

## Copyright Undertaking

This thesis is protected by copyright, with all rights reserved.

**By reading and using the thesis, the reader understands and agrees to the following terms:**

1. The reader will abide by the rules and legal ordinances governing copyright regarding the use of the thesis.
2. The reader will use the thesis for the purpose of research or private study only and not for distribution or further reproduction or any other purpose.
3. The reader agrees to indemnify and hold the University harmless from and against any loss, damage, cost, liability or expenses arising from copyright infringement or unauthorized usage.

### IMPORTANT

If you have reasons to believe that any materials in this thesis are deemed not suitable to be distributed in this form, or a copyright owner having difficulty with the material being included in our database, please contact [lbsys@polyu.edu.hk](mailto:lbsys@polyu.edu.hk) providing details. The Library will look into your claim and consider taking remedial action upon receipt of the written requests.



THE HONG KONG  
POLYTECHNIC UNIVERSITY  

---

香港理工大學

Department of Industrial and Systems Engineering

# SYSTEM STUDY AND DESIGN OF A MULTI-PROBE MISSION FOR PLANETARY IN-SITU ANALYSIS

PETER SIMON WEISS

A thesis submitted in partial fulfillment of the  
requirements for the degree of  
Doctor of Philosophy  
November 2009

# CERTIFICATE OF ORIGINALITY

I hereby declare that this thesis is my own work and that, to the best of my knowledge and belief, it reproduces no material previously published or written, nor material that has been accepted for the award of any other degree or diploma, except where due acknowledgement has been made in the text.

\_\_\_\_\_

Peter Weiss

Hong Kong, 20<sup>th</sup> July 2009

# ABSTRACT

*Planetology has gained an overall picture of most surfaces of solar system bodies through observation satellites and robotic landers. However a novel method for the exploration of extraterrestrial surfaces is needed to complete remote observations with a global network of in-situ measurements. Miniaturized surface penetrators are a promising concept to fill the gap between remote observations and in-situ measurements.*

*This work investigates the feasibility of the deployment of a large number of geochemical measurement instruments, integrated into high-velocity penetrators. The objective was to develop a mission strategy and architecture for a multi-microprobe planetary exploration system.*

*To determine the quantity of probes needed, a landing site decision support system was developed in ArcGIS. The system uses a method to calculate the uncertainty in geochemical datasets in order to identify locations with high measurement uncertainty. This methodology was applied on data of the lunar surface: The identification of ISRU elements in the lunar soil is one of the highest objectives in the future attempts to return to the Moon. Thirty-one locations on the Moon are identified that can be used to perform ground control checks of the abundance of these elements. The ultimate goal of such a mission would be to develop a model of the surface abundances of elements that span the overall lunar surface.*

*Based on this quantity as base specification, a miniaturized high-velocity penetrator concept is developed. Different carrier structures were analyzed through empirical formula and hydrocode simulations in LS-DYNA. The goal of this investigation was to evaluate the ruggedness of the carrier shell, evaluate the penetration depth and its impact behavior. A soil model of the lunar soil had to be developed to perform the numerical analysis. The result of this work was a modified penetrator design which is better suited to geochemical surface analysis.*

*Several works identify the sampling mechanism for soil analysis as weak element in the development of high-velocity penetrators. Different sampling strategies are reviewed and novel methods suggested. Based on a technological analysis a sampling system that works like a vibrating conveyor was designed further. The efficiency of the system is evaluated analytically. The work concludes with a design of a high-velocity penetrator for geochemical analysis that can be deployed in large numbers on the surface of extraterrestrial surfaces.*



# RESUMÉ

*Aujourd'hui la planétologie a acquis, grâce aux sondes robotiques, une image relativement complète des surfaces planétaires de notre système solaire. Cependant une nouvelle méthode d'exploration des surfaces extraterrestres est nécessaire, afin de compléter les observations en orbite par des mesures in-situ. Dans ce contexte, les pénérateurs miniaturisés sont un outil prometteur pour réduire le fossé entre ces télé-observations et les mesures in-situ.*

*L'objet de cette thèse est d'étudier la faisabilité du largage d'un grand nombre d'instruments géochimiques grâce aux pénérateurs de haute vitesse. Il s'agit d'une part de développer une stratégie de missions et d'autre part de mettre en place l'architecture d'un tel système d'exploration planétaire par des microsondes.*

*Un système informatique décisionnel (Decision Support System, DSS) a été développé sous ArcGIS. Ce système utilise une nouvelle méthode pour calculer les incertitudes des données géochimiques, afin d'identifier les endroits où mesures supplémentaires (in-situ) seront nécessaires. Cette méthode a été appliquée aux données de la surface lunaire : A ce titre, l'identification des éléments ISRU est un des objectifs principaux pour permettre l'exploration de la lune par des hommes dans l'avenir. Trente-et-une positions sur la surface de la lune ont été identifiées comme intéressantes pour prendre des mesures. L'objectif ultime d'une telle mission est de développer un modèle des caractéristiques de ces éléments, sur une envergure totale de la surface lunaire. Sur cette base, un nouveau concept de pénérateurs haute-vitesse miniaturisé est développé. Différentes structures mécaniques correspondant à un tel système ont été analysées par des formules empiriques et des simulations en hydrocode par LS-DYNA. Le but de cette investigation est d'évaluer d'une part la rugosité des différentes architectures, d'autre part la profondeur de la pénétration dans le sol, et enfin le comportement d'impact en général. Un modèle du sol lunaire a dû être développé pour effectuer les analyses numériques. Le résultat de ce travail a mené à une forme modifiée de la conception des pénérateurs ; forme qui sera mieux adaptée pour des analyses géochimiques. Plusieurs publications ont déjà identifié le système d'échantillonnage comme l'élément faible dans le développement des pénérateurs de haute vitesse. Au cours de cette thèse, différentes stratégies d'échantillonnage sont revues, et de nouvelles méthodes sont proposées. Sur la base de cette analyse technologique, un système d'échantillonnage fonctionnant comme un convoyeur vibrant a été développé avec plus de détails. L'efficacité de ce système a également été analysée.*

*Ce travail s'achève sur la conception d'un pénérateur de haute vitesse pour l'analyse géochimique, pénérateurs qui pourraient être largués en grand nombre sur des surfaces extraterrestres.*

# ZUSAMMENFASSUNG

*Die letzten Roboter Missionen zu den Planeten und Monden unseres Sonnensystems haben der Wissenschaft ein gutes allgemeines Bild der Oberflächen dieser Himmelskörper geliefert. Neue Methoden werden jedoch in der Zukunft benötigt, um diese Fernmessungen mit einem oberflächenübergreifenden Netzwerk von in-situ Daten zu vervollständigen. Miniaturisierte Hochgeschwindigkeitspenetratoren sind ein vielversprechendes Konzept, um eine grosse Anzahl von Analyseinstrumenten an verschiedenen Oberflächenpositionen zu platzieren.*

*In der folgenden Arbeit wird die Machbarkeit eines solchen Systems unter verschiedenen Aspekten studiert. Das Ziel dieser Studie ist die Entwicklung einer Missionsstrategie und Systemarchitektur für solche Hochgeschwindigkeitsspenetratoren. Ein Landing Site Decision Support System wurde in ArcGIS entwickelt. Eine Methode um die Genauigkeit in geochemischen Datensätzen zu berechnen wird vorgestellt. Die Methode erlaubt es, Orte auf einer Planetenoberfläche zu identifizieren, deren Messungen Inkonsistenzen aufweisen. Die Methode wurde auf Datensätze der Mondoberfläche angewendet: Die Identifizierung von sogenannten ISRU Elementen im Mondregolith stellt eine hohe Priorität für die zukünftige Rückkehr des Menschen auf dem Mond dar.*

*31 Positionen auf der Mondoberfläche wurden auf diese Weise ermittelt, welche sich für Oberflächenmessungen anbieten. Das Ziel einer solchen Mission wäre es letztendlich ein genaues Model der Elementvorkommen der Oberfläche des Mondes zu erstellen. Ein miniaturisiertes Hochgeschwindigkeitspenetratorensystem wurde entwickelt, basierend auf dieser Anzahl an Proben als Basisspezifikation. Verschiedene Projektilformen wurden mittels empirischer Formeln und in Hydrocode-Simulationen in LS- DYNA analysiert. Das Ziel dieser Forschung ist die Robustheit verschiedener Architekturen zu ermitteln, die Eindringtiefe in die Mondoberfläche zu errechnen, und das Aufschlagverhalten den Proben zu studieren. Ein Model der Mondoberfläche musste für die numerische Analyse entwickelt werden. Das Ergebnis dieser Arbeit ist ein modifiziertes Penetratoren, dessen Design für geochemische Untersuchung der Oberflächen optimiert wurde. Verschiedene andere Arbeiten stellten fest, dass das Probenentnahmesystem ein Schwachpunkt in der Entwicklung von Hohgeschwindigkeitsspenetratoren darstellt.*

*Verschiede Strategien und neue Methoden zur Bodenprobeentnahme werden vorgestellt. Ein System, welches auf dem Prinzip des Schwingförderers basiert wurde weiterentwickelt. Die Effizienz dieses Systems wurde analytisch ermittelt. Die Arbeit schließt mit der Vorstellung des Designs solcher miniaturisierter Hochgeschwindigkeitsspenetratoren für geochemische Untersuchungen ab, welche in großen Mengen auf Oberflächen abgeworfen werden können.*

## ACKNOWLEDGEMENTS

My choice to pursue a Ph.D after having already worked for five years has raised many questions and doubts. However, developing space technology and doing a Ph.D has been a long time dream for me. Luckily I had a strong support of my wife for this adventure, albeit the large impact on our own family life. My thanks go foremost to my wife and our two kids who followed me into this adventure; they had to sacrifice a lot for this endeavor.

*Stéphanie, Awa, Raphael, je vous aime le plus profondément de ma vie!*

Leaving Europe had obviously also a great impact to my family in Germany and France. They encouraged me -each one in his or her own way- to pursue what I was set up to do. In particular I wish to thank my parents and my brothers for their help and love during this time. This project would not have been possible without them and I will ever be grateful that they have given me this possibility.

Prof. Kai-Leung Yung of the Hong Kong Polytechnic University accepted me in his research team. During the three years that I spend with him he was always available for my many questions and provided great help in technical problems and personal issues. Although he has a lot of work already I never heard from him “I have no time today, please let’s make an appointment next week”. I am aware that this is more than a Ph.D student can expect; I will always be thankful for having me given the chance to work with him.

During my time in Hong Kong I had the help of many local friends who introduced me in the life in China with all its cultural aspects. I deeply wish that I will often get a chance to come back to this great place and meet with them in the future. In particular I would like to thank Sam Lam, Sam Choi, Winnie Leung, Ko, T.C., Jan, Nicole, Jack, Jackson and Matthew.

Towards the end of this work we were forced to leave Hong Kong due to a serious health issue in my family. I think under normal circumstances this would have been the end of my work if it would not have been for the help of my best-man – and best friend: Frederic Gauch was always there for us during these three years and especially at the end, when he managed to give me a place in COMEX where I could finalize my work. I am uncertain I will be able to return back to him all what he has done for me and my family the last years; but I will try my best!

## PUBLICATIONS DURING THE RESEARCH PERIOD

1. Weiss, P., Yung, K.L., 2009. Feasibility study of a lunar landing area navigation network deployed by impacting micro-probes, accepted to Planetary and Space Science.
2. Leung, S.W.W., Weiss, P., 2010. Integrated design framework for payload deployment flexible parallel mechanism, submitted to the 10th International Symposium on Artificial Intelligence, Robotics and Automation in Space.
3. Weiss, P., Yung, K.L., 2009. Navigation beacons based on penetrators deployed during lunar landing, submitted to the Global Lunar Conference, Beijing, China.
4. Weiss, P., Leung, W., Yung, K.L., 2009. Feasibility study for Near-Earth-Object tracking by a piggybacked micro-satellite with penetrators, accepted, Planetary and Space Science.
5. Weiss, P., Yung, K.L., Kömle, N., Ko, S.M., Kaufmann, E., Kargl, G., 2009. Thermal drill sampling system onboard high-velocity impactors for exploring the subsurface of Europa, *Advances in Space Research*, doi 10.1016/j.asr.2010.01.015
6. Weiss, P., Shi, W.Z., Yung, K.L. 2009. Attribute uncertainty modeling in lunar spatial data, submitted 14th International Symposium on Spatial Data Handling Theory, modeling and concepts in Geospatial Information Science.
7. Weiss P., Yung K.L., Kömle N., Ko S.M., Kargl G., Kaufmann E., 2009. A thermal drill head for the exploration of subsurface ice layers on Europa, *Proceedings of the International workshop “Europa lander: science goals and experiments”* Space Research Institute (IKI), Moscow, Russia.
8. Weiss, P., Yung, K.L., 2009. Mission Strategy Decision Support System for robotic lunar landing, *Planetary and Space Science*, 57, pp. 1434-1445.
9. Weiss, P., Shi, W.Z., Yung, K.L. 2009. Attribute uncertainty modeling in lunar spatial data, *International Journal of Remote Sensing*, 31, pp. 197 - 211. doi: 10.1080/01431160902882611.
10. Küppers M. et al., 2008. Triple F - A Comet Nucleus Sample Return Mission, *Experimental Astronomy*, 23, pp. 809-847.

11. Kömle N.I., Weiss P., Yung K.L. 2008. Considerations on a suction drill for lunar surface drilling and sampling, *Acta Geotechnica*, 3, pp. 201-214.
12. Weiss P., Yung K.L., Ng T.C., Kömle N., Kargl G. and Kaufmann E., 2008. Study of a melting drill head for the exploration of subsurface planetary ice layers, *Planetary and Space Science*, 56, pp. 1280-1292.
13. Weiss P., Yung K.L., 2007. Closing the gap between remote observation and rover explorations: Lunar exploration by multiple micro-probes, *Proceedings of the 9th ILEWG International Conference on Exploration and Utilization of the Moon*, Editors: B.H. Foing, S. Espinasse and G. Kusters.
14. Weiss P., Leung W., Ng T.C., 2007. Houyi – Asteroid Apophis tracking and sampling system, *Mission Design Award of The Planetary Society*.
15. Weiss P., Yung K.L., Ng T.C., Wai Leung W.S. and Choi S., 2007. Integrated Sampler Downhole Hammering Drill Head (ISDHH) for soft and hard soil sampling, *Proceedings of the European Geosciences Union General Assembly*, Vienna.
16. Weiss P., Yung K.L., Ng T.C., Kömle N., Kargl G. and Kaufmann E., 2007. Study of a melting drill head for the exploration of subsurface planetary ice layers, *Proceedings of the European Geosciences Union General Assembly 2007*, Vienna.

# CONTENTS

CHAPTER 1 Introduction.....	2
1.1 A new scientific rationale in space research .....	2
1.2 Objectives of the dissertation.....	4
CHAPTER 2 Literature Review .....	6
2.1 Future objectives of planetary exploration .....	6
2.2 Multiprobe mission concepts and their development methodology .....	11
2.3 GIS-based landing strategy decision support systems .....	20
2.4 EDLS and sampling design considerations.....	23
CHAPTER 3 Research Methodology .....	25
3.1 Problem formulation .....	25
3.2 Methodology of the investigation .....	26
3.3 Research contribution and originality of the work .....	28
3.4 Originality of the proposed work.....	30
CHAPTER 4 Landing strategy decision support system.....	32
4.1 GIS-based decision support system for lunar exploration .....	32
4.2 Uncertainty in lunar GIS data to determine potential landing sites .....	33
4.2.1 Sources of uncertainty in remotely sensed data.....	34
4.2.2 Probability estimation by elemental inter-correlation: Example Oxygen..	37
4.2.3 Extending this method to all elements .....	45
4.2.4 Identification of landing sites based on uncertainties in ISRU elements...	46
4.3 Landing strategy decision support system .....	54
4.3.1 Introduction of technical restriction for the exploration methods .....	55
4.3.2 Capabilities and constraints of the three exploration strategies.....	58
4.3.3 Landing Strategy Decision Support System process .....	60
4.4 Resulting design considerations.....	63
CHAPTER 5 Analysis and modeling of high-velocity impacting probe.....	65
5.1 Basic specifications for the deployment of micro-probes.....	66
5.1.1 Impact velocities .....	66
5.1.2 Soil properties .....	74
5.1.3 The lunar environment.....	84

5.2 Analysis of the carrier design .....	87
5.2.1 Methodology to determine the penetration depths.....	87
5.2.2 Impact behavior simulation in hydrocode.....	95
CHAPTER 6 Feasibility study of a high velocity impact sampling system .....	111
6.1 Payload integration study.....	111
6.1.1 Technological readiness study for geochemical analysis instruments.....	111
6.1.2 Integration into high-velocity micro-penetrators .....	113
6.1.3 Description of the strawman payload suite .....	117
6.1.4 Conclusions and design requirements for the sampling mechanism .....	119
6.2 Review of geochemical sampling apparatus.....	120
6.2.1. Mars-96 sampling strategy.....	121
6.2.2. Deep-Space-2 micro sampler.....	122
6.2.3. Integrated sampling device for penetration moles .....	123
6.2.4. Bio-inspired micro-drill .....	124
6.2.5. Suction-drill .....	126
6.2.6. Shacking sampling system.....	128
6.2.7. Chladni-Sampler .....	129
6.2.8. Vibrating conveyor .....	135
6.2.9. Conclusions on the concept studies .....	137
6.3 Modeling of the vibrating conveyor as sampling system .....	139
6.3.1. General considerations in vibrating conveyor applications .....	140
6.3.2. The problem of the probe's orientation .....	148
6.4 The integration of the sampling mechanism in the projectile.....	150
6.5 Conclusions on the sampling system .....	154
CHAPTER 7 Conclusions and suggestions for future research.....	155
References.....	159

# LIST OF FIGURES

- Figure 1:** Viking '75 scientific instrument integration from Holmberg et al, (1980).
- Figure 2:** Multiprobe missions can deliver multiple ground-truth data spots to orbital observation.
- Figure 3:** Left: Schematic design of the Deep-Space2 probes. Right: Photograph of the probe (JPL DS 2007).
- Figure 4:** Clockwise: Evolution of the DS-2 architecture. (courtesy of NASA, retrieved from [http://nmp.nasa.gov/ds2/pictures/misc/b121698\\_02.html](http://nmp.nasa.gov/ds2/pictures/misc/b121698_02.html))
- Figure 4:** Architecture of the Mars-96 penetrators (Zakharov 2007).
- Figure 5:** From Shiraishi et al, 2007: The Lunar-A penetrator after impact tests at the Sandia Laboratory.
- Figure 6:** Photograph of the mock-up penetrator of the LunarEX proposal traversing 2 meters of concrete at a velocity of 300 m/s (Smith et al., 2007).
- Figure 7:** Concept design of the Europa Microprobe from Atzei and Falkner (2003).
- Figure 8:** Difference between EDL for atmospheric and atmosphereless bodies in the Solar system
- Figure 9:** Proposed study methodology.
- Figure 10:** Overview on the elements of the development of a multiprobe mission.
- Figure 11:** Factors leading to uncertainties in lunar spatial data
- Figure 12:** Negative correlation between Oxygen and Titanium.
- Figure 13:** Negative correlation between Oxygen and Iron.
- Figure 14:** Positive correlation between Oxygen and Aluminum.
- Figure 15:** Positive correlation between Oxygen and Silicon.
- Figure 16:** Relation of Oxygen to Calcium.
- Figure 17:** Negative correlation between Oxygen and Magnesium.
- Figure 18:** Uncertainty estimation in Oxygen abundances by comparison with other abundance datasets that exhibit a correlation.
- Figure 19:** Uncertainty chart for Oxygen by comparison with Ti, Fe, Mg, Si and Al.
- Figure 20:** Uncertainty charts for Titanium, Iron and Aluminum. The chart of Fig 18 and the ones of Titanium and Iron show a concentration of the derivation of values in the Oceanus Procellarum region. This fact offers the possibility to refine the models by separating the values into two categories.
- Figure 21:** Determination process based on the abundance value of certain ISRU elements and their related uncertainty.
- Figure 22:** Proposed landing sites for geochemical investigation. The numbers indicate the cell ID of the measurements. Three categories of locations were identified: blue with high Oxygen abundances, red with high Titanium or Iron abundances and green those with high Aluminum values.



**Figure 23:** The abundance values for Oxygen, Titanium, Iron and Aluminum classified per priority, cell ID and category.

**Figure 24:** Comparison of the proposed landing sites with those of the previous Apollo missions on a Aluminum-Titanium chart.

**Figure 25:** Identical comparison as of Fig. 23 but on an Oxygen-Iron chart.

**Figure 26:** Topography chart of the Moon with the elevations as measured by the Lunar Prospector mission.

**Figure 27:** Surface slopes as derived through Eq. 5 with a cut-through surface profile at the 31<sup>st</sup> longitude east.

**Figure 28:** Landing Strategy Decision Support System.

**Figure 29:** Operational ranges of 300km for a rover mission. The background chart shows the slopes identical to Fig. 27.

**Figure 30:** Additional landing site proposals from other sources (red stars) in comparison with the above identified surface cells (white triangle).

**Figure 31:** Variation of the impact speed as function of the initial velocity, the orbit altitude, the topographic variation and the gravity on the Moon.

**Figure 32:** (A) Descent phases of Lunar-A and (B) the architecture of the LunarEX proposal to ESA's Cosmic Vision Call (NSSDC, 2009; Gowen et al., 2009).

**Figure 33:** The ratio between the penetrator mass  $M$  and the propellant mass  $M_{Prop}$  as function of the exhaust velocity.

**Figure 34:** The concept of a tether-based deceleration system.

**Figure 35:** Density models of the lunar soil as function of the depth.

**Figure 36:** Compression strength models for the lunar soil

**Figure 37:** Shear modulus  $G$  as function of the applied pressure (adapted from Khalid et al., 2009).

**Figure 38:** Elastic modulus  $E$  as function of the applied pressure (adapted from Klosky et al, 2000 and Khalid et al., 2009).

**Figure 39:** Attenuation of a radio signals in different frequency bands at depths levels of lunar regolith. The assumed electrical conductivity  $\sigma=10^{-9}$  S/m.

**Figure 40:** Attenuation of a radio signals in different frequency bands at depths levels of lunar regolith. The assumed electrical conductivity  $\sigma=10^{-9}$  S/m.

**Figure 41:** The two model shapes considered for the study (left to right): Slim ogive shape with a diameter of 100mm and a flat ogive shape with a diameter of 200mm.

**Figure 42:** Flow chart of Young's penetration equations. The bold lines show the approach taken for the here presented impact penetrators.

**Figure 43:** Penetration depth plots for the models of Young and Holsapple.

**Figure 44:** Estimation of the penetration depth and crater shape based on Young ( $d_{max}$  and  $d_{tmax}$ ) and Holsapple ( $d_{min}$  and  $d_{tmin}$ ).

**Figure 45:** Model of the lunar soil in LS-DYNA.

**Figure 46:** Penetration of the projectile in the soil with erosion of cells.

**Figure 47:** Penetration depths at different initial velocities for the large ogive penetrator (diameter 200mm; length 70mm).

**Figure 48:** Penetration of the large ogive projectile at 244 m/s.

**Figure 49:** Penetration of the large ogive projectile at 70m/s and 186m/s into the enclosed and 5meter soil model.

**Figure 50:** Penetration depths of the large projectile (diameter 200mm) into the lunar soil model. Red and blue values are the corresponding depths calculated through the formula of Young and Holsapple.

**Figure 51:** Penetration profiles of the slim probe at different impact velocities. Red graphs show penetration profiles of projectiles with normal nose and blue graphs show those with a blunted nose.

**Figure 52:** Orientation of the probe during its penetration at an initial speed of 244m/s.

**Figure 53:** Penetration depths of the slim projectile (diameter 100mm, length 200mm) into the lunar soil model. Red and blue lines are the profiles calculated from Young's and Holsapple's formula.

**Figure 54:** Bounce off behavior of the probes at attack angle of 40°.

**Figure 55:** Screenshot of the bouncing-off of the larger probe at a smaller attack angle.

**Figure 56:** The deformation of the projectiles at an impact of 360m/s.

**Figure 57:** Projectile shape with deceleration mechanism adapted for geochemical soil analysis.

**Figure 58:** Penetration profiles of the probe with stoppers.

**Figure 59:** Deformations of the stoppers after a 128m/s speed impact.

**Figure 60:** Decelerations at different orbital heights.

**Figure 61:** Rough estimation of the payload space that would be required to deploy 36 microprobes. **Figure 62:** Design of the high-velocity penetrator carrier shell.

**Figure 62:** Design of the high-velocity penetrator carrier shell.

**Figure 63:** Principal elements of an APXS. The spectrum shown in the upper right inlet shows the Mermaid Dunes measured on Mars by Pathfinder (courtesy Economou, 2001).

**Figure 64:** The APXS onboard the Mars Pathfinder (courtesy NASA/JPL-Caltech).

**Figure 65:** The different phases of the sampling strategy.

**Figure 66:** The Mars-96 sampling apparatus.

**Figure 67** High-velocity penetrator adapted Sampling device based on the Mole micro-sampler design. (1) Projectile shell, (2) actuator, (3) sampling cavity, (4) sample recipient and (5) analysis instruments (i.e. APXS not in scale).

**Figure 68:** The drilling method of the wood wasp.

**Figure 69:** Lateral integration of the bio-drill described by Gao et al. (2006; 2007). (1) Projectile's shell of 100mm diameter, (2) APXS, (3) Bio-drill, (3a) foldable metal tape and pin-crack mechanism, (3b) electronics. Green path indicates the sampled particles falling into a collection funnel installed above the analysis instrument.

**Figure 70:** Schematic architecture of the Implementation of a suction drill mechanism into a high-velocity penetrator shell: [A]: Schematic architecture of the device (1) projectile shell,

(2) particle access channel, (3) gas tank with pyrotechnic bolt valve, (4) analysis chamber (5) particle filter and (6) APXS. [B] CFD simulation of the gas flow inside the system in COSMOSFlowXpress (not shown: the trajectory of the flow towards the rear of the probe after the filter).

**Figure 71:** Schematic architecture of the vibration sampler for mobile units: (1) unbalanced rotary mass, (2) motor, (3) reduction gear for the shutter, (4) sample inlet, (5) shutter, (6) unloading valve, (7) spring, (8) unloading funnel.

**Figure 72:** The principle of Chladni-plates: A rectangular or circular plate (2) is brought into vibration by a loudspeaker (1). Powder which was put on the plate will align in specific patterns as function of the frequency and the plate's geometry as shown in the inlets on the right side.

**Figure 73:** The deformation of a circular plate as function of the number of modes  $n$  and  $m$ .

**Figure 74:** The working principle of a Chladni-Sampler.

**Figure 75:** Concept of the impact sampling system integrated into the shell: The projectile disposes of several inlets on its perimeter. While impacting (direction of the large white arrow) soil particles will be projected into the sampling chamber.

**Figure 76:** Inner structure of the Chladni sampling mechanism: The particles follow the blue path. They enter the probe during impact through the inlets in the penetrator's shell [1]. An actuator (here electromagnetic vibrator) [2] induces a vibration to the Chladni Plate [3]. The soil particles travel as a function of the frequencies used towards the centre of the plate where they fall into the trap [4]. An APXS [5] is aligned atop of the centre to take measurements of the particles composition in the trap. Measured particles are discarded into a second chamber [6] below the plate. The system allows continuous measurement of the particle flow from the perimeter into the discard chamber.

**Figure 77:** The two basic construction principles of a vibrating conveyor: (top) introduction of a time-dependant force which makes the items jump forward and (bottom) forward shifting of the items along the conveyor.

**Figure 78:** The integration of a vibration conveyor as sampling system into the high-velocity penetrator. The soil enters the probe during impact through inlets [1] that are integrated in the shell. A piezoelectric actuator [2] drives the vibrating conveyor [3] to push the particles into the analysis chamber [4]. The chamber can be opened by a system of Shape Memory Alloy shutters, once the measurement by the APXS [5] is finalized.

**Figure 79:** The vibrating conveyor can even work if the probe remains at a large inclination angle.

**Figure 80:** The vector diagram of Jung to determine the slippage between the particle and the conveyor. At point A both, the conveyor and the particle, move with its maximum speed forward.

**Figure 81:** At point B the inertia of the particle overcomes the friction and the particle starts to slip forward.

**Figure 82:** At point C the vector enters again the friction phase; the particle starts decelerating.

**Figure 83:** At point D the system enters a second slipping phase. This time the particle starts to slip backwards (negative  $x$  direction) due to the acceleration of the conveyor.

**Figure 84:** A stepwise inclination of the conveyor's surface will assure that the particles move rather forward than backward.

**Figure 85:** Simulation of the jump of a particle on the conveyor. The red line traces the path of the particle, while the blue line indicates the displacement of the conveyor.

**Figure 86:** Integration of the sampling channel into the projectile.

**Figure 87:** Horizontal position of the probe (with  $F_N$  pointing downwards). The active surfaces are marked in red. Each channel disposes of two active surfaces, where the shadowed ones are looking outwards of the figure.

**Figure 88:** The movement of the conveyor  $x_{Conv}$  is restrained to be inferior of the travel of the actuator  $x_{Actu}$ .

**Figure 89:** The conveyor disposes of three active surfaces.

**Figure 90:** Design of the microprobe with integrated sampling apparatus. [1] Sampling aperture, [2] vibrating conveyor, [3] piezoelectric bending actuator, [4] APXS, [5] batteries.

# LIST OF TABLES

**Table 1:** Decision Table for the Oxygen correlation estimation. The percentage in the last column shows the occurrence of cells.

**Table 2:** The percentage of correct values within one sigma deviation of different elements resulting from the correlation rules as described in 4.2.2. The input elements (left column) were used to derive the output elements (first row).

**Table 3:** The weight factors for the different surface cells in terms of elemental abundances.

**Table 4:** The landing site locations with the measurement objective (OP = Oceanus Procellarum; \* Central point of a 5°x5° cell).

**Table 5:** Landing site proposals. Sites with identical numbers in brackets are proposed as duplicate sites in the references.

**Table 6:** Payload weight on various host missions.

**Table 7:** Velocity components used for the study

**Table 8:** Recommended bulk density values for the lunar soil as function of depth.

**Table 9:** Recommended Compression Indexes.

**Table 10:** Recommended values for the cohesion and the friction angle as function of the penetration depth. Both values are used to derive the shear strength as indicated in Eq. (5.6).

**Table 11:** Summary of the soil parameters and used values for the modeling.

**Table 12:** Recommended values for some of the characteristics of the lunar surface.

**Table 13:** Summary of different types of ionization radiation at the lunar surface (Vaniman et al., 1991).

**Table 14:** Soil parameters with its units used for the lunar soil model 005-SOIL\_AND\_FOAM in LS-DYNA.

**Table 15:** Material parameters for the model 024-PIECEWISE\_LINEAR\_PLASTICITY with its units used for the projectile model.

**Table 16.:** The impact characteristics of the two probe shapes.

**Table 17:** Capabilities of instruments for geochemical analysis. “n.d” means that there is no data available for its accuracy. “n.a” means that the technology is not applicable for this kind of mineralogical investigation.

**Table 18.:** Operational parameters of geochemical analysis instruments. Instrument references are, unless otherwise indicated, the same as in Tab.17. “n.d” means that no data is available for this instrument. Brackets in the weight column indicated different versions of the instrument.

**Table 19:** Comparison of different sampling strategies. The number in brackets show the ranking within the systems studied here. Fields marked with \* are estimations.

**Table 20:** Battery technologies.

**Table 21:** Estimated power consumption

# ABBREVIATIONS

AES	Auger Electron Spectroscopy
AOA	Angle Of Attack
APX	Alpha Proton X-Ray
APXS	Alpha Proton X-Ray Spectroscopy
DSS	Decision Support System
CFD	Computational Fluid Dynamics
CSV	Comma-Separated Value
EDLS	Entry, Descent and Landing System
EOP	Exterior Orientation Parameters
FEA	Finite Element Analysis
GIS	Geographic Information System
GRS	Gamma-Ray Spectrometer
HIPS	Highly Integrated Payload Suites
IOP	Internal Orientation Parameters
IR	Infrared
ISRU	In-Situ Resource Utilization
MASCON	MASs CONcentrations (variations of the gravity field of a planet or moon)
MER	Mars Exploration Rover
NMR	Nuclear Magnetic Resonance
RMSE	Root Mean Square Error
SEMPA	Scanning Electron Microscope and Particle Analyzer
SMA	Shape Memory Alloy
SPE	Solar Particle Events
SRP	Self-Recording Penetrometer
TOF	Time-Of-Flight
TRS	Technology Reference Study
VIS	Visual
XPS	X-Ray stimulated Photon Spectroscopy
XRD	X-Ray Diffraction analysis
XRF	X-Ray Fluorescence
XRS	X-Ray Spectrometer
UHV	Ultra High Vacuum
UV	Ultraviolet
VIS	Visible (spectrum)

# LIST OF SYMBOLS

$\Delta e$	change in volume
$\Delta x_{TGE}$	difference to the mean surface
$a$	acceleration (gravity)
$A$	cross-sectional area; amplitude
$c$	Cohesion
$C_c$	compression index
$d$	depth / diameter
$d_{min/max}$	primary penetration depth
$d_{tmin/max}$	final depth of the crater
$E$	Young's modulus
$f$	frequency
$G$	shear modulus
$g$	gravitational constant
$K$	bulk modulus
$K_H$	mass scaling factor hard soil
$K_S$	mass scaling factor
$L_n$	nose length
$M$	Mass (spacecraft)
$m$	number of circular modes
$M_{prop}$	mass of ejected propellant
$n$	integer
$N$	nose performance coefficient
$n$	number of radial modes
$q$	the mass flow of the propulsion
$R$	Radius (Moon)
$S$	Young's index of penetrability
$S_R$	conveyor's displacement
$\beta$	slope
$t$	time
$v$	velocity
$V$	volume
$v_0$	initial speed
$v_e$	exhaust velocity (of propellant)
$x$	element abundance
$y$	element abundance
$z$	Altitude
$z_{ij}$	vertices at longitude $i$ and latitude $j$
$z_{\lambda\phi}$	vertices at longitude $\lambda$ and latitude $\phi$
$\alpha$	intercept
$\Gamma$	jump coefficient
$\lambda$	longitude
$\mu$	friction constant
$\pi_2$	gravity-scaled size parameter
$\pi_3$	soil strength group
$\pi_V$	cratering efficiency factor
$\rho$	density
$\sigma_{max}$	maximum conductivity

$\sigma_v$	applied vertical stress
$\tau$	shear strength
$\nu$	Poisson's ratio
$\Phi$	latitude
$\Phi$	angle of repose
$\omega$	angular speed





*Amongst the twelve men that walked on the Moon  
there was only one geologist.*

# CHAPTER 1

## Introduction

### **1.1 A new scientific rationale in space research**

The exploration of our Solar System and in particular Earth's Moon with robotic probes has gained a new momentum through numerous new missions that are planned for the coming decade (Zheng et al., 2008; Foing and Ehrenfreund, 2008; Hovland and Foing, 2007; Green, 2007, Polishchuk, 2007). Robotic explorers have acquired a glimpse into the most mysterious worlds of our Solar System such as the surface of planet Venus or Saturn's moon Titan. However, novel techniques will be needed to deliver the necessary amount of data to establish globally valid models of these extraterrestrial surfaces: Mission architectures using a single lander approach will not be sufficient to fill the information gap between orbital observations and the in-situ ground measurements. In this work a system design for a multiple probe exploration missions is developed and evaluated as solution to deliver ground measurements.

A multiple probe mission is a mission that delivers not a single lander onto an extraterrestrial surface, but that deploys various, rather simple explorers on different locations of a planet or moon. The probes are deployed by an orbiting craft and descend on various regions of the target. This global deployment scheme allows the development of a more comprehensive model of the surface properties.

The concept of a deployment of multiple probes onto a planetary or lunar surface itself is not new. A detailed discussion of previous multi-probe mission designs will be given in the following chapter. However, several issues will be addressed in this work, which were not sufficiently elaborated in precedent studies:

The work will start by determining a minimal number of probes that are necessary to retrieve sufficient data to globally model the geochemistry of the target's surface. This quantity will be derived independently from how many probes can technically be carried by a host space-craft at a first stage. Methodologies developed in the field of Geographic Information Systems (GIS) will be applied to determine a necessary quantity of probes (and their landing location), based on the determination

of uncertainty in geochemical surface data and the fulfillment of set mission goals. The engineering specifications for the micro-probe development are then derived as a function of the necessary number of landing sites.

The second problem to be tackled in this study is the lack of geochemistry sampling instruments that are suited to the operational constraints of micro-probe missions (potential high decelerations, small size and low energy consumption). Smith and co-workers (2007) identify the sample acquisition process as the weak link in the in-situ sampling process for impacting microprobes. Sampling techniques for geochemical surface analysis will be developed, analyzed and evaluated. Special consideration will be given to the integration of the instrument into the architecture of a high-velocity penetrator. The operational requirements will limit the range of instruments that can be used in such an exploration scenario. A novel type of a sampling mechanism for high velocity impacts will be presented in this work. The design of the probe is verified by mathematical models of its dynamic behavior and through hydrocode simulations of the high-rate loading phenomena that will occur during impact on the surface.

## 1.2 Objectives of the dissertation

This research was to develop a mission strategy and architecture for a multi-micro-probe planetary exploration system. The study was about how such systems can be deployed onto a target's surface in order to deliver significant scientific data (System Strategy) and how such a system shall be designed to accomplish the before mentioned mission (System Architecture).

To achieve the overall goal the following objectives have to be attained:

- i) To answer the question of how many of such probes are necessary to perform geochemical analysis of a surface (in our case the Moon).
- ii) Then we study the feasibility of high-velocity impactors: The impact process is analyzed through numerical models of different probe shapes and a model of the lunar soil. The objective is to optimize the probe architecture for such deployment scenario.
- iii) The sampling mechanism was identified as weak element in the development of high-velocity impactors. Different strategies were studied in respect to the requirements of an impacting microprobe. Its expected performance is derived through theoretical models and led to a design of a system.

To reach the objectives, the following four phases have to be pursued:

- **Phase A:** Identification of the objectives for future solar system exploration missions based on previous missions and techniques.
- **Phase B:** Development of a landing strategy decision support system to optimize the number of probes, and to show its validity by applying it to the exploration of Earth's Moon.

The precedent phases A and B delivered the key elements for the following design and design verification process in phases C and D: namely a number of probes and the system's functionalities.

- **Phase C:** Investigation on the microprobe design that complies with the payload and system requirements identified in Phase A, B and C. The design

was validated through analysis and simulation the impact process. Different projectile forms were analyzed in order to derive an optimal shape for the above identified investigation.

- **Phase D:** Technology assessment in terms of miniaturization potential and space-fitness for the soil analysis instrumentations. The sampling mechanism was identified as the weak member in the process chain from sample acquisition to sample analysis. Sampling strategies were studied and a novel sampling method for impacting probes was investigated.

The following research identifies candidate scientific instruments for future exploration missions by studying previous mission profiles and payload. For this we will limit the research on studying the use of analysis instruments for micro-probe application, the design of the analysis instruments itself, is beyond the frame of the work. Limits will be established in terms of mass and payload through the number of probes that are needed for the exploration of a specific surface. The figures were established based on a lunar deployment scenario while the methodology used here is applicable to other atmosphereless object in the solar system. The payload architecture of the micro-probes needs to comply with those limits in order to remain feasible.

A Geographic Information System based on ArcGIS® was used to analyze the target's geology and morphology and to derive a landing strategy by taking account mission objectives and system capabilities. Previously proposed landing targets were completed by a list of sites that were derived through the study of attribute uncertainty in elemental abundance measurements (Weiss et al., 2009). The algorithms that will be proposed are based on the attempt to evaluate this uncertainty of the target's surface (Longley et al., 2005). This spatial analysis delivered a number of impacting probes that are needed to be deployed onto the surface. This number defined the maximum size of each system and its payload integration. The research concludes with a conceptual system design of the micro-probe and its sampling mechanism.

# CHAPTER 2

## Literature Review

The following Literature Review will cover four main fields that are significant for this study.

An overview on the elaboration of future mission objectives will be given will be given in the first section. This review will present what kinds of missions have been fulfilled so far and which were the (scientific) driving forces behind those. It will then extrapolate this knowledge to future missions and derive their potential objectives.

In the second section different multi-probe approaches will be presented. The review will resume the scientific driving force behind these studies and review their technical design. The methodology that led to their architecture will be studied.

In the third part we will study the determination of landing sites for previous missions. An emphasis will be given on the use of GIS for such studies and how those can help to determine necessary Ground Control Points (GCP).

The last part of this review will study some general considerations for the design of the probes. Especially aspects such as the Entry Descend and Landing (EDL) strategy are to be considered in an early phase of the study since several assumptions can be done at the definition phase. These assumptions will be compared to other referenced design studies with similar objectives.

### **2.1 Future objectives of planetary exploration**

The evolution of the objectives behind space exploration missions is well illustrated by Sharpe (1970), Williamson (2006), Woods (1989) and Ball et al., (2007):

Engineering objectives were in the foreground of the first years of Solar System exploration. New technologies had to be developed and tested that made it possible to land humans on the Moon and the first robotic explorers on Mars.

Nowadays science objectives are the driving force behind such missions: Robotic exploration probes enable scientists to investigate the different worlds of our solar

system such as Venus with its thick cloud layer (Bienstock, 2003). Huygens descend through Titan's atmosphere in 2005, unveiled the last completely unknown surface in the Solar System (Ball et al., 2007). Orbiting spacecraft such as Magellan or MarsExpress furthermore mapped the surfaces to a detail in the range of meters (Simpson, 2001).

Planetology has gained in the last decades a relatively complete *general* picture about the structure of the planets and their moons. The exploration process will now shift from global mapping to detailed search for landing sites, utilizable in-situ resources (ISRU) and signs of remnant or existing life.

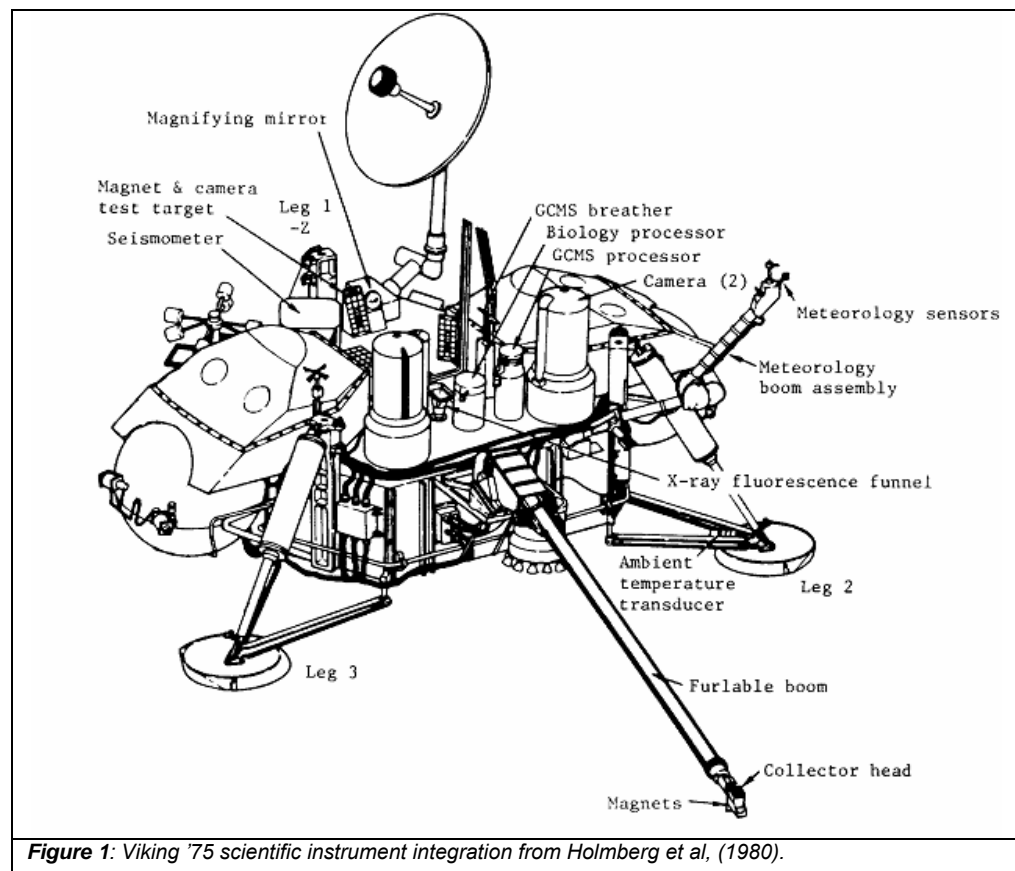
While orbiting spacecraft can deliver a global chart of a planetary surface, in-situ measurements are needed for detailed surface analysis.

The development of sensorial payloads for planetary exploration probes illustrates the shift of the mission objectives from *engineering* assessments to *scientific* goals (Sharpe, 1970; Winchester, 2006; Williamson, 2006; Ball et al., 2007):

- The first systems were developed to prove technological feasibilities: The first landings on the Moon by Russian and American probes carried few scientific sensors onboard but many engineering sensors that helped to monitor the condition of the spacecraft. One typical example for such kind of mission was the first American soft-landing on the Moon within the frame of the Surveyor Program: The Surveyor landers carried a large set of engineering sensors to determine the landing performance and the surface characteristics of the target area as described by Choate (1969), Sharpe (1970) and Williamson (2006). The bearing strength of the surface was computed by photographic means and by force measurements using an automatic scoop.
- The second type of probes was developed to reach the most unknown worlds of our solar system: The surface of Venus and its atmosphere was completely unknown before the arrival of the Russian Venera systems (Hunter, 1978; Basilevsky et al., 2007). Those probes carried amongst some engineering sensors mostly scientific sensors to gather data of the Venusian atmosphere. The latest type of such probes was the European Huygens lander that delivered

first pictures of Titan's surface and returned various scientific measurements (Lebreton et al., 2005).

- The third type of probes are scientific workhorses that carry large numbers of very specific and highly sophisticated sensor payloads onboard to analyze the soil and environment for the research of specific items such as evidences of life. Examples for such probes are the Viking landing stations on Mars. These systems carried a large number of scientific instruments and experiments which operated for almost one year on the Martian surface. Holmberg and co-workers (1980) list the extensive number of analytical instruments onboard of Viking in order to analyze the Martian soil, atmosphere and potential biology. Figure 1 illustrates the integration of this equipment into the lander structure (from Holmberg et al., 1980). Another such example is the forthcoming ExoMars mission which will search for indices of life in up to two meters depth of the Martian soil (Vargo J. 2006; Vargo J. 2004b).





However, a novel type of probe will be needed in the future in order to fill the gap between global observations from orbit and the few in-situ sampling missions in the surface. These probes will help to model global maps of a planet's landforms and its mineral composition.

The Moon can be considered nowadays as primary target for a near-future, in-depth exploration campaign: While orbiting craft have charted maps of high detail of its surface, future landing systems will be needed to explore the abundances of raw materials, high value volatiles and isotopes such as Helium-3. Kulcinski et al. (1990) predicts future prospects in the mining of the Moon's minerals and its use for human exploration. A concise overview of the benefits and the need of a return to the Moon by humans or robots can be found in Crawford (2004). Neal (2009) resumes how much was learned during the first stage of lunar exploration and what is left to explore in the post-Apollo era. The author compiled a comprehensive list of reasons to return to the Moon, with reference to the space policies of leading space-exploring nations.

Robotic exploration was, and will again be the precursor in the preparation of crewed interventions on the lunar surface (Boyle et al., 1962; Wilhelms, 1985; Spudis and Taylor, 1992; Wargo and Hill, 2007; Valero et al., 2007; Plescia et al., 2007). In this function, its primary mission goals are: (i) the reconnaissance and cartography of safe, hazard-free landing sites (Jolliff et al., 2009; Chin, 2007), (ii) the in-situ study of the chemical composition of the surface in order to locate resources and evaluate the feasibility of the in-situ use of elements such as water, hydrogen, oxygen and helium and the mining of rare elements (Haskin, 1985; Podnieks and Roepke, 1985; Meek et al., 1985; Matsumoto et al., 2007; Kulcinski et al., 1990; Spudis and Hood, 1992; Swindle, 1992), (iii) the characterization of the radiation environment, the lunar atmosphere and space hazards (Gerzer, 2007; Plescia et al., 2007; Foing and Ehrenfreund, 2008) and more general (iv) the test of new technologies needed for human exploration (Foing and Ehrenfreund, 2008).

The ultimate goal of lunar robotic development is supposed to lead to a teleoperated infrastructure as supports to human exploration. But apart from this precursor function, robotic missions can also help to unravel other questions about the Moon or its space environment (Crawford, 2004), such as: (i) the lunar origin (National Research Council, 2006), (ii) the identification of the geological processes that

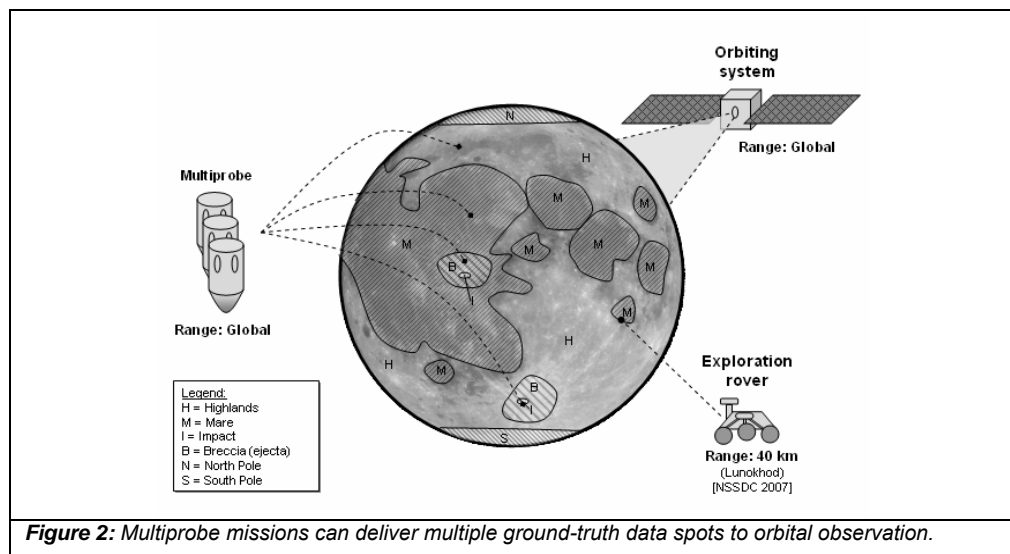
formed the surface (i.e. cratering, space weathering, volatile delivery or volcanism) to establish comparative Earth-parallels and estimate the absolute surface age (Wilhelms, 1987; Foing and Ehrenfreund, 2008; Flamini and Ori, 2007), (iii) the composition at sites of known stratigraphy context in order to extrapolate and model composition at unsampled sites and to allow calibration of orbital measurements (colour and gamma-ray) (Wilhelms, 1985; Wilhelms, 1987), (iv) the crust, the composition and state of the lunar core (National Research Council, 2006; Wilhelms, 1985; Lognonne et al., 2007; Schmitz et al., 2007; Tanaka et al., 2007) or (v) astronomy from the lunar surface, eventually on the Far Side, shielded from the electromagnetically noisy Earth (Spudis and Hood, 1992; National Research Council, 2006; Tanaka et al., 2007).

Three categories of exploration activities are derived from the objectives and will be used for the following considerations: (a) Reconnaissance, cartography and high resolution photography of the location, (b) in-situ science using instruments such as microscopic imagers, spectrometers (Mössbauer, APXS, Thermal Emission, Laser emission) or seismic instruments, and (c) sample return which represents the highest effort either by manned or robotic means.

In the following study a robotic micro-probe system is studied, which has as objective to support the activities for the location and quantification of in-situ resources. But while some elements can be detected by observational means, others need to be identified by in-situ means or through sample return missions. Single spot sampling or rover missions give only evidence about a very limited region of interest. A multi-probe approach bears the potential to deliver mineralogical data on a larger number of locations on the Moon. Those would confirm and complete remote observations from orbit with “ground-truth” points of data. Figure 2 sketches such a scenario in a very simplified manner: The main region types of the Moon are marked schematically: Lunar mare, highlands, impact craters, breccia, the North and South Pole. Orbiting system can deliver a global map. Rovers have a range that would allow traveling from one region to another if the landing spot is well chosen. But their range does not allow investigation in a larger scale (i.e. three regions). A micro-probe mission on the other hand with multiple probes can deliver data from several regions which could be correlated with the orbital observations. This need can be illustrated through a

terrestrial example: a single probe landing in Earth's Sahara desert would hardly be able to deliver a representative overall picture of Earth's morphology and geochemical diversity. This comparison seems obvious; but fact is that all lunar probes landed on the equatorial region of the Moon. We have no in-situ data or samples from its poles or the Far Side.

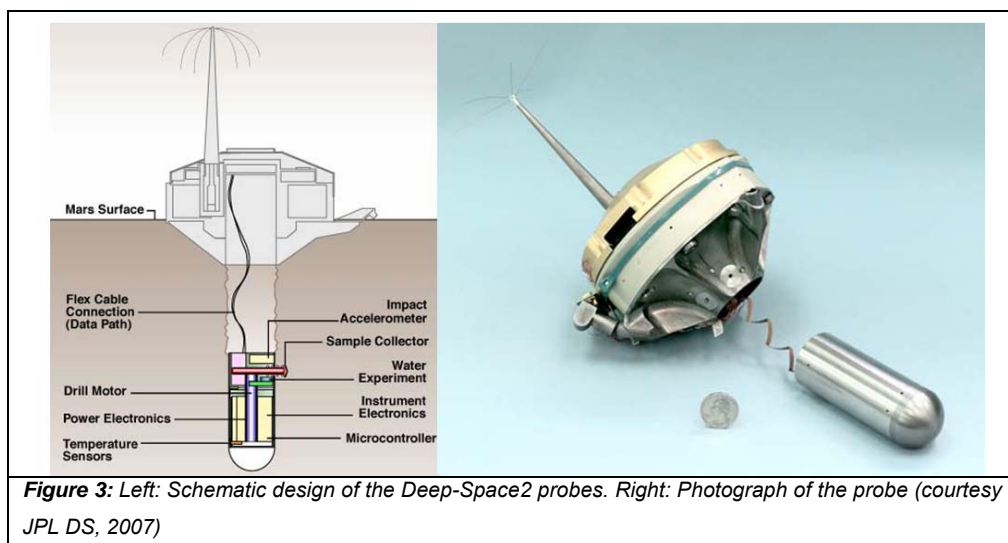
Microprobes, equipped with a geochemical payload, represent a middle-way between orbiting satellite and a large landing craft. Due to miniaturization it will be possible to accommodate larger quantities of identical probes into one single mission. The probes are deployed over various places on the surface and deliver in-situ measurements to the global cartography. In Gavit and Powell (1996) it is underscored that networks of landing probes will be *essential to the understanding of dynamic planetary systems*. In the following section, different existing multi-probe concepts will be presented.



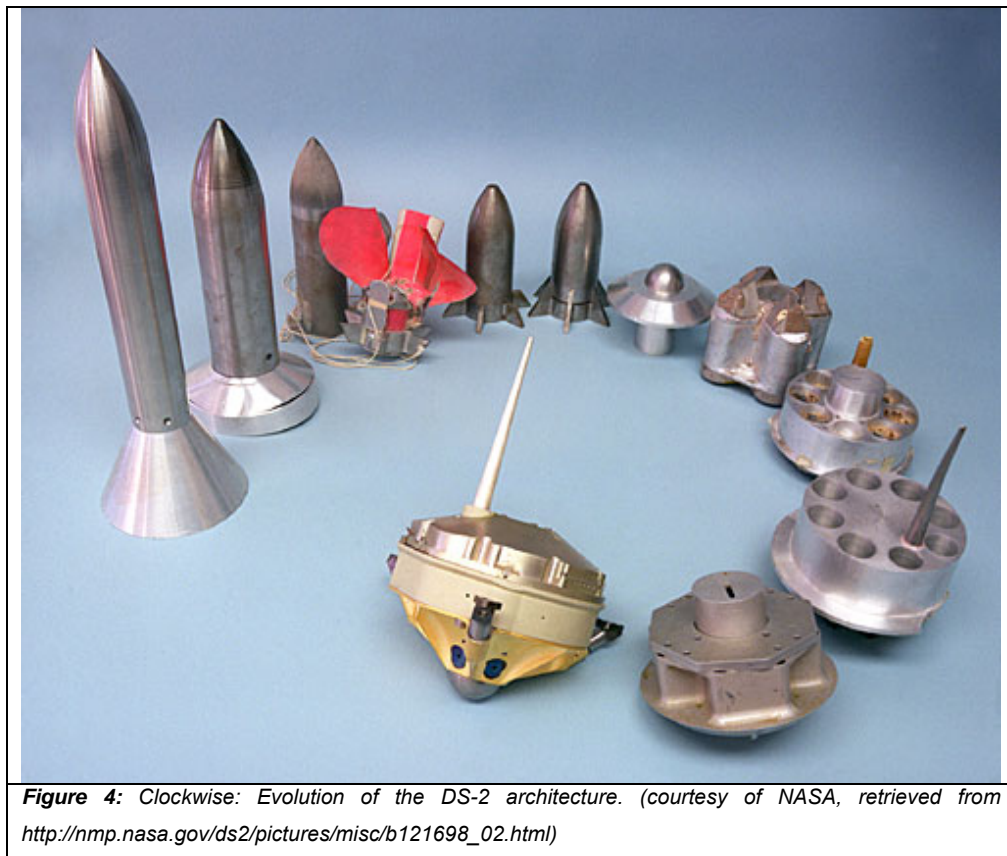
## 2.2 Multiprobe mission concepts and their development methodology

The concept of a multiple probe mission is not new and was applied with success in the exploration of Venus during the Venus Pioneer mission in 1978 where three probes descended into the Venusian atmosphere (Hunter, 1978; Winchester 2006). Also the Vega probes to Venus can be considered as a multi-probe approach since each mission hosted a balloon with scientific instruments and a landing system (Chassefière et al., 2009).

An example for what can be referred to as “micro-probe” is the *Deep Space 2* penetrators of the *Mars Polar Lander* (Gavit et al., 1990; Gavit and Powel 1996): This mission intended to deploy two miniaturized impact probes from a larger landing vehicle (Mars Polar Lander). The probes were supposed to penetrate 0.5 to 2 meters into the Martian soil (Gavit and Powel 1996). Both systems were highly miniaturized and had a weight of around 2.4kg. The expected impact velocities were around 150m/s to 250m/s. The probes relied on aerodynamic deceleration through the heat shield in the descend phase. The consecutive impact shock was estimated at 10 000g and the system was designed to withstand over 80 000g. The design of the probes was dictated by the constraints of the host mission towards Mars (Gavit and Powel 1996). It was essential during its design that the integration into the lander led to little modifications for the latter: The two probes were mounted onto the spacecraft’s stack in a balanced configuration to minimize landing inertia in the case the probes were not to be launched. No spin stabilization was required upon release since the entry system was designed to passively stabilize upon atmospheric entry. Finally, no electrical interface was foreseen between the lander itself and the probes. Whilst impacting, the fore body of the probe separated from the aft body which remained on the surface for communication purpose. Apart from pressure sensors, all scientific instruments were integrated in the fore body: A motor-driven soil sampler, and H<sub>2</sub>O experiment, temperature sensors and a 3-axis accelerometer were integrated in each probe. Figure 3 shows the schematic design and a photograph of the final system. Unfortunately, both probes and the lander failed to communicate back to Earth upon estimated arrival. The exact reason for this mission failure is unknown.

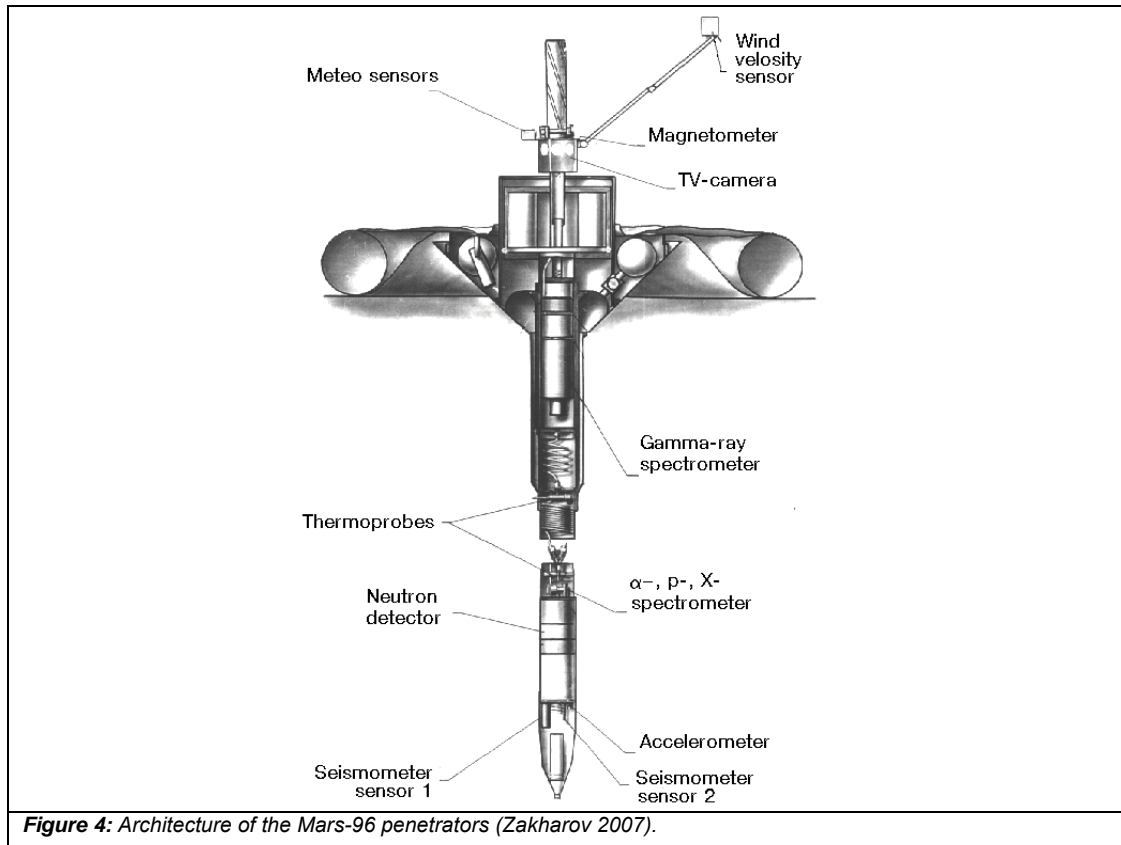


The penetrator's shell design and internal elements were extensively tested through airgun impact tests and airplane drops from high altitude. The impact tests by airgun are described by Lorenz et al. (2000). The penetrator's design was altered several times as a result of these tests. Its evolution can be seen in Fig. 4 from a projectile shaped form towards its final flight-version. Internal elements of the micro-probe, such as its batteries, also underwent impact trials (Frank et al. 1998).



A second, very similar penetration probe was developed earlier for Mars. The Mars-96 mission, described by Zakharov (1996), was intended to deliver a seismometer, neutron detectors, thermo probes, alpha-spectrometers and gamma-spectrometers up to 6 meters into the soil. The aforementioned Deep-Space2 system architecture resembled the Mars-96 much in design, but the Mars-96 mission was significantly heavier than the Deep-Space2 probes, with a weight of 100kg each for two penetrators. Figure 5 illustrates the resemblance of both mission concepts.

A further significant difference between both systems is that the heavier Mars-96 system does not dispose of a sample retrieving mechanism. The soil analysis is done via windows in the penetrators structure (Smith et al., 2007). Mars-96 failed during mission launch and never reached its destination Mars.



Little information can be found on the methodology that was used by the Russian scientists to come up with the innovative design of Mars-96. The probes are expected to have gone through similar impact test as those described above for Deep-Space-2. The planned MetNet mission to Mars can be considered as successor of Mars-96 since it is developed by the same institutions with very similar objectives to Mars-96. The mission is planned to be brought to Mars by the coming Phobos-Grunt mission. The mission homepage (<http://metnet.fmi.fi/>) gives information about the tests to evaluate the different system components: The penetrator architecture of MetNet was validated through impact tests by airgun and drop tests from airplanes. One of the critical elements in MetNet's architecture is the inflatable entry and descent system. Its functionality was tested through aerodynamic stability tests and material tests for the heat shields.

A third multi-probe mission concept that was almost brought to reality is the Japanese Lunar-A mission which was cancelled in February 2007 (Shiraishi et al., 2007). The orbiting spacecraft was planned to carry two 13 kg impacting penetrators, which would have been released in 40km altitude in vicinity of the Apollo 12 and 14 landing sites. Each penetrator was equipped with seismometers and heat flow experiments. This data could have been compared to previous Apollo measurements. Here it is also interesting to remark that following to the presentation of Shiraishi and co-workers (2007) the mission was ultimately cancelled by JAXA due to a lack of redundancy “*because of only two penetrators*” were used. It is now under discussion to integrate four of the Lunar-A penetrators onto the planned Russian Luna-Glob mission. The Luna-Grunt mission was even more ambitious before becoming an international cooperation between Russia and Japan: it was planned to impact more than a dozen penetrators on the Moon by one single mission (Ball and Lorenz, 1999). Ten small probes would have impacted in a diameter of 10km to form a small seismic array. These probes would have withstood impact velocities of up to 2600m/s. Two large penetrators would have impacted at speeds between 60m/s to 100m/s to form a wideband seismic network. Finally one polar penetrator would have been dropped in permanently shadowed craters at the poles. The probes were tested through airgun tests similar to those done in the frame of the Deep-Space-2 development at the Sandia Laboratory: The tests described by Shiraishi et al (2007) validated the penetrator structure and survivability of the communication system. Figure 5 shows the penetrator’s shell after an impact.



Apart from these missions there are several design studies on multi-probes that are of interest to this subject.

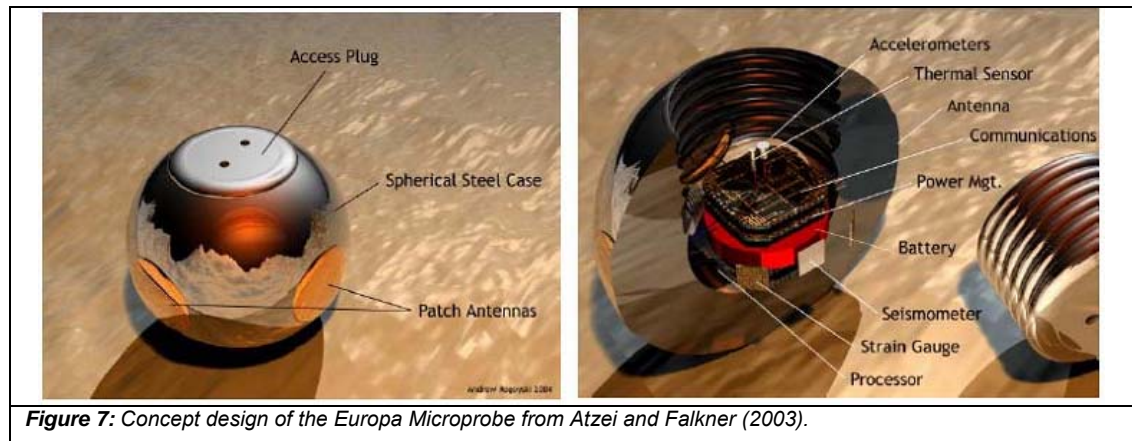
Smith and co-workers (2007) presented a multi-probe mission concept to the Cosmic Vision Call of the European Space Agency. The proposal, called “LunarEx” proposes to impact four penetrators onto the surface of the Moon. This study can be seen as the successor of a previous proposal, “MoonLITE”, with similar ideas (Gao et al., 2007). LunarEx is supposed to host micro-seismometers, a geochemistry package, a water/volatiles detector, a heat-flow experiment and an impact accelerometer onboard of each penetrator (Smith et al, 2007; 2007b; 2009). The design of the probe and its payload profited from research done in the defense area, previous mission developments as mentioned above and ballistic tests done by QinetiQ Ltd. as shown in the Fig. 6. The expected decelerations in the case of a lunar impact are around 10 000g with a penetration into the soil between 2m and 5m. Crawford and Smith (2007) mention the possibility to gather “ground-truth” data for geochemical analysis and preparation of future lunar exploration activities. The authors of the proposal identified as potential impact sites the poles, the Far Side and one Apollo site for calibration means. While the study stresses that many payload components are readily



available for such a mission scenario, the method of geochemistry sample retrieving was identified as critical development (Smith et al., 2007).



The European Space Agency launched a Technology Reference Study (TRS) on the utilization of micro-probes for the exploration of Jupiter's moon Europa in the context of possible liquid water below the surface (Atzei and Falkner 2003; Atzei et al., 2006). In the first version of this study, only one single probe with a weight of below 1kg was considered to be impacted onto the European surface. The micro-probe was to carry spectrometers in the visible and NIR range, a gas chromatograph, a Raman spectrometer, a seismometer and a microphone to listen to sound waves in the ice (Atzei et al., 2006). The technical challenges identified in this study were, amongst others, the development of highly integrated payload suites (HIPS) and the development of a low-resource, high-speed impact probe. Another point mentioned in the study is the challenge to assure a stable orientation of the device while descending onto (an atmosphereless) target to assure the focusing of the cameras during the descend phase (Atzei et al., 2006). The concept of integrating a microprobe onto a mission to Europa was first abandoned due to budgetary restrains. However the idea to deploy impacting penetrators has gained a new momentum due to the efforts of the authors of the LunarEx proposal mentioned above (Gowen et al., 2009).



To resume on the concept of multiple (micro) probes:

The different authors mentioned above stress the potential advantages and technical challenges of such mission concepts. The advantages were resumed earlier by Periminow (1999) on the design of the Mars descend probes of the Russian Venus program: *“I felt it was necessary to build a multipurpose versatile spacecraft that would be able to simultaneously explore Mars and Venus and solve the scientific and technical problems that appear during the flight. To reduce production costs, decrease the time required for developing and building the spacecraft, and enhance the probability of a successful flight, it was planned not to make significant changes in the design of the spacecraft and its onboard systems.”*

The approach proposed in this work goes into the direction of the design philosophy of the Russian engineers: A mission that includes a large number of descent systems will have several advantages compared to classical single probe systems:

### **Scientific outcome**

As shown above, landing probes have widened our knowledge about the solar system’s bodies. But detailed information on the surface conditions, a planet-wide “ground-truth” for the remotely observed data, is missing.

### **Mission reliability**

The utilization of multiple landing systems will increase the chances for mission success. If one probe in a single-probe mission fails, the whole mission fails. If one probe in a multiple-probe mission fails, there will still be a data return from the other systems.

The technical challenge of this work is the integration of highly miniaturized instruments to characterize the geochemical environment of the target. The probes will need to be reduced in size and weight in order to integrate a large number of such probes into one single mission. This eventually requires that no soft-landing deceleration system is integrated in the probes (i.e. retro-rockets). The probes therefore will descend in free fall to the atmosphereless target.

In order to evaluate the feasibility of this approach it will be necessary to simulate the effects of the high velocity impacts of the system onto the target. The methodology that was used in the abovementioned missions was based on impact tests via airgun or high-altitude drops from airplane. Another methodology is applied in this work by studying the impact of different shell forms through numerical simulation. This approach has several advantages: Its first obvious advantage is that such simulation can be done without the need of complex, expensive and potentially dangerous high-velocity impact trials. The costs associated with such trials are out of the reach of many institutions, therefore there is an urging need to develop accurate methods to simulate such processes (i.e. similar to crash-test simulations in the car industry). The development of a soil model for planetary surfaces in hydrocode can lead to a useful application in various coming missions (including soil-vehicle interactions in low velocity).

The number of landing sites that are necessary to acquire a global network of measurements is studied as baseline specification for the development of the microprobes. The used case study will concentrate on the exploration of Earth's Moon since this is the primary target for coming space missions.

In the following section, we will study, how other works have addressed the issue of landing site determination and outline a methodology proposed here to solve this issue by studying the effects on geochemical attribute uncertainty. In the frame of this review we will also list several other GIS developments which work with data of solar system bodies.

### **2.3 GIS-based landing strategy decision support systems**

A landing site selection is a very sophisticated process: It needs to satisfy the demands of the mission scientist and fit to the payload suite of the spacecraft. But also mission aspects such as vehicle security must be taken into consideration (Grant et al., 2004). The ratio of influence between these different aspects varies depending on the mission philosophy: A rover mission will search for highest landing security (e.g. acceptable rock abundances and surface slopes) and can accept remotely positioned areas of scientific interest (since it can drive to the interesting spots). An immobile landing station on the other hand needs to hit exactly the area of scientific interest. The mission constraints for the Mars Exploration Rovers (MER) mission are discussed by Grant et al., (2004). The candidate area was limited by security constraints to only five percent of planet Mars. In other words, 95% of Mars' surface was not suited for the landing of rovers. Engineering parameters that influence the consideration of the landing site include altitude, ellipse dimensions and orientation, latitude, slopes, surface relief (hazard-free), trafficability, winds, minimal temperatures, albedo, dust, load bearing surface and radar reflectivity (Ball et al., 2007). As science criteria Grant et al., 2004 mention the evidence of water activity, climate or geological history, preservation of biotic materials, site diversity and Earth analogues. The 155 initially proposed candidate sites were at the end limited to 2 sites, since only two rovers were sent to Mars.

For the strategy of this multi probe mission it is the scientific choice of the landing site that shall become the main design factor (contrary to the engineering or security factors for single lander missions). A GIS-based Decision Support System is presented in the following chapter which uses lunar geochemical data to derive potential landing sites for a multi-probe deployment. The development for such an application is novel, however there exist several other GIS applications that use data of extraterrestrial surfaces:

In Maguire, Goodchild and Rhind (1991), several definitions of "Geographic Information Systems" are listed which vary slightly in their conception. In this section some GIS applications in the field of planetology and selenology are reviewed that fit to these definitions. In this context it is rather interesting to have a look at the first

definition given by the US Department of Environment that says that GIS is “*a system for capturing, storing, checking, manipulating, analyzing and displaying data which are spatially referenced to the Earth.*” Planetary applications would therefore clearly not fit into the field of GIS systems, since moreover the prefix “geo” referees to the Greek word for “Earth”. A system that uses planetary data other than Earth’s would therefore probably be called *AIS* for “Astrographic Information System”. Despite this, we will continue to refer to such system here as GIS.

One definition cited in the abovementioned work is “*Any manual or computer based set of procedures used to store and manipulate geographically referenced data*”. The aspect “manual” is of interest here, since it allows including other storage media than digitalized data. Given this definition, one of the first GIS developed for applications other than Earth is the landing site detection in the US Apollo program: Prior to Neil Armstrong’s historic footstep several unmanned orbiters and probes mapped the lunar surface in order to detect a safe and scientifically interesting landing site. To be named here are the US Ranger and Surveyor Program, but also the Russian Lunar Program. Each craft delivered a set of photographs, either from orbit or while descending (and ultimately crashing) onto the surface. The maximal resolution achieved by descending craft (Ranger 4 to 9) was at 0.3 meters. Today these images can be retrieved from the National Space Science Center of NASA that stores the different photographic sets and also other instrument measurements from those vehicles. At the time of Apollo this data was manually reviewed in order to come up with suitable landing sites as described in the definition above.

A further definition for GIS given in Maguire et al., (1991) is “*an information technology which stores, analyses and displays both spatial and non-spatial data.*” An example in which this definition can be applied is the NASA Planetary Data System. This database combines different datasets from NASA’s robotic missions in the Solar System. The data can either be searched following to its target (all planets, major asteroids and known moons and other astronomical features such as stars, nebulae and galaxies) but also instrumental data or spacecraft search is possible. The user retrieves the data via several search and filter functions. The variety of data ranges from photographs, to spatially referenced instrument data in CSV-format to general description of the instrument used.

A third definition cited in Maguire et al., (1991) is “*a decision support system involving the integration of spatially referenced data in a problem-solving environment.*” This definition brings a third aspect to the GIS: While the first two definitions described the type of data and its storage, this definition gives a hint about the utility of the system: to solve a specific problem. In Earth based GIS it becomes quickly obvious that most GIS are developed to answer a particular question (i.e. the fastest way from New York to Boston, crime patterns or the displacement of Homo neanderthalensis by Homo erectus). Also in space science, spatially referenced data is processed to answer to specific questions concerning our Solar System and its bodies or to establish geographic models of planets or moons. Just to mention one example, Choi and coworkers (2007) developed surface models for some of the large gas giants exists to i.e. search to predict the behavior of the outer cloud layers of these planets. Image mosaics transmitted by the Galileo spacecraft were processed in order to measure wind speeds in Jupiter’s Great Red Spot and to establish models of this phenomenon. Another example that resembles to terrestrial applications is Helium-3 abundance estimation on the lunar surface. Several indicators lead to an estimation of the abundances of this element (Johnson et al., 1999): Ilmenite ( $\text{FeTiO}_3$ ) retains  $^3\text{He}$  better than other elements and can be measured from orbit by Gamma-Spectroscopy. A first index to establish an abundance map of  $^3\text{He}$  is to measure the Titanium concentrations on the surface. A second factor that can be used is the solar irradiance since this is the element that transports the  $^3\text{He}$  into the surface and its distribution is not identical over the whole surface due to shielding in Earth’s magnetic field. Johnson and co-workers built up a GIS for the estimation of  $^3\text{He}$  abundance on the Moon by applying these two factors based on data from the Lunar Prospector. The results were repeated and further elaborated by Fa and Jin later (2007). The resulting Lunar GIS tries to predict the abundance of Helium-3 by combining remote measurements of Titanium and the solar irradiance since Helium-3 cannot be measured directly by remote observations nowadays.

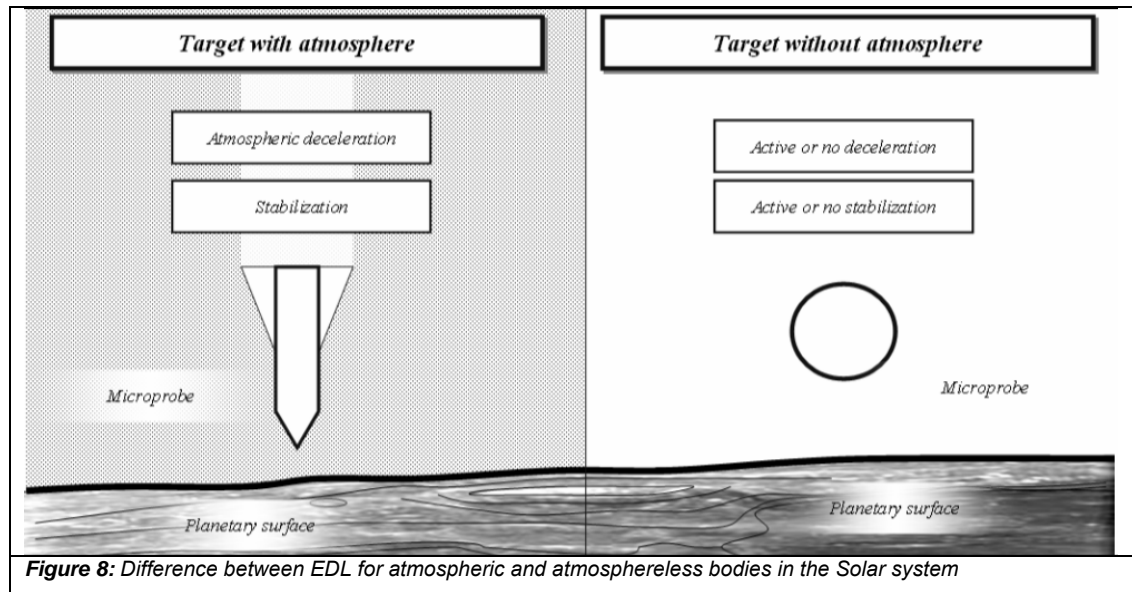
These tree examples of Geographic Information Systems in planetology and astronomy illustrate the various possibilities in this field. In Chapter 4 we will present a GIS-based Decision Support System to derive future landing spots for robotic missions to the Moon.

## **2.4 EDLS and sampling design considerations**

While the actual design of the microprobes will be subject to the last step of this work some general assumption can be made here based on the overall objective of the study:

While this case study will be based on an application for the coming lunar exploration, it is intended to design a probe that can ultimately be used for different targets without major modification. This will call for special considerations on the Entry, Descend and Landing System's (EDLS) concept:

Our Solar System bodies can be separated into two main classes that determine the EDLS of a landing probe: Bodies with atmosphere (Venus, Earth, Mars, the large Gas Giants and Saturn moon Titan), and bodies whose gravitational force is too low or which are too close to the Sun to sustain a permanent atmosphere (Mercury, the dwarf planets, Earth's Moon, the asteroids and most of the moons from the other planets) (Bakich 2000). Missions to atmosphere-possessing objects can use parachutes to decelerate the probe. Missions to atmosphereless bodies cannot use this possibility. Allouis and co-worker (2006) present technologies that can be applied for future landers on planet Mars. But these methods consequently exclude targets such as the Earth's Moon, where either an active deceleration system is needed, or where the probe needs to survive high impact velocities. Furthermore, as outlined by Atzei et al., (2006), atmospheric bodies allow stabilizing the probe by the use of fins or similar devices. This possibility is not given for targets without atmosphere. The issue of stabilizing the microprobes must be handled otherwise.



Possibilities for stabilizing a probe in an atmosphereless body are (i) an omnidirectional probe concept, where sensors work independently to the orientation of the system, (ii) and active stabilization system based on thrusters, which are largely prohibitive in terms of weight and size, and furthermore call for the development of a navigation system, (iii) a system based on reaction wheels that are commonly used in satellite technology and (iv) a spin-stabilized system.

A first resume on the design that can be drawn at this stage of the study is that the micro-probe's EDLS cannot be based on deceleration systems that use atmospheric friction since this would exclude a large number of targets. The attenuation of the impact will be further analyzed in this study.



# CHAPTER 3

## Research Methodology

The overall objective of the proposed study is the system design and evaluation of a multi-probe mission. This study will address several issues that have not been addressed, or have not been addressed sufficiently, in previously works. In this chapter, we will formulate the remaining problems in multi-probe mission design. And we present our methodology to solve those. In the last section of this chapter we discuss the expected contributions of new knowledge in this field and evaluate its originality.

### 3.1 Problem formulation

As it was shown in the previous chapter, the concept of a multi-probe deployment *per se* is not new. Various concepts can be found in the literature, ranging from real mission to design concepts (Gao et al., 2007; Smith et al., 2007; Atzei et al., 2003; Zhenming et al., 1999; Zakharov 1996). In this study, several aspects of multi-probe deployments will be studied that have, to our knowledge, not been addressed sufficiently in previous works:

- i) Multiple probes serve the purpose to enhance our knowledge of a planet's or moon's surface. However, the number of probes that are proposed in previous works is mainly based on system design aspects. To our knowledge, there is no study that tackles the problem of multi-probe landing sites by studying, independently from the probe's final design, the number of probes to confirm a geochemical surface model on a global scale. The method that is applied uses the notion of spatial data uncertainty to derive the number of probes. The study will be done in the frame of a Geographic Information System (GIS) based on ArcGIS®. The study will be using data from the Moon, namely orbital measurements of the Lunar Prospector and Clementine missions. It is expected that this GIS and Ground Control Point (GCP) determination methodology represent a

valuable tool in the process of decision for future landing missions even beyond the subject of multi-probes presented here.

- ii) To answer the questions which are set up through the mission objectives, payloads will be needed that can measure specific surface features while complying with the design of impacting multi-probes. This work will deliver a technology assessment of space instruments with emphasis on miniaturization versus space and landing compatibility. The need for such an assessment with particular focus on microtechnology was already stressed by Kraft (2005), Gershman and Wallace (1999), Ellery et al., (2006) and the Committee on Planetary and Lunar Exploration (1999). These authors underline the necessity to develop certain critical elements in the micro-probe design, such as geochemical sampling apparatus, structural analysis for high impact survival and techniques and stabilization methods for EDL. The study will try to seek and evaluate answers to these problems. Special emphasis will be given on sampling mechanisms for micro-probes since this activity fits well in the expertise of the Hong Kong Polytechnic University with its various activities in planetary sampling tools for Beagle2 and Phobos-Grunt (Yung et al., 2000; Towner et al., 2006; Weiss et al., 2007; Weiss et al., 2007b).

### **3.2 Methodology of the investigation**

#### Methodology phases A and B:

The methodology used for this approach can be resumed as presented in Fig. 9. The study started in outlining the future mission objectives of space exploration in order to determine, what kind of data will be acquired by the micro-probes. The results of these considerations were reported in the literature review of the previous chapter.

A Landing Strategy Decision Support System (DSS) was then developed using the case of a deployment of such probes on the lunar surface. The goal of this effort was to derive the number of probes that are necessary to gather sufficient in-situ data to establish a valid geochemical model of the surface. The Landing Strategy DSS consists of two steps:

1. Measurement uncertainties in elemental abundance data sets are evaluated by cross-correlation. This process led to a number of locations with high spatial uncertainties in the geochemical surface composition. The system was established based on orbital data from the Clementine (Nozette, 1995) and Lunar Prospector mission (Kellog 2007; Hubbart 2002), and in-situ measurements of the Apollo missions (Heiken et al., 1991). By implementing element abundance data sets into the GIS, we will be able through comparison and uncertainty considerations to designate an uncertainty factor to each surface element of the Moon (Shi 2007; Weiss et al., 2009). The list of sites is completed by landing site proposals of other authors as input for the Landing Strategy Decision Support System.

Landing strategies for the landing sites are derived in the final process step. These take into account the system capabilities of three kinds of exploration systems (micro-probes, landing stations and exploration rovers). Each site will be assigned to one exploration system, resulting thus in a number of micro-probes.

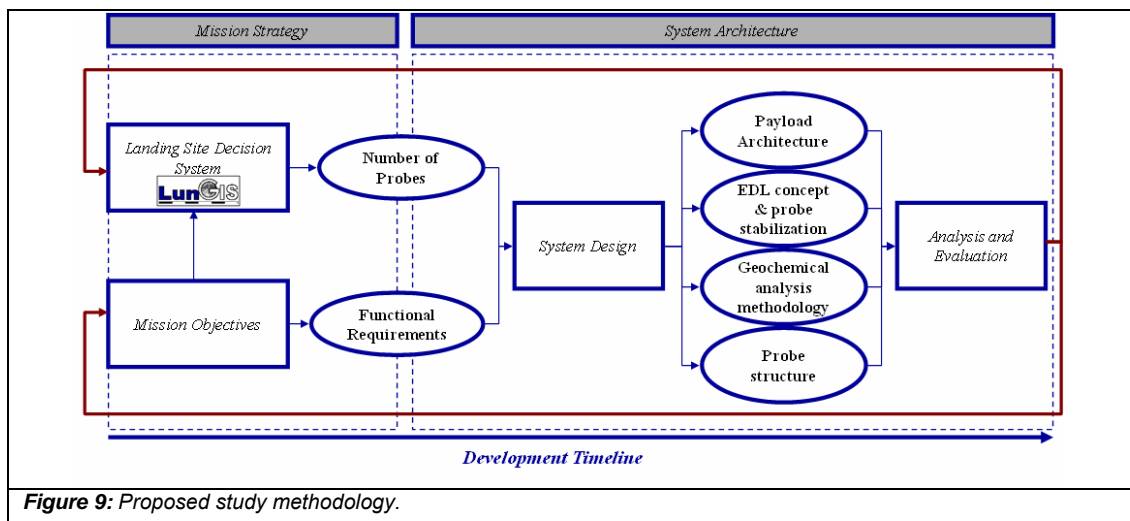


Figure 9: Proposed study methodology.

### **Methodology Phases C and D:**

The number of probes and the functional requirements will be the two main baseline specifications that will be delivered to the second work package of the study (System Architecture). While in the first part, a Mission Strategy was established (objectives and landing sites), the second part will develop, analyze and evaluate a micro-probe design.

Payload packages that comply with the functional requirements will be identified in a technology assessment. A baseline figure, on an overall available host space and weight (based on the study of effectuated and planned piggyback missions), will be used. This data will deliver the overall space and weight that the microprobe system can require.

In order to be validated, the structure of the probe and models of its payload need to be assessed in terms of impact ruggedness and survivability. To simulate and analyze some of the complex impact problems, Zhengming and co-workers (1999) refer to the use of FEA software such as LS-DYNA. The outcome of this last phase shall be the evaluation and analysis of the impact behavior of such system, to create the understanding on what processes have to be considered for the future design of such systems.

### **3.3 Research contribution and originality of the work**

This research will contribute new knowledge and techniques to the following fields:

- A novel method and algorithms to determine the optimum number of landing sites that are necessary to cover the areas of scientific interest. It was discussed in the literature review that current multi-probe mission design studies are mainly based on engineering specifications. In this work, the attribute uncertainty of a surface is studied. From this is derived, in a justifiable manner, the number of probes that are necessary to achieve this goal. It is expected that this work will contribute methods to model the uncertainty of planetary GIS data and thus the understanding of the interpretation of such datasets for future exploration attempts. We expect to gain a list of scientifically significant sites for the coming lunar exploration.
- The second outcome of this work will be the derivation of a lander platform able to deliver the required instrumentation packages based on coherent geological data and a technically feasible design. As it was shown in the works mentioned in chapter 2, major brick stones are still missing in the development of such probe concept. These components need to be developed in order to

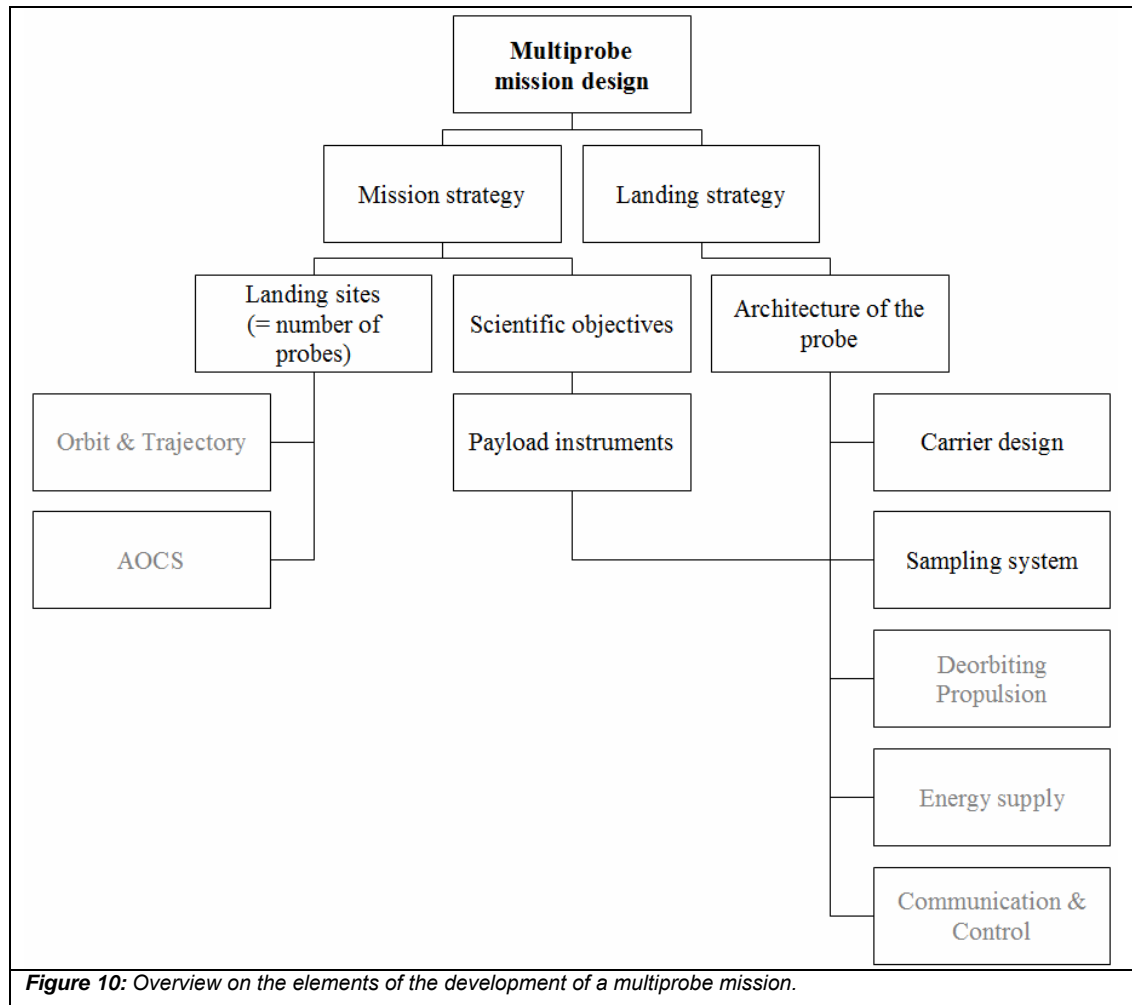
make geochemical investigations with micro-probes feasible. Focus was on the development of sampling methods for high-velocity impact environments.

- The third outcome of this work will be the understanding generated in the evaluation of the performance of such equipment under the given mission constraints. While impact tests with prototypes are technically difficult, analytical tools and methodologies will be of major importance for such development.

The proposed work aims to clarify several key points in the development of a multi-probe mission for a global scale geochemical analysis. The fact that this work starts with the development of a Decision Support System for lunar landing sites may make the work seem fragmental. This step is, however, necessary in order to establish a baseline specification on how many probes are needed for a surface wide geochemical network. This approach will show that the number is much higher than in any previously proposed concept.

Figure 10 shows the elements that set up the development of a multiprobe mission. Most of them are studied in this work to validate the micro-probe concept. The cases in light grey color are not explicitly worked out; however, some of these aspects are discussed in the following chapters. The energy supply and de-orbiting propulsion for example, will not be developed in detail. However, we will estimate the mass of these systems in order to calculate the overall mass of the novel probe concept.

This research methodology aims to validate the concept of a multiprobe mission for global surface investigation. Its objective at the end is to come up at the end with an overall design of such a microprobe and its feasibility.



### 3.4 Originality of the proposed work

The proposed work is original in various manners:

- i) Establishing a multi-probe mission based on a founded GIS study is novel in itself. Previous studies looked into the issue of potential landing sites after the development of the hardware concept, thus undervaluing the advantage of multi-probe concepts to reach multiple spots on the surface. This study will look into the issue from a bottom-up approach: first the potential scientific outcome will be evaluated by this novel GIS system, on which the development of the probes themselves is based.
- ii) The factor of uncertainty estimation and Data Quality of lunar element abundance data is another novel aspect. Uncertainty in GIS data is a factor

that we are beginning to master now for terrestrial applications. Its consideration, while of utmost importance for the coming exploration decade, is not well understood and very specific for lunar applications.

- iii) The development of a system for high-g impacting probes is novel in itself and can find various applications in the field of planetary sampling techniques. In order to master such technology, clear understanding of impact processes and effects must be established. This study will derive a valid concept based on the knowledge gained here.

# CHAPTER 4

## Landing strategy

### decision support system

#### 4.1 GIS-based decision support system for lunar exploration

The objective of a multi-probe mission can be twofold:

- i) It can confirm measurements that have been done by an orbiter through delivering GCP, or the “ground-truth”, to the remote measurements.
- ii) It can deliver measurements in a resolution scale that are not achievable by orbiting craft.

The multi-probes will therewith close the gap between orbital measurements and large scale in-situ laboratories such as rovers or landing stations in delivering higher “Data Quality” for specific regions on the Moon. The mention of Data Quality is thus of utmost importance since it describes the content and certainty of surface information that we dispose of (Shi, 2007). The definition of Data Quality can be found with Longley and co-workers (2005):

- **positional accuracy**  
(the spatial error referring the value),
- **attribute accuracy**  
(the percentage of error measured value),
- **temporal accuracy**  
(uncertainties that are induced by temporal processes or factors),
- **logical consistency**  
(the fidelity of relationships),
- **completeness**  
(of the data and references),

Each measurement on the Moon - or elsewhere - is subject to these factors. Therefore, those can be used to describe the accuracy of data on different locations on the Moon. As it can be seen from the first three points, uncertainties play a major role in the evaluation of surface data. There exist three kinds: spatial uncertainty (a possibility of



error in the position of a feature), attribute uncertainty (the possibility of error in the measurement of a feature), and temporal uncertainty (errors or changes that are brought to a feature by temporal dependant processes). Uncertainties can be qualified in different ways, but the outcome “*must always be a notation that provides the language for reasoning and allows decision-makers to evaluate the potential presence of errors in GIS data*” (Zhang and Goodchild 2002).

In the following, we will express uncertainty within lunar data by the notion of probability. Based on the probability estimation, we will derive landing sites for micro-probes that serve as ground control checks to confirm orbital measurements, that means to eliminate (or reduce) uncertainty.

#### **4.2 Uncertainty in lunar GIS data to determine potential landing sites**

The Moon has shifted back into the focus of scientific interest. While in the last 35 years (1973 to 2008) only eleven missions were sent to the Moon, ten missions are already planned to be launched in the coming decade. One of the main objectives of this effort will be to chart precise maps of elemental abundance that can be used for in-situ resource utilization (ISRU) for future manned landings (Landis, 2001; Espinasse and Di Pippo, 2007). Consequently the precision, or inversely uncertainty, of such data needs to be considered for the choice of future landing sites.

The Landing Strategy Decision Support System that is presented here will work with two different types of site proposals: 1) Site proposals from other authors mentioned in works before and 2) site proposals that result from the following study on uncertainties in geochemical surface data (of ISRU elements).

In this section we discuss the source of uncertainties (with emphasis on lunar datasets) and present a methodology to evaluate those.

Uncertainty of a model is a function of its scale, the precision of the measurements used for it and the potential error that those inhibit. A known positional error does not necessarily decrease the Data Quality (Longeley et al., 2005; Shi 2008), since it can

be corrected. It is the unknown error that leads to misinterpretation and reduce the quality of the outcome.

The challenge of uncertainty evaluations in lunar data is to quantify the accuracy of remotely sensed surface data at the local scale. In terrestrial GIS applications, the process of quantifying geophysical products is termed “validation”. Validation of remotely sensed data is achieved by analytical inter-comparison to ground control checks, reference data or model outputs (Justice et al., 2000). Validation has to be distinguished from calibration here, which is the determination of a system’s response to known inputs. In geophysical applications, validation can thus be achieved by the collection of in-situ measurements or the comparison to independent, but identical in content, satellite observations. In the case of the Moon very little ground-control points exist that can be used to validate orbital measurements. Extrapolating this existing data to the whole surface of the Moon would lead to errors.

In this approach, we will work with the datasets of the Lunar Prospector mission which delivered a set of mineral abundance measurements of the lunar surface. At the time of edition of this text, there were no identical datasets of such measurements available from other spacecraft. Therefore no comparison to identical observations is possible for instance. Another method had to be developed to estimate the uncertainty in mineral abundance measurements for the Moon.

The methodology developed here evaluates the uncertainty by analyzing the correlations between orbital measurements of different elements (that were done by the same mission). The uncertainty is estimated based on the deviation of the measured value from the though-correlation-expected one. The method was applied on different ISRU elements. The uncertainty of each of these elements for a specific location on the Moon is combined to derive an overall probability of accuracy for this location.

#### **4.2.1 Sources of uncertainty in remotely sensed data**

Before presenting this novel method, we discuss the various sources that can lead to uncertainties in remotely sensed data. The list presented below is certainly not exhaustive, and emphasizes GIS data for the Moon (i.e. selenographic data).

Various factors influence the precision of remote measurements. They can be categorized according to their consequence, leading to i) positional uncertainties, ii) attribute uncertainties or iii) temporal uncertainties. Positional and attribute uncertainties are considered of high importance in selenographic data, while temporal uncertainties play a minor role in this context due to slow geological processes and the low frequency of observation coverage.

Attribute uncertainties affect the second major element of spatially referenced data: the measurement. It is possible to categorize these different factors by their origin:

### **System limitations**

Instrument related uncertainties are mainly influenced by the measurement capabilities, the resolution (and footprint), its actual temperature and the Internal Orientation Parameters (IOP) of the instrument (Munsell and Smith, 2007; Genetay et al., 2003; Feldman et al., 1999; Satellite Imaging Corporation, 2007; Habib et al., 2004). Thus the final attribute uncertainty is highly dependant on the hardware architecture that is used for each mission. Specific works on recent missions can be found for the Neutron Spectrometer onboard the Lunar Prospector with Genetay et al., (2003), where the authors estimate the uncertainty for neutron data at 2% ( $2^\circ \times 2^\circ$  surface cell). The abundance of Iron, as measured by the Lunar Prospector Gamma-Ray spectrometer, is discussed and compared to earlier measurements taken in the frame of the Clementine mission by Lawrence et al., (2001). Returned samples of the Apollo era served to post-calibrate Clementine measured abundance data. Jolliff (1997) compares the measurements of Clementine's UV-VIS measurements with the abundance measurements done on the Apollo 17 site. The correlations allow the extensions of this knowledge on a regional scale, namely to unsampled areas in Taurus Littrow.

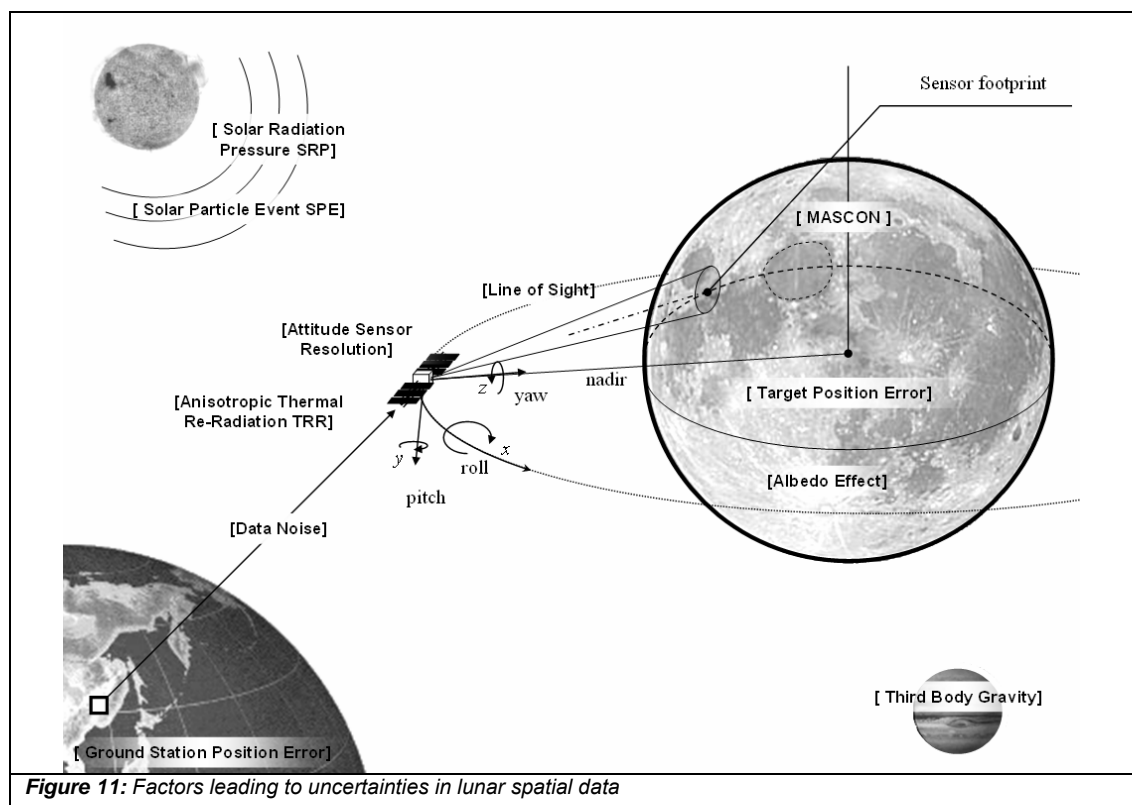
### **Mission limitations**

The mission design and spacecraft's ephemeris further determine the accuracy with which the measurements are taken. Exterior Orientation Parameters EOP, the spacecraft's altitude and orbital velocity accuracy limit the amount of radiation captured by the instruments onboard (McEwen and Robinson, 1997; Pieters and

Englert 1993; Williams and Zuber, 1998; Spudis et al., 2005). Solar Particle Events (SPE) and the Sun's relative position further influence the measured data and lead to uncertainties in the measurement (Pieters and Englert, 1993). Third bodies' influence decreases the accuracy of the satellite's position knowledge which, in return, increases the uncertainties of its measurement data.

### Target specific limitations

Similar to the positional uncertainties discussed above, some characteristics of the target and its surface can determine the precision with which the surface is analyzed. The following factors can therefore be considered as georeferenceable uncertainties in lunar GIS data: terrain morphology, surface roughness, surface albedo, surface temperature and MASCONS, which each can bring variations in the remote (Pieters and Englert, 1993; Williams and Zuber, 1998; Spudis et al., 2005; PDS, 2007). Figure 11 resumes schematically the factors mentioned above.



**4.2.2 Probability estimation by elemental inter-correlation: Example Oxygen**

A novel method to evaluate the uncertainty in remotely measured data was developed (Weiss et al., 2009). This method allows evaluating the probability of justness of abundance measurements by inter-correlating different elemental measurements. The advantage of this methodology is that it can work without Ground Control Points. Neither does it need independent datasets of the same kind. Both are very limited or nonexistent for the lunar surface.

Precondition of this approach is that there is some correlation rule between the elements. A method to evaluate this is to analyze the regression lines between abundances of the different elements. The fitting function of the regression line is given in (1), with its parameters  $\alpha$ , the intercept and  $\beta$ , the slope ( $x$  and  $y$  signify the abundance values for element  $x$  and element  $y$ ),

$$y = \alpha + \beta x \quad (4.1)$$

where the intercept is

$$\alpha = \left( \sum_{i=1}^n y_i - \beta \sum_{i=1}^n x_i \right) / n \quad (4.2)$$

The slope can be used to determine if there is a correlation between the two elements  $x$  and  $y$ .

$$\beta = \frac{L_{xy}}{L_{xx}} = \frac{\sum_{i=1}^n (x_i - \bar{x})(y_i - \bar{y})}{\sum_{i=1}^n (x_i - \bar{x})^2} = \begin{cases} > 0 \rightarrow \text{positive correlation} \\ \approx 0 \rightarrow \text{no simple correlation} \\ < 0 \rightarrow \text{negative correlation} \end{cases} \quad (4.3)$$

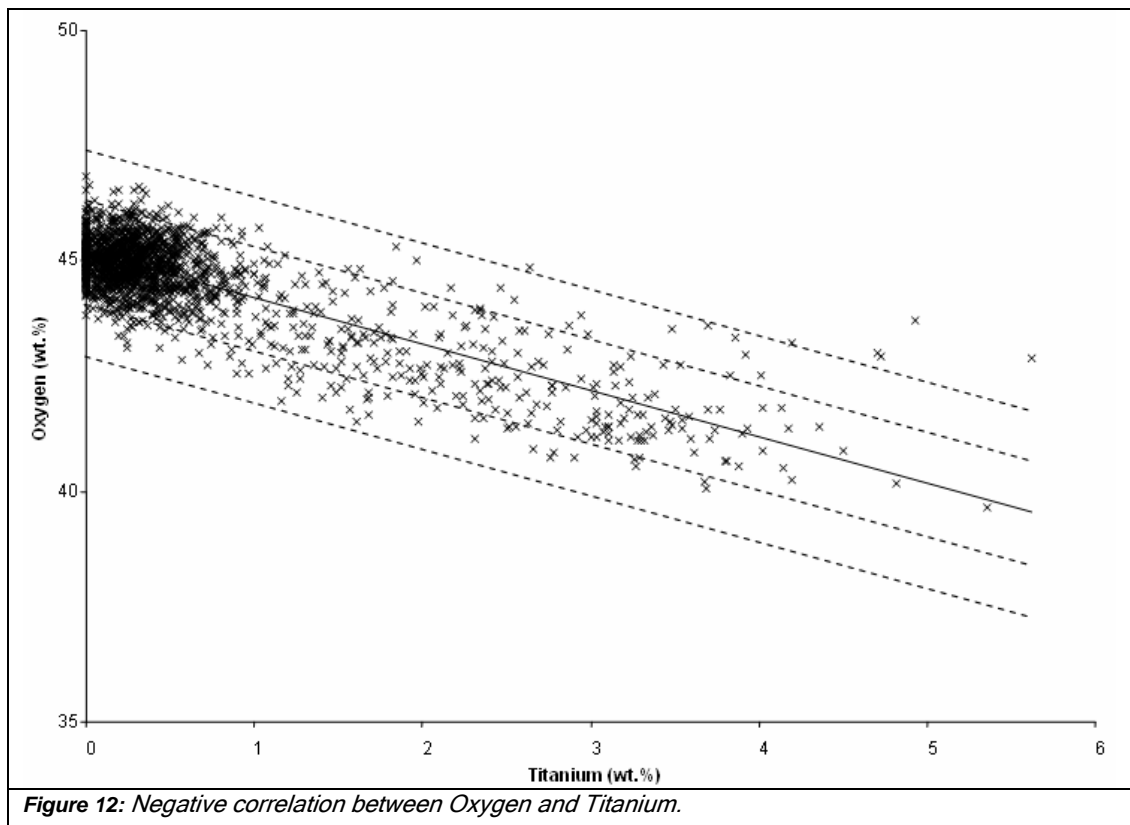
**Application on the example of Oxygen**

The bulk of the lunar material is composed of the eight major elements: Oxygen (60%), Silicon (17%), Aluminum (10%), Calcium (5%) and Magnesium (5%), Iron (2.5%), Titanium and Sodium (1% together). The correlations amongst these elements' oxides which were derived from the returned samples by Apollo are discussed by Haskin and Warren (1991). The authors state a negative correlation between Aluminum oxide ( $\text{Al}_2\text{O}_3$ ), Iron oxide ( $\text{FeO}$ ) and Magnesium oxide ( $\text{MgO}$ ), and between Calcium oxide ( $\text{CaO}$ ) and Iron oxide.  $\text{Al}_2\text{O}_3$  correlates with  $\text{CaO}$ , Silicon

dioxide ( $\text{SiO}_2$ ) correlates to Iron oxide and Magnesium oxide ( $\text{MgO}$ ) and Titanium dioxide ( $\text{TiO}_2$ ) each correlate positively with Iron oxide.

Identical plots as those of Haskin and Warren can be produced for the measurements of the Lunar Prospector mission (Prettyman et al., 2002) by correlating the abundance of different elements. Seven of the eight major element datasets are available in 5° data products from the PDS Geosciences Node. There were no measurements done of Sodium by the Lunar Prospector. To evaluate the certainty of the Oxygen dataset, we plot correlation diagrams for Oxygen with each of the remaining six elements (Fig. 12 to Fig. 17).

While Titanium, Iron and Magnesium exhibit a slight negative correlation to the abundance of Oxygen (with a slope of  $\beta_{\text{O-Ti}}=-1.0134$ ,  $\beta_{\text{O-Fe}}=-0.2723$  and  $\beta_{\text{O-Mg}}=-0.3027$  respectively), Aluminum and Silicon show a positive correlation (the slopes are  $\beta_{\text{O-Al}}=0.2839$  and  $\beta_{\text{O-Si}}=0.4199$ ). No correlation can be stated to the abundance of Calcium, and its dataset is excluded from the following modeling of Oxygen abundance uncertainties. These correlations can be used to estimate an Oxygen abundance value at a certain position as function of the abundance of the other elemental values.



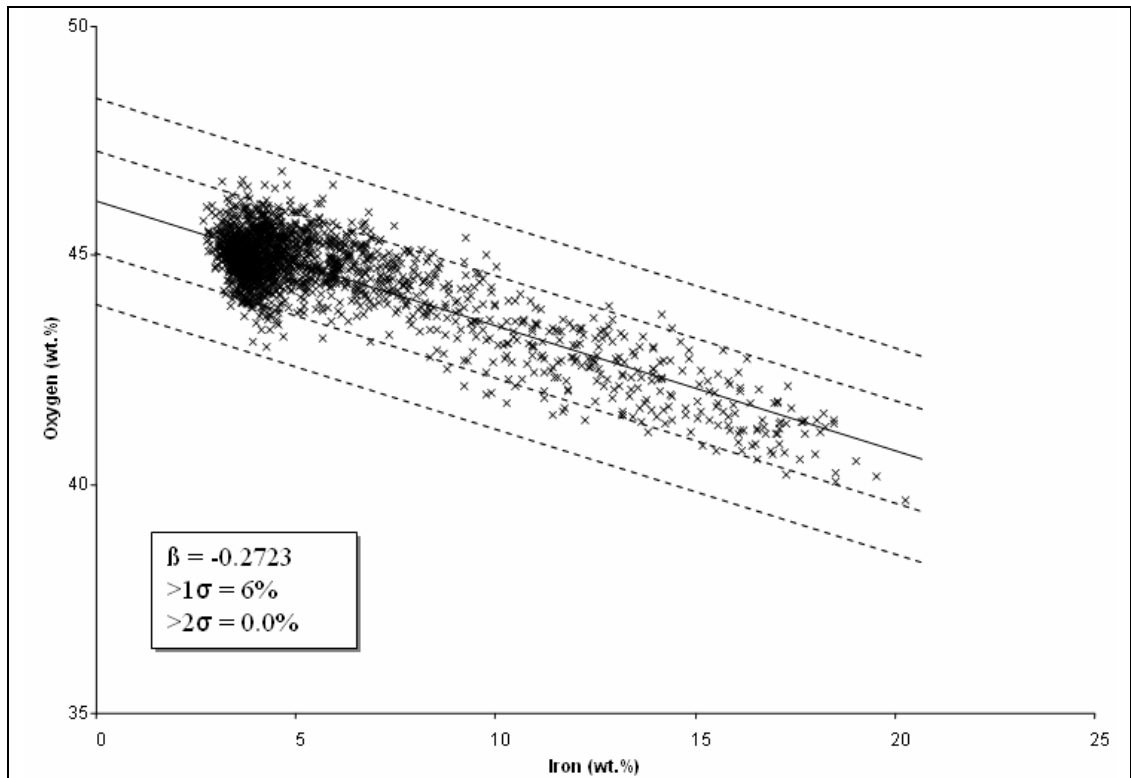


Figure 13: Negative correlation between Oxygen and Iron.

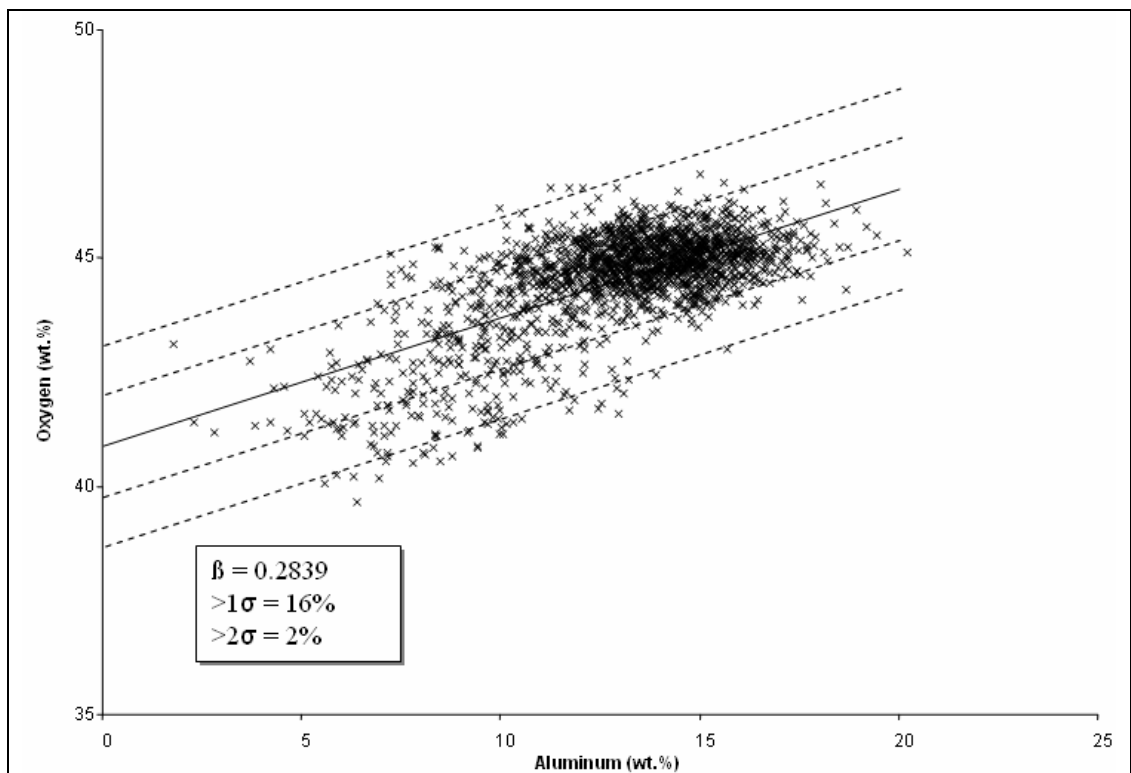
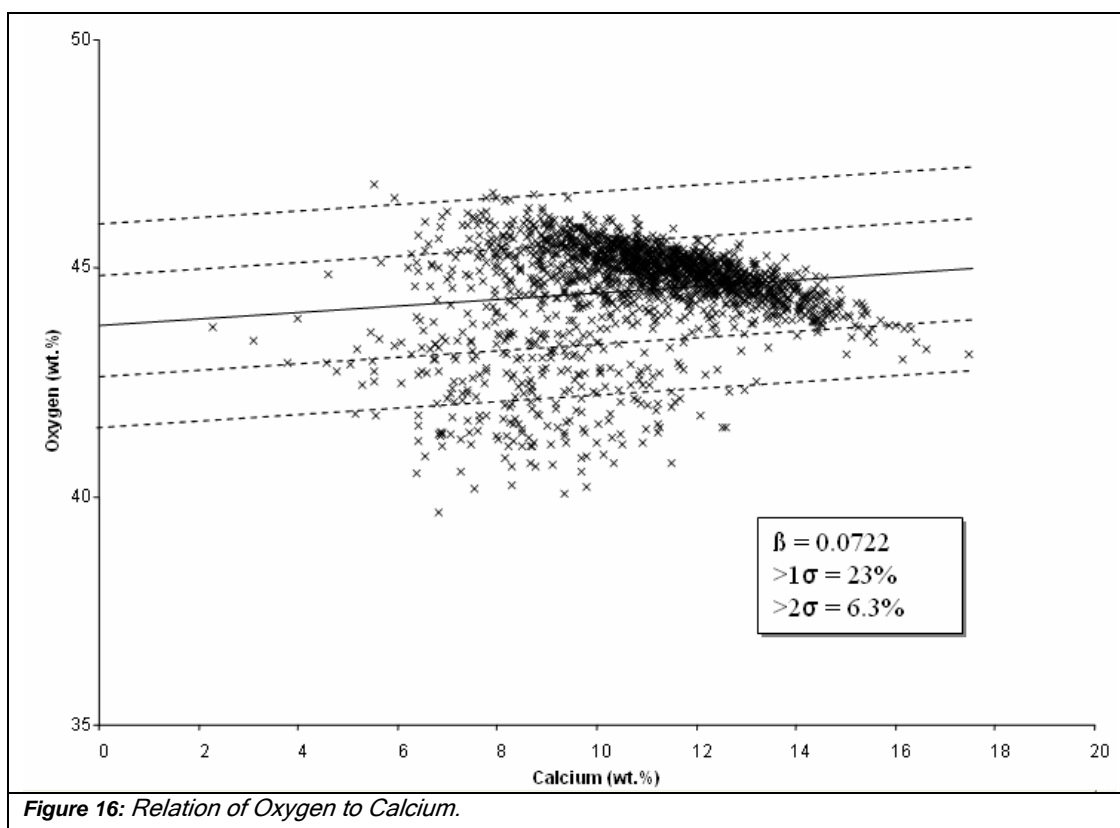
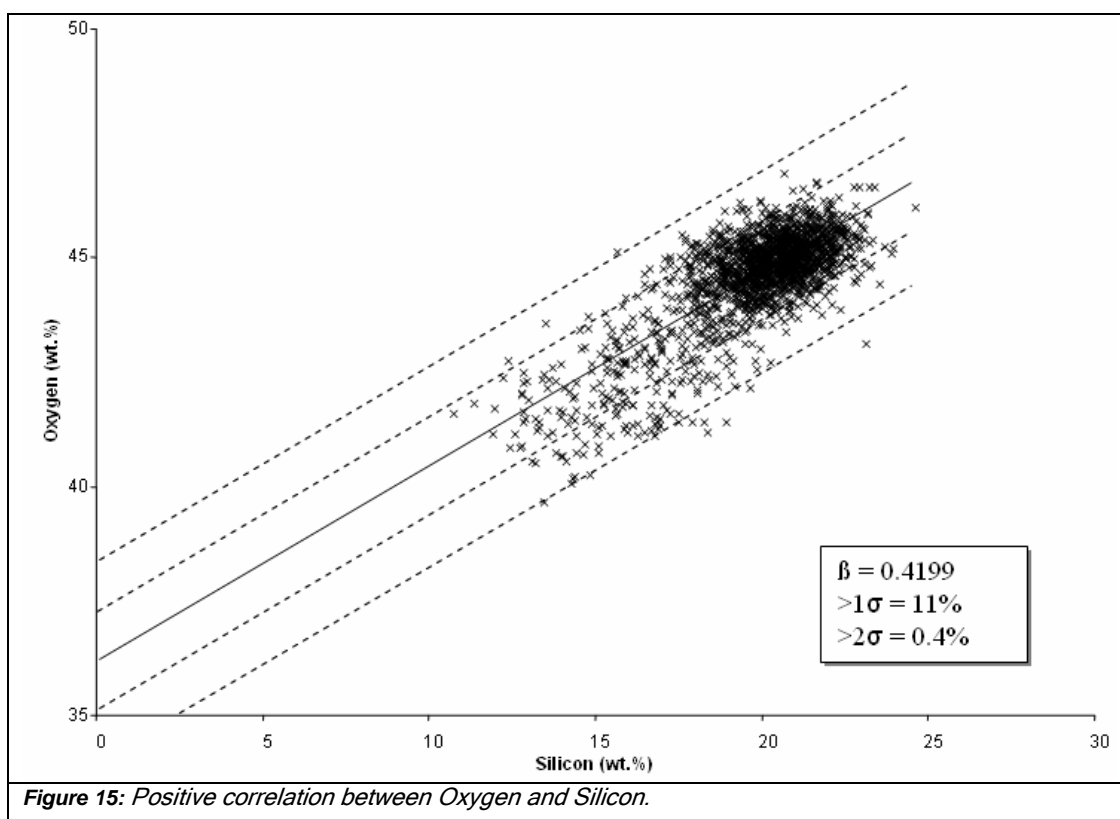
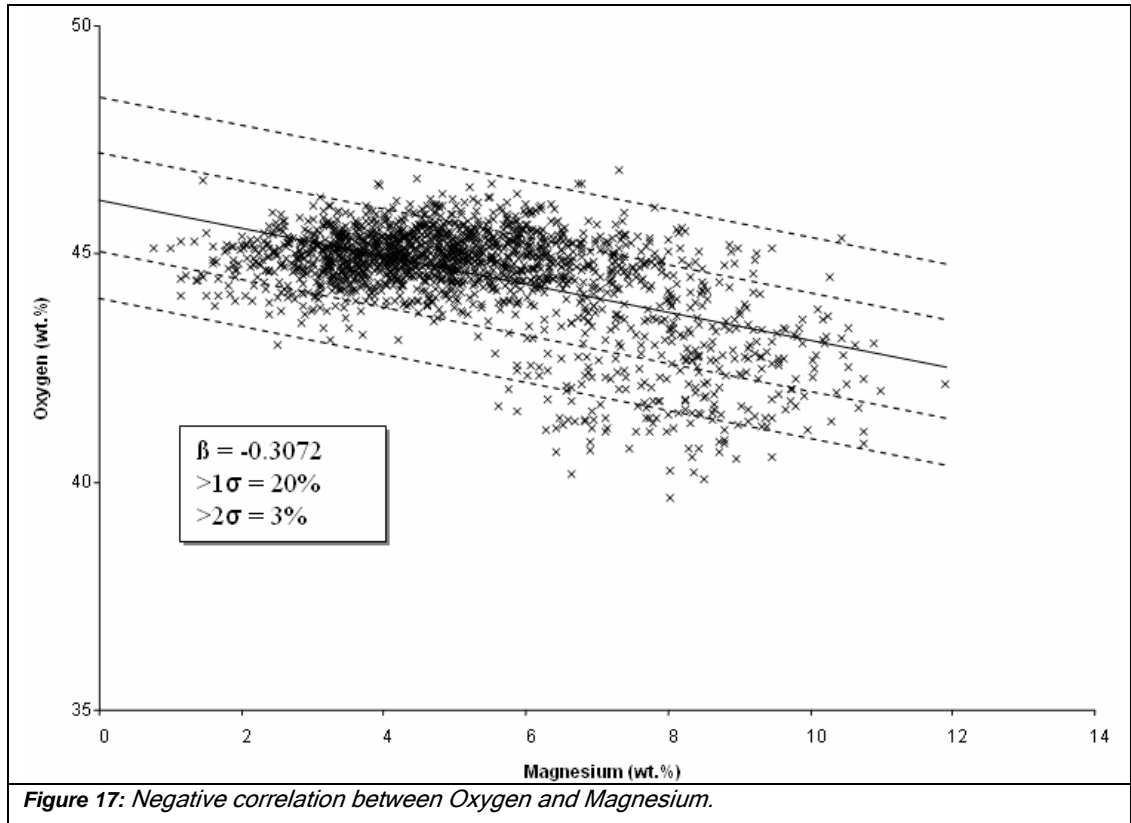


Figure 14: Positive correlation between Oxygen and Aluminum.





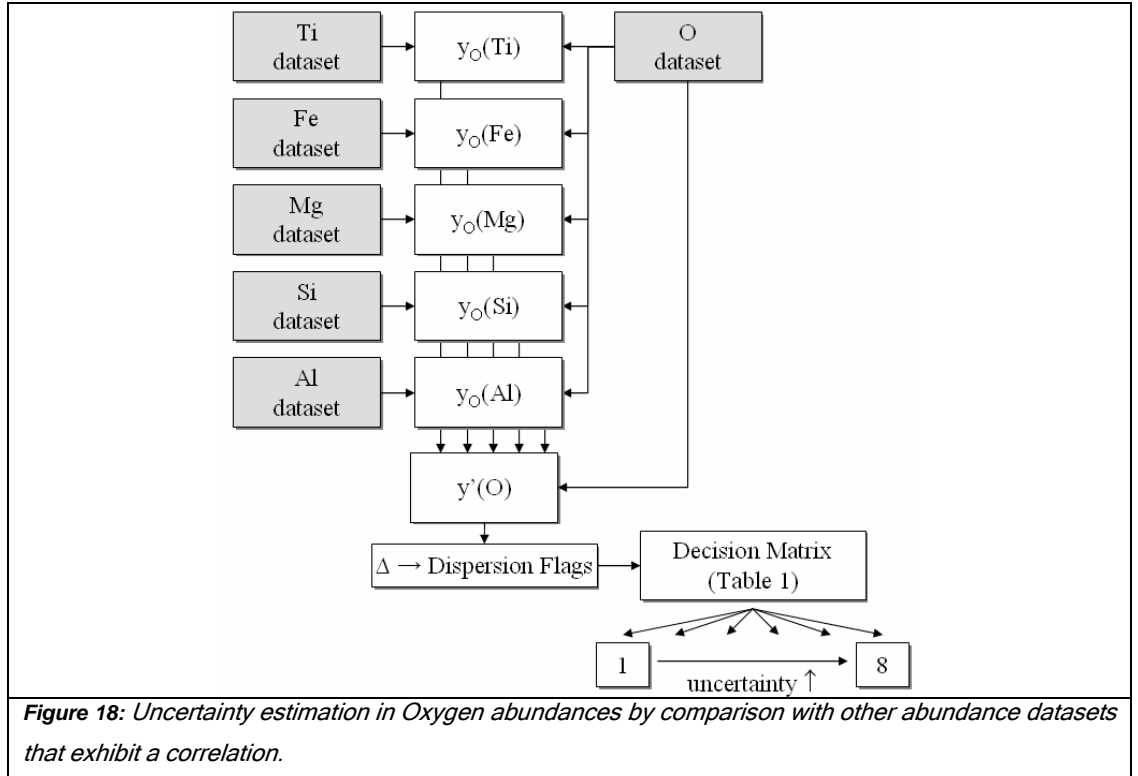


A Root Mean Square Error analysis between the so produced datasets and the actual measured one states a minimal RMSE for Iron of 20wt.%, followed by Titanium (21wt.%), Aluminum (27wt.%) and Magnesium (30wt.%). The dashed lines in the graphs of Fig. 12 - 17 show values that lie outside the boundaries of one and two sigma.

These outliers can be caused by faulty measurements, or can indeed represent an exotic soil mixture that does not follow the correlation rule. Since the correlation diagram is composed of two elements, it cannot be clearly identified, which one of the measurements caused the outlier. But a cross-comparison between the correlation results of all elements can help to further identify the origin of the deriving measurement. Therefore, we need to identify the outlying values before being able to verify if a surface cell is an outlier in more than one correlation rule. Surface cells deviating from correlation can be classified corresponding to their extent of dispersion. As the weighting factor for this consideration, we use multiples of the standard deviation with  $y'$  being the actual value to be compared to the expected value  $y$  as derived through Eq. (4.1). Eq. (4.4) below shows the three cases that were differentiated for the uncertainty estimation:

$$\left| \frac{\alpha + \beta x - y'}{\sigma} \right| = \begin{cases} < 1 \rightarrow \text{no dispersion} \\ \geq 1 \rightarrow 1 \text{ sigma (flagged 1)} \\ \geq 2 \rightarrow 2 \text{ sigma (flagged 2)} \end{cases} \quad (4.4)$$

By this method, all datasets can be compared to flag cells that derive from the assumed correlations. This analysis was applied for instance only on all five Oxygen correlations (the one of Calcium is not used), and the results are registered in a number of flags per surface cell. The Oxygen abundance estimates, which were derived as function of the Iron content, agreed in 94% of the surface cells with the actual measured value (within the one-sigma margin). Titanium reaches 92%, Silicon 89%, Aluminum 84% and Magnesium 80%. To determine the source of the outliers, we evaluate which are the surface cells that show outlying values for several elements. Figure 18 shows this process schema which was applied to derive uncertain cells for Oxygen measurements.



In order to draw conclusions on this result, a decision matrix was used as shown in Tab. 1. The consideration behind this approach is that soils that underwent similar

formation processes are expected to exhibit similar elemental mixtures. The abundances on the surface should, therefore, follow rules that can be expressed in a mathematical model.

Shows a cell a deriving value from this rule then the uncertainty in this cell is high: either its measurement value is erroneous or its surface composition derives from the assumed model and is therefore exotic. The occurrence of non-fittings within one single cell is counted: if only one single estimated value derives from the measured one, then high uncertainty can be assigned to this element that delivered the estimated value and not to Oxygen (see Tab. 1). We extended this criterion, allowing two deriving values from Oxygen measurement without decreasing the certainty of the latter (this occurred in 35% and 19% of the cells respectively). However, if three or more of the calculated values derive from the actual measured one, then high uncertainty is assigned to the measured Oxygen value itself. In less than 1% of all measurements (10 surface cells in total), all of the calculated values were beyond the one-sigma range. While, on the other hand, in 65% of all surface cells, the calculated value based on the element correlation and the measured Oxygen value fitted well in the one-sigma criterion.

*Table 1: Decision Table for the Oxygen correlation estimation. The percentage in the last column shows the occurrence of cells.*

$y_o(\text{Ti}) = y'_o$	$y_o(\text{Fe}) = y'_o$	$y_o(\text{Mg}) = y'_o$	$y_o(\text{Si}) = y'_o$	$y_o(\text{Al}) = y'_o$	<b>Conclusion</b>	<b>%</b>
yes	yes	yes	yes	yes	$\rightarrow y'_o$ certainty $\uparrow$	65%
any 1 element does not fit					$\rightarrow y'_o$ certainty $\uparrow$ element cert. $\downarrow$	35%
any 2 elements do not fit					$\rightarrow y'_o$ certainty $\uparrow$ elements cert. $\downarrow$	19%
any 3 elements do not fit					$\rightarrow y'_o$ certainty $\downarrow$	8%
any 4 elements do not fit					$\rightarrow y'_O$ certainty $\downarrow$	3%
no	no	no	no	no	$\rightarrow y'_O$ certainty $\downarrow$	1%

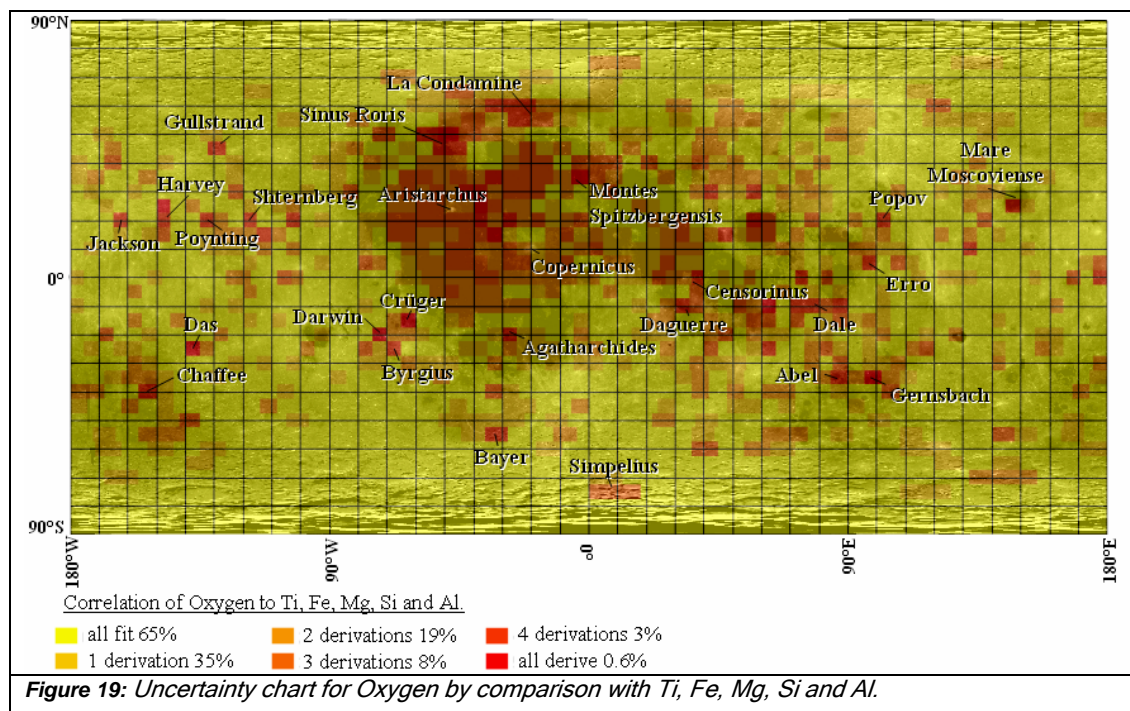
## Result and discussion

The result of this estimation is charted in Fig. 19. The chart shows that 65% of all surface cells remained inside the one-sigma margin for all elements of the correlation comparison (the datasets have 1790 cells at a resolution of  $5^\circ$ ). Cells that derived in one or more elemental comparisons were marked in increasing red color. The Oxygen

abundances of the majority of the Far Side, the Poles and large regions of the Near Side can thus be estimated certain by the correlation check with the other five elements.

High derivations occur in the Oceanus Procellarum basin (between the craters Aristarchus and Copernicus, the South-Eastern border of Sinus Roris), partly the Mare Imbrium (with uncertainty peaks at Montes Spitzbergensis), the western limb of Mare Frigoris (crater La Condamine).

The Far Side abundance shows fewer deviations from the Oxygen correlation model: 78% of the predicted cell values fit to the measured value (within the 1-sigma range). Nevertheless, deviations occur in the South-Pole Aitken basin (at crater Chaffee near, but not at, mare-filled crater Apollo), Mare Moscoviense and several other single spots.



These considerations can now be extended by studying the spatial distribution of the uncertain marked surface cells: if those are isolated between measurements with high certainty, then there is a high probability that those originate from an error in the remote measurement itself. This could be referred to as measurement uncertainty.

On the other hand, uncertain-flagged cells that are clustered might indicate that the soil properties in this region indeed do not fit the correlation model. There is thus an

uncertainty in the soil's composition leading to the fact that the correlation rule does not apply on such areas.

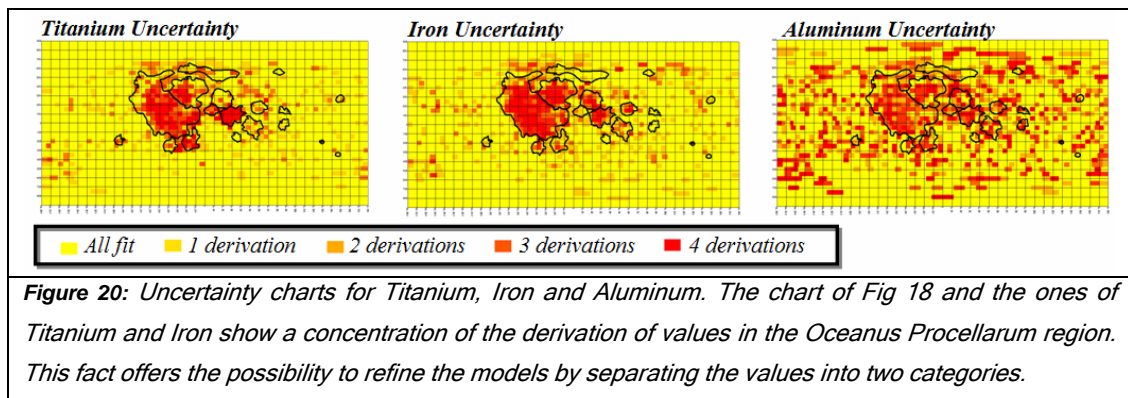
The method presented above allows estimating the certainty of mineral abundance data from remote observations. The uncertainties for the other five elements were evaluated based on the above presented method.

### 4.2.3 Extending this method to all elements

The same method was applied to the other above mentioned elements. The result of this exercise is a correlation matrix of the seven elements between each other. Tab. 2 shows the percentage of correct values within one sigma deviation. Fig 20 shows the charts of uncertainties for the ISRU elements of main interest.

*Table 2: The percentage of correct values within one sigma deviation of different elements resulting from the correlation rules as described in 4.2.2. The input elements (left column) were used to derive the output elements (first row).*

↘ Output element							
	O	Si	Ti	Al	Fe	Mg	Ca
O		89%	93%	83%	94%	76%	69%
Si	89%		90%	72%	87%	80%	71%
Ti	92%	87%		84%	98%	80%	77%
Al	84%	74%	88%		90%	82%	71%
Fe	94%	86%	97%	90%		85%	88%
Mg	80%	83%	87%	82%	89%		82%
Ca	77%	76%	85%	72%	84%	83%	
↑ Input element							



This study leads to two interesting results:

- a) It helps to identify regions in which large derivations of the correlation rule exist. As indicated above there are two possible explanations for this: either the measured values are fault in this particular location (measurement error), or the composition of the soil is exotic at the particular spot. We dispose of two methods to estimate which one of the two cases is more probable. The first is to consider whether the measurement value derives for more than one correlation rule. The second is to look into the spatial extend of the derivation (is it a single cell or a whole region). If a whole region is concerned, then there is a high chance that that the particular region exhibits an exotic soil composition. It is these locations that we consider interesting for in-situ exploration.
- b) The second outcome of these considerations is not directly related to the subject of a landing strategy decision support system: From Tab.2 it can be seen that some elements can be predicted with a relatively high accuracy as function of another element. Titanium abundance for example, can serve to estimate the abundance of Iron with a one-sigma derivation for only 2% of the surface cells. This is now very interesting in the case where maps of Titanium are available with higher resolutions than those of Iron. For the Lunar Prospector mission, this is effectively the case, where we dispose of maps in 2 degree resolution for Titanium, while those of Iron achieved only 5 degree. By observing the charts of Fig. 19 and 20, it becomes clear, that the deriving values are concentrated around the Oceanus Procellarum region. The here presented soil model could therefore be separated into two specific regions (i.e. "Oceanus Procellarum Model" and "Highland-Model") to refine the prediction method as a function of other element abundance.

#### **4.2.4 Identification of landing sites based on uncertainties in ISRU elements**

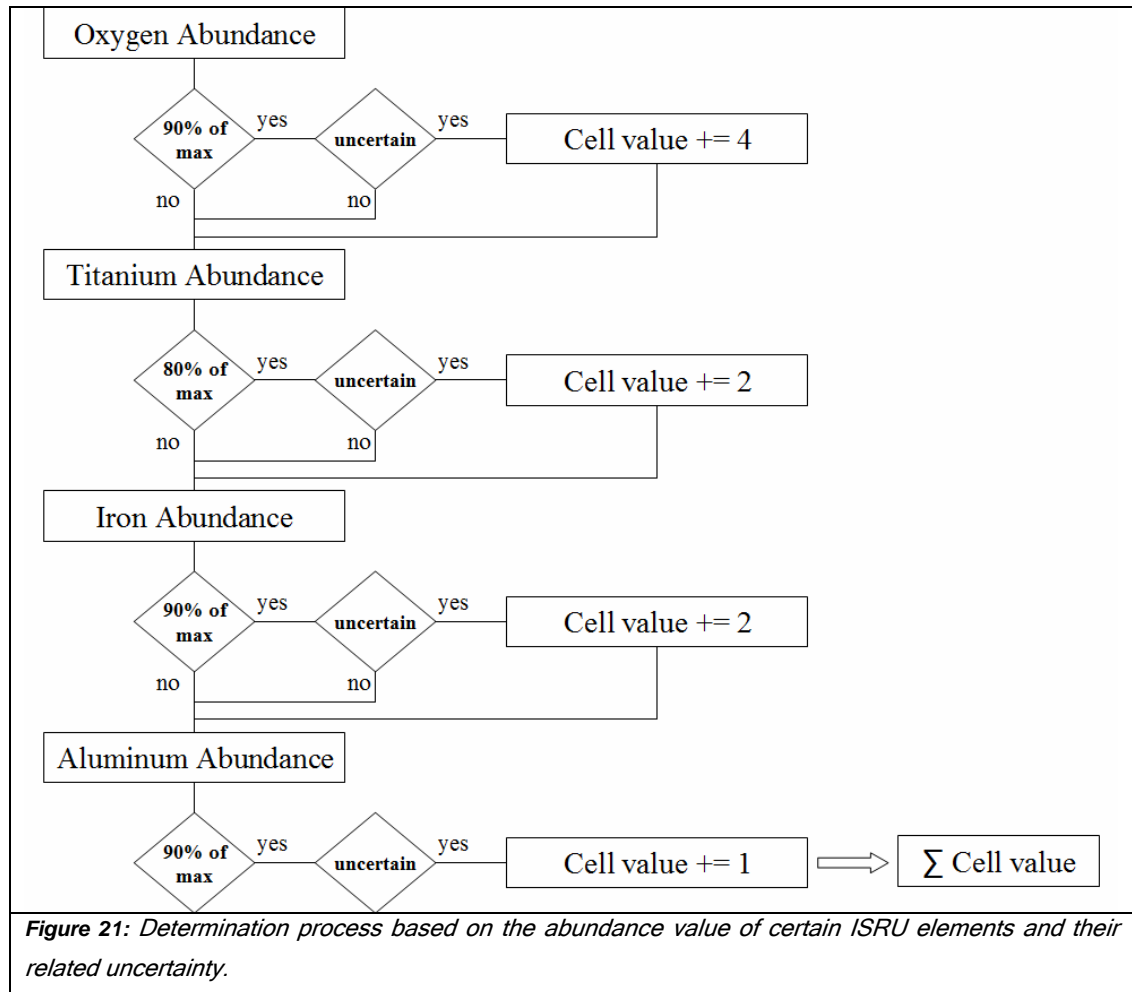
The method to evaluate uncertainties for Oxygen in 4.2.2 and 4.2.3 could be extended now to all seven elements (actually there are further datasets of the Lunar Prospector available in 5 degree resolution that could be used; those are Uranium, Potassium and

Thorium). However, it would not be realistic to plan the deployment of an in-situ exploration for a site where elements that are not of direct interest for ISRU are uncertain. We consider that it will be a primary objective for future robotic missions to evaluate the usability of ISRU elements in the lunar soil as support to human exploration. Those elements are Oxygen, Hydrogen and the metals Titanium, Iron and Aluminum. The goal of ISRU in this context is the production of life support elements (Oxygen and Hydrogen) and the potential to mine and exploit metals for construction purposes in the future.

The Hydrogen charts of the Lunar Prospector mission were in 2 and 0.5 degree resolution. Therefore, those cannot be used for the correlation study above. However, we assign a higher weight to locations where there is a high abundance of Hydrogen. The highest priority is given to places where there is a high but uncertain abundance of Oxygen. Those are to be verified by robotic missions. The third weight factor is given for a high, but uncertain, abundance of Titanium and Iron, since one of its oxides, Ilmenite ( $\text{FeTiO}_3$ ), has several geochemical properties that are of interest for ISRU exploitation. Ilmenite is known to fix Solar-wind-implemented elements better than other rock forms. Third, and lowest, priority is given to a high, but uncertain, abundance of Aluminum. Magnesium and Calcium were assigned no importance for the following considerations. Tab. 3 resumes the weight factors for the above stated elements. Fig 21 illustrates the decision process that uses the four abundance measurements and its uncertainties.

*Table 3: The weight factors for the different surface cells in terms of elemental abundances.*

<b>Condition</b>	<b>Weight Factor</b>
High oxygen abundance (at least 90% of the maximal value) with high uncertainty	4
High Titanium abundance (at least 80% of the maximal value) with high uncertainty	2
High Iron abundance with(at least 90% of the maximal value) high uncertainty	2
High Aluminum abundance (at least 90% of the maximal value) with high uncertainty	1
Magnesium	0
Calcium	0



The resulting landing sites with assigned importance are shown in Fig. 22. Fig 23 shows the abundance values of each site (to be identified by their Cell ID number in Fig 22 and Fig 23). It is to be noted here that the motivation behind this exercise is to identify surface regions where there is not only a high inconsistency between the element abundances, but also where there are potentially high values of these ISRU minerals. Therefore, many sites were not considered in Fig 22 that have a high uncertainty, but which are not of primary interest due to the fact that those have low values for Oxygen, Titanium, Iron or Aluminum. The result comes up with 38 different sites. A first, but too preliminary, result would be that 38 impactors are needed to determine the mineral constitution of these locations. This number can be optimized:

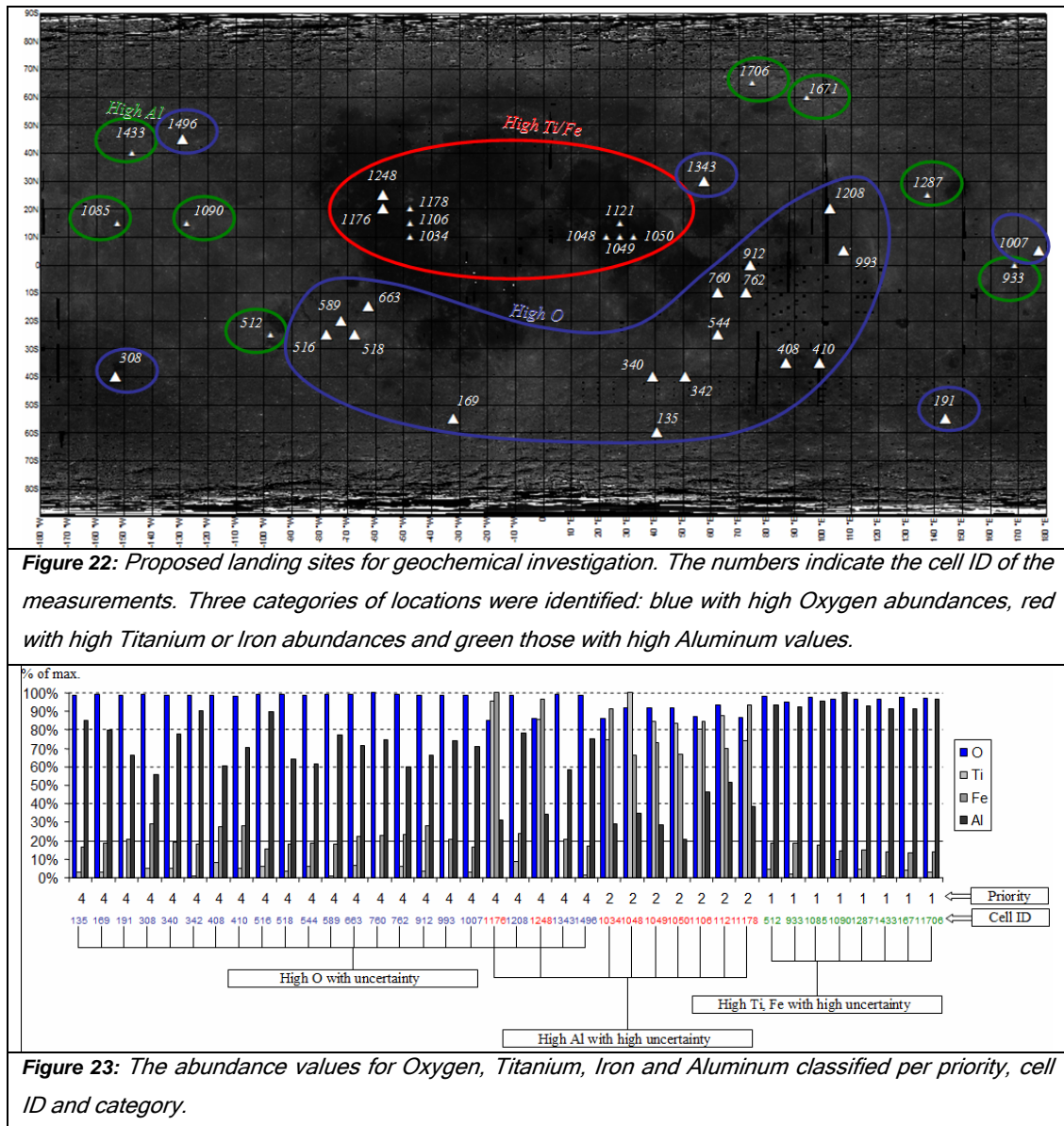
Many sites show similar abundance and uncertainties. One can see from Fig 23 that there are basically three categories of sites: a majority of locations with high oxygen abundance that has little metal abundance. Those are located (with some exceptions)



in a belt marked blue on the southern frontier of the Oceanus Procellarum. Its main extension lies on the Near Side, while it is interrupted at the Far Side of this altitude.

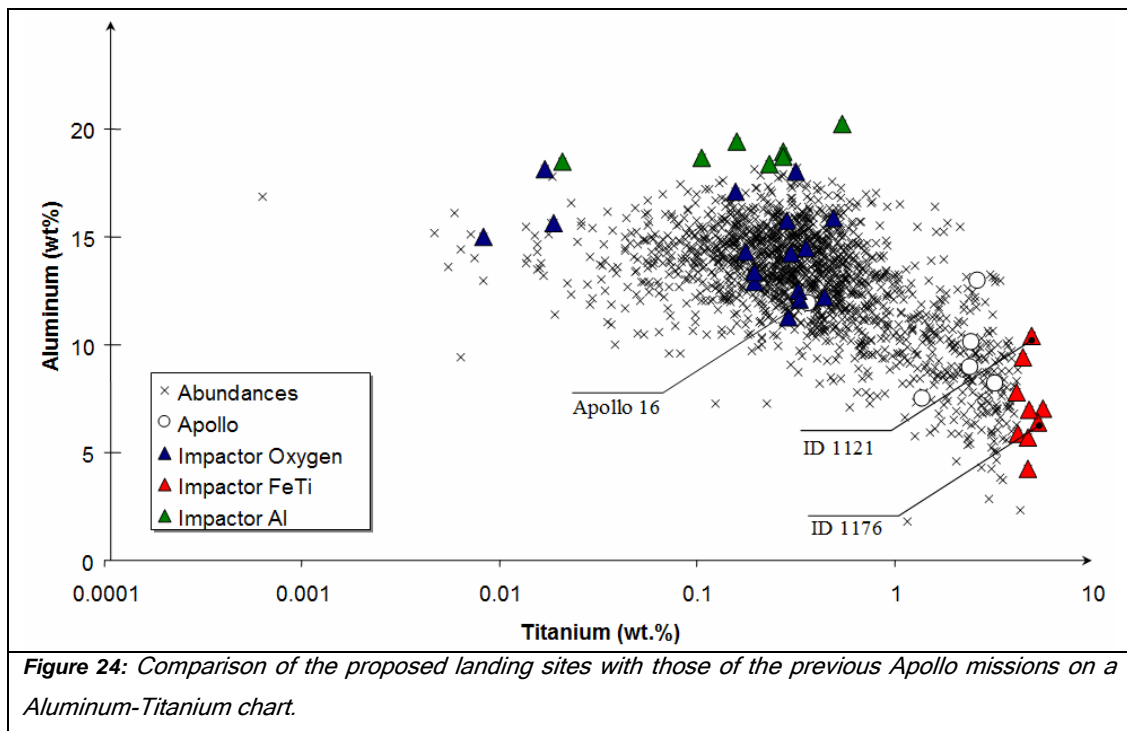
A second group is located in the Oceanus Procellarum. Those locations have little oxygen abundance (below 80%) but have large quantities of Iron and Titanium with high uncertainties in one of both elements. The reason for the deviation was mentioned before, so it is very likely that the correlation-model that we established before does not deliver correct values for mare regions.

And third group can also be emergent from our list which is locations that have a high Aluminum abundance and uncertainties. Since these regions are located in the Highland regions of the Moon, those also show high values for Oxygen.



The regions of the Moon can be separated into two categories corresponding to their elemental distributions: the Mare regions, which are rich in Titanium and Iron but depleted in Aluminum and Oxygen, and the Highland regions, which are rich in Aluminum and Oxygen but have low abundance of Titan and Iron. Fig. 24 and Fig 25 chart the abundance in pairs of these elements with indication of the proposed landing sites and previous Apollo landing sites. The charts show that the Apollo missions are concentrated in regions with similar chemical characteristics. However, those do not represent the bulk of the surface composition. One exception is Apollo 16, which landed in Descartes highlands next to the borderline between ancient volcanic flows and tephra. The geochemistry of the Apollo 16 site stands out to those of the other five manned landing sites. It is the only site that has highland characteristics as defined above.

The landing site proposals are charted in the same figures. The proposed landing sites would correct or confirm high abundance data of the ISRU elements. In all cases, these probes would reach locations of chemical composition that have not been explored in-situ before. These measurements would, therefore, fill the gaps in ground truth data for the lunar surface, which would help to establish global models of elemental distribution.



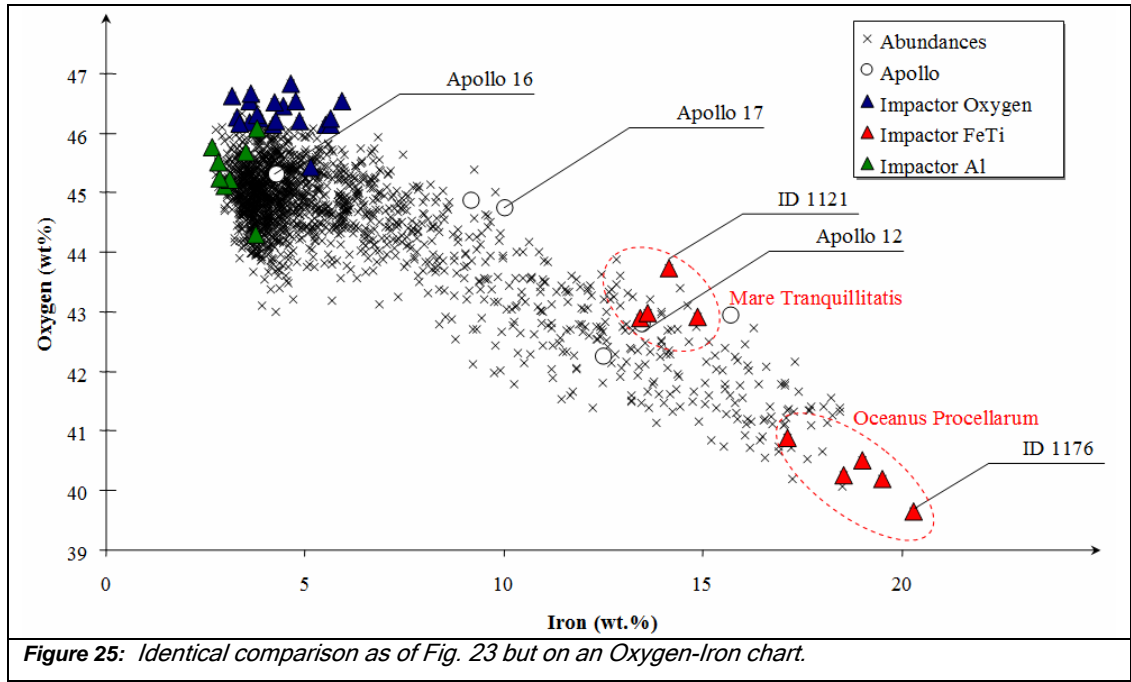


Figure 25: Identical comparison as of Fig. 23 but on an Oxygen-Iron chart.

In a second step, we will identify similar landing targets based on the criteria that if two or more sites are located in proximity and exhibit similar element abundances, since those can be combined into one single target. The charts of Fig. 24 and Fig. 25 illustrate that the proposed sites are clustered in groups. By comparing the proximity of its values (in the charts) with the proximity of its location, it becomes clear that the Titanium-Iron impactor landing sites have similar elemental abundance while being within close spatial distance. For this reason it is not necessary to cover all landing points. We reduce the five sites of the Oceanus Procellarum and the four sites of Mare Tranquillitatis to one single probe each. As a substitute for the Oceanus Procellarum impactor sites we chose ID 1121 for its high Iron value and because of the fact that the probe lands in the borderline between Mare Tranquillitatis and Mare Serenitatis. Sites ID 1048, ID 1049 and ID 1050 are eliminated from the further considerations. Equally, we chose site ID 1176 for the Oceanus Procellarum cluster, which replaces ID 1034, 1106, 1178 and 1248. The other proposed sites are quite distinct in their abundance measurement and their spatial distance and are kept maintained as a landing target. The new number of targets is reduced and 31 probes are proposed to establish a geochemical measurement network on the lunar surface. Tab. 4 resumes the assumed landing sites identified above.

Table 4: The landing site locations with the measurement objective (OP = Oceanus Procellarum; \* Central point of a 5°x5° cell).

ID	Lat*	Lon*	Location	Objective	Remarks
135	-60	40.5	crater Nearch	O measurement	
169	-55	-32	between craters Schiller and Scheiner	O measurement	
191	-55	144	north of crater Prandl	O measurement	
308	-40	-153	SPA south of crater Apollo	O measurement	
340	-40	39	crater Brenner	O measurement	
342	-40	51	crater Young	O measurement	
408	-35	87	crater Abel	O measurement	
410	-35	99	crater Gernsback	O measurement	
512	-25	-97.5	South of Mare Orientale	Al measurement	
516	-25	-77.5	South of crater Eichstadt	O measurement	
518	-25	-67.5	Southwest of crater Byrgius	O measurement	
544	-25	62.5	crater Petavius	O measurement	
589	-20	-72.5	west of crater Darwin	O measurement	
663	-15	-62.5	between crater Byrgius and OP	O measurement	
760	-10	62.5	crater Langrenus	O measurement	
762	-10	72.5	east of crater Kapteyn	O measurement	
912	0	74.25	between Mare Smithii and Mare Foecunditatis	O measurement	
933	0	168.75	crater Coriolis	Al measurement	
993	5	107.5	crater Al-Khwarizmi	O measurement	
1007	5	177.5	south of crater Tiseliuss	O measurement	
1034	10	-47.5	south-west of crater Marius	Fe-Ti measurement	Substituted by ID 1176.
1048	10	22.5	south of crater Ross	Fe-Ti measurement	Substituted by ID 1121.
1049	10	27.5	south of crater Jansen	Fe-Ti measurement	Substituted by ID 1121.

1050	10	32.5	between crater Jansen and Sinas	Fe-Ti measurement	Substituted by ID 1121.
1085	15	-152.5	crater Henyey	Al measurement	
1090	15	-127.5	south of crater Fersman	Al measurement	
1106	15	-47.5	OP between crater Marius B and C	Fe-Ti measurement	Substituted by ID 1176
1121	15	27.5	between Mare Tranquillitatis and Mare Serenitatis	Fe-Ti measurement	Retained as single site for the Mare Tranquillitatis impactors (substitutes IDs 1048, 1049 and 1050)
1176	20	-57.5	between crater Galilaei W and Seleucus A	Fe-Ti measurement	Retained as single site for the Oceanus Procellarum impactors (substitutes IDs 1034, 1106, 1178 and 1248)
1178	20	-47.5	crater Aristarchus	Fe-Ti measurement	Substituted by ID 1176
1208	20	102.5	north of crater Popov D	O measurement	
1248	25	-57.5	between crater Herodotus and Seleucus	Fe-Ti measurement	Substituted by ID 1176
1287	25	137.5	crater Siedentopf	Al measurement	
1343	30	57.5	crater Burckhardt	O measurement	
1433	40	-147	Crater Fowler N	AL measurement	
1496	45	-129	crater Gullstrand	O measurement	
1671	60	94.5	between crater Belkovich and Compton	Al measurement	
1706	65	75	between crater Hayn and Hayn A	Al measurement	

The study of potential landing sites for a geochemical network of impacting probes is not complete without taking into consideration potential alternative exploration strategies for the proposed sites. A rover mission, for example, could be more effective compared to multi-probe landings if it is able to cover a larger number of those sites (i.e. one single rover mission could cover three or more sites and thus replace three or more missions). Furthermore, the above identified sites are compared to other site proposals in order to evaluate if additional scientific objectives, apart from geochemical analysis, are of interest for a particular location. In this case, it might be wiser to send a larger, more sophisticated system to cover the specific spot.

In the next section, a Landing Strategy Decision Support System is described which takes into account the technical capabilities of different exploration means to explore locations on the lunar surface.

### **4.3 Landing strategy decision support system**

This section will present the last step in the identification of landing spots for geochemical measurement networks. It will compare the locations of the sites identified above in order to evaluate if another exploration method would be more effective than impacting penetrators. We compare the sites listed above with a number of other landing site proposals in order to see if one of them is of interest from other scientific investigations.

A Landing Strategy Decision Support System (DSS) was developed, which combines different types of exploration methods with landing site proposals based on technical constraints and geological properties of the locations. Three types of strategies are defined, namely rover missions, immobile landing stations and impacting probes. The capabilities and restrictions of each system are taken into account and compared to the scientific objectives of the proposed landing sites. The DSS is based on the same GIS application as described above.

As a ground rule, it was considered that impacting penetrators are the most (cost) effective exploration method. A maximum of sites is therefore to be covered by impacting micro-probes.

If a certain number of sites can be combined by a single rover mission, then the rover is to be preferred as mission strategy.

If a certain site is mentioned by other proposals for a scientific rationale different than geochemical measurements, then a rover or landing station mission is to be preferred.

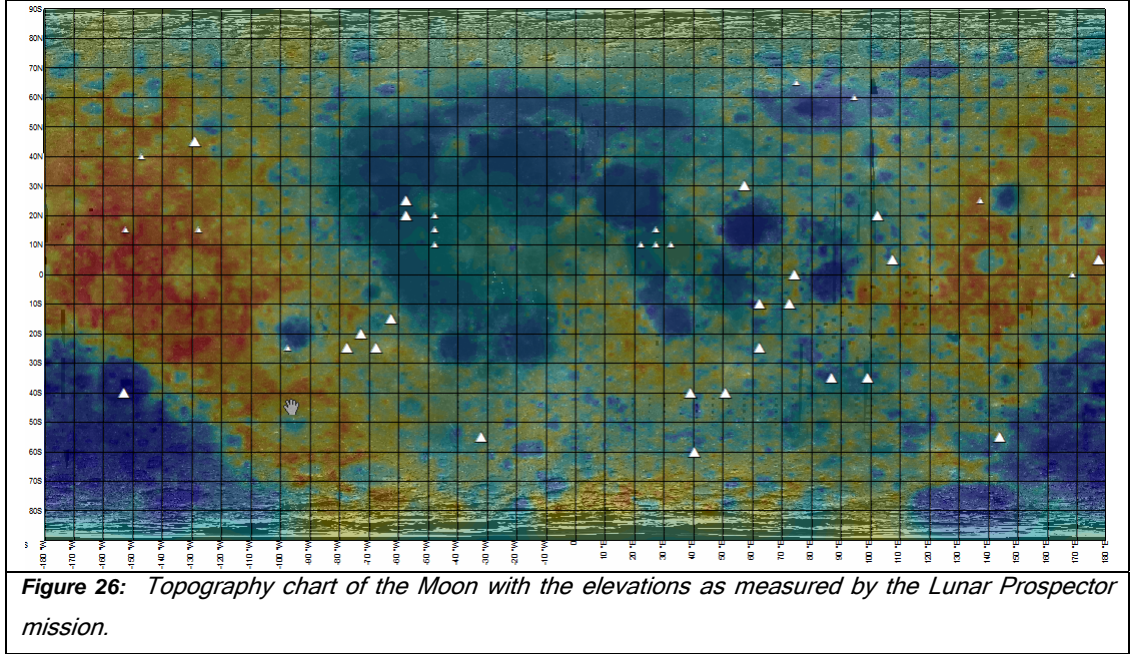
Both of the latter can only be landed on locations that permit a safe operation of the equipment.

#### **4.3.1 Introduction of technical restriction for the exploration methods**

The first step in the mission strategy decision process is the definition of the parameters for each site that lead to technical, spatial and temporal limitations for robotic missions:

1. Far Side locations require the communication be via a relay satellite, which increases the overall mission effort and costs (Okada et al., 2006). Such locations, although scientifically attractive, are most often not considered for mission studies, leading to an exclusion of 41% of the lunar surface (if regions visible in libration are considered as still acceptable).
2. The elevation of a location determines the propulsion effort of a rocket-assisted descent landing strategy, although its variation can be considered small compared to the orbital component of the velocity. In the case of an impacting probe, the impact velocity will vary as function of its topography. The variation from the Moon's Theoretical Gravitational Equilibrium (TGE) ranges from -9.06km (in the South-Pole-Aitken Basin, crater Antoniadi) to +10.75km (southern rim of the Dirichlet-Jackson Basin) (Araki, et al., 2009b). While the security and power effort of landing systems is penalized in low altitude locations, those bear the potential to analyze deep interior material (Tompkins and Pieters, 1999; Okada et al., 2006; Tanaka et al., 2007, Crawford, 2004).

3. Slopes and surface roughness reduce the chances of a safe landing (at a kilometric scale) and a rover's trafficability (at a metric scale). A roughness in a kilometric scale can be statistically evaluated as a function of altitude variance by using topographical data. Data for the evaluation of the surface roughness in a scale of meters is not available yet, but future orbiters such as the US Lunar Reconnaissance Orbiter (LRO) will deliver Digital Elevation Maps with a maximum resolution of meters at sites of interest. An example which uses altimetry data from the US Clementine mission can be seen in Fig. 26 (Williams and Zuber, 1998). The LIDAR dataset that was used to produce this chart originated from the PDS Geosciences Node of NASA and the Washington University in St.Louis. It has a resolution of 1 degree relative to a spheroid of radius 1738 km at the equator.



To derive the slope angle  $\alpha$  in a range of kilometers, each measurement point is compared to its eight adjacent vertices,

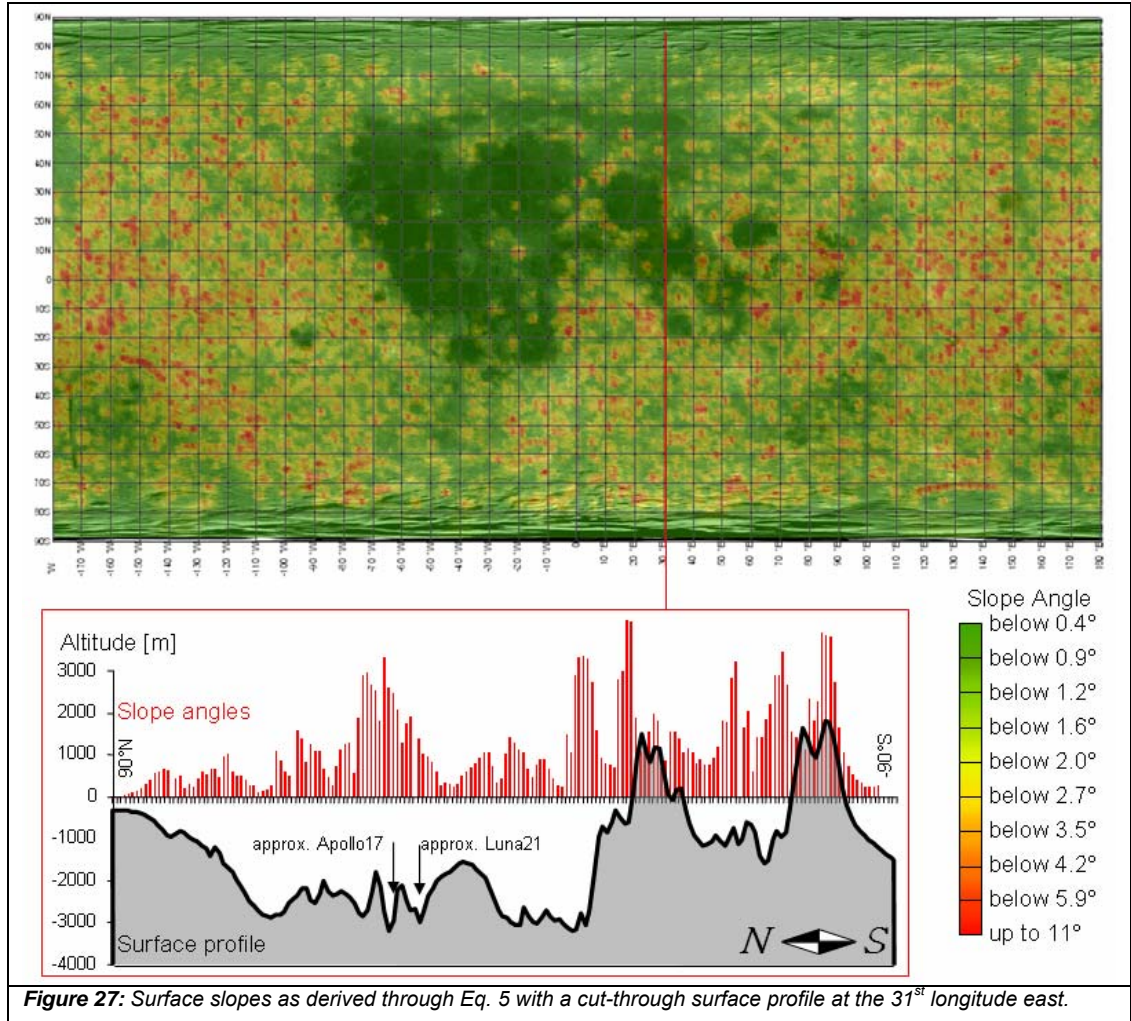
$$\alpha = \text{atan} \left[ \frac{\Delta(z_{ij} - z_{\lambda\phi})}{x_{zij; z\lambda\phi}} \right] \quad (4.5)$$

$$x_{zij; z\lambda\phi} = \text{acos} \left[ \left[ \sin(\phi) \sin(j) \right] + \left[ \cos(\phi) \cos(j) \cos(i-\lambda) \right] R \right] \quad (4.6)$$

where  $z_{ij}$  is the neighbor vertices at longitude  $i$  and latitude  $j$  and  $z_{\lambda\phi}$  is the analyzed vertices at longitude  $\lambda$  and latitude  $\phi$ . The simple distance  $x_{zij; z\lambda\phi}$  between both



locations can be approximated via the spherical law of cosines in formula (4.6).  $R$  stands for the Moon's radius (here assumed 1738km). The expression inside the brackets needs to be transformed to radians to be correct. The resulting chart is shown in Fig. 27 with an extract of the topology profile along the 31<sup>st</sup> longitude east. Angle values above 2° can be considered as critical for the landing operation's safety (Grant et al., 2004). In the chart of Fig. 27, such regions are marked from yellow to red.



This model can deliver a rough idea about the surface morphology. However, it has two major weaknesses: 1) the polar regions must be discarded from these considerations since these regions have yet not been covered with precise LIDAR measurements (the slopes on both poles are certainly higher than in the model above), and 2) the Clementine measurements can only deliver a data roster in kilometric scale (in the best around 8 km). The model can only be used to give a very schematic

picture of the surface morphology, while surface roughness data on a meter or decimeter scale is of pre-eminent importance for the landing's safety and ultimately for the mobility on the surface in a hazard-free environment. Topographical datasets in resolutions high enough to allow a detailed modeling in this scale do not exist yet on a global scale but only for specific regions. Future and recent missions like the Japanese Kaguya, the Indian Chandrayaan-1 and the US LRO will considerably improve the resolution of the topological charts of the Moon. The data of these missions will produce more precise surface roughness charts than the one presented above. However, the principle of using this data, at a kilometric scale to evaluate landing security remains valid.

4. The list of surface-dependant limitations to the mission is completed by time-variant constraints, such as surface light conditions (Thompson, 1964). A system is constrained to operate during the lunar day if it is not able to cope with the large temperature variations and missing solar radiation for power supply during the lunar night. The operational time is limited to two weeks in this case, consequently also reducing the operational radius as function of terrain trafficability and rover speed. Okada and co-workers (2006) limit the operation time of the Japanese SELENE-B rover to 10 Earth days, where the solar elevation angle and solar irradiation allow robotic operations.

#### **4.3.2 Capabilities and constraints of the three exploration strategies**

Above, potential landing sites and mission restrictions were described. In the following section the Decision Support System will be presented that assigns a landing strategy to these locations. The applied process is shown in Fig. 28. We differentiate three categories of robotic missions:

##### **Rover Missions:**

Soft-landing landers with a Lunokhod rover that is able to negotiate long distances as geological fieldtrips. The advantage of a mobile vehicle is that it can investigate several sites if those are located in a certain distance. The Russian Moon rovers Lunokhod 1 and 2 have traveled 10.54km and 37km over the Moons' surface in the

1970 and 1973 respectively. The Mars Exploration Rovers have not yet broken this distance record, but operate since 2004 in the harsh and dusty Martian environment. The Lunokhod rovers were larger than the MER rovers which was one of the reasons why those vehicles could negotiate longer distances. The rover size has on the other hand, large implications for the mission architecture and its costs. The power supply is another factor that significantly determines the operation time of the robot on the surface, thus its range. Lofgren (1993) considers operation radii for coming missions of 100km, while Spudis and Taylor (1992) go even beyond the 500km mark. For this study, we assume that a rover is able to drive a total distance of 300km. Rovers carry equipment to perform geochemical analyses, and they can send back high-resolution images of the landscape. If the lander that delivered the rover to the surface has a sample return vehicle, then samples can even be send back to Earth from the location near to the landing site. It is assumed that the rover requires smooth terrain for safe landing (slopes  $< 2^\circ$ ) (Grant et al., 2004). Rover missions are justified in the following study if: a) several sites lie in the operation range of the vehicle, or b) the site is considered as opportunity to perform age determination or sample return.

#### **Landing Station:**

Immobile soft-landing systems similar to craft like the Surveyor, Viking or Mars' Phoenix. The station can be equipped with a manipulator arm which gives it an operation range of approximately one meter. Landing stations can carry subsurface sampling mechanisms (scoops, drills or moles) to investigate deeper layers of the soil. It can deliver samples back to Earth if it is equipped with a return vehicle. Like the rovers, it is assumed that it requires smooth terrain for safe landing (slopes  $< 2^\circ$ ) (Grant et al., 2004). Landing station missions are justified if the site is considered as opportunity to perform age determination or sample return and therefore requires more sophisticated instruments as those that can be carried by an impactor.

#### **Impacting Probes:**

Ballistic probes are released from an orbiting satellite and impact on the surface without the use of a retro-rocket. The survivability of the on-board instruments depends upon, amongst other factors, the impact velocity, thus the altitude of release and trajectory parameters of the satellite. It will be assumed, for instance, that the

probe and some of its instruments are robust enough to perform in-situ science on a limited spatial scale. This issue is to be studied in more detail in the following chapters 5 and 6.

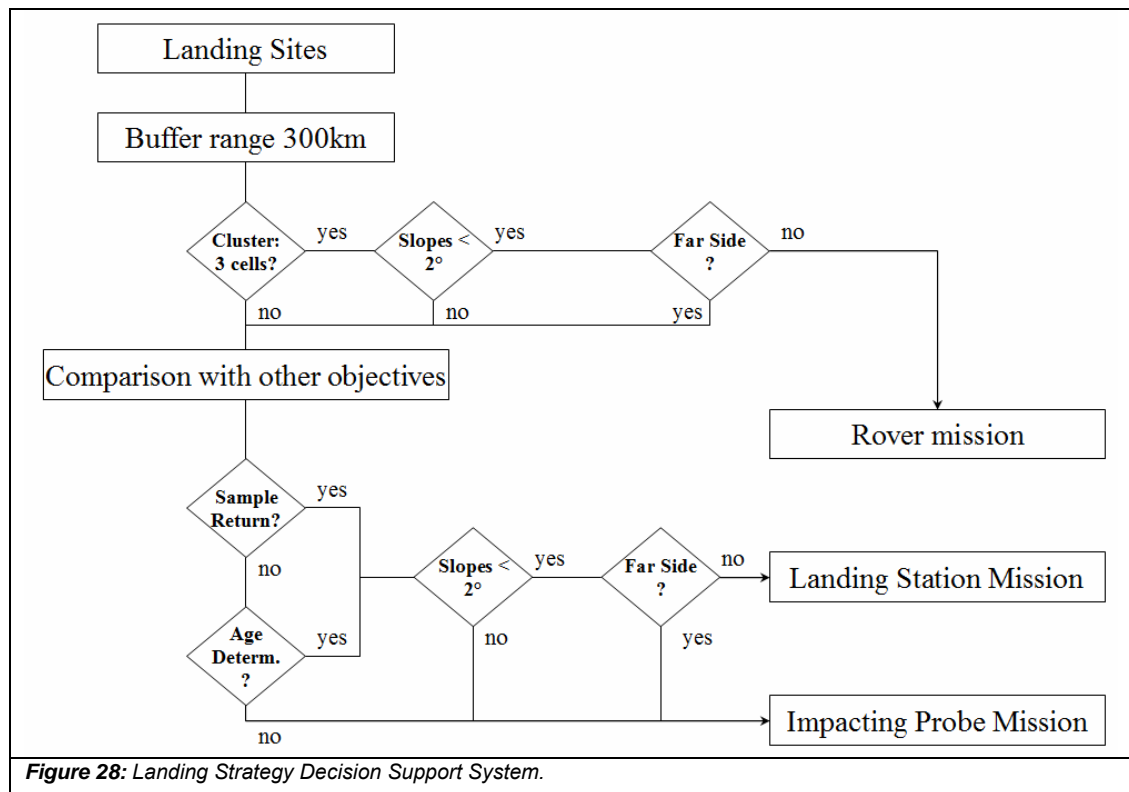
### **4.3.3 Landing Strategy Decision Support System process**

Figure 28 shows the Decision Support System process diagram. A range of 300km will be assigned to each landing site. In a first step, clusters of more than three sites will be identified that lie inside a 300km range. It is assumed that one of the sites needs to have slope angles of less than  $2^\circ$  in order to assure a safe landing of a rover or a landing station (Grant et al., 2004). If this is not the case, then the sites are assigned for a penetrator mission. A rover or landing station that operates on the Far Side needs a relay satellite for the communication with the ground stations. Since this will further affect the mission costs, we assume that such sites are assigned to be penetrator mission sites: a penetrator will be deployed from an orbiting craft and operate only a short period while the satellite can relay back data to Earth.

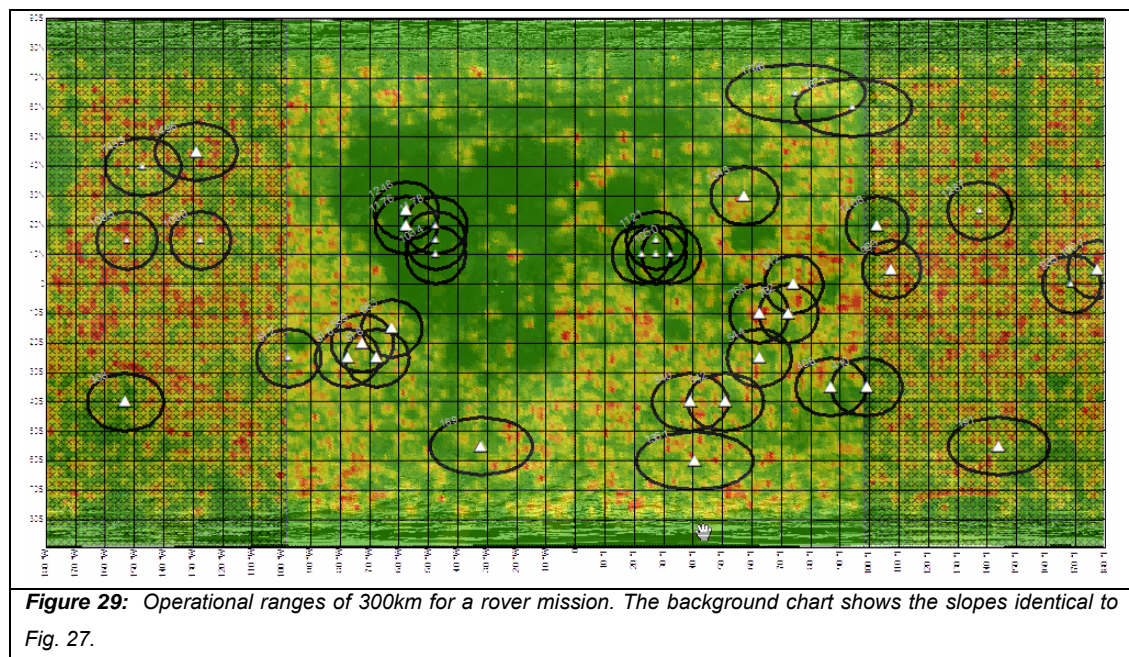
After having clustered some sites to a single rover mission, we will examine if there exist other landing site proposals that target a similar site as those mentioned above. In this case, there might be additional mission objectives that would call for a more sophisticated instrument than an impactor. Such site would then be assigned to a landing station.

Figure 29 shows the first step in this process: a range of 300km was assigned to each landing site. Several sites can be clustered in a perimeter of 300km and would, therefore, be an opportunity for a rover mission. Both Titanium-Iron groups (in the Mare Tranquillitatis and Oceanus Procellarum) can be combined in this way. The slopes at these locations are below  $1^\circ$  and would, therefore, permit a safe landing. A third group of interest is situated around crater Darwin (cell ID 516, 518 and 589). A fourth site close to crater Byrgius (ID 663) is located at a distance of 335km from this area. The terrain at this region is more rugged than the Mare regions before, with maximum slopes of  $3^\circ$  to  $4^\circ$ . However, one of the sites south of crater Eichstadt (ID 516) offers an even terrain with slopes below  $1^\circ$  for the deployment of a rover. All other sites cannot be clustered to three in a range of 300km. These considerations

would eliminate the remaining impact landing locations at the mare regions for the further study. However, this judgment is arbitrary because we already reduced these locations to two distinct sites. A rover mission could only cover a maximum of 3 sites at the same time (assuming an operational range of 300km). All other locations are spaced in distances, which make them difficult to reach with a single rover.



**Figure 28:** Landing Strategy Decision Support System.



**Figure 29:** Operational ranges of 300km for a rover mission. The background chart shows the slopes identical to Fig. 27.



In a second step, we examine additional landing site proposals for landing sites from other authors. The objective of this study is to identify eventual supplementary mission objectives at sites that lie inside the surface cells that were identified above. Three categories of exploration objectives were derived: (CP) Reconnaissance, cartography and high resolution photography of the location, (IS) in-situ science using instruments such as microscopic imagers, spectrometers (Mössbauer, APXS, Thermal Emission, Laser emission) or seismic instruments, and (SR) sample return which represents the highest effort either by manned or robotic means. The proposed sites, their location, objective and references are indicated in Tab. 5, and Fig. 30 charts those locations (red stars) in comparison with the surface cells that were identified (white rectangles). It can be seen than none of these sites is located inside one of the surface cells: therefore there are no additional mission objectives that have to be taken into consideration for the above mentioned landing sites.

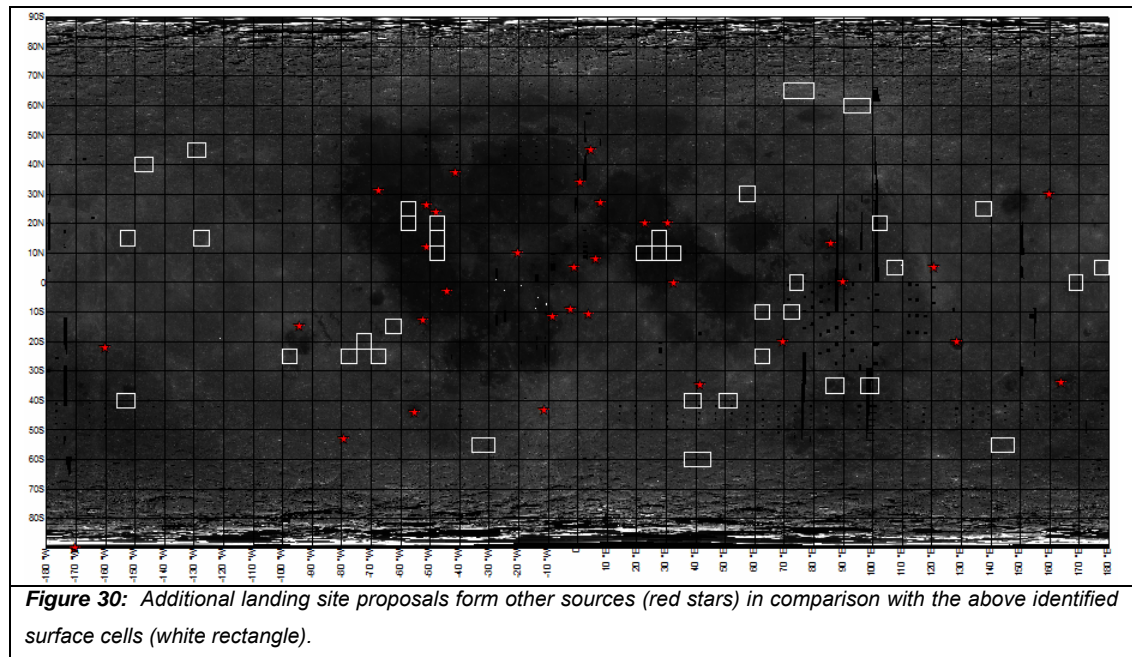


*Table 5: Landing site proposals. Sites with identical numbers in brackets are proposed as duplicate sites in the references.*

Position (lat. / long.)	Feature	Goal	Req.	References
-11S / 4.1E	Albategnius[1]	Volcanism	(CP)(IS)	(Wilhelms, 1985)
27N / 8E	Apennine	Age, composition and spectra calibration	(CP)(IS)	(Wilhelms, 1985)
23.7N / -47.4W	Aristarchus[4]	Composition	(IS)	(Okada et al, 2006)
33.9N / 1.2E	Aristillus[4]	Composition	(IS)	(Okada et al, 2006)
20N / 71E	Balmer[3]	Age and composition	(IS)(SR)	(Wilhelms, 1985)
-0.4S / 32.7E	Censorinus	Age and composition	(IS)(SR)	(Head, 1970)
20N / 23E	C. Mare Serenitatis	Age and spectra calibration	(CP)	(Wilhelms, 1985)
31N / -67W	Copernican Mare	Age and composition	(IS)(SR)	(Wilhelms, 1985)
10N / -20W	Copernicus[4]	Feature anal., age and composition	(IS)(SR)	(Head, 1970; Greeley, 1974; Wilhelms, 1985; Okada et al, 2006)
-11.8S / -8.1W	Davy-Crater Chain	Composition and age	(IS)(SR)	(Head, 1970)
-3S / -44W	Flamsteed P	Spectra calibration	(CP)	(Head, 1970; Wilhelms, 1985)
37N / -41W	Gruithuisen[2]	Volcanism	(CP)(IS)	(Wilhelms, 1985)
-13S / -52W	Hansteen[2]	Volcanism	(CP)(IS)	(Wilhelms, 1985)
7.8N / 6.3E	Hyginus	Feature anal., composition	(CP)(IS)(SR)	(Head, 1970, Greeley, 1970)
5N / 121E	King	Age and composition	(IS)(SR)	(Wilhelms, 1985)
-34S / 164E	Mare Ingenii	Composition	(IS)	(Wilhelms, 1985)
13N / 86E	Mare Marginis	Age and composition	(IS)(SR)	(Wilhelms, 1985)
0.0N / 90E	Mare Smithii	Precursor, composition	(CP)(IS)	(Spudis and Hood, 1992, Swindle, 1992)
11.9N / -50.8W	Marius Hills	Composition and age	(IS)(SR)	(Head, 1970, Greeley, 1974)
-15S / -94W	Maunder	Age and composition	(IS)(SR)	(Wilhelms, 1985)
5N / -1W	Murchison	Composition	(CP)(IS)	(Wilhelms, 1985)
-35S / 42E	Crater Brenner	Age and composition	(IS)(SR)	(Wilhelms, 1985)
-9S / -2W	Ptolemaeus[1]	Volcanism	(CP)(IS)	(Wilhelms, 1985)
-44S / -55W	Schickard[3]	Age and composition	(IS)(SR)	(Wilhelms, 1985)
-89.6S / -170W	South-Pole ELT	Human Precursor, composition	(CP)(IS)	(Spudis et al, 1985, Smith et al. 2007)
-22S / -160W	SPA, South Wilsig	Age and composition	(IS)(SR)	(Wilhelms, 1985)
30N / 160E	Steno Q-N	Age and composition	(IS)(SR)	(Wilhelms, 1985)
20.2N / 30.8E	Taurus-Littrow	Age and composition	(IS)(SR)	(Taylor, 1992)
-20S / 129E	Tsiolkovsky	Composition	(IS)	(Wilhelms, 1985)
-43.4S / -11.1W	Tycho	Feature examination, composition and age	(CP)(IS)	(Head, 1970; Greeley, 1970; Okada et al, 2006; Crawford et al., 2007)
45N / 5E	Vallis Alpes	Composition	(CP)(IS)	(Wilhelms, 1985)
26N / -50.8W	Vallis Schröteri	Volcanism (sinuous rille)	(CP)	(Head, 1970)
-53S / -79W	Yakovkin	Composition	(CP)(IS)	(Wilhelms, 1985)

#### 4.4 Resulting design considerations

In the previous sections, we found out that 38 probes would be needed to cover all the identified surface cells. Nine sites had similar surface compositions and could be combined. We, therefore, conclude that a number of 31 probes would be needed to cover all spots of interest.

The study of the rover range led to the conclusion that three clusters could be reached by a single rover however, those combine three sites each where two of the clusters are located in the mare regions that were, in any case, reduced to two distinct landing sites.

The cluster around crater Darwin offers the possibility to deploy a rover. This strategy would eliminate three further sites while it remains to be discussed if a rover mission to this spot is more cost effective than the deployment of impacting probes.

In conclusion, we assume that 31 probes are needed to establish a geochemical surface measurement network with impactors. We use this figure as input for the design of the probe.

The following chapters have as the objectives to derive a design for such impacting probes and to evaluate the feasibility of a multi-micro-probe mission with a large quantity of probes. In order to gain a frame figure for the weight and size of the single micro-probe it is interesting to study the payload weight of previous missions. We are not interested here in the overall weight of a specific satellite, but rather in the weight that was assigned to its instruments: the micro-probe system, as it is proposed here, is to be considered here as an additional *instrument* for an orbiter, along with other devices such as cameras and spectrometers. Candidates for such missions are those that used a similar system like the one proposed, such as the Indian Chandrayaan-1 and the Russian Luna-Glob which did, or are to, deploy an impacting system to the Moon. Tab. 6 summarizes the data of these missions. Assuming a number of 31 probes whose weight takes 30% to 50% of overall instrument weight, we conclude that a single probe can weigh between 0,3kg and 5kg.

*Table 6: Payload weight on various host missions.*

<b>Mission Name (year)</b>	<b>Instrument</b>	<b>Instrument weight</b>
Chandrayaan (2008)	Moon Impact Probe	35kg (ISRO, 2009)
Luna-Glob (2012)	Lunar-A penetrators	2 x 13kg (NSSDC, 2009)
LunarEx (proposal)	Penetrators	4 x 13kg (Smith et al., 2007)
Mars Express (2003)	Beagle-2	33,2kg (NSSDC, 2009b)
Cassini	Huygens	319kg (NSSDC, 2009c)



# **CHAPTER 5**

## **Analysis and modeling of high-velocity impacting probe**

We studied a global deployment strategy of a geochemical micro-probe network in the previous chapter. The mission objective of this network is to take in-situ measurements on the lunar surface in order to establish a global model of the abundance of ISRU elements. The availability of these elements will be a crucial factor in the future exploration of the Moon by astronauts, since those can serve to sustain long-duration missions on the Moon. The result of this study was that it indicated that a quantity of 31 probes would be needed to be deployed on the surface. Based on previous mission payloads, we derived one first basic specification of feasibility, namely the weight of each probe should be between 0.3kg and 5kg in order to keep the overall weight of such instrument (i.e. the totality of probes) in an acceptable weight range.

In this chapter, we will narrow down our study of the micro-probe design by studying the technical feasibility of such a system. The architecture of a micro-probe can be separated into three major components: the carrier, which is the shell that penetrates into the soil; household components such as batteries and communication; and the scientific payload, which are the instruments to perform surface investigations.

The following study will investigate the design of the carrier and its household systems to sustain high velocity impacts. We will evaluate the suitability of different projectile designs to deliver a scientific payload onto the surface and establish a model for the impact process.

In a second step, we will study the scientific payload of a microprobe by identifying instruments that fulfill the mission objectives (geochemical analysis of the soil) and are capable of sustaining high decelerations during the impact. Based on this, we will derive the specifications for the sampling system that is needed to transport soil from the perimeter of the probe into the scientific instruments in its inner housing.

## 5.1 Basic specifications for the deployment of micro-probes

The probes are dispatched from a satellite that orbits the Moon. Table 6 summarizes some previous and planned missions that deployed impacting probes onto extraterrestrial surfaces. The idea is that all probes are deployed by the same craft through one single mission. The weight and size of the micro-probes and their deployment mechanism must correspond to those of typical surface instruments to keep their integration feasible.

Basic specifications on the micro-probe deployment from orbit need to be established before it is possible to verify different design options for a micro-probe system. Parameters of importance are the impact velocity, the properties of the lunar soil and sub-soil in order to model the impact process and the lunar environment to derive design constraints. The impact velocity will be one major input factor for the design of the probe.

### 5.1.1 Impact velocities

The impact velocity of a micro-probe system impacting on the Moon is a function of the deployment speed, the orbit's altitude, gravity and topography. These factors depend on the ephemeris of the satellite orbiting the Moon. It is not the objective of this study to derive an optimized trajectory to cover, for example, all impact locations identified above. Therefore assumptions will be made about the impact velocity that the penetrator will reach. The impact velocity  $v$  of an object that is released in orbit can be calculated through the formula of a free fall (5.1) where  $a$  is the surface gravity,  $v_0$  is the initial velocity,  $z$  the spacecraft's altitude above the TGE, and  $\Delta x_{TGE}$  is the difference to the mean surface.

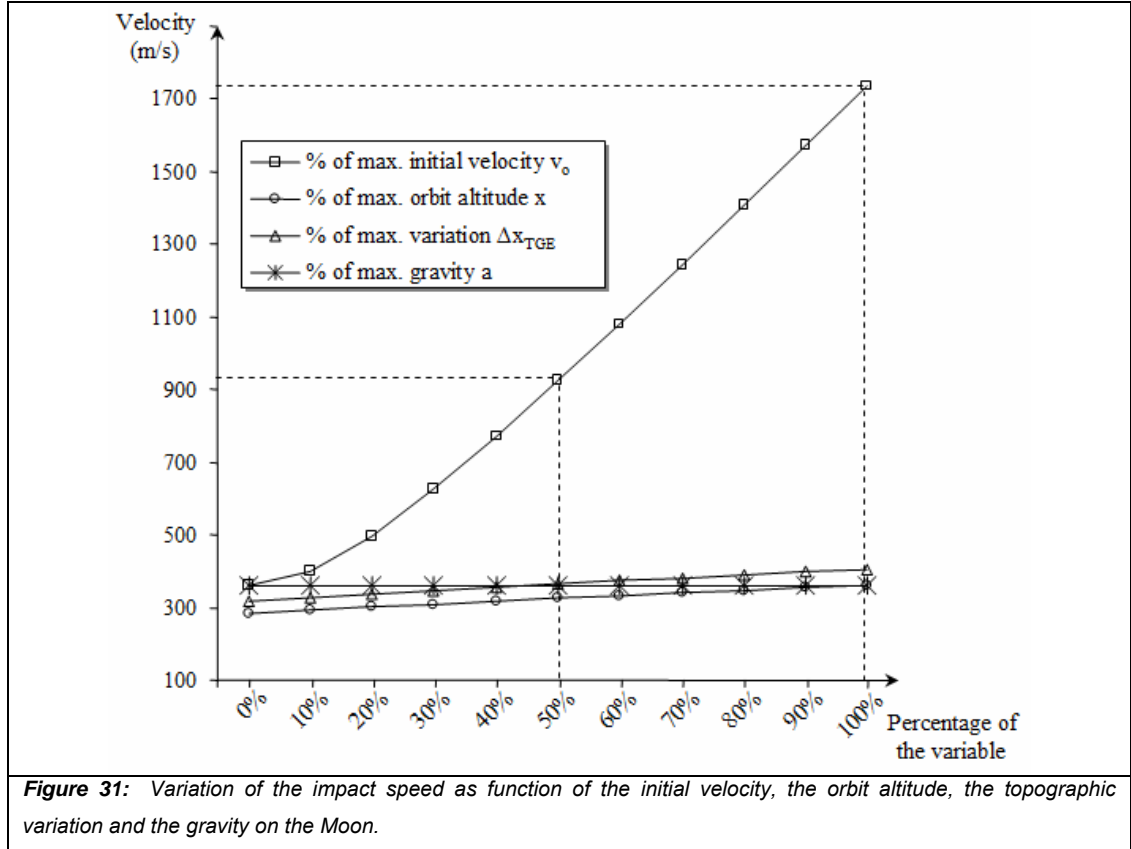
$$v = \sqrt{2 a (z + \Delta x_{TGE}) + v_0^2} \quad (5.1)$$

All these variables change according to the spacecraft's orbit and location:

- The lunar gravity  $a$  exhibits variations from its equatorial surface gravity ( $1.622\text{m/s}^2$ ). The latest spacecraft Kaguya, established the so far most precise map of the lunar surface gravity (Namiki et al., 2009). Its gravitational field can vary from  $1.619\text{m/s}^2$  to  $1.625\text{m/s}^2$  depending on the surface gravity below the spacecraft.

- The altitude  $z$  depends on the ephemeris of the satellite around the Moon. For the following study, we assume an orbit for the deploying spacecraft of 25km to 40km altitude.
- The difference of the ground to the TGE is, like the gravity, a surface-dependent variable. A topographical chart is shown in Fig. 25. The Japanese Kaguya also performed laser altimetry of the surface shape of the Moon with unprecedented resolution and coverage (Araki et al., 2009). Previous maps used Clementine data which had large uncertainties beyond  $80^\circ$  latitude. Kaguya was the first orbiter that delivered a topographic map of the Poles with a resolution of  $0.015625^\circ$  in latitude and  $0.179^\circ$  in longitude. The Moon's topography spans 19.81km according to this new data. Its lowest point is the Antoniadi crater (-9.06km), and the highest point is located at the rim of the Dirichlet-Jackson Basin (10.75km) (Araki et al., 2009b).
- The initial velocity needs to be separated into a vertical component and a horizontal component. A vertical initial velocity can be introduced by the release mechanism of the probe, which needs to accelerate the probe for the separation with the spacecraft. The horizontal component of the initial velocity of a probe is inherited from the orbiting velocity of the spacecraft. As maximum forward velocity, we use the de-orbiting speed of 1680 m/s for the Moon in a Hohmann Transfer as estimation for the following calculations. As minimum forward velocity, we consider the case where there is an active deceleration system (retro-rockets) integrated into each probe. The Japanese Lunar-A penetrators, which are planned to fly onboard a Russian craft, use rocket power to cancel the orbital component of the velocity (Shiraishi et al., 2007). In this case, the vertical velocity becomes zero.

Figure 31 plots the change in velocity for a penetrator based on the variation of each above-mentioned parameter. All parameters were fixed in the chart to the following values:  $a=1.622\text{m/s}^2$ ,  $z=40\text{km}$ ,  $\Delta x_{\text{TGE}}=0$ ,  $v_0=0$  except those which were varied as indicated (in percent from minimum=0% to maximum=100%).



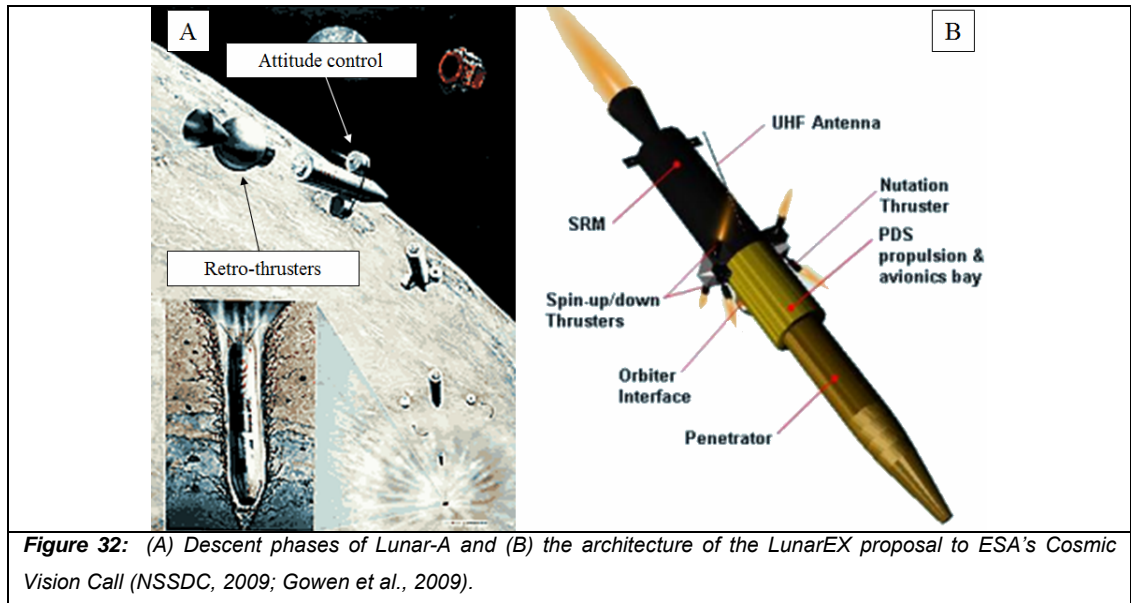
It becomes obvious that the horizontal velocity has the highest impact on the overall velocity vector of the system. This leads to a serious design challenge for a multi-probe mission with a large quantity of probes. In order to assure the survival of the carrier and its payload, the large horizontal velocity needs to be reduced; but in order to assure the feasibility of reaching all locations indicated above, each probe needs to be as small as possible, while its size and weight will be penalized by the deceleration mechanism. To solve this problem, there exist several solutions which will be discussed in the following text.

#### **a) Deceleration by retro-rockets**

Most of the before-mentioned penetrator proposals make use of a retro-rocket system to cancel the horizontal component of the impacting system. The Japanese Lunar-A mission, which is now under discussion to be integrated into the Russian Luna-Glob 1 mission, is planned for 2012 (Shiraishi et al., 2007). The orbiting spacecraft was planned to carry two 13kg missile-shaped penetrators that would have been released in 40km altitude in vicinity of the Apollo 12 and 14 landing sites. The penetrators

would impact at speeds of 250m/s to 300m/s. They were successfully tested at an impact speed of 330m/s at the US Sandia Laboratory (Shiraishi et al., 2007). Each penetrator is equipped with seismometers and heat flow experiments. Lunar-A would use a set of retro-thrusters which are jettisoned before impact. Figure 32 (A) shows an artist's view of the penetrators with its thrusters (NSSDC, 2009). Little information is available about the exact design of the deorbit rocket engines.

The UK LunarEx proposal uses an identical concept to eliminate the horizontal speed component (Smith et al., 2007; 2009). The descent modules are released at periapsis and perform a deceleration burn to decelerate -1675m/s. Each penetrator has a total mass of 36kg, where 23kg are used for the deorbit motor and altitude control (Gao et al., 2008). The penetrators impact after 3.5 minutes of free fall at speeds around 300m/s. The probe architecture was tested through trials in the UK with an impact velocity of 310m/s (Gowen et al., 2009). Fig 32 (B) shows the concept of the descent of the UK Penetrator, as an example for a mission to Europa (Gowen et al., 2009).



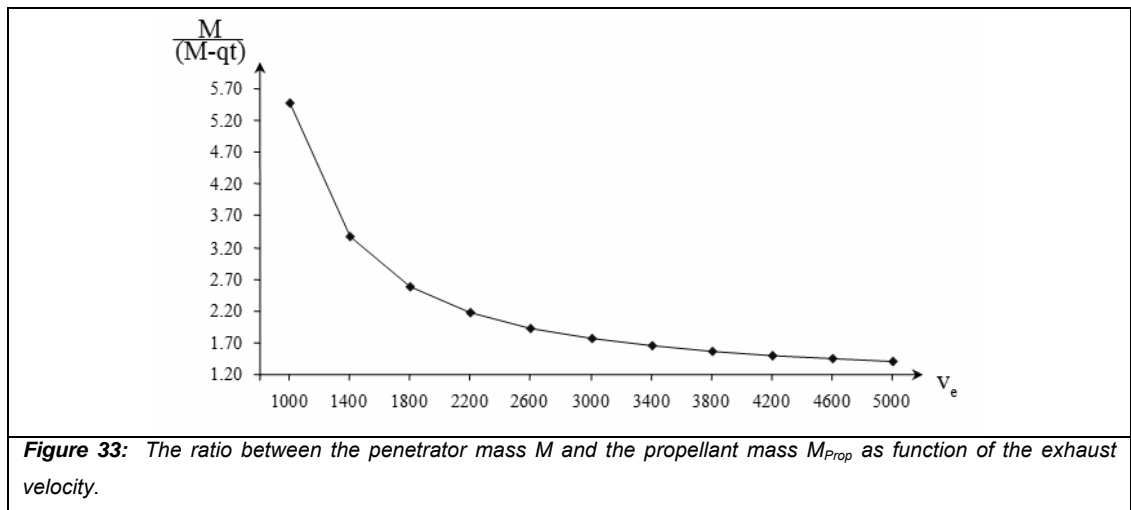
The integration of a deorbit motor will penalize the overall weight of the probe. This fact is problematic in the scenario described above, where a large number of probes need to be deployed. The available payload space and weight will be reduced by the mass that is needed for each single retro-rocket. The mass that is required to achieve a  $\Delta v$  of 1700m/s in order to cancel the horizontal velocity can be estimated through the impulse of a rocket system in Eq. (5.2) where  $v_e$  is the exhaust velocity of the

propellant,  $M$  is the spacecraft mass (before the maneuver),  $q$  is the mass flow of the propulsion, and  $t$  the time (Braeunig, 2008):

$$\Delta v = v_e \ln \left( \frac{M}{(M-qt)} \right) \quad (5.2)$$

The term in the large brackets describes the ratio of spacecraft mass  $M$  before the maneuver, to its mass after the maneuver, since the term  $qt$  is the mass  $M_{\text{prop}}$  of ejected propellant. It is this ratio which is of interest for our consideration since it will deliver an approximation of how much of the probe's mass needs to be assigned to the propulsion system. Equation (5.3) shows Eq. (5.2) resolved after this ratio. Figure 33 shows the plot of the ratio for different exhaust speeds ranging from 1000m/s (solid rocket) to 5000m/s (bipropellant rocket). The corresponding ratios of penetrator mass  $M$  to propellant mass  $M_{\text{prop}}$  ranges from 29% to 82%. For the further study, it can be assumed that at least 60% of the total mass  $M$  needs to be assigned to the deorbiting system, if chosen as solution.

$$\frac{M}{(M-qt)} = e^{\left( \frac{\Delta v}{v_e} \right)} \quad (5.3)$$



### **b) Deceleration by space tether**

On September 25, 2007, ESA performed a tether satellite test, onboard a Russian Foton-M3 vehicle, which had the objective to deploy a re-entry capsule by the use of a long cable. The concept of this mission was to deorbit a capsule through a momentum transfer (Kruijff and Van der Heide, 2009). The system was developed by students and was named Young Engineer's Satellite 2 (YES2) (ESA, 2007). Similar

systems were already successfully tested at previous missions, but YES-2 was, so far, the largest structure deployed in space. Its 0.5mm diameter Dyneema® tether had a length of 30km.

The concept is to reduce the orbital velocity of the re-entry capsule through its cable link to a deployment satellite in higher orbit: The capsule gains velocity during its descent through its lower orbit until a stage where the tether length is reached. At this point the system starts to swing back, until it reaches a lower speed, the one of the deployment craft, but at a lower orbit. Figure 34 illustrates the concept.

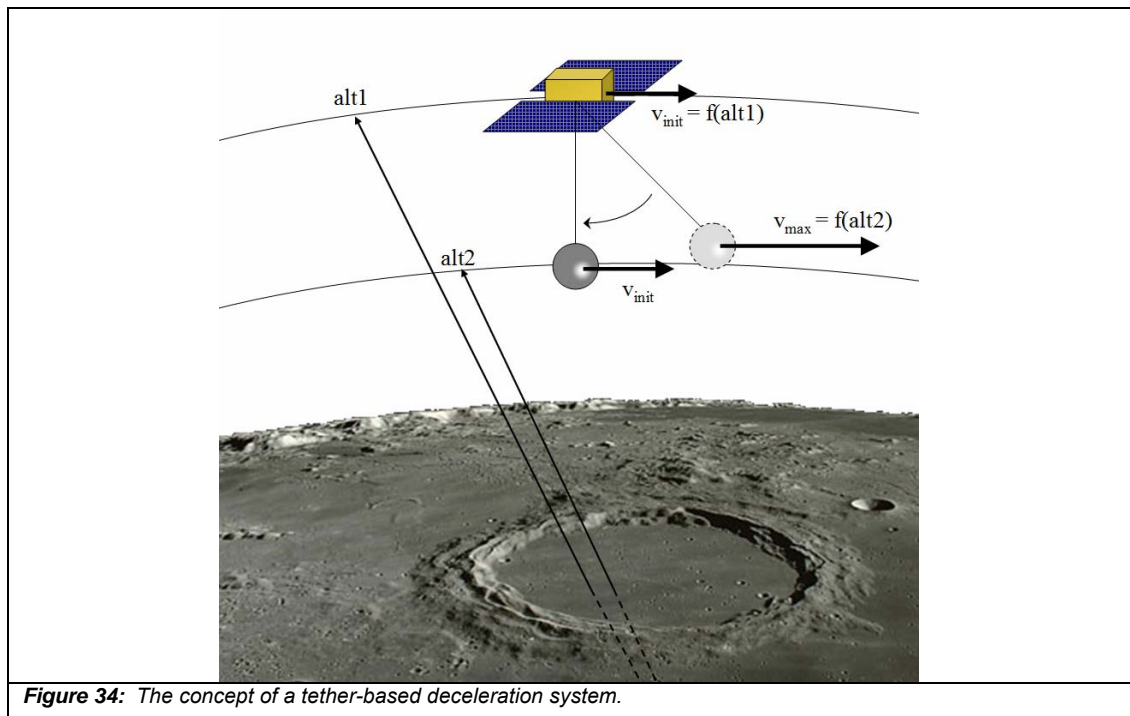


**Figure 34:** The concept of a tether-based deceleration system.

A similar concept could be a solution for the problem of reducing the horizontal velocity of impacting probes. The probes are “robed” down from a higher orbit where the deployment craft travels with lower horizontal velocity. Once the cable reaches its end, the micro-probe would be decelerated to a speed that would be lesser than the normal orbital speed at this altitude.

Although the idea is appealing, it quickly turns out that it is not feasible from a technical point of view. In order to reduce the orbital speed to a range of around 300m/s, it would be necessary that the deploying craft orbit the Moon at 54 000km.

The cable would require a volume of  $43\text{m}^3$  taking into consideration the specifications of the YES-2 satellite.

### **c) Deployment from a landing craft**

A third option to achieve smaller impact velocities is to deploy the probe from a landing spacecraft. The concept of an ad hoc landing micro-probe network foresees to deploy penetrators in a sequence during the landing approach of a larger lander (Weiss and Yung, 2007). Free-falling, without a deceleration system, those would impact prior to the touchdown of the main lander. A vision system could deliver high resolution photography of the surrounding landing site, which could be used to assess the local environment of the area for potential hazards to surface mobility (rover) and identification of locations of interest. While the optical system will not survive the impact, the telecommunication device will continue working after the impact. This device will serve as beacon to determine the location of the rover during its excursions. The probes will establish an ad hoc network to support the navigation of the robot. The probes can furthermore carry instruments that identify buried water ice. In this configuration, the probe can be deployed into permanently shadowed areas where its instruments would identify ice, if present. The impact sites of one or several probes will be in the reach of the rover. It is, therefore, possible to examine the impact site of the probe. This would deliver insights about the impact condition of this instrument as a technological assessment for future penetrator missions. The possibility to “revisit” impactor-type mission sites is only given in the constellation with a landing mission. The analysis of the impact site will enable scientists to examine fresh ejecta from up to 3m depth through the instruments of the rover.

While this concept is an attractive payload opportunity for the coming phases of manned lunar exploration, it cannot, as it stands, be used to establish a global network of geochemical impactors. The spatial extent between the different sites is too large to allow a clustering of several sites into a single lander mission.

### **d) No horizontal deceleration**

The last option is to not use any deceleration mechanism and to develop a system that is able to attenuate the shock of impact for a velocity of around  $1700\text{m/s}$ . This speed corresponds to those of Kinetic Energy Penetrators (KEP), a type of ammunition. The



technology to assure the survival of the shell (or the carrier) can be derived from the field of weapon technology. A typical KEP design uses tungsten carbide or depleted uranium as projectile material (Trueman et al., 2004).

While the carrier structure can be adapted to these high velocity impacts, it is unlikely that sensitive scientific instrument payloads could withstand the decelerations. A penetrator that complies with such high impact velocities will only carry a reduced payload package, which is certainly not able to perform geochemical measurements as identified above.

### **Conclusions**

The study showed that the only technical valid option for the deceleration of the system is the use of a de-orbiting propulsion. The second concept, using a tether, does not lead to reasonable reduction of the speed, while the third does not comply with the mission objectives. The option to let the penetrator impact with a high horizontal velocity will reduce the range of scientific instruments.

An actively decelerated system will eliminate the horizontal velocity. Table 7 lists the velocity components used for the further study.

*Table 7: Velocity components used for the study*

<b><i>Component</i></b>	<b><i>Speed [m/s]</i></b>
Vertical velocity $v_z$	360
Horizontal velocity $v_{x/y1}$	0

### **5.1.2 Soil properties**

In order to simulate and analyze the impact processes onto the lunar surface, it will be necessary to establish a soil model with specific parameters. In the following section, we will discuss the needed parameters for our model.

Two processes dominate the creation of the lunar soil: volcanism and high-velocity impacts of (micro-) meteoroids. While the first was more dominant on the mare regions of the Moon, the second process appears on the global scale of the surface. It is estimated that the whole lunar surface is covered with a layer of several meters to tens of meters of loose regolith resulting from the permanent space weathering of micrometeoroids (Vaniman et al., 1991b). This fact has a big advantage for the modeling of surface processes (such as high-velocity impacts): there is no distinct simulation necessary for Mare-type terrain and Highland-type terrain, because from a geomorphologic point of view, both surface types can be considered to be the same in the first meters of the surface above the bedrock. However, contrarily to Earth, there is a complete lack of aqueous erosion and weathering, which makes it difficult to find adequate simulants for lunar soil on Earth.

The Apollo astronauts and Russian robots brought back some 382kg of samples of the lunar soil to Earth (Vaniman et al., 1991). In addition to that, and more important for this study, numerous soil experiments were performed on the surface to determine the in-situ properties of the soil that are needed for geotechnical engineering. However, many questions about the soil's characteristics remain, and the samples represent only a small fraction of all existing soil forms on the Moon. The samples that researchers on Earth had at their disposition were small in quantities, which made it difficult to perform geotechnical tests since those require normally larger quantities of soil. Still, this geotechnical data is needed to establish a model of the surface characteristics to predict the impact process of a penetrator. In this section, we review different sources on the soil data and derive a set of parameters to model the soil of the Moon. Some of the parameters reported in the literature are derived from measurements on actual lunar soil. Others, such as the Elastic Modulus, Poisson's ratio and Bulk modulus needed to be derived from tests with lunar stimulant (Khalid et al., 2009). While there certainly might exist differences between these simulants and the real soil on the Moon, this data, nevertheless, is a close approach to the lunar reality. We discuss

potential differences between the model based on this data and the reality in this chapter.

#### **a) Soil density**

Before the first human landings confirmed our current understanding of the characteristics of the lunar soil, many speculations circulated about its nature, and its dangers. An anecdote which illustrates this dilemma was that the first Apollo Lunar Modules (LM) disposed of an extendable antenna, which would have made it possible to communicate with Earth even in the case where the lander would have sunken into the soil. Although the previous robotic missions sent back a large amount of data on the soil's density, scientists feared that the soil could not withstand the load of the lander and that the vehicle would sink into it.

The bulk density is one of the soil's prime parameters which can only be measured precisely in-situ. Observations from the Surveyor missions indicated a soil density of about  $2.4\text{g/cm}^3$  to  $3.1\text{g/cm}^3$  (Scott, 1970). Returned core tube samples from Apollo 11 to 14 gave some further estimation of the soil's density, but the samples are known to have been compressed, if initially loose, through the sampling process. And, if the soil was initially dense, the sample would have been loosened through the shearing action of the sampling tool. Both processes led to higher or lower figures for the soil density measured on Earth than those which can be expected on the Moon. The best estimates that were achieved through returned samples state a soil density between  $0.75\text{g/cm}^3$  to  $1.75\text{g/cm}^3$  for the Apollo 11 site,  $1.6\text{g/cm}^3$  to  $2.0\text{g/cm}^3$  for the Apollo 12 site, and  $1.45\text{g/cm}^3$  to  $1.6\text{g/cm}^3$  for the Apollo 14 site (Carrier et al., 1991). The rotary drill on the Russian Luna 16 lander also delivered a sample, whose density was estimated at around  $1.2\text{g/cm}^3$ , back to Earth. The modification of the soil led to a compression in length of the sample, which makes it difficult to establish a depth dependant model of the bulk density. These measurements were improved with a novel kind of sampling drill onboard Apollo 15 to 17. The drill's wall was thinner, while its diameter was larger, which reduced the disturbance of the core through the sampling process. The densities on the Apollo 15 site was consequently estimated at  $1.36\text{g/cm}^3$  to  $1.85\text{g/cm}^3$ , the one of Apollo 16 was  $1.40\text{g/cm}^3$  to  $1.80\text{g/cm}^3$ , and the Apollo 17 site  $1.57\text{g/cm}^3$  to

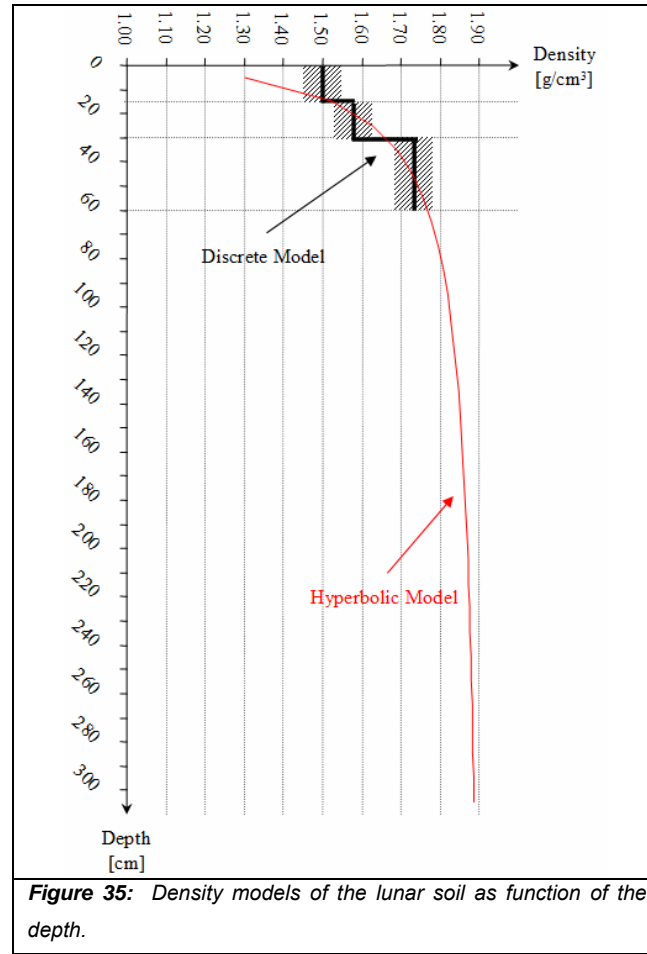
2.29g/cm<sup>3</sup>. These values are estimated to be representative for the in-situ densities on the lunar soil.

Two models for the soil density arose of these studies: a discrete model with specific values for depths up to 60cm, and a continuous model that is based on a hyperbolic relation between the depth and the density (Carrier et al., 1991 and references herein). Table 8 depicts the recommended density values for specific depths. Figure 35 shows these values plotted in a depth-density diagram, together with the hyperbolic curve of the second model as described by Eq. (5.4):

$$\rho = 1.92 \frac{z + 12.2}{z + 18} \quad (5.4)$$

*Table 8: Recommended bulk density values for the lunar soil as function of depth.*

<b><i>Depth [cm]</i></b>	<b><i>Density [g/cm3]</i></b>
0 to 15	1.50 ± 0.05
15 to 30	1.58 ± 0.05
30 to 60	1.74 ± 0.05
<b><i>Consolidated values:</i></b>	
0 to 30	1.58 ± 0.05
0 to 60	1.66 ± 0.05



### **b) Compressibility and compressive strength**

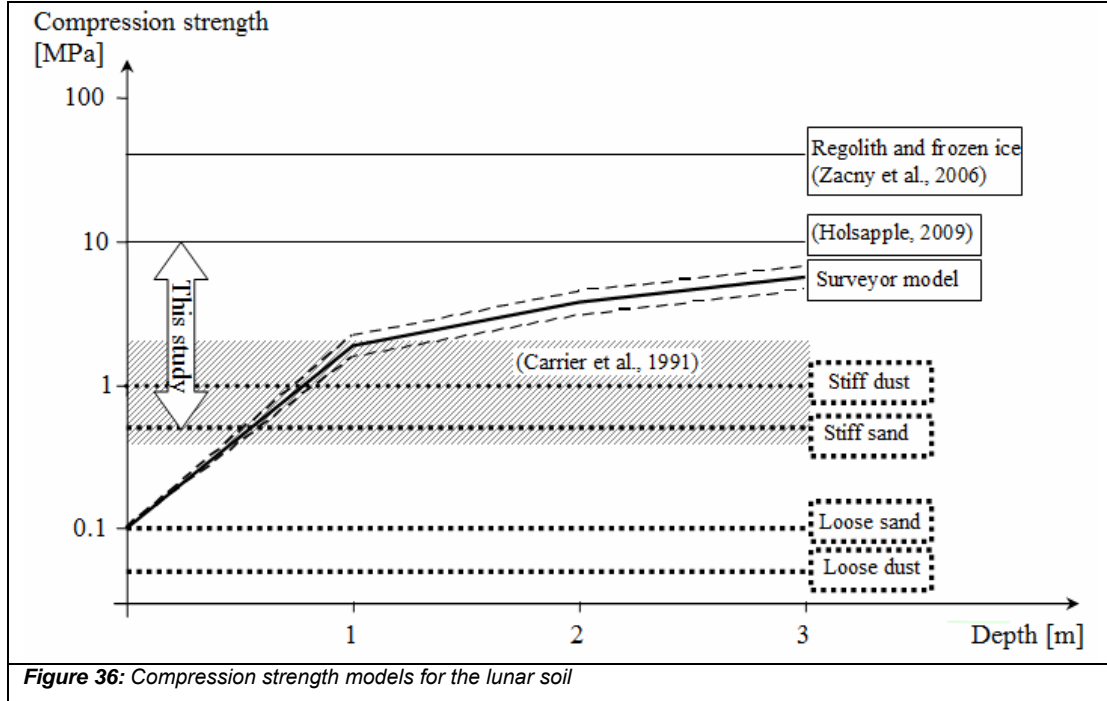
Compressibility describes the volume change when a confining stress is applied to the soil (Carrier et al., 1991). The compression of the soil can be explained by two different phenomena: the slippage and reduction of voids in the soil at a relatively low applied stress, and the particle breakage and reduction of internal voids at higher stress values. The compression is described by the compression index  $C_c$ , which expresses the ratio of change in volume  $\Delta e$  to the change in logarithm of applied vertical stress  $\sigma_v$ . Different experiments were done on returned samples to derive reasonable values for  $C_c$ , which are indicated as recommended values for loose and dense soil in Tab. 8 (Carrier et al., 1991 and references herein).

$$C_c = \frac{\Delta e}{\Delta \log \sigma_v} \quad (5.5)$$

*Table 9: Recommended Compression Indexes.*

<b><i>Constitution</i></b>	<b><i>Compression Index <math>C_c</math></i></b>
Loose	0.3
Dense	0.05

The compressive strength of a material is defined as its capability to withstand a pushing force. When the limit of this strength is reached, the material is compressed, or crushed, to a smaller volume. Impact force histories gained during the Surveyor mission showed a bearing strength of the soil, which is dependent of the depth: its rate is  $1.87 \pm 0.33$  MPa/m (Ball and Lorenz, 1999 with references herein). Carrier et al. (1991 with references herein) list compression strengths of 0.4MPa to 2MPa depending on the mission (Lunar and Apollo) and depending on the location where the penetration measurements were done (intercrater regions showed lower compression strengths than crater walls or sections that are covered with small rocks). Holsapple (2009) uses for his calculations a strength value of 10MPa for regolith. Zacny and co-workers (2006) state a compressive strength for lunar regolith simulant of 40MPa. However, the sample used here was a mixture of ice and regolith and therefore exhibits higher strength values than uncontaminated regolith. Kochan and co-workers (1999) work with compressive strength values for lunar soil that are based on physical analogues on Earth: loose dust = 0.05MPa, loose sand = 0.10MPa, stiff sand = 0.50MPa, and stiff dust = 1.00MPa. Figure 36 shows these different estimations in reference to the depth model of the Surveyor measurements (Ball and Lorenz, 1999). For the following study, we use a minimum value for the compression strength of 0.5MPa (stiff sand) to a maximum value of 10MPa (Holsapple, 2009)



### c) Shear Strength

The shear strength is the combination of the soil's cohesion and the perpendicular component of the normal stress that is applied to the surface. Its estimation for the lunar soil is based on various in-situ experiments that were done in the frame of the Apollo program and the Russian Luna robots. Tests on samples returned to Earth also delivered data for the shear modulus of lunar soil. However, these samples were highly disturbed artificially (sieving and re-compaction) and altered naturally (through the increased gravity on Earth during the measurements). The in-situ experiments however, were refined throughout the Apollo program, crowned by the deployment of the Self-Recording Penetrometer (SRP) used in Apollo 15 and 16.

The Mohr-Coulomb Eq. (5.6) indicates the components of the shear strength  $\tau$ : cohesion  $c$  and friction angle or angle of repose  $\Phi$ ,

$$\tau = c + \sigma \tan \Phi \quad (5.6)$$

where  $\sigma$  is the normal stress perpendicular to the failure surface. Table 10 depicts the best in-situ estimates for the cohesion and friction angle based on the data reported in Carrier et al. (1991). Higher shear strength values correspond to higher relative densities of the soil. The measurement location in terms of geological history furthermore influences the shear strength. The Lunokhod robots performed

penetrometer measurements on the crater walls, crater floor and inter-crater areas which each showed specific values for cohesion and friction angle.

*Table 10: Recommended values for the cohesion and the friction angle as function of the penetration depth. Both values are used to derive the shear strength as indicated in Eq. (5.6).*

<b>Depth [cm]</b>	<b>Cohesion <math>c</math> [kPa]</b>		<b>Fiction Angle <math>\Phi</math> [°]</b>	
	Average	Range	Average	Range
0 to 15	0.52	0.44 – 0.62	42	41 - 43
15 to 30	0.90	0.74 – 1.10	46	44 - 47
30 to 60	3.00	2.4 – 3.8	54	52 - 55
<b>Consolidated values:</b>				
0 to 30	0.90	0.74 – 1.10	46	44 – 47
0 to 60	1.60	1.3 – 1.9	49	48 - 51

Khalid et al., (2009) evaluated the geotechnical properties of NASA's lunar soil simulant JRC-1A. Their data reveals that the shear modulus approaches a maximum value with rising confining pressure. Figure 37 shows the plot of their values (symbols) for two sample densities and the approximated function-curve (dashed). For the simulations, we will use the maximum value of the higher density curve of the experimental results in Khalid et al., namely a shear modulus  $G$  of 27.9MPa.

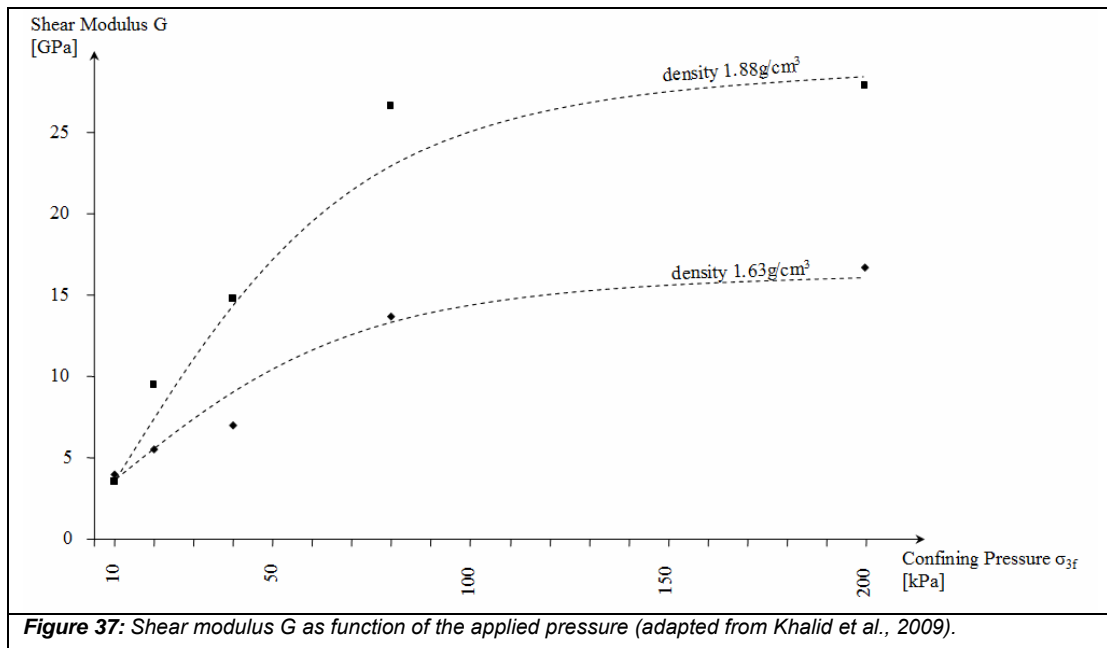
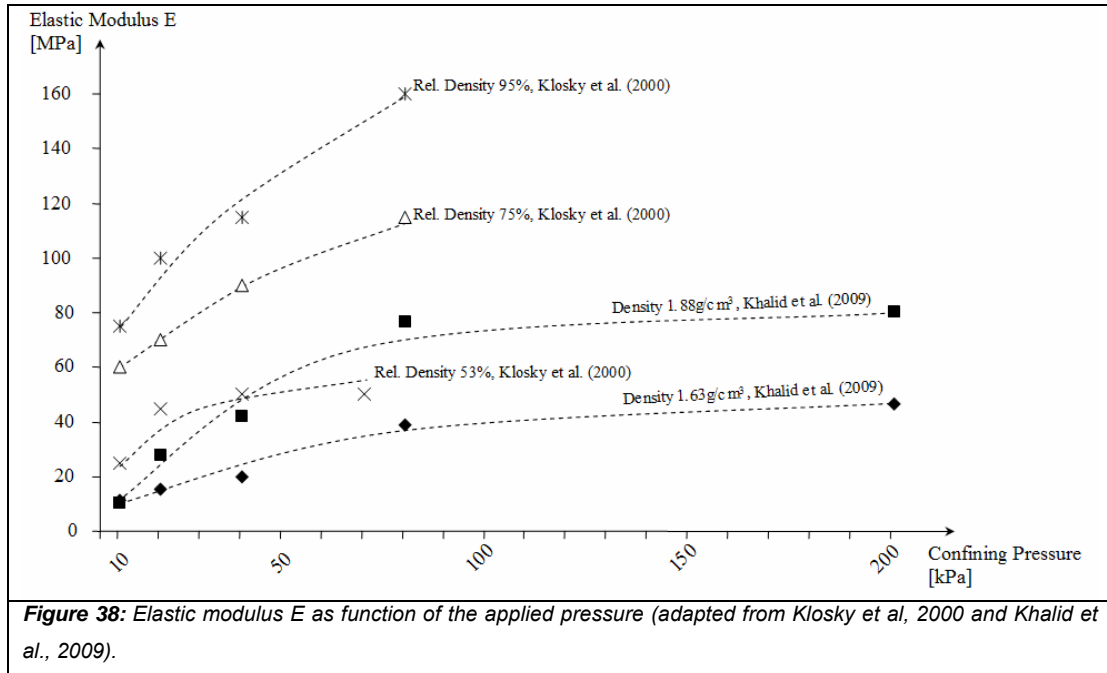


**Figure 37:** Shear modulus  $G$  as function of the applied pressure (adapted from Khalid et al., 2009).



#### d) Young's Modulus

To simulate the strain and displacement behavior of the lunar soil, Young's modulus  $E$  and the bulk modulus  $K$  are needed as elastic constants. These values are gained through experiments with triaxial compression tests. Little data can be found on the determination of these parameters on existing soil samples: miniature shear tests were performed by Ronald F. Scott on a 1.1g soil sample returned with the Surveyor 3 scoop (Carrier et al., 1991). Klosky et al. (2000) determined the Young's modulus of lunar regolith simulant (JSC-1) as function of the relative density and confining stress. The values reported by Klosky and co-workers are significantly higher than those reported by Khalid et al. (2009) under identical conditions. Figure 38 shows the two experimental results in comparison. For the following simulations, we use the maximum value of Khalid's experiment of 80MPa for a soil density of  $1.88\text{g/cm}^3$  as Young's modulus  $E$ .



#### e) Poisson's ratio

The Poisson's ratio for the soil can now be calculated from the elastic parameters of the material, namely the shear modulus  $G$  and the Young's modulus  $E$ :

$$\nu = \frac{E}{2G} - 1 \quad (5.7)$$

For the above-assumed values (for the simulation), we get a Poisson's ratio of 0.43, which represents the higher limit of  $\nu$  as stated for sand (0.2 to 0.45). Khalid et al. (2009) calculated ratios between 0.40 to 0.47 for their experiments, with a mean of 0.427.

#### **f) Bulk Modulus**

The bulk modulus  $K$  relates the change in stress to a volumetric strain. For isotropic materials, it can be inferred from the Poisson's ratio and the  $E$  modulus:

$$K = \frac{E}{6(0.5 - \nu)} \quad (5.8)$$

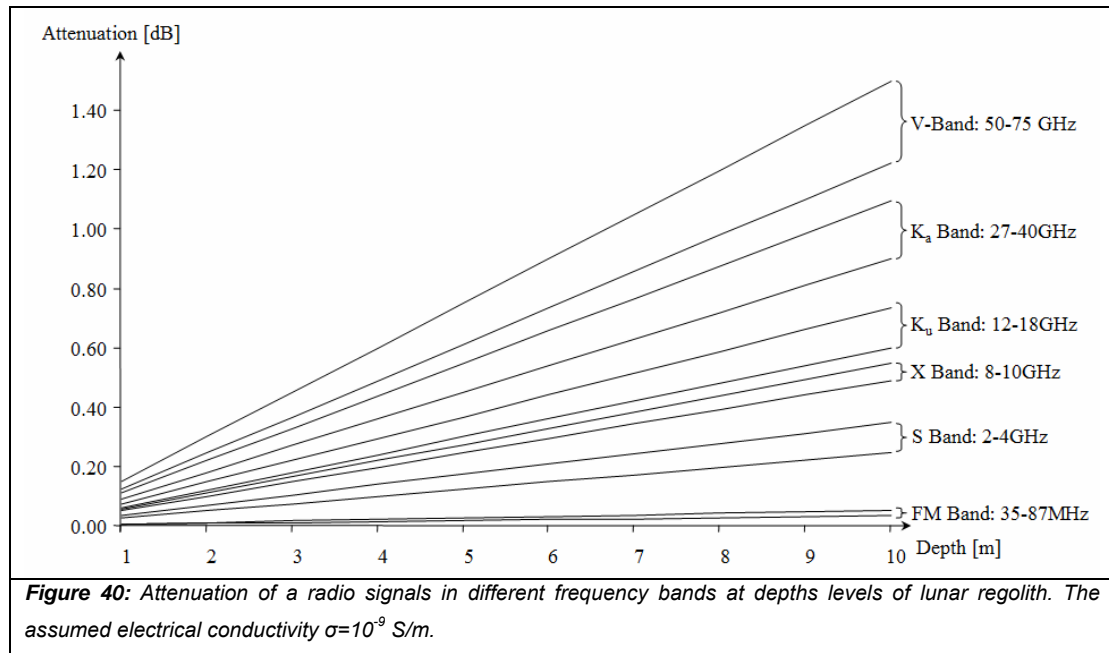
This calculation results in a bulk modulus  $K$  of 190MPa for the above-mentioned data ( $E=80\text{MPa}$  and  $\nu=0.43$ ).

#### **g) Electrical conductivity and resulting radio signal penetration**

Above parameters are related to the mechanical properties of the lunar regolith. It is, however, also necessary to discuss the electrical conductivity of the surface material to estimate to which depth a buried probe can transmit radio signals to an orbiting satellite. The conductivity  $\sigma$  of the lunar regolith is known to be very low (similar to its thermal conductivity). Its values vary from  $10^{-14}$  S/m on sunlit material to  $10^{-9}$  S/m in permanently shadowed areas (Carrier et al., 1991). This characteristic makes it an excellent medium for deep-penetrating radio transmission. The attenuation of a radio signal can be calculated from Eq. (5.9). Fig 40 shows its result at different depth levels of lunar regolith for different frequency bands (the assumed maximum conductivity assumed here is  $\sigma_{\max}=10e^{-9}$  S/m).

$$\text{Attenuation [dB]} = 0.173 \sqrt{f [\text{Hz}] \sigma} d \quad (5.9)$$

The radio signal can, therefore, be relatively low, since little power losses are expected through the penetration of the soil medium. This fact is advantageous for the overall power budget of the probe, which has to be kept low to reduce the size and weight of the batteries.



### Summary of the soil properties

The review of the soil properties above serves to establish penetration models for different impactor shapes. Concluding this review, we will present in Tab. 11 a summary of the identified value ranges and the values that have been chosen for our models.

*Table 11: Summary of the soil parameters and used values for the modeling.*

Parameter	Value or range	Model value	Used in model (see section 5.2.1)
Density	1.50 g/cm <sup>3</sup> (0-15cm)	1.50 g/cm <sup>3</sup>	<i>Holsapple model</i>
	1.58 g/cm <sup>3</sup> (15-30cm)		
	1.74 g/cm <sup>3</sup> (>30cm)	1.74 g/cm <sup>3</sup>	<i>Lagrangian model</i>
Comp. Strength	0.05 MPa to 40 MPa	10 MPa	<i>Holsapple model</i>
Shear Modulus	0 MPa to 27.9 MPa	27.9 MPa	<i>Lagrangian model</i>
Young's Mod.	10.3 MPa to 160 MPa	80 MPa	
Bulk Modulus	190 MPa	190 MPa	<i>Lagrangian model</i>

### **5.1.3 The lunar environment**

The lunar environment itself will add several constraints to the design of the micro-probe. While those will not play a major role in the impact process, those are important for the choice of certain technologies and materials to assure the survival of the system in this, for an Earthling's understanding, harsh environment. In this section, we will review the current knowledge of the environmental parameters on the lunar surface, and its implications for the technologies used. Table 12 shows the main parameters that have to be taken into account for the lunar surface environment.

*Table 12: Recommended values for some of the characteristics of the lunar surface.*

Parameter	Values	Reference
Temperature ranges	-183°C to 123°C	Vaniman et al., 1991b; JAXA, 2009
Surface temperature	-153°C to 107°C	Vaniman et al., 1991b
Gravity (at equator)	1.62m/s <sup>2</sup>	Vaniman et al., 1991b
Ionizing radiation		
Dust adhesion	Metal: 0.02N/cm <sup>2</sup> to 0.03N/cm <sup>2</sup> Painted surfaces: 0.1N/cm <sup>2</sup>	Scott & Zuckerman, 1971

#### **a) Temperature ranges**

Microwave and infrared observations of the Moon from terrestrial observatories allowed quite early estimations about the surface temperature of the Moon and its variations (Pardo et al., 2005). Early on, it was speculated that its range of temperatures might be extreme, ranging from more than minus two hundred degrees Celsius in regions of permanent shadow, to over one hundred degrees Celsius in areas that are permanently lit by sunlight. The Japanese Kaguya satellite revealed that no regions exist that are permanently exposed to the Sun as initially expected (JAXA, 2009). However, craters at the poles are effectively permanently shadowed and exhibit temperatures of around -183°C.

Apart from these temperature extremes, based on the location on the lunar surface, temporal fluctuations of the lunar surface temperature are equally immense. Apollo 15 to 17 left temperature probes on the surface that recorded the change of temperature during the lunar day and night. Those measurements revealed a mean fluctuation of around 280° at equatorial latitudes. Heat flow experiments showed a further very interesting fact: the lunar soil is highly isolating in its first centimeters of depth; the

first 30cm of the lunar soil reduce the fluctuation of  $280^\circ$  to mere  $\pm 3^\circ$  in this depth. This phenomenon bears a clear advantage for insulation problems of lunar equipment: it is sufficient to bury such devices in a depth below the 30cm to protect it from the harsh temperature fluctuations between lunar day and lunar night.

### **b) Gravitation**

The reduced gravitation of  $1.62\text{m/s}^2$  on the lunar surface is another obvious difference to the terrestrial environment. The effect of gravitation was discussed in the previous sections in terms of its influence on the impact speed. However, the gravitation also influences the effectiveness of the transport of material inside the sampling system of the micro-probe: the reduced gravitational force will make particles tend to lift off more easily and fall down and repose slower than on terrestrial applications. In general, less force is needed to lift sample material.

### **c) Ionizing radiation**

The radiation encountered on the lunar surface consists of protons, electrons and some heavier nuclei that originate from the solar winds, solar flares and galactic cosmic rays (Vaniman et al., 1991b). We shall not discuss the source and detection of these particles (a concise summary can be found at Vaniman et al., 1991), but it is worthwhile to mention some of the threats to devices on the lunar surface. Major effects through these nuclei are sputtering on exposed surfaces. Penetrating ions are known to alter semiconductors by ionizing the silicon and silicon oxide layers of these devices. This effect can permanently damage the equipment, or lead to data loss in mass storage media. To protect semiconductor devices, insulating layers of silicon are sometimes applied as an insulator against the incoming radiation. Also, the regolith layer can be used to shield equipment from radiation effects. Silberberg et al. (1985) estimate that 2m regolith shielding is sufficient for the protection of living tissues (astronauts) against solar flares. Table 13 gives a summary of different radiation nuclei, their respective energies and penetration depths.

*Table 13: Summary of different types of ionization radiation at the lunar surface (Vaniman et al., 1991)*

Type	Energy	Penetration Depth
Solar Wind	0.3 to 3keV/u	$\mu\text{m}$
Solar Cosmic Rays	1 to 100MeV/u	mm to cm
Galactic Cosmic Rays	0.1 to 10GeV/u	cm to m

**d) Dust**

One of the major challenges that future human or robotic explorers of the Moon will face is dust. The lunar dust is known to be composed of fine particles, with grain sizes between 45 $\mu\text{m}$  to 100 $\mu\text{m}$ . The grains have sharp features, similar to fresh volcanic ashes on Earth. The dust presents a hazard to human health and sensitive mechanical devices since it adheres to surfaces and accumulates in devices. For robotic equipment, this fact has to be taken into consideration for the design of any mechanism that uses moving parts. The astronauts of Apollo used a specially designed brush to clean their equipment (notably the LRV) and the Russian Lunokhod 2 rover is believed to have been disabled by dust that covered and insulated its radioactive heater (Chaikin, 2004). Scott and Zuckerman (1971) investigated the long-term effects of lunar dust on the sampling mechanism of the Surveyor 3 lander. They report that the dust adheres to metallic surfaces with 0.02N/cm<sup>2</sup> to 0.03N/cm<sup>2</sup> and to painted surfaces 0.1N/cm<sup>2</sup>. This property of the lunar dust will lead to several design guidelines for mechanical devices used in or on the lunar soil:

- (1) Any moving mechanism that is supposed to work over longer periods on the lunar soil should be sealed from the outside surface.
- (2) If appropriate sealing of a mechanism is not possible, then the system should be equipped with an auto-cleaning device that evacuates accumulations of dust at sensitive spots.

**Summary of the environmental parameters**

The review of the lunar environment above serves as frame specification for the design of the carrier system of the penetrators. The above values do not directly influence the modeling of the impact processes (except the gravity). However, factors like the dust, radiation, and temperature ranges will be used as input to the choice of technologies and materials in section 5.3 and chapter 6.

## **5.2 Analysis of the carrier design**

The previous section summarized the main characteristics of the lunar surface and the specifications of the micro-probe system. In the following, we will study different carrier designs. Emphasis will be given on the study of the projectile's shape and its influence on the impact behavior of the probe on the lunar soil. First, the penetration depth will be estimated by two empirical formulas of Young (1997) and Holsapple (1993; 2009). The result of this calculation will be compared with simulations in LS-DYNA of two different probe shapes. The LS-DYNA simulation, however, goes beyond the calculation of the penetration depth:

- 1) It will deliver an estimation of the entry stability of the probe, to see, for example, if the system bounces off at a specific angle of attack.
- 2) It will show the stability of the probe to penetrate through the medium in order to see what its final orientation angle is.
- 3) Although we will use a simplified model of the projectile, it will show the deformation that can be expected at high-velocity impacts.

Based on the results of this work, we will derive an optimal penetrator shape for the impacting micro-probes.

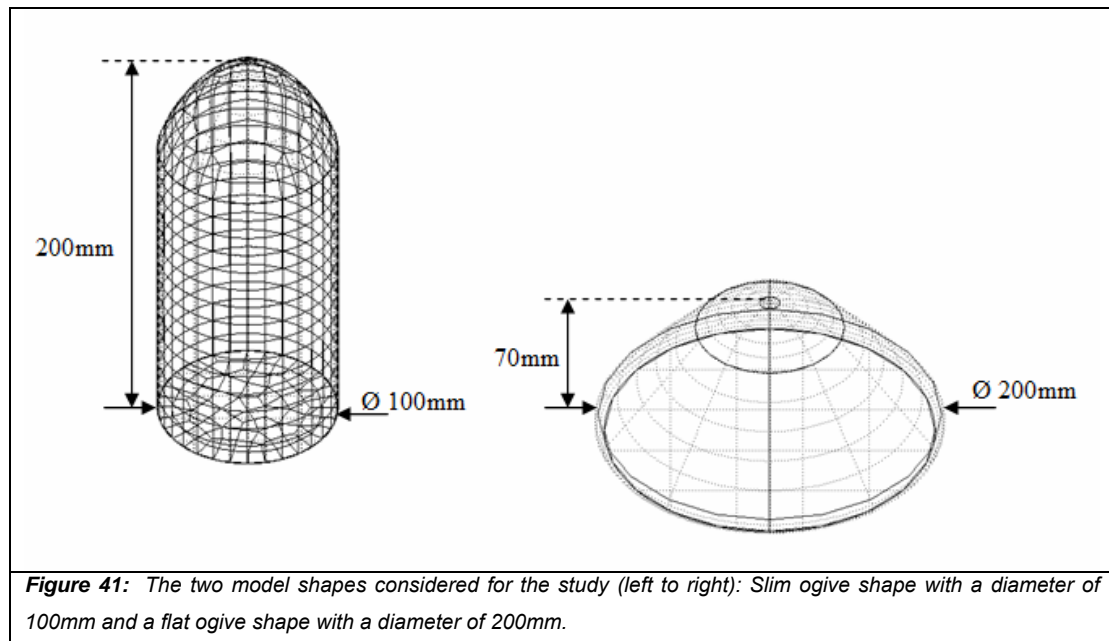
### **5.2.1 Methodology to determine the penetration depths**

The survival of the system and its functionality will be determined by its capability to mechanically withstand the impact on the lunar surface and its burial depth. The latter is an important factor for several reasons. It firstly determines the subsoil layers that the system will reach. The here presented mission concept does not seek to penetrate as deeply as possible into the soil; rather, its objective is to remain at the surface to perform the measurements. The penetration depth will influence the design of the communication system. The microprobes need to be able to communicate with the orbiter even when buried in the soil. However, the electrical conductivity of the regolith is known to be low and will not significantly attenuate the radio communication in the first meters. On the other hand, it is advantageous for the

operation of the probe to penetrate deeper than 30cm in order to insulate the system from large thermal fluctuations. The optimal burial depth is, therefore, below 30cm.

### **The shape of the probe**

The shape of the penetrator determines the penetration capabilities. This development can profit from design studies that were done for penetration systems as mentioned above. In this section, we will evaluate the penetration depth that can be reached by microprobes through different empirical estimations. Two probe shapes were used for the calculations: a 100mm diameter, dart-shaped penetrator with ogive nose-form, and a 200mm diameter, flat penetrator with ogive nose-form. Both models have the same volume and an approximate weight of 5kg<sup>1</sup>. Figure 41 shows the two design concepts with its main parameters.



The impact velocity of the system depends on the deployment altitude and initial velocity that was inherited through the deployment mechanism. For the following study, we assume a vertical velocity ranging from 70m/s to 360m/s. The speeds correspond to a deployment from 1.5km to 40km altitude.

---

<sup>1</sup> This value is assumed considering a filled body using Titanium as reference material. The final weight of the probe will be calculated based on a strawman payload package and a specific thickness for the projectile's walls.



The models were first evaluated using formula frameworks for impact calculations developed by Young (1997) and Holsapple (1993). The equations developed by Young are based on experiments carried out at the Sandia National Laboratories and bring into relation the penetration depth of a ballistic projectile, its geometry and target properties. Holsapple established formulas for an identical purpose, but independent from the projectile's geometry. Those can also be used to estimate the excavated volume of the crater. However, Holsapple's formulas become imprecise for velocities below 1km/s, which is the case in this application.

### **Penetration depths following Young (1997)**

Young (1997) established a mathematical framework of penetration equations based on experimental results at the Sandia National Laboratories. The formulas allow prediction of the penetration depth of a ballistic projectile, based on its geometrical characteristics and the target's properties. The formulas to be used depend on the projectile's shape, velocity and the target properties. Fig. 42 shows the flow chart of these operations derived from Young's work. The penetration depth  $D$  for the impacting system can thus be derived through formula (5.10) with the Young's index of penetrability  $S$  (also "S-Number"), the nose performance coefficient  $N$ , the probe's mass  $m$ , the cross-sectional area  $A$ , its velocity  $V$ , and the mass scaling factor  $K_S$  ( $K_H$  being the factor for hard soil). All variables are either predefined or can be calculated from the formulas given in Fig. 42. Young's index of penetrability can be computed if the compressive strength and quality of the soil is known (Young, 1997). For lunar impact scenarios, there is little sense in trying to compute this value through the formula given by Young, due to the fact that the "quality of soil" cannot be quantified. However, the author states example values for typical soil types, which can be used to set a range of S-numbers for lunar applications. Fig. 40 shows the plot of penetration depths, based on the above-stated probe geometries and velocity ranges. The S-numbers used here were 2 to 9, thus "*2-Dense, dry, cemented sand. Dry caliche. Massive gypsite and selenite deposits.*" to "*9-Moderately dense to loose sand, no cementation, water content not important*" (Young, 1997). It needs to be stated here that it is the determination of a realistic S-number that is the weakness of this approach.

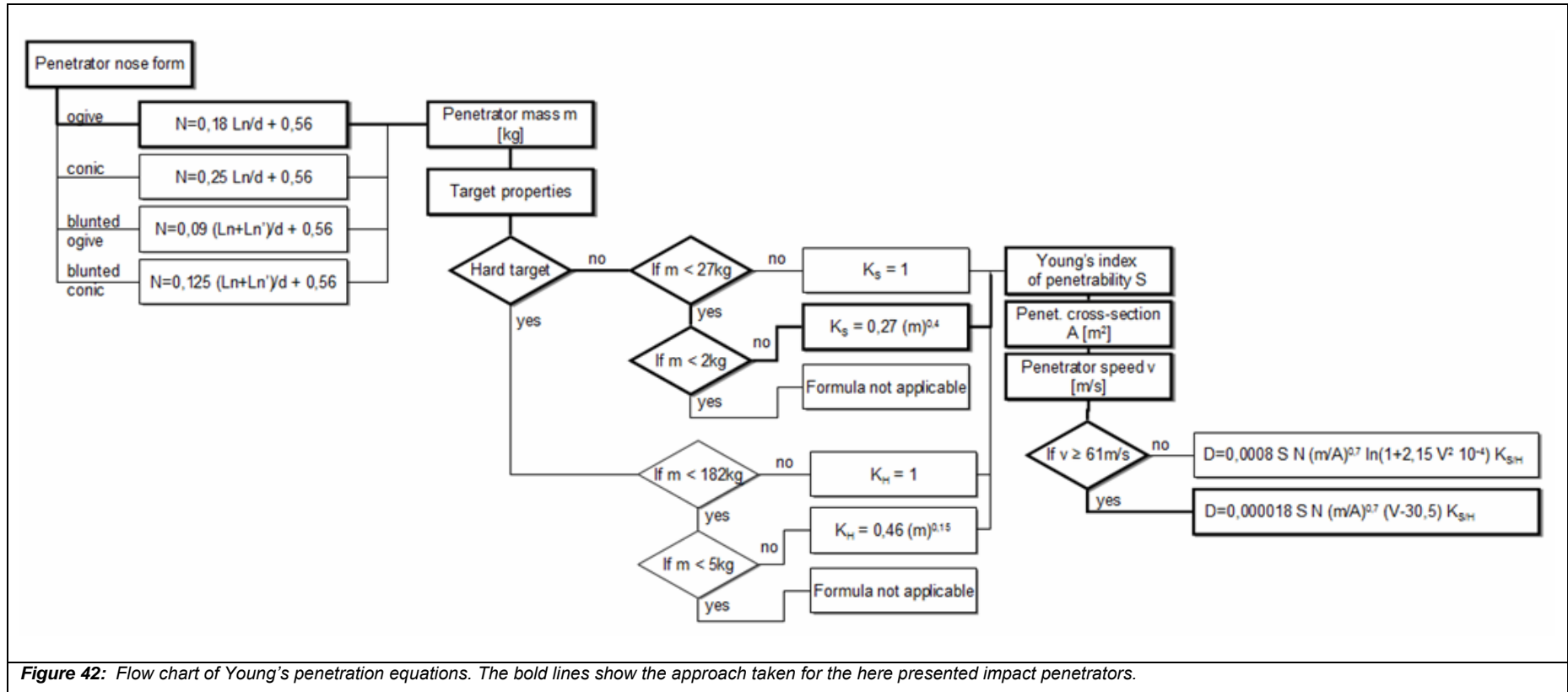
$$D=0,000018 S N (m/A)^{0,7} (V-30,5) K_{S/H} \quad (5.10)$$

The nose performance coefficient  $N$  for ogive nose shapes can be calculated following (5.11), where  $L_n$  is the nose length and  $d$  its diameter.

The nose length for the 100mm diameter ogive shaped penetrator is 50mm, while the one of the flat, ogive shape is 70mm. The mass  $m$  was set to 5kg.

$$N=0,18 L_n/d + 0,56 \quad (5.11)$$

The result of this calculation is presented in Fig. 43, in comparison with the penetration estimation based on Holsapple's formulas. This computation confirms the obvious fact that the slimmer probe shape will penetrate deeper into the soil: the 100mm diameter penetrator will reach depths up to 1,1m, depending on the soil's penetrability, while it can be expected that the flat shaped, 250mm diameter penetrator will not go beyond 30cm at maximum speed.



**Penetration depths following Holsapple (1993)**

Holsapple (1993) uses another method to calculate the parameters of high-velocity impact crater formation, which is of particular interest if the crater shape and excavated volume need to be calculated. However, the Holsapple's Scaling Laws fit impact speeds above 1km/s, such as those which occur in collisions between natural solar system objects. The speeds are beyond the velocity ranges of artificial impacts discussed here and, therefore, can only be used as rough estimation (i.e. Holsapple's formula does not take into consideration the shape of the projectile since it uses a point-source for the impact). It is nevertheless reported that the Scaling Law for the hypervelocity impacts fits experimental data from older experiments with lower velocities by Worthington (see references in Holsapple; 1993).

Holsapple derives the impact crater shape through a cratering efficiency factor  $\pi_v$  which includes a gravity-scaled size parameter  $\pi_2$  and the soil strength group  $\pi_3$ . All three factors are dimensionless.

$$\pi_v = K_1 \left\{ \pi_2 \left( \frac{\rho}{\delta} \right)^{\frac{6v-2-\mu}{3\mu}} + \left[ K_2 \pi_3 \left( \frac{\rho}{\delta} \right)^{\frac{6v-2}{3\mu}} \right]^{\frac{2+\mu}{2}} \right\}^{\frac{3\mu}{2+\mu}} \quad (5.12)$$

The factors  $K_1$ ,  $K_2$ ,  $v$  and  $\mu$  are target dependent. The values for lunar regolith are reported with Holsapple (1993), namely  $K_1=0.132$ ,  $K_2=0.26$ ,  $v=0.33$  and  $\mu=0.41$  which were used for the following calculations. The ratio  $\rho$  to  $\delta$  is the density ration of the target to the penetrator. The gravity-scaled size parameter  $\pi_2$  is calculated through the surface gravity  $g$ , penetrator radius  $a$  and its velocity  $v$ . The results presented in Figure 43 are based on the values stated for the 100mm diameter penetrator.

$$\pi_2 = \frac{g a}{v^2} \quad (5.13)$$

The soil strength group  $\pi_3$  combines the target strength, its density  $\rho$  and the penetrator's speed  $v$ . The target density suggested by Holsapple for lunar soil was 1,5g/cm<sup>3</sup>. In our calculation, we use the consolidated value of 1.66g/cm<sup>3</sup> for a depth between (0-60cm) as found above.

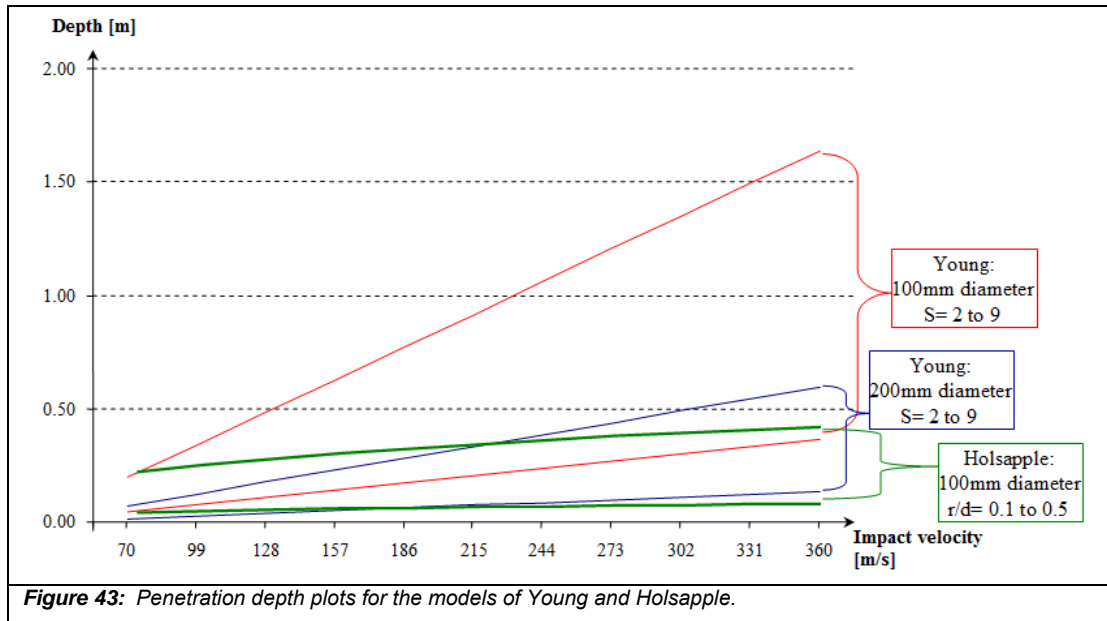
$$\pi_3 = \frac{Y}{\rho v^2} \quad (5.14)$$

The volume of crater excavation can now be derived through its relation to the cratering efficiency in formula (5.13). The relation of the cavity radius to the excavation volume of the crater is presented in formula (5.14).

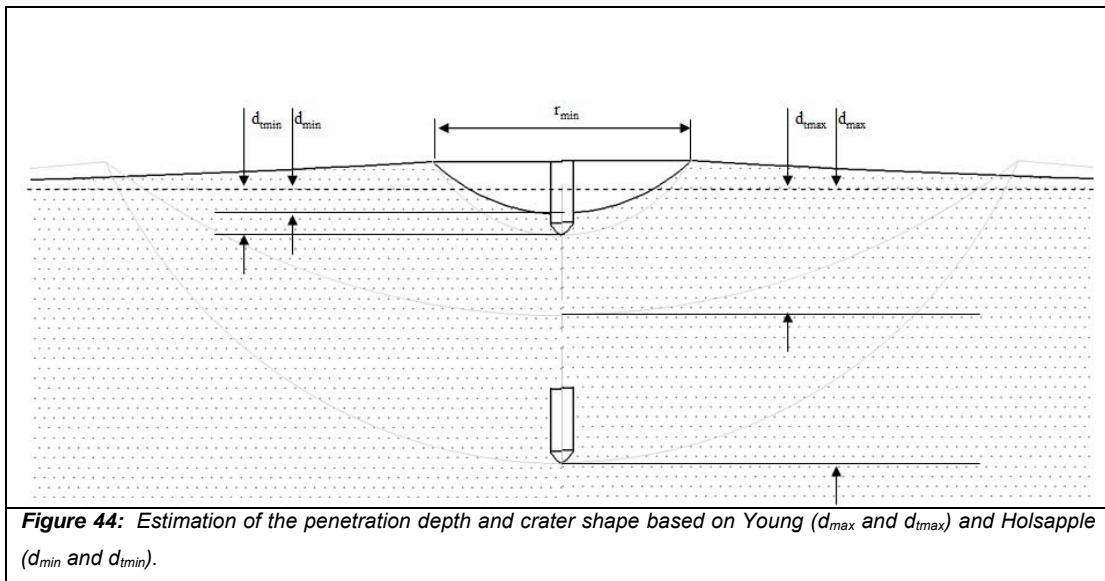
$$V = \frac{\pi_V m}{\rho} \quad (5.15)$$

$$r = 1,33 V^{0,33} \quad (5.16)$$

The maximal impact depth is reached prior to the maximal radial growth (McKay et al., 1991). It is for this reason that the crater floor rebounds, and is filled with ejecta and material from the collapsing walls. Consequently, it is hard to define a realistic relationship between the cavity radius and its final depth. The ratio between  $r$  and  $d$  varies, following the literature, from 0.1 to 0.5 (Holsapple, 1993; McKay, et al., 1991 and references herein). Both values are used as range limits in the results presented in Fig. 43.



The crater shape parameters are shown in scale in Fig. 44. The figure indicates in scale the two depths for the estimations of Holsapple (minimum) and the Young formula (maximum), where  $d_{\min/\max}$  is the primary penetration depth and  $d_{\text{tmin/max}}$  is the final depth of the crater (taking into account the refill of the cavity with ejecta material).



### **5.2.2 Impact behavior simulation in hydrocode**

Following the empirical estimations of the penetration depth by the formula of Young and Holsapple, a model in LS-DYNA® was built to simulate the impact of the probe. Using such model bears not only the possibility to calculate the simulation depth, but also to evaluate the penetration behavior of the probe (i.e. under different angles of attack). Conclusions can, therefore, be made of the capability of the system to perform satisfactorily even if the probe impacts with a horizontal speed or on surface slopes. Kinetic penetrator simulations are a domain typically found in military applications, and various tools are used nowadays in this field to simulate the behavior of projectiles on different targets. LS-DYNA is an explicit finite element code processor to analyze large deformations in structures. Structural and soil deformations, as those that will occur in high velocity impacts, cannot be simulated with implicit calculation methods.

#### **5.2.2.1 A soil model for impact simulations**

The challenge in impact simulations is the definition of the model for the soil: geotechnical parameters need to be translated into engineering parameters; both fields of science do not have identical definitions for material behavior. Soil models are normally based on the pressure dependant yield surfaces (Mohr-Coulomb) while metallic structures are modeled based on the Von Mises yield behavior. Secondly, we have very little knowledge about the properties of the lunar soil. The data is limited to the experiments of the Apollo program and the Russian and American robotics landers. Some results could be obtained by experiments on Earth that were performed on returned lunar soil samples, but the quantity of these soils and their potential alternation during the return flight limited the scale of possible experiments. Furthermore, our “ground-truth” knowledge is limited a restrained region of the Moon (see precedent discussions), with little or no information about the soil characteristics in the highlands and the poles, for example. The samples were retrieved from depths up to 3m; the properties beyond this depth can only be assumed and have not been verified in-situ as yet. For these reasons, it must be borne in mind that the following simulations that are based on the models that are derived from the current understanding of the lunar soil.

The soil was modeled in LS-DYNA in a Lagrangian model. The different projectile shapes were impacted on a cylindrical soil model of a diameter of 700mm and a depth of 2000mm. The soil model has 10 000 nodes. Its total size and mesh size were chosen in function of the calculation capabilities of the time of calculation necessary for each run. Figure 45 shows the upper part of the soil model with the large ogive probe in its initial position. The projectile body was defined as a rigid body in the first penetration tests. That means, while the soil was subject to deformations, the projectile's shape did not change. Large deformations as those will appear during the impact and will lead to tangling of the mesh nodes (which would, at a certain extent, stop the simulation). An erosion criterion was therefore introduced, which eliminates cells that exhibit a too large strain. In the following models, this erosion factor was set to 60% of the shear strain at failure (see Fig. 46.). The drawback of this method is that compaction and friction between the projectile and the soil are reduced. This leads to higher penetration depths.

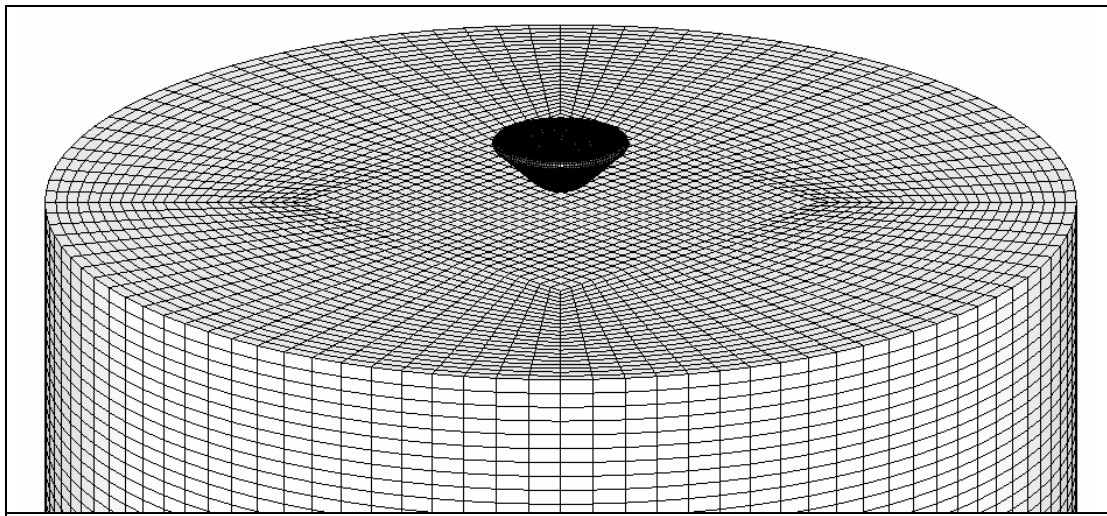
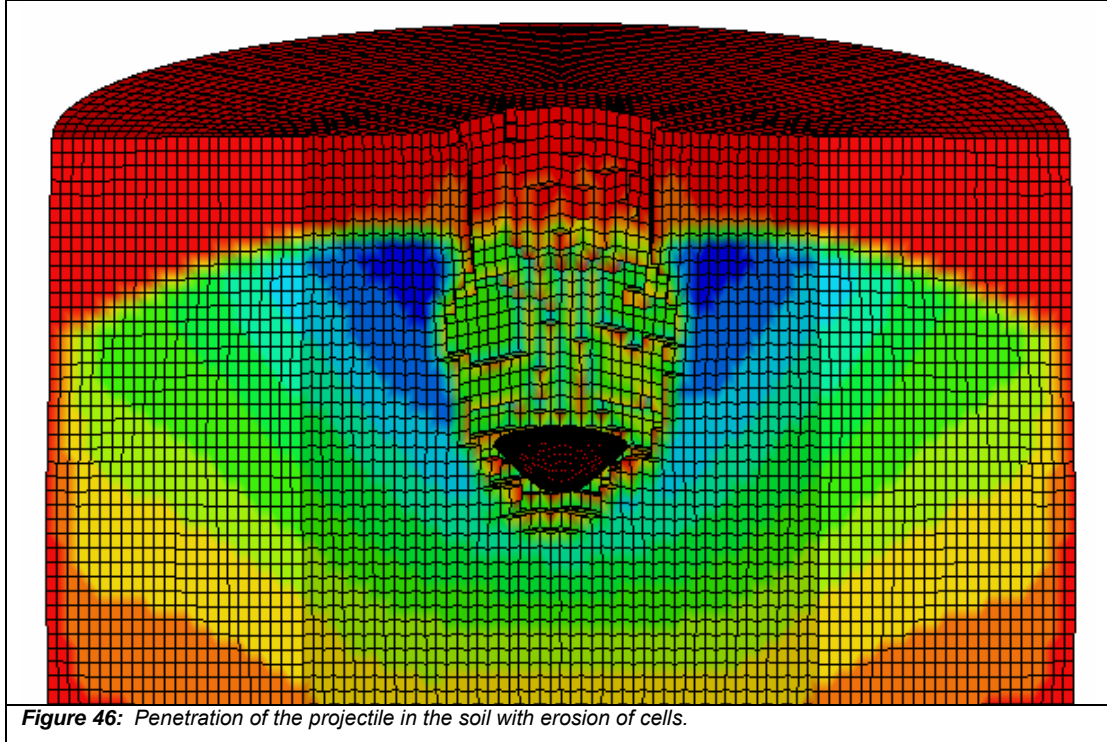


**Figure 45:** Model of the lunar soil in LS-DYNA.





Several soil models are available in LS-DYNA: Reid et al. (2004) evaluate LS-DYNA soil model 147-MAT-FHWA\_SOIL. The model is an isotropic material with a modified Mohr-Coulomb surface for the simulation of roadside safety structures (LSTC, 2007). Hayward (2007) uses soil model 014-MAT-SOIL\_AND\_FOAM\_FAILURE to perform penetration tests of a micro-dart into Martian soil. Following a communication with LSTC, we have chosen a basic soil model for our simulations: 005-MAT-SOIL\_AND\_FOAM. Its behavior is, to some extent similar to the behavior of a fluid. Its advantage for lunar soil simulation is that it works with a limited number of defined soil parameters.

Consistent units are defined throughout the model in order to assure its functionality. In our simulations all units are expressed in millimeter, milliseconds, kilogram, kilonewton, and giga-Pascal. The soil parameters of model 005 are shown in Tab. 14.

*Table 14.: Soil parameters with its units used for the lunar soil model 005-SOIL AND FOAM in LS-DYNA.*

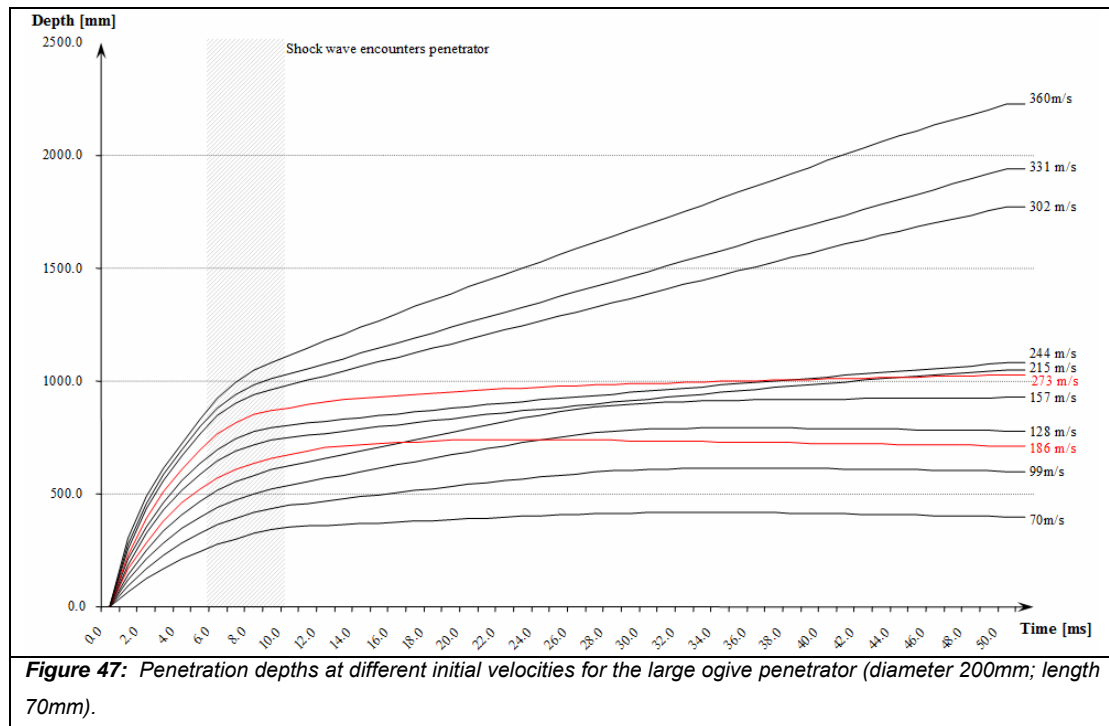
Mass density	1.74e-6 kg/mm <sup>3</sup>
Shear Modulus	0.0279 GPa
Bulk Modulus	0.19 GPa

### 5.2.2.2 Penetration depth and impact behavior

A series of simulations was run in LS-DYNA to evaluate the penetration behavior of the projectiles into the soil. The two shapes as shown in Fig. 41 were used. Its values can be compared with the results from Young's and Holsapple's formula. LS-DYNA offers the possibility to follow a specific node's trajectory and trace its displacement. The penetration curves were retrieved by plotting the vertical displacement (y-direction in the model) over the time.

#### Ogive probe 200mm diameter, 70mm length

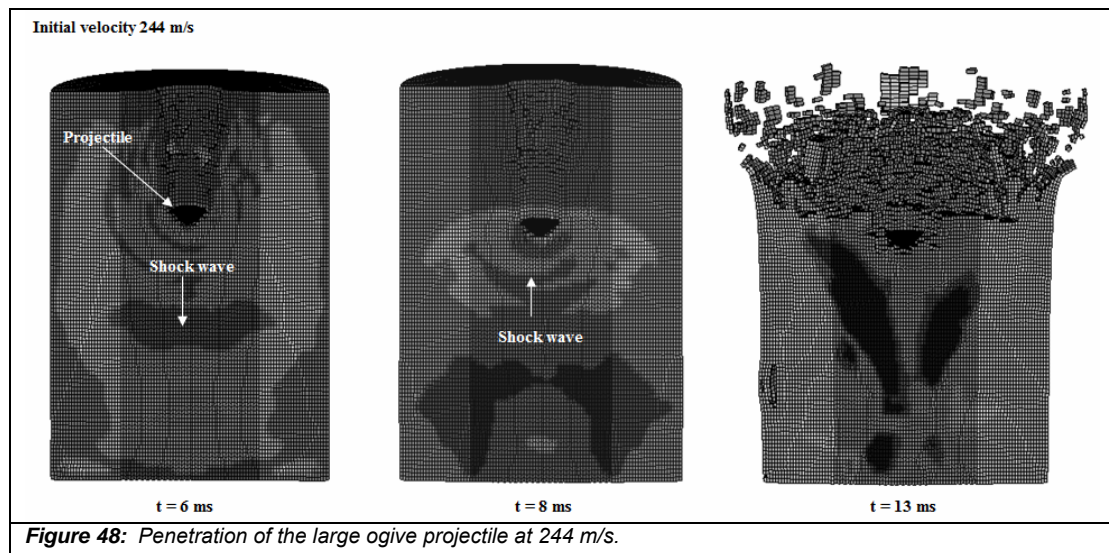
The first simulations were run with the larger projectile: the 200mm diameter 70mm length probe. Fig 47 shows the penetration results for increasing initial speeds.



The graph shows, in the majority of the measurements, a constant increase of penetration depth with increasing initial velocity. However, the penetration depths are much lower, as expected, at the speeds of 186m/s and 273m/s. This effect is related to the modeling of the soil. The progress of the projectile can be separated into two phases: (i) The initial penetration of the projectile where the acoustic shock wave travels in the same direction as the projectile at the velocity of sound of the material, and (ii) the crater forming phase where the shockwave was reflected by underlying

material (in our model, the boundaries of the soil model) and ultimately lifts off the surface material of the soil. One first observation is that the shock wave is not scattered back in the two cases where the penetration depths are inferior to the expected ones (186m/s and 273m/s). In an additional model, side walls were modeled around the walls and bottom of the soil, to force the shock wave to be reflected to the upper part of the cylinder. Figure 49 shows the penetration depths of an impactor with a speed of 70m/s and 186m/s in the enclosed soil model. The chart reveals the effect of the uplifted material on the probe's penetration. In the case of the 70m/s impact the probe is lifted out of the model (no gravity is implemented in the model, which means that, in reality, the material and the probe would fall back into the cavity). A third model was created where the soil cylinder has a height of 5m. The penetration depths at 70m/s and 186m/s are also shown in Fig. 49. It can be seen that the cylinder shape has, in these ranges, little influence on the penetration behavior. The probes reach identical final depths like the 3m model.

The five meter model certainly approaches more the reality that can be found on the lunar surface (it is expected that the regolith depth varies on the Moon between 5m and 20m). However, the larger model requires significantly more computation time and its results are similar to the ones of the 3m model.



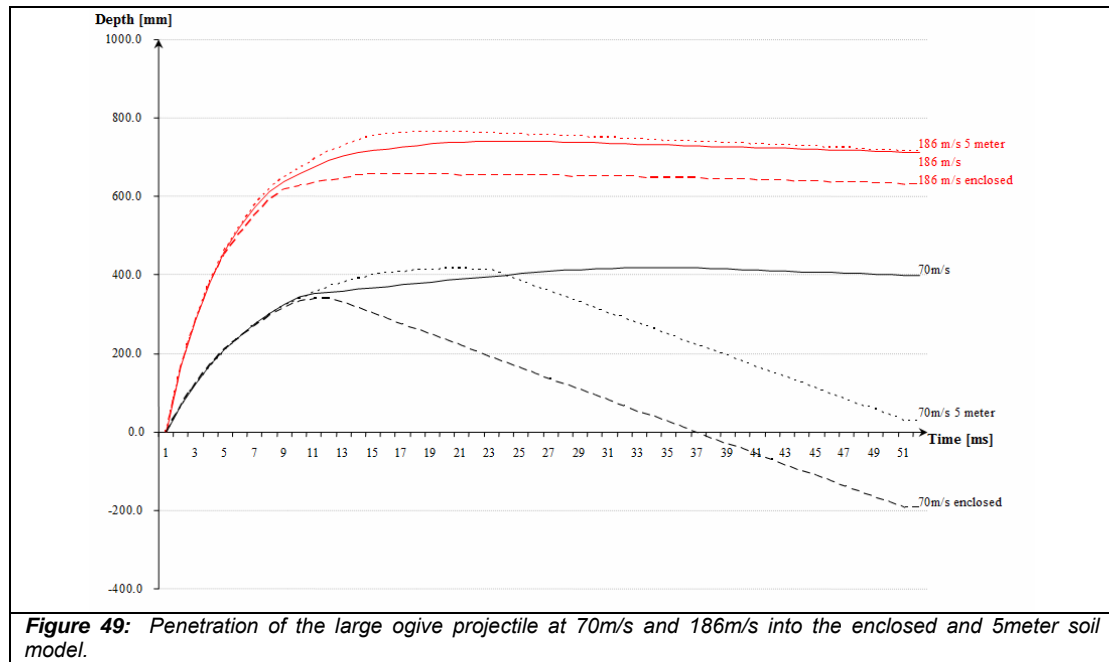
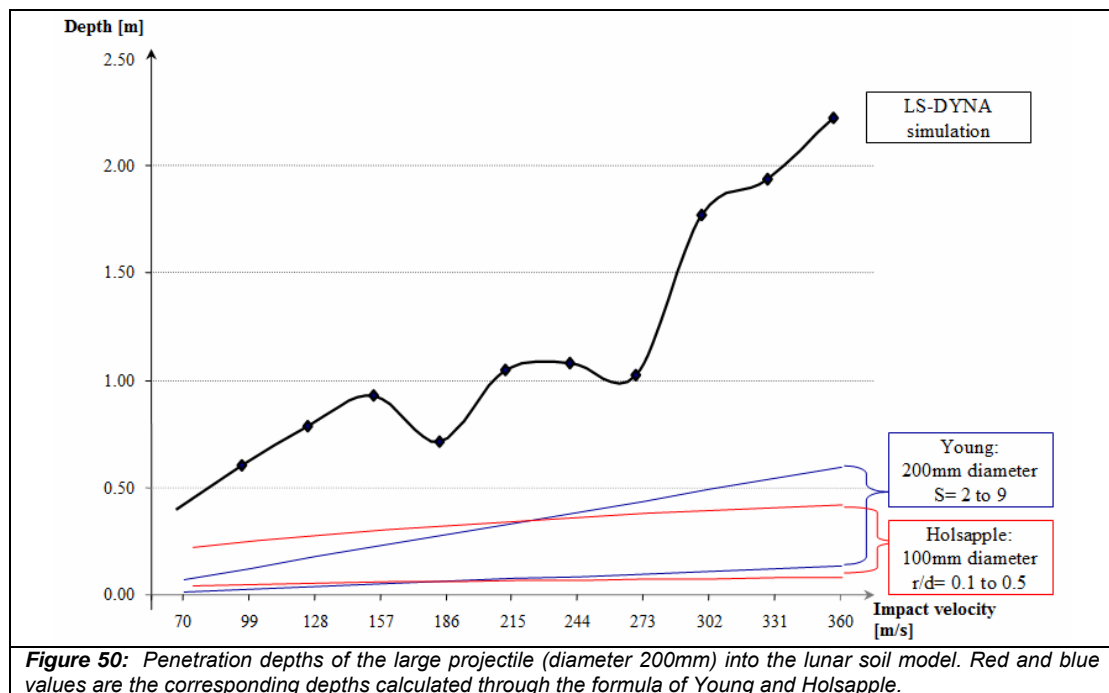


Figure 50 shows the penetration profile of the large projectile obtained by LS-DYNA in comparison to the previously calculated data through the formula of Young and Holsapple. The final penetration depth varies with the definition of the erosion factor (set to be 60% of the shear strain at failure; see section 5.2.2.1). The penetration values of LS-DYNA are above the ones calculated by the formula. However, those depths approach previously estimated values by Smith et al., (2009) for a similar probe deployment.



### Ogive probe 100m diameter, 200mm length

The slim shaped probe (diameter 100mm, length 200mm) was tested in a second series of penetration simulations. Figure 51 plots the penetration profiles of the projectile at different impact velocities. The graphs show a constant increase of the final penetration depth with increasing velocity. At 244m/s, the projectile diverts from its vertical path. Similar observations can be made for the speeds of 302m/s, 331m/s and 360m/s. The probes reach lower penetration depths at these speeds, as expected, from the precedent plots. Figure 52 depicts the path of the probe and its orientation during impact. As it can be seen, the probe diverts from its initial vertical orientation and comes to a rest at a horizontal position. The nose of the probe was blunted to improve the ricochet resistance of the probe. The same simulation was done with the penetrator at impact speeds of 244m/s and 360m/s. The blunted nose improved the projectile's capability to remain on the horizontal penetration path and led consequently to higher penetration depths for these probes (see blue graphs in Fig. 51).

Figure 53 plots the penetration depths of the slim projectile shape in comparison to the previously calculated impact profiles by the formulas of Young and Holsapple.

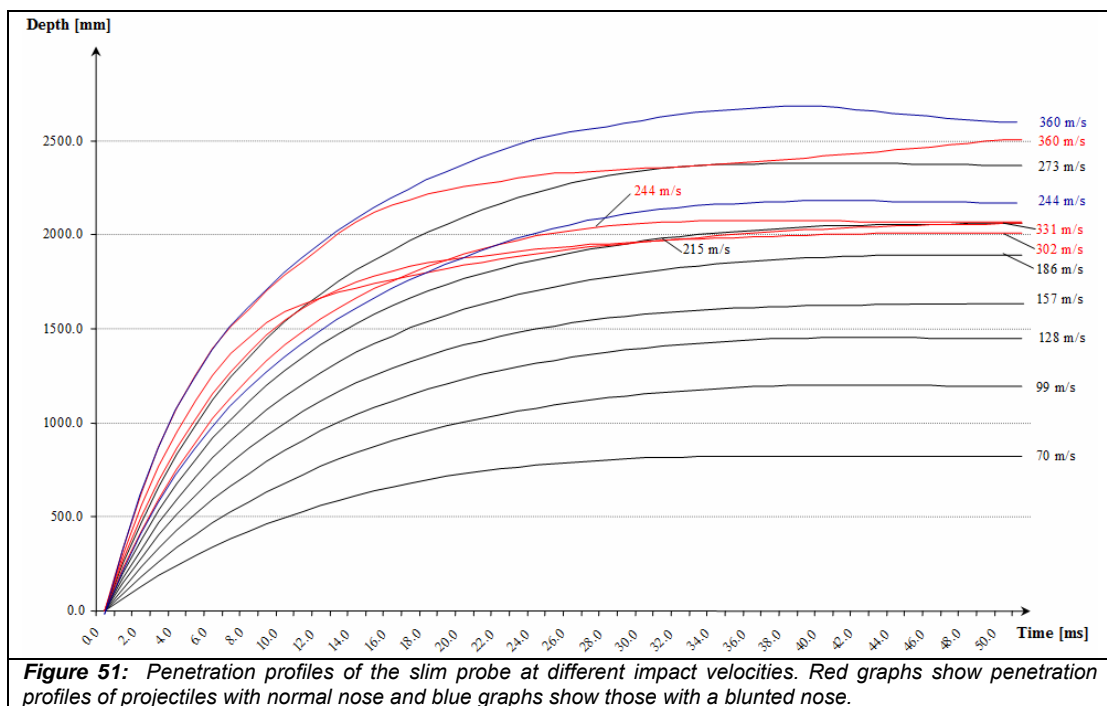


**Figure 51:** Penetration profiles of the slim probe at different impact velocities. Red graphs show penetration profiles of projectiles with normal nose and blue graphs show those with a blunted nose.

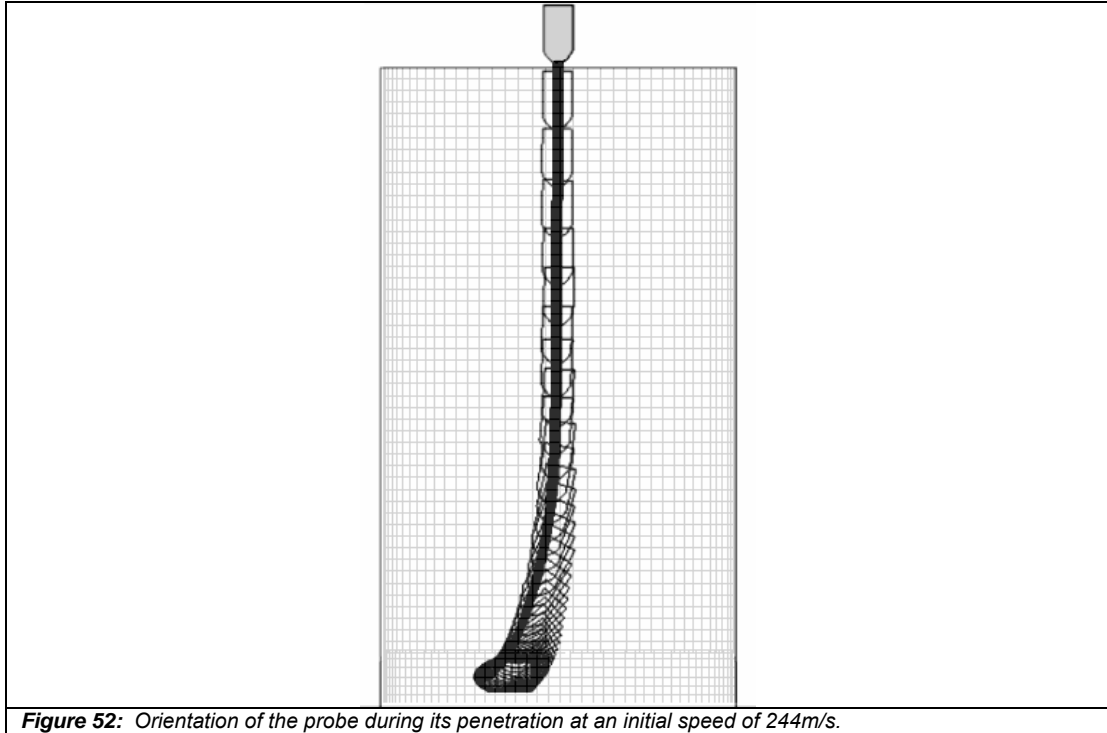


**Figure 52:** Orientation of the probe during its penetration at an initial speed of 244m/s.

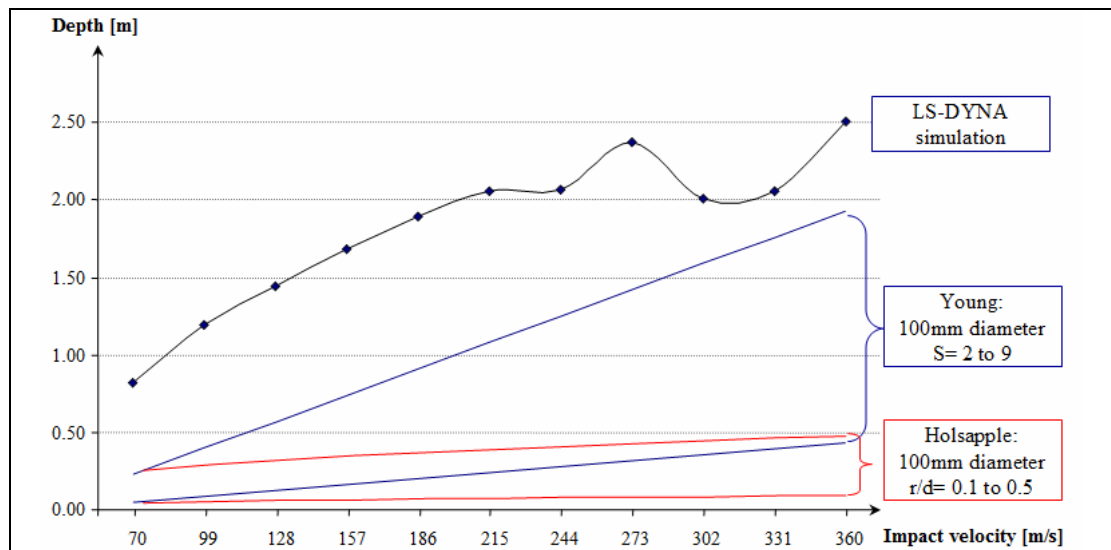


**Figure 53:** Penetration depths of the slim projectile (diameter 100mm, length 200mm) into the lunar soil model. Red and blue lines are the profiles calculated from Young's and Holsapple's formula.

### 5.2.2.3 Impact behavior

The impact behavior of the projectile was evaluated under different angles of attack AOA (which is the angle between the surface and the direction of flight of the probe). The interest of this study is to evaluate the bounce-off behavior of the probe; it must be assured that the probe's body is buried in the soil.



Simulations were run under changing AOA to determine the angle under which the different probes bounce off the surface. Figure 54 shows the result with an AOA of  $40^\circ$  for both probe shapes. In both cases, the probe remains buried in the soil after impact (although the penetration depth remains shallow).

Beyond an angle of  $40^\circ$ , the large diameter probe bounces off the surface as shown in Figure 55. The slim probe still penetrates into the soil until an angle of around  $20^\circ$ , where it slips out of the surface after impact.

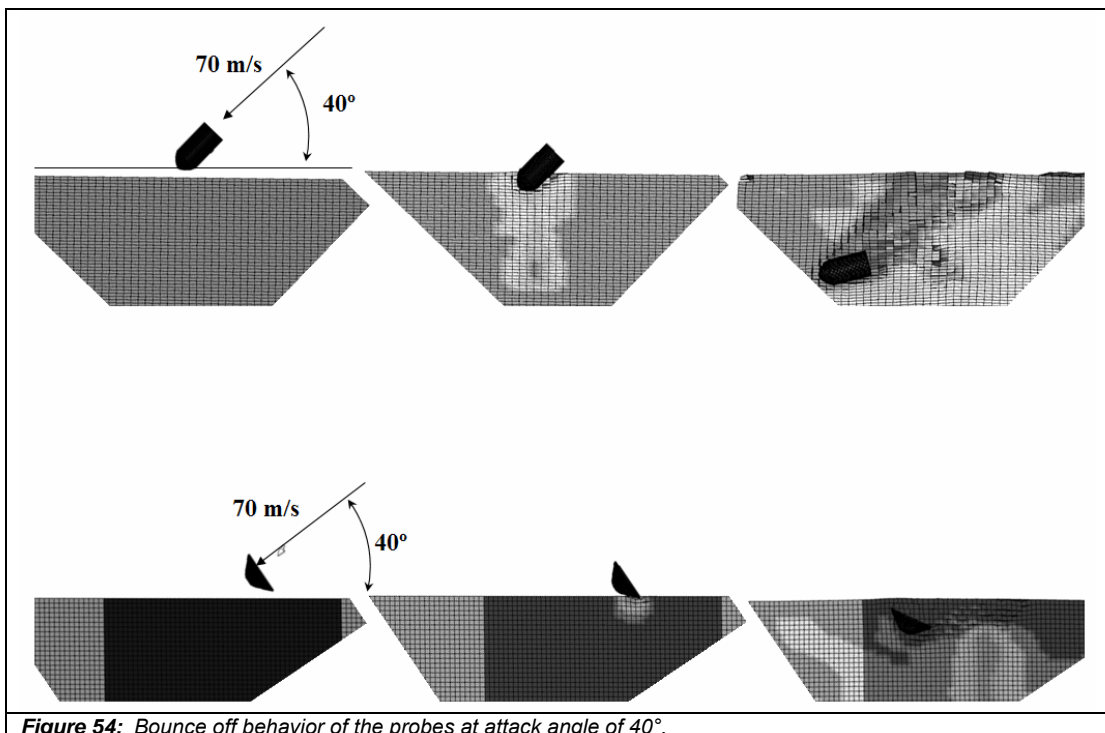


**Figure 54:** Bounce off behavior of the probes at attack angle of  $40^\circ$ .

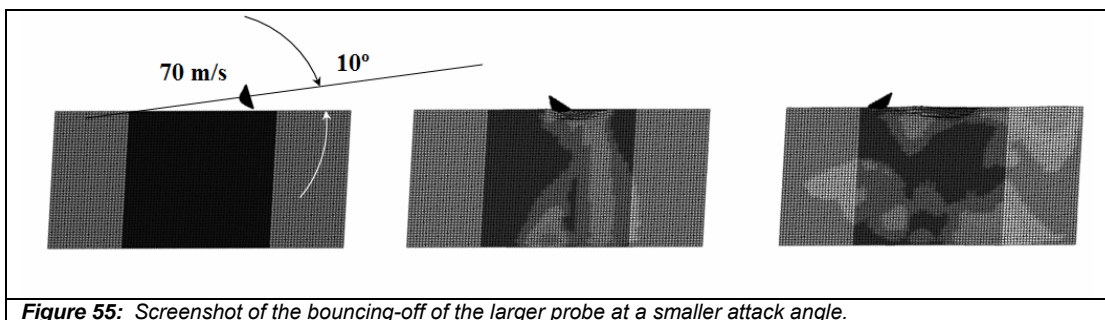


**Figure 55:** Screenshot of the bouncing-off of the larger probe at a smaller attack angle.

#### 5.2.2.4 Structural deformation of the carrier

In a last series of simulations, we studied the deformation of the penetrators upon impact on the soil model specified in 5.2.2.1. In this case, we used an elastic material model for the projectile, based on the material parameters of Titanium. The used

parameters are reported in Tab. 14. The overall body of the probe was defined to be of the same material since only a simplified model of the projectile could be used. A second simplification was that the probe was defined as a shell with a thickness of 20mm (the version of LS-DYNA used did not allow to import more complex structures of the projectile, such as a filled nose, for example). However, the simulation allows a qualitative evaluation of the probe's deformation.

*Table 15.: Material parameters for the model 024-PIECEWISE LINEAR PLASTICITY with its units used for the projectile model.*

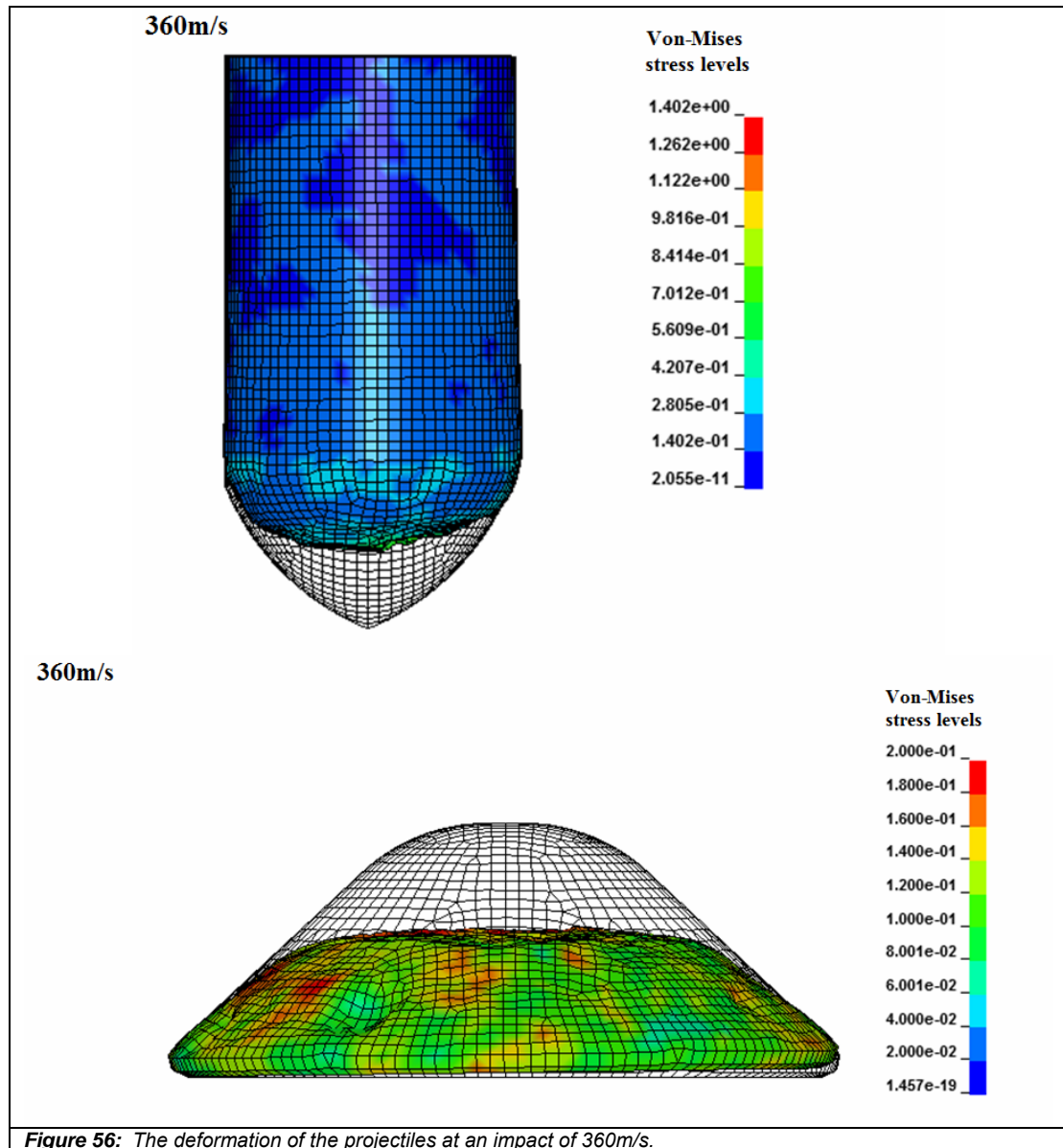
Mass density	4.5e-6 kg/mm <sup>3</sup>
Young's Modulus	116 GPa
Poisson's Ratio	0.3
Tangent Modulus	0.2 GPa

Figure 56 presents the shapes of both projectiles after an impact of 360m/s. The simulation shows that the plastic deformation is concentrated on the area that directly hits the target. The slim probe is mainly deformed at its nose, while the large ogive projectile is deformed over its whole cross-section.

A result of this study is the finding that a larger probe will need a frontal shock attenuation structure. There are several possibilities to compensate for the deformations on the frontal parts of the large probe, such as having a thicker frontal shell, honeycomb structures, or even airbags. However, each of these methods will increase the weight of the structure of the carrier, and thus decrease the available weight of its payload.

The slim probe has the disadvantage that it penetrates deeper into the soil. However, its structure is better suited for an impact scenario. The frontal part of penetrator shells is commonly filled; whereas, the rear part can be used to integrate payload systems.





#### 5.2.2.5 Projectile shape design adapted to geochemical exploration

Before resuming the conclusions on this study the objectives of this analysis shall be reviewed:

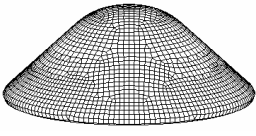

- 1) The system shall mechanically survive the impact of velocities up to 360m/s. Deformations that occur during these impacts shall not affect instrument spaces inside the shell.
- 2) Deep subsurface burial is not a requirement of the mission. Its objective is to measure the abundance of elements at the surface and shallow subsurface of

the soil. The probe shall be buried as shallow as possible; however, below 30cm to reduce the thermal fluctuations.

- 3) It must be assured that the probe penetrates the soil and does not bounce off. The system shall dispose of a large tolerance to the angle of impact.

Table 16 resumes the main findings of the above study for the two types of probes. None of the architectures represents an optimized solution for the here discussed application.

*Table 16.: The impact characteristics of the two probe shapes.*

		
Penetration depth at 360m/s	2230mm	2510mm
Penetration depth at 70m/s	390mm	820mm
Entry stability: Minimal angle of impact	40°	20°
Penetration stability	yes	no
Deformation as % of original volume	~ 30%	~ 10%

- The results show one major problem in both designs: the reached penetration depths are too deep. The larger shape reaches already 39cm at the lower impact velocities, while both projectiles penetrate over 2m into the soil at speeds above 360m/s.
- The small cross-section projectile shows a higher stability with increasing angles of attack. With the current geometry it is able to penetrate at angles around 10°, while the large diameter probe starts bouncing off the surface at less than 40°.
- However, the larger diameter probe shows a stable penetration path, which partly can be explained by its shallow overall penetration length. The slimmer probe tends to derive from its initial orientation at higher speeds (>244m/s). Any sampling mechanism would need to comply with a possible re-orientation of the probe at its final position.

- The distribution of the plastic deformation of the projectile's shell is not identical between the larger cross-sectional probe and the slim probe. The deformed parts are limited to the frontal nose part for the latter. The large diameter probe is deformed over its total cross-section, which will lead to a significant reduction of the payload spaces.

Based on the above findings, a novel projectile shape had to be found which fits the requirements of a geochemical exploration penetrator. The novel design is a trade-off between the slim probe and the large disc-shaped probe. Its penetrator depth shall be similar to the one of the larger diameter projectile. Its penetration behavior and deformations shall be similar to the small diameter projectile.

Different architectures that had a larger dish-shape structure at the rear of the slim projectile were tested in LS-DYNA. The motive behind this design is to offer a similar deformation pattern as the slim probe, while decreasing the penetration depth. It was found that the rear disc needs to have a significant size to stop the probe at shallow depths. Such design is not compliant with the integration of a large quantity of probes into one single mission (many large diameter probes will require a large deployment structure). The solution to this problem is depicted in Fig. 57: the probe deploys stoppers that are arranged in an umbrella-like pattern. The proposed design has an apparent diameter of 270mm in its deployed mode while only having a diameter of 120mm in the transport mode. The stoppers are fixed to the rear of the probe and are extended by a spring mechanism as shown in the below figure. Upon impact, soil will be compacted and accumulated below the stoppers.

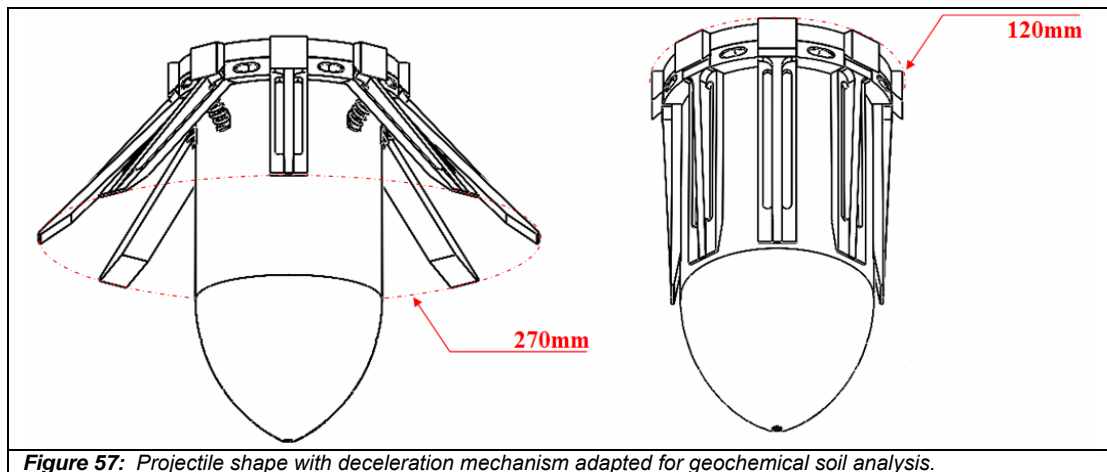


**Figure 57:** Projectile shape with deceleration mechanism adapted for geochemical soil analysis.

The depth profiles at different speeds of the above depicted shape were calculated through LS-DYNA simulations (see Fig. 58). At 157m/s the projectile still remains below a 1m burial. It was shown above that the radio transmission through the layer of regolith is not critical. However, a secure trade-off between minimizing the penetration depth and maximizing the impact velocity (and therefore the deployment orbit) has to be found. The maximal penetration depth at a maximal speed of 360m/s is around 1.5m. It is important to keep in mind that a similar probe, without stoppers, penetrates 2.5m into the soil.

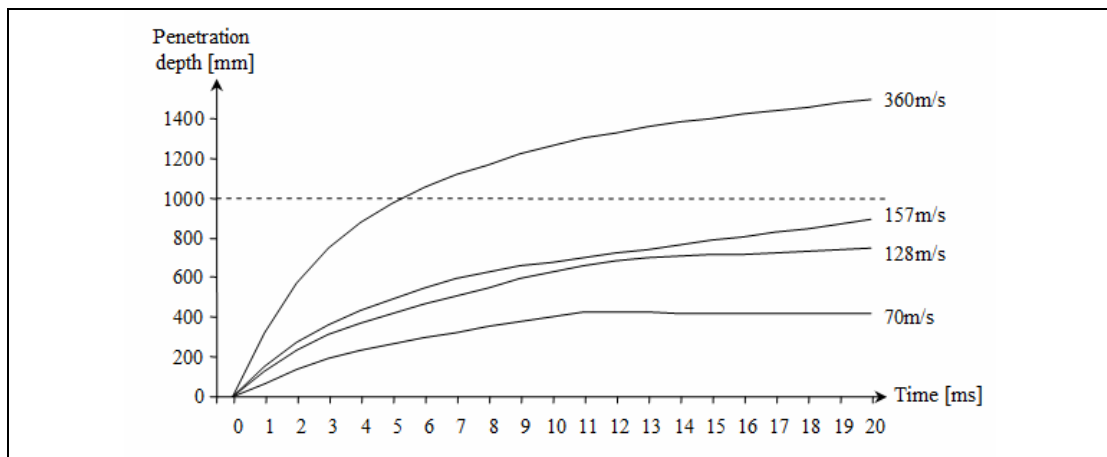


**Figure 58:** Penetration profiles of the probe with stoppers.

Figure 59 shows the resulting deformation of the projectile at this speed. The mechanical parameters of Titanium were assigned to the body of the probe. The simulation shows that the stoppers are able to withstand the impact. Their state, however, has no relevance for the further functionality of the system once the probe is at rest. It is also of interest to note that the resulting deformation of the nose section of the probe is reduced.

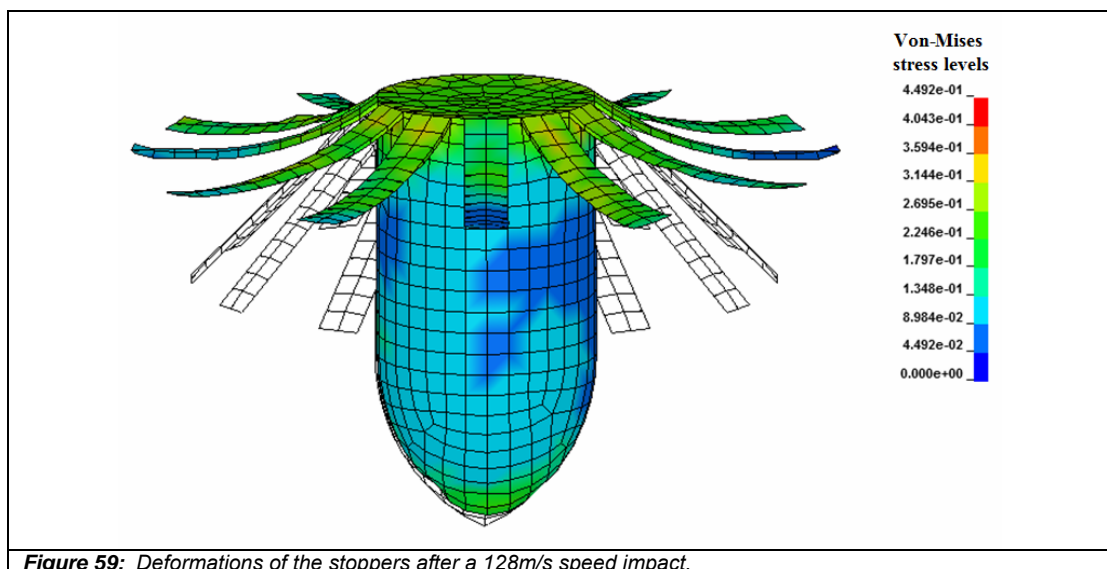
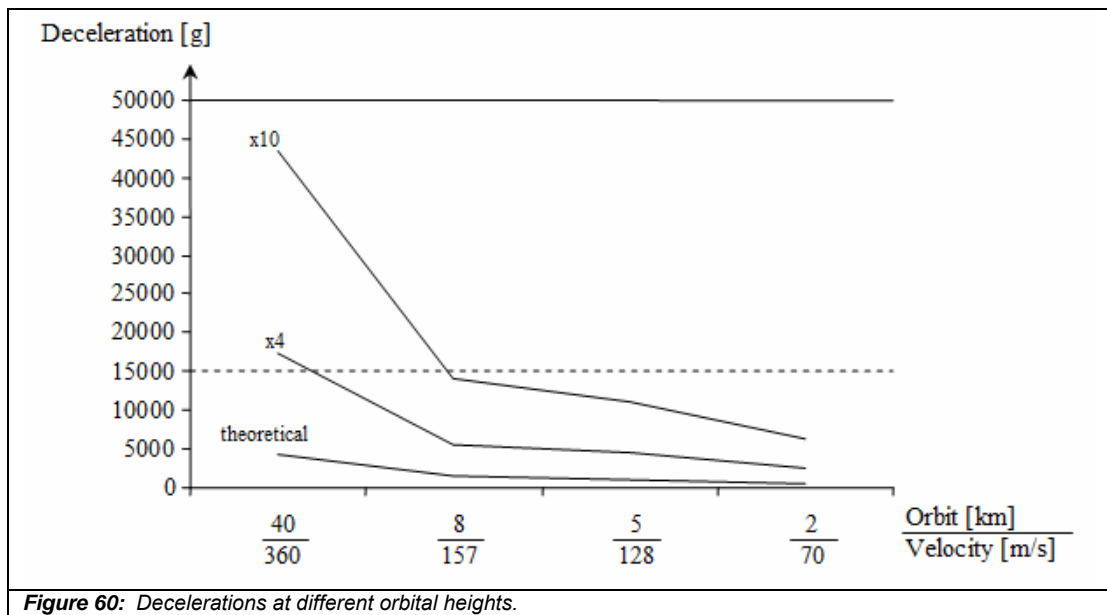


**Figure 59:** Deformations of the stoppers after a 128m/s speed impact.

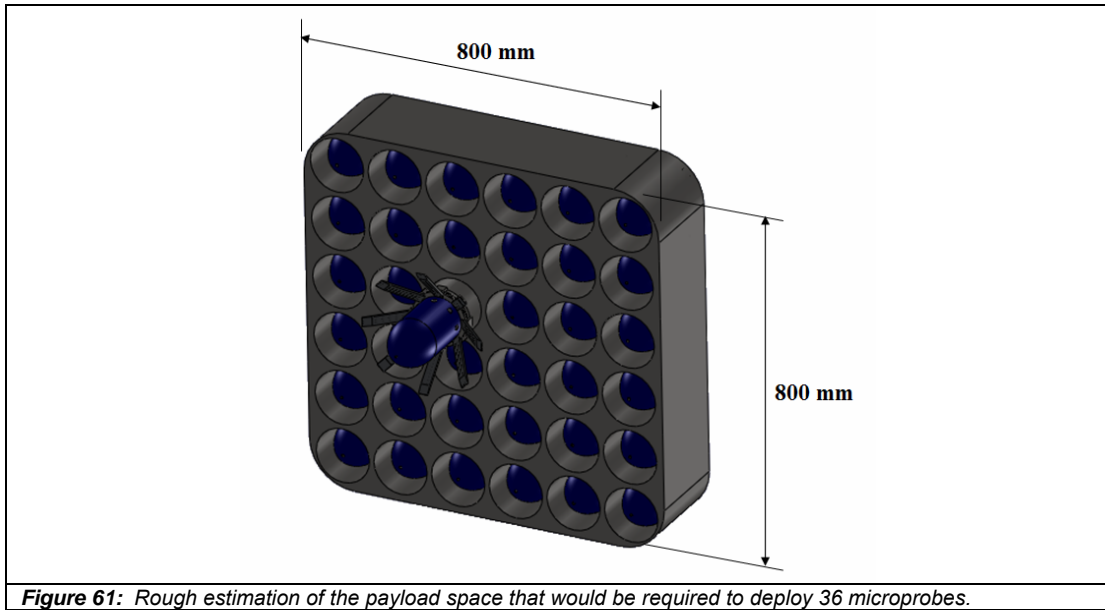
While high decelerations have the advantage to reduce the penetration depth, those will lead to a higher risk of equipment being destroyed upon impact. The theoretical mean of the deceleration can be calculated through formula (5.17). However, the through impact trials observed g-forces have a mean of 4x this theoretical value with peaks up to 10x of this theoretical value (R. Gowen, private communication).

$$a = \frac{v^2}{2x} \quad (5.17)$$

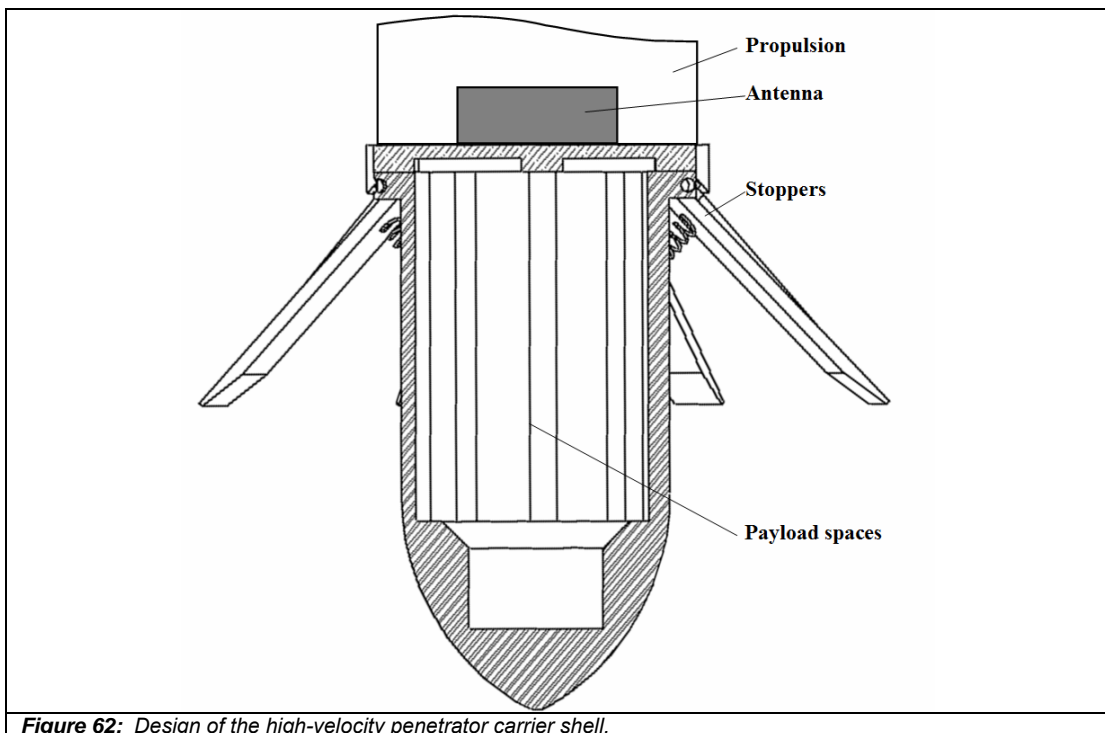
The theoretical decelerations and their corresponding estimated real values are plotted in Fig. 60. A secure g-force limit, based on the rating of electronics in military artillery shells is 15 kgee. From the graph, it can be seen that an impact velocity of 128m/s results just below this value (with the 10x peak estimation).



Based on this projectile design, we can estimate the overall payload space necessary for the mission described above: a simple integration study can give an idea about the size of the deployment mechanism that such a quantity of probes would require (see Fig. 61). The probes are aligned in a 6x6 pattern (therefore a total of 36 probes, and not 31 as required). The overall space that such a system would require is a structure of 800mm x 800mm (length around 400mm depending on the propulsion system which is not designed here).



The design of this microprobe is depicted in Fig. 62. The location of the propulsion and the antenna are only indicated. The shell has a payload compartment in the middle of the projectile. The carrier alone has a weight of 3.7kg. The overall system parameters, including the sampling mechanism and payload instrument, will be completed in the last chapter.



# CHAPTER 6

## Feasibility study of a high velocity impact sampling system

After having developed a mission strategy and a carrier system for high-velocity penetrators, we are now coming to the final step of this work: the development of an adapted sampling mechanism for penetrators dedicated to geochemical surface analysis. We will first select an analysis instrument that fits the mission objectives while being adapted to the integration in high-velocity impact penetrators. The development of the analysis instrument itself is not in the frame of this work; the selected instrument is solely used as strawman payload for the development of an adapted sampling strategy. Different sampling mechanisms were evaluated on the basis of their utilization in the frame of a high-velocity penetrator mission. Based on this technology review, a novel sampling method is derived, which works on the principle of a vibrating conveyor. The mechanism is designed and integrated into the above-developed carrier structure. The work will conclude with a forecast of the overall system parameters and the feasibility to integrate the penetrator array into a host mission.

### 6.1 Payload integration study

#### **6.1.1 Technological readiness study for geochemical analysis instruments**

In this section, we will identify different payload instruments which act as candidates for the geochemical soil analysis in the frame of an impacting micro-probe mission. The instruments will be evaluated for this study in terms of their compliance to the mission objectives and their adaptability to utilization inside a high-speed penetrator. The mission scenario described in Chapter 4 identified Oxygen, Iron, Titanium and Aluminum as elements of interest. Especially, Oxygen will be a primer element for in-situ resource utilization of the short- to medium-term lunar exploration. Table 17 lists possible payload instruments for geochemical analysis with their respective

measurement capabilities (we are mainly interested in their capabilities to determine elemental abundance). We will not deliver a detailed description of each measurement method. The reader is referred to the work of Meyer et al., (1996) which gives a comprehensive overview on these methods and their application in space exploration.

*Table 17: Capabilities of instruments for geochemical analysis. “n.d.” means that there is no data available for its accuracy. “n.a.” means that the technology is not applicable for this kind of mineralogical investigation.*

Instrument type; (Reference/s)	Element quantification accuracy [weight%]				
	O	Fe	Ti	Al	[H]
Alpha-proton-X-Ray Spectrometer (APXS); (Meyer et al., 1996; Smith et al. 2009)	±0.7	±0.4	±0.15	±0.4	<i>n.a.</i>
Gamma-Ray Spectrometer (GRS) (Meyer et al., 1996; Yin and Trombka, 1988)	<10*				<10*
X-Ray Spectrometer (XRS); (Meyer et al., 1996 Smith et al., 2009)	n.d.	±0.03	n.d.	n.d.	n.d.
Scanning Electron Microscope and Particle Analyzer (SEMPA); (Meyer et al., 1996)	<i>n.a.</i>	±0.2	±0.2	±0.2	<i>n.a.</i>
X-Ray Stimulated Photon Spectroscopy (XPS); (Meyer et al., 1996; Reniers and Tewell, 2005; Seah, 1993)	Overall energy resolution 0.28eV				<i>n.a.</i>
Auger Electron Spectroscopy (AES); (Meyer et al., 1996; Reniers and Tewell, 2005; Seah, 1993)	Relative energy resolution $\Delta E/E = 1.2$ .				<i>n.a.</i>
Mössbauer Spectrometer; (Meyer et al., 1996; Mars Moessbauer Group, 2009)	<i>n.a.</i>	1%	<i>n.a.</i>	<i>n.a.</i>	<i>n.a.</i>
Laser Time-Of-Flight (TOF) Mass Spectrometer; (Rohner et al., 2003; McEntire et al. 1996, Wüest et al., 2007)	10% for several elemental abundances.				
Nuclear Magnetic Resonance Spectrometer (NMR); (Meyer et al., 1996; Yen et al., 1999)	0.1%	<i>n.a.</i>	<i>n.a.</i>	<i>n.a.</i>	0.1%

\* Measurement accuracy is time dependant: a 10-h measurement can reach precisions of 1% for all stated elements concentrations.



*Table 17 continued.*

<b>Instrument type; (Reference/s)</b>	<b>Mineral identification accuracy (No specific elemental analysis)</b>
Visual Imagery (UV-VIS-IR); (Meyer et al., 1996, Jakeš, 1997)	<i>Mineral texture identification up to a 100<math>\mu</math>m scale.</i>
IR Spectrometer; (Basilevsky et al., 2004; Silverman and Chistensen, 2006, Meyer et al. 1996, Salisbury et al., 1997)	<i>Capable to differentiate major mineral type spectra with an accuracy of <math>\pm 2\%</math> to 5%.</i>
X-Ray Diffraction Analysis (XRD); (Meyer et al., 1996)	<i>Mineral abundances around 5%.</i>
Raman Spectroscopy (Meyer et al., 1996, Courrèges-Lacoste et al. 2007)	<i>Abundance up to 5%.</i>

### **6.1.2 Integration into high-velocity micro-penetrators**

A second set of criteria to be considered for the strawman payload suite of a penetrator mission is the operational requirements: Table 18 gives details of the technical specifications of each above-mentioned instrument.

Looking back at Tab. 17 it can be seen that there are several analysis techniques that are capable to deliver precise measurements of the quantities of elements in the lunar soil. However, several of these instruments can be eliminated due to their respective size and weight (see Tab. 18). We set a weight threshold of 1kg for the instrument in order keep the overall weight of the penetrator low. The analysis and development of the analysis instrument is not part of this work, we therefore set a criteria that only instruments that have been flight proven (or better that have been already integrated in a penetrator) are qualified. A shorter list of possible payload instruments emerges from these criteria: The APXS, the XRS, the Mössbauer spectrometer, the Laser Time-of-Flight spectrometer, and the Raman spectrometer. The latter is mainly used to analyze minerals, it cannot identify specific elements. It is not a specific objective of this mission to identify minerals, although the elemental composition could be interfered from a mineral known. The Mössbauer spectrometer and XRS deliver accurate measurements of iron; however, other elements cannot directly measured by

this technique. The remaining two instruments are the APXS and the Time-of-Flight Laser spectrometer. The APXS has, however, two specific advantages: its measurement capabilities are higher than those of the laser spectrometer, and this instrument was part of space missions (i.e. Surveyor and Pathfinder) and even high-velocity penetrator missions (Mars-96).

Based on this state-of-the-art, we will continue the penetrator design on the basis of an APXS for the penetrator mission. In the following section, we will review the functionality of this instrument and study a sampling strategy to deliver soil into the penetrator.

Table 18.: Operational parameters of geochemical analysis instruments. Instrument references are, unless otherwise indicated, the same as in Tab.17. “n.d” means that no data is available for this instrument. Brackets in the weight column indicated different versions of the instrument.

Tech. heritage			System specifications						Critical issues			
Instrument	Penetrator application	Flight proven system	Weight	Size [mm <sup>3</sup> ]	Power	Duration	Temp. range	Data trans.	Radiation sensibility <sup>2</sup>	Moving parts <sup>3</sup>	Optical system	Specific sample preparation
<b>Alpha-proton-X-Ray Spectrometer (APXS):</b> (1) Surveyor Models	No	Yes	4.30kg	171x165x133 178x165x102	1.2W	3h		2750Byte	Yes	No	No	No
(2) Pathfinder Model & Mars96 Model	No Yes		0.55kg	70x80x65 Ø 52 x 65mm	0.33W	n.d.	>-120°C	16kByte				
<b>Gamma-Ray Spectrometer (GRS)</b> <sup>4</sup>	No <sup>5</sup>	Yes <sup>4</sup>	6.00kg	n.d.	10W	30sec <sup>6</sup>	n.d.	n.d.	Yes	No	No	No

<sup>2</sup> Electronics (damage) and the measurement itself. Many instruments are sensitive to external radiation which can influence the measurement.

<sup>3</sup> Not considered are any mechanisms to bring the sample to the instrument or to position the instrument on the sample.

<sup>4</sup> Flight proven models were built for orbiter missions (i.e. Apollo 16, Lunar Prospector and Mars Odyssey). However, no system was utilized for direct surface science so far. The technical data presented here is based on the study of Yin and Trombka (1988).

<sup>5</sup> Evans et al (1986) describes the efforts to develop a GRX for the comet nucleus mission CRAF. The instrument was to be deployed through a penetrator.

<sup>6</sup> Meyer et al. (1996) page 12.

<b>X-Ray Spectrometer (XRS)</b>	Yes	Yes	0.26kg	120x80x15 Ø 47 x 47mm	4W	3h	n.d.	50kByte	Yes	No	No	No
<b>SEMPA</b>	No	n.d.	11.90kg	500x200x300	22W	20min	n.d.	n.d.	n.d.	Yes <sup>7</sup>	No	Yes <sup>8</sup>
<b>X-Ray Stimulated Photon Spectroscopy (XPS)</b>	No	No	n.d.	n.d.	Sever. watts	1min - 10min	n.d.	n.d.	No	Yes <sup>9</sup>	Yes <sup>10</sup>	No
<b>Auger Electron Spectroscopy (AES)</b>	No	No	n.d.	n.d.	n.d.	n.d.	n.d.	n.d.	No	No	No	No
<b>Mössbauer Spectrometer</b>	No	Yes	0.40kg	50x50x90	1W	n.d.	n.d.	60kByte	Yes	Yes	No	No
<b>Laser Time-Of-Flight Mass Spectrometer</b>	No	Yes	0.50kg	Ø 60 x 150	3W	n.d.	n.d.	n.d.	No	No	Yes	No
<b>Nuclear Magnetic Resonance Spectrometer</b>	Yes <sup>11</sup>	Yes	0.15kg	n.d.	5W	n.d.	n.d.	n.d.	No	No	No	No
<b>Visual Imagery</b>	No	Yes	n.d.	n.d.	>1W	n.d.	n.d.	n.d.	No	Yes <sup>12</sup>	Yes	No
<b>IR Spectrometer</b>	No	Yes	3kg	n.d.	6W	n.d.	-30°C to +30°C	Data link 80bps	No	Yes	Yes	No
<b>X-Ray Diffraction Analysis (XRD)</b>	No	n.d.	n.d.	n.d.	n.d.	n.d.	n.d.	n.d.	Yes	Yes	No	No
<b>Raman Spectroscopy</b>	No	Yes	0.85kg	190x150x190	n.d.	n.d.	>77K	n.d.	No		Yes	No

<sup>7</sup> Stepping motor for the line raster of the beam and ion pump (Albee and Bradley, 1987)

<sup>8</sup> Sample coating (Albee and Bradley, 1987)

<sup>9</sup> Scanning system.

<sup>10</sup> System of lenses.

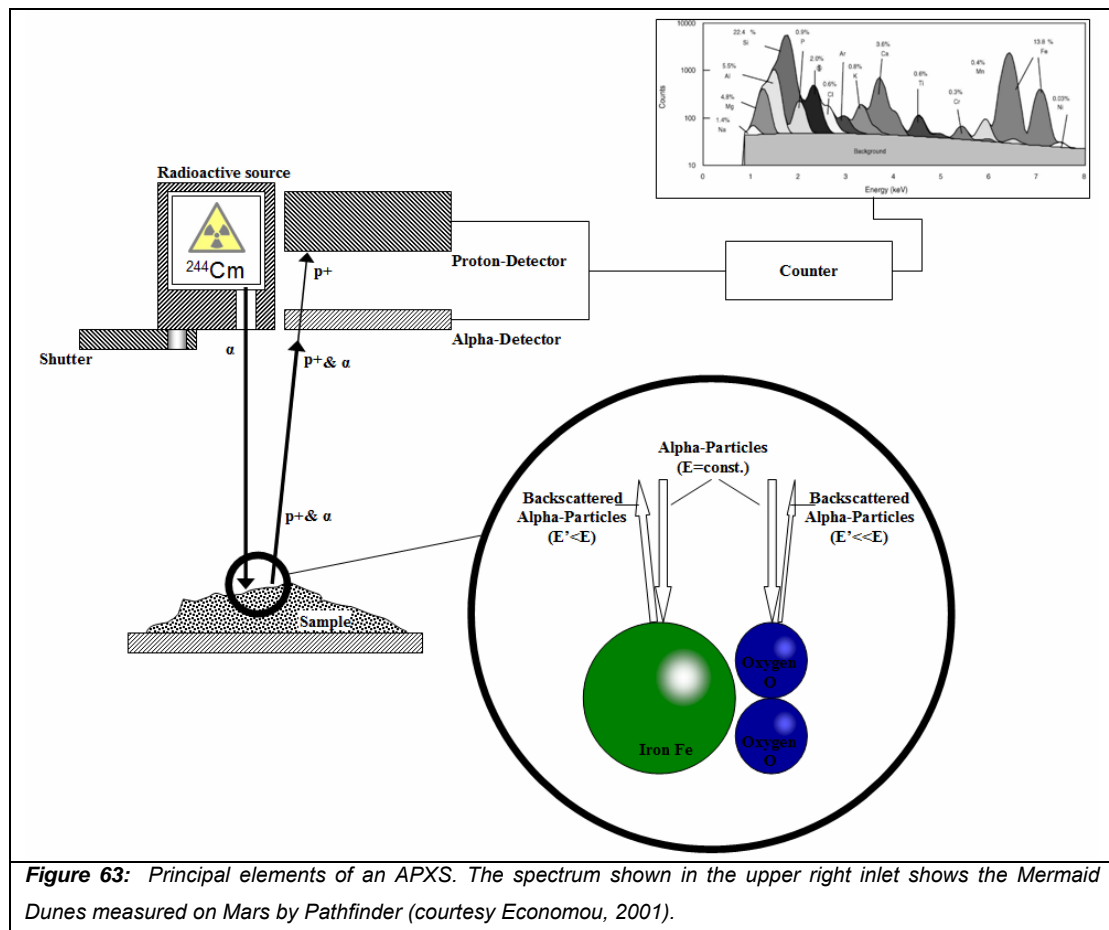
<sup>11</sup> Proposed concept based on DS-2 mission (Yen et al. 1999).

<sup>12</sup> Focusing and sample positioning.

### 6.1.3 Description of the strawman payload suite

From both the analytical and technical capabilities, it comes out that the APXS might be the most suited instrument for geochemical analysis by penetrators. The following study will be based on the use of such device inside the penetrator.

Alpha-Proton X-Ray spectrometers radiate the sample with alpha-particles. The backscattered particles have different energies, depending on the target's nucleus mass. The number of particles per energy thus gives the information about the constitution of the sample. Figure 63 shows the main elements of this instrument. The APXS which was used in the Mars Pathfinder mission is shown in Fig. 64. All mentioned elements (except the electronics) were included in the sensor head.



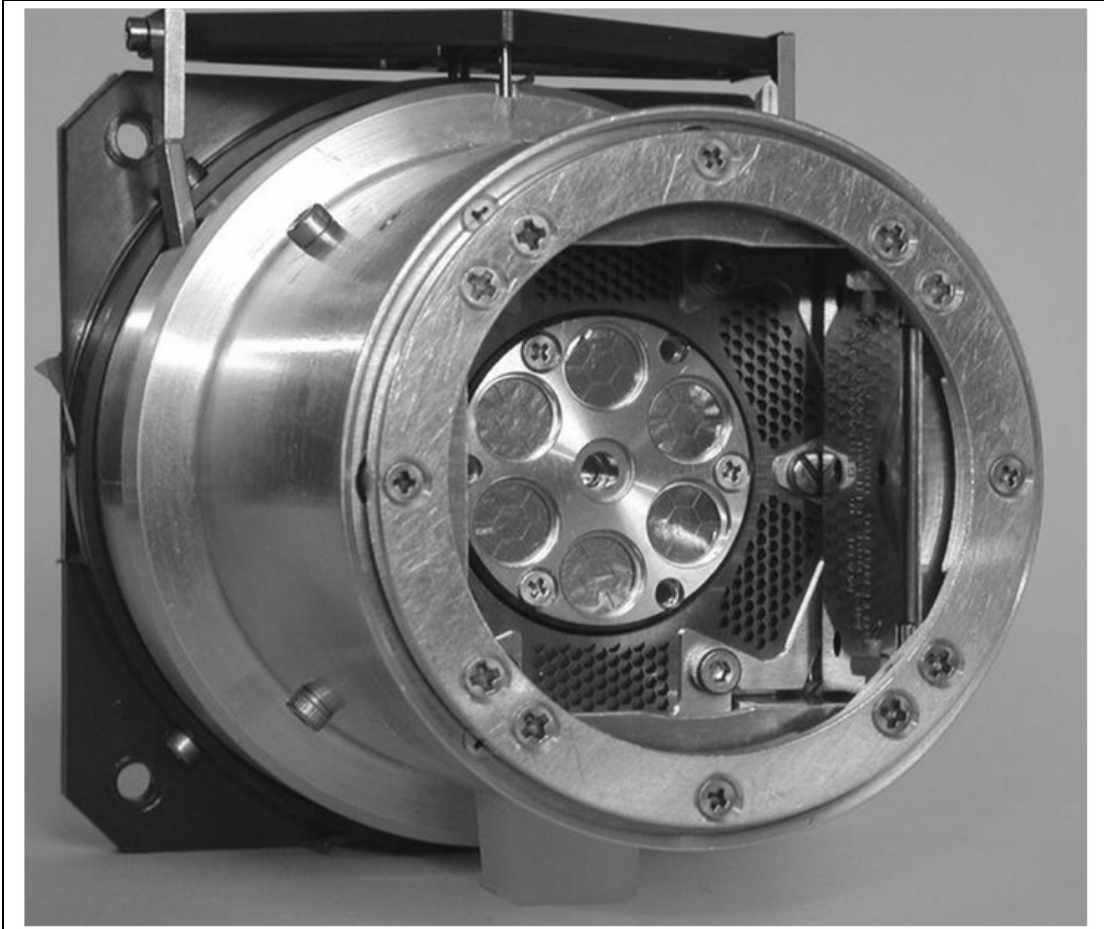


**Figure 64:** The APXS onboard the Mars Pathfinder (courtesy NASA/JPL-Caltech).

A preliminary version of such instrument was already used during the US Surveyor missions to the Moon (Meyer et al., 1996). The in the Surveyor utilized instrument showed good results in the identification of lighter elements (Turkevich et al., 1966). However, Hydrogen could not be measured directly, and the resolution of heavier elements such as Iron was rather bad. The application of this process is of particular interest for planetary surfaces that do not dispose of an atmosphere that could interact with the emitted alpha-particles and protons. The principle of this measurement method is that the sample is exposed to a radioactive source (alpha particles and X-Rays). The alpha-particles are scattered in the nuclei of the sample's atoms which, in turn, produces protons and fluorescence X-Rays. Three processes take place once the particles hit the target surface: (i) elastic scattering of the alpha-particles with the nuclei, (ii) nuclear interaction of alpha particles with light elements, and (iii) excitation of the atomic structure and subsequent X-Ray production (Economou, 2001). The scattered alpha-particles inherit a specific energy that depends on the

atomic mass of its target. The produced particles are, therefore, counted in ratio of their energy, which allows determining the elemental chemistry of rock and soil. The sample that is to be analyzed by APXS does not require a specific preparation, but needs to be brought to the instrument in a distance sufficiently close to the source and sufficiently far to allow the scattered particles to penetrate into the detectors.

Based on the success of the in-situ analysis of the lunar surfaces by the Surveyors, APXS became a tool in many space missions. Current APXS are substantially miniaturized compared to the Surveyor versions (Economou, 2001). The Russian Mars-96 mission carried an APXS in the penetrator's forebody (Surkov and Kremnev, 1998). The instrument was high-g rated and supposed to measure the concentrations of elements with back-scattering energies from 150KeV to 7MeV (alpha-particles) and 400keV to 7MeV (protons). These ranges would have identified elements in the atomic mass range from Carbon to Iron. Its sensitivity is reported to have been 0.2 to 0.5 vol.%. Sadly, Mars-96 never reached the Red Planet, but was lost in an accident in Earth's orbit. An identical instrument was developed for the US Pathfinder mission to Mars. The instrument was qualified to operation temperatures down to -120°C (Economou, 2001). Its radioactive source consists of Curium-244 and the counting proton detector was based on a thin (35µm) silicon charged particle detector for the alpha particles and a thick (800µm) proton detector.

#### **6.1.4 Conclusions and design requirements for the sampling mechanism**

Based on the above study, we can determine several requirements for the sampling system of the micro-probe. As "sampling system", we define here the mechanisms that retrieve a soil sample from the surrounding regolith and deliver it to the analysis instrument (here, the APXS). The sample should have a quantifiable volume. It needs to be directly exposed to the ray of alpha-particles, since APXS is a surface analysis method. We intend to build a system that can process several samples. That means once a sample is measured, it needs to be evacuated, and a new sample is delivered. Ideally, this is done by guaranteeing that no residues remain in the sampling chamber to avoid cross-contamination between the samples.

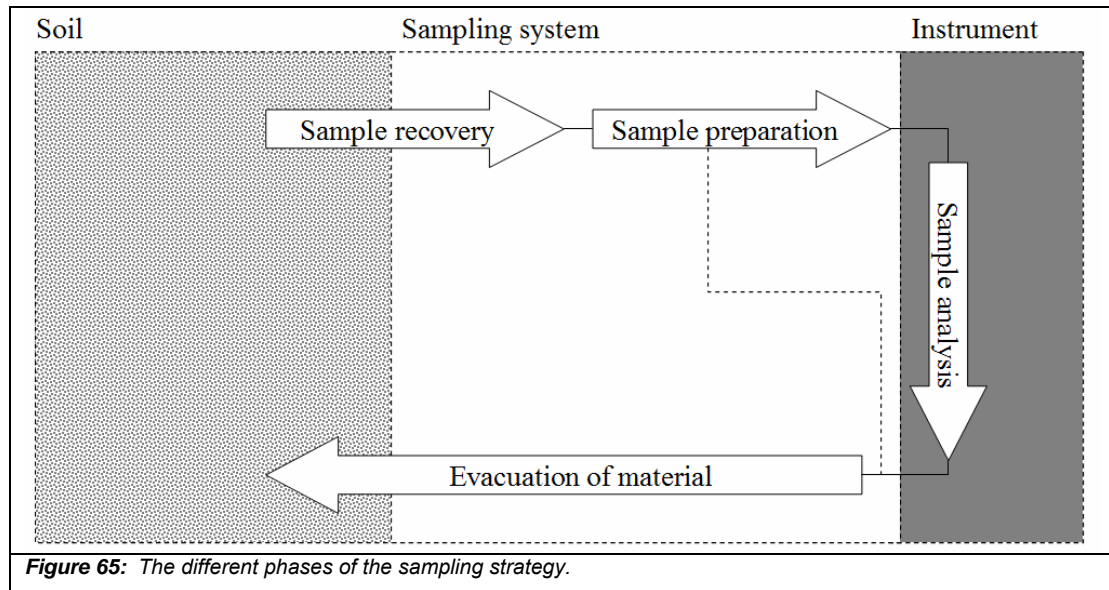
## 6.2 Review of geochemical sampling apparatus

Geochemical soil analysis is only one objective that is attractive for high-velocity penetrator missions. Amongst other mission goals are seismic measurements of the target body (i.e. Lunar A, LunarEx/MoonLITE), accelerometry measurements (i.e. Huygens, Rosetta) or, “simply”, the creation of an artificial impact event to examine the ejecta formed by the impactor (i.e. DeepImpact, Lunar Prospector, LRO).

Geochemical analysis of surface material, however, can be considered as the technically most challenging analysis method for penetrator missions due to two reasons: a) it requires highly sensitive analysis instruments, which is potentially more sensitive to damage during the impact, and b) it requires a proper sample recovery and sample handling strategy. The development of the latter is the subject of this chapter. Before evaluating different techniques, we will define the necessary steps in the sampling process. Figure 65 shows the main phases of a sampling strategy:

- 1) Sample recovery: The sample is taken from the close proximity of the probe. In the case of harder material, it has to be broken up from the larger agglomerate, and be transported into the probe. In the case of granular soil, it can be directly transported into the probe. We assume that the penetrator system only needs to handle granular soil. The lunar regolith consists mainly of particles below mm-size. Harder rock will be scattered during the impact of the probe.
- 2) Sample preparation: The sample will be prepared depending on the analysis method. Preparation methods can be the sieving of the soil to allow only particles with a certain size to enter the analytical chamber. Larger boulders are evacuated from the probe.
- 3) Sample analysis of the soil by the instrument. This process can, depending on the method used, include the heating of the sample.
- 4) Evacuation of the sample: This step is only necessary if several samples need to be analyzed or if a large amount of sample is to be examined. In this case, it would be ideal to assure that no material remains in the analysis chamber to avoid cross-contamination between the samples.





Sampling strategies of previous and planned missions are evaluated under the aspect of fulfilling the requirements of the above mentioned sampling strategy. Emphasis will be given on the constraints of a high-velocity penetrator mission, in terms of survivability, energy consumption and space. The following list contains mechanisms that have been developed for specific penetrator missions, sampling apparatus concepts that can be adapted to penetrator missions and also novel concepts.

### **6.2.1. Mars-96 sampling strategy**

The Russian Mars-96 mission had the objective to launch two penetrators into the surface of Mars. Its science objective was the determination of the physical characteristics of the rock, TV-surveying of the environment, and the measurement of the elemental composition of the sites (Surkov and Kremnev, 1998). It is the last mission goal that is of interest in the following study: In Mars-96 it was planned to bombard a 50mm diameter soil sample with alpha-particles from the APXS (Rieder and Wänke, 1996; Wänke, 2009). The sampling strategy did not include any active sampling mechanism. The soil was expected to fall into the analysis chamber during the impact and separation of the forebody and the afterbody. This simple sample strategy (without an active sampling mechanism) is certainly adapted to the high-deceleration constraints of penetrator missions. However, it relies on the uncertain condition that sufficient soil falls back on the analysis instrument. Figure 66 shows the schematic architecture of the forebody with its soil analysis apparatus.

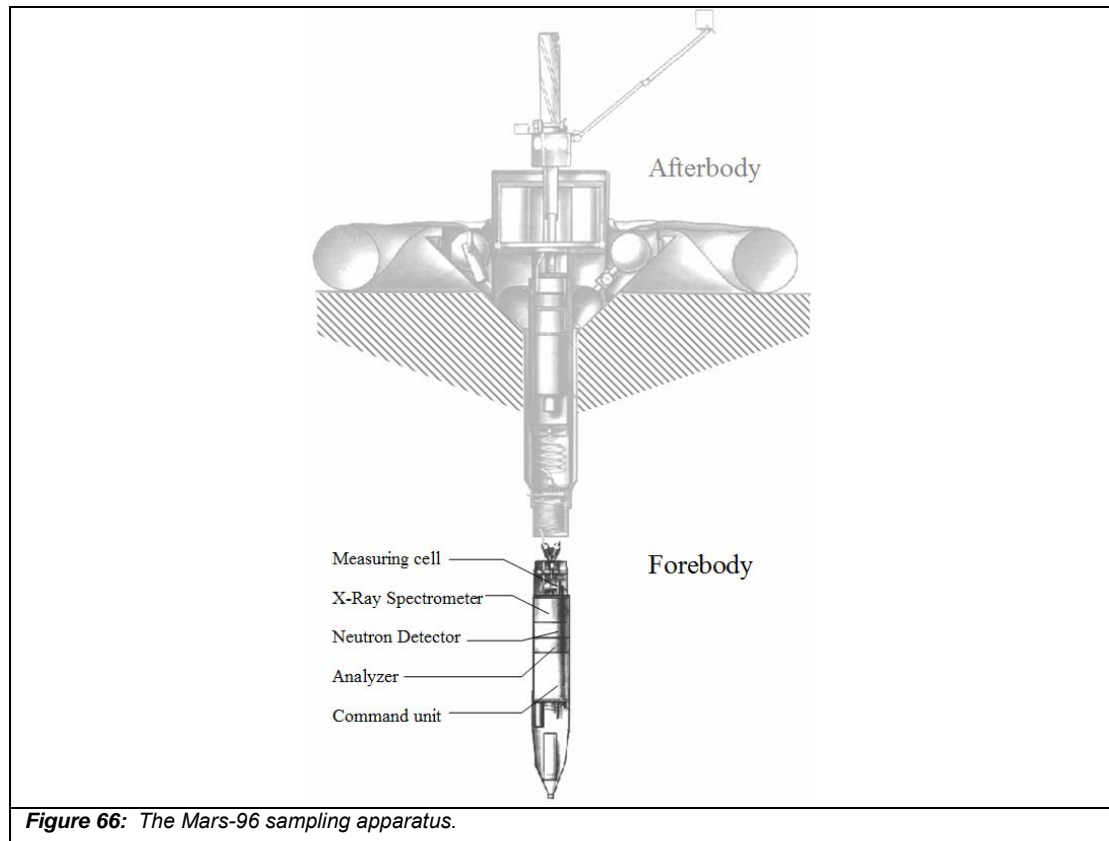


**Figure 66:** The Mars-96 sampling apparatus.

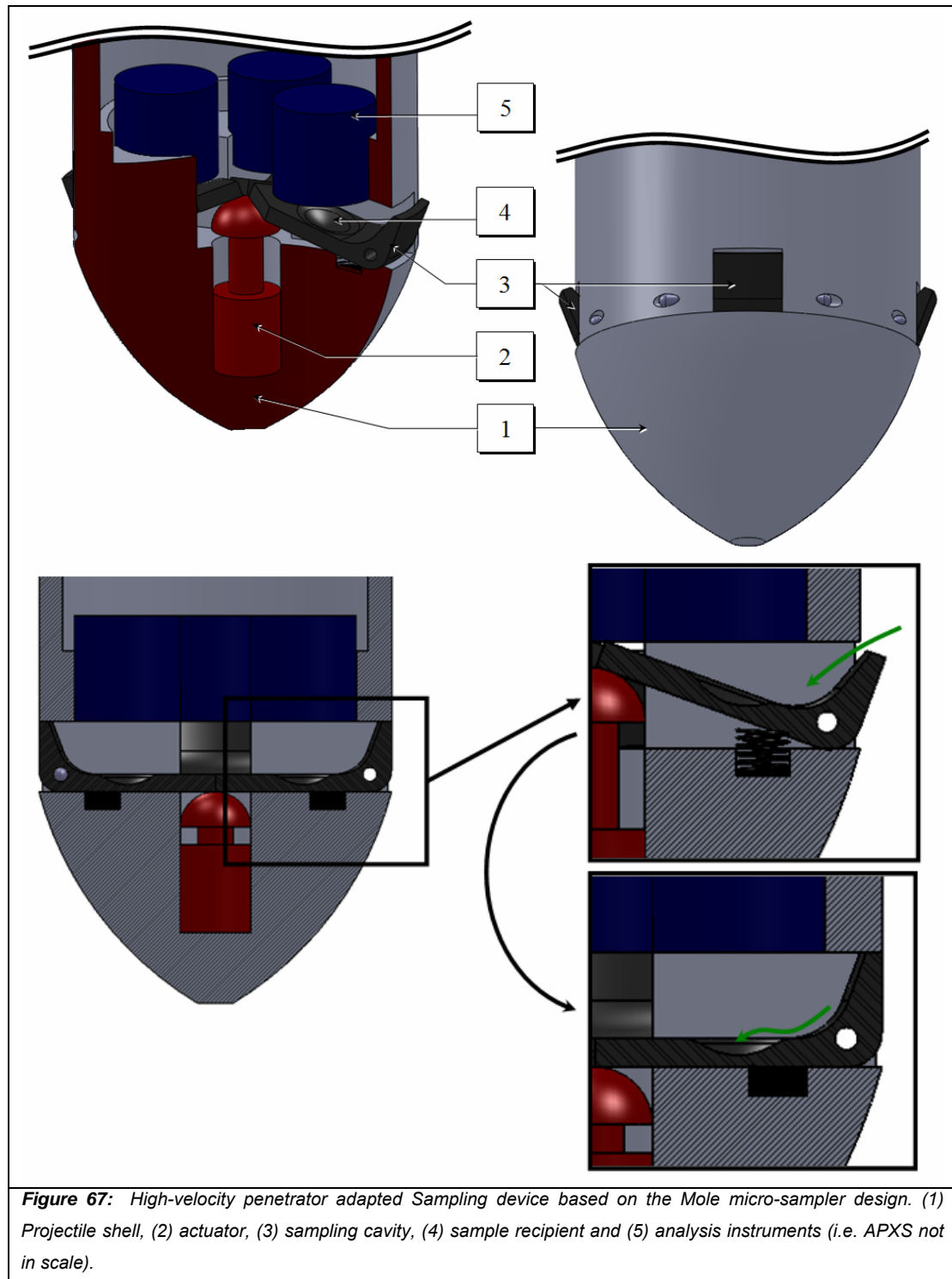
### **6.2.2. Deep-Space-2 micro sampler**

Another sampling mechanism developed for a Mars mission was the US Deep-Space 2 probes. Both penetrators disposed of a micro-drill which was supposed to drill laterally into the soil to retrieve a sample for analysis (i.e. the Evolved Water Experiment) (Mining and Luers, 1999). The drill consisted of a micro-motor which drives an auger laterally from the probe's side-wall into the soil (JPL DS2, 2009; Blue 1999). The driving motor was a precious metal DC-motor (Faulhaber MicroMo 1016) which was planned to operate during six minutes to transport around 100mg of Martian soil into the system. The sample would have been off-loaded into a 6mm in diameter analysis chamber which was sealed pyrotechnically. The whole ensemble had a weight of 50g and a volume of 11cm<sup>3</sup>. Critical components of the DS-2 microprobe have been tested through air gun impact tests at the Energetic Materials Research Test Center in New Mexico (Blue, 1999). These tests confirmed the probe's capability to survive its Martian impact.

**6.2.3. Integrated sampling device for penetration moles**

Kochan et al., (1991) present a study on different sampling mechanisms for a planetary mole. One concept which was referred to as “Integrated Sampling Device” by the authors uses the hammering mechanism of the mole to be activated (in contrast to the autonomous sampling device which needs a specific actuator). The sampling apparatus includes an annular cavity which is integrated into the mole’s tip. The specifications for the integration of such a sampling device into a high-velocity penetrator are similar to the ones of the DS-2 sampling method. The sample cavity could, however, be actuated by a hammering device, in contrast to the rotary auger drill of the DS-2 system. Utilizing a shock mechanism to obtain samples from the surrounding soil has the advantage that it delivers a higher force to penetrate the compacted regolith. The mechanism can be based on a larger range of actuators (rotary and linear). While Kochan et al. suggest the integration of the cavity into the front tip of the mole, alternative locations such as at the rear part are imaginable and would offer a better protection of the mechanism against damage during the impact.

Figure 67 shows the possible integration of a sampling cavity based on the mole sampling device. An actuator pushes the four sampling cavities outside the perimeter of the probe once it has penetrated the soil. The actuator here is only schematically shown. It can be a hammering mechanism as described by the works above or a linear actuator such as a piezoelectric device or shape memory alloy (SMA). The latter two systems offer a better adaptation to high-g applications (monolithic structure; no moving parts). However, their displacement is little, which would limit the extension of the cavity into the surrounding soil. SMAs and piezo-actuators can be operated at high frequencies. This would offer the possibility to move the cavity in a manner that the particles are shaken into the system. The sample will slide into the sample recipient below the analysis instrument once the cavity is closed again.



#### 6.2.4. Bio-inspired micro-drill

A concept which was proposed as a penetrator sampling device is the biomimetic micro-drill described by Gao et al. (2006 and 2007b). This device was studied in the frame of an European Space Agency project on bionics and space systems design to sample low-gravity targets such as asteroids by impacting probes. The concept is

inspired by the nesting technique of wood wasps which use an ovipositor to drill holes into trees to parasitize the wood-boring larvae that feed deep inside dead trees (see Fig. 68). The advantage of this technique is that it requires little axial force to penetrate. The drill is composed of two shells that move in reciprocating manner. Backward-pointing teeth prevent the drill from sliding backward while presenting little resistance to forward movement. The drill concept was developed and tested in laboratory by Gao et al., and the authors conclude that such system presents an energy-efficient alternative to classical drilling systems.

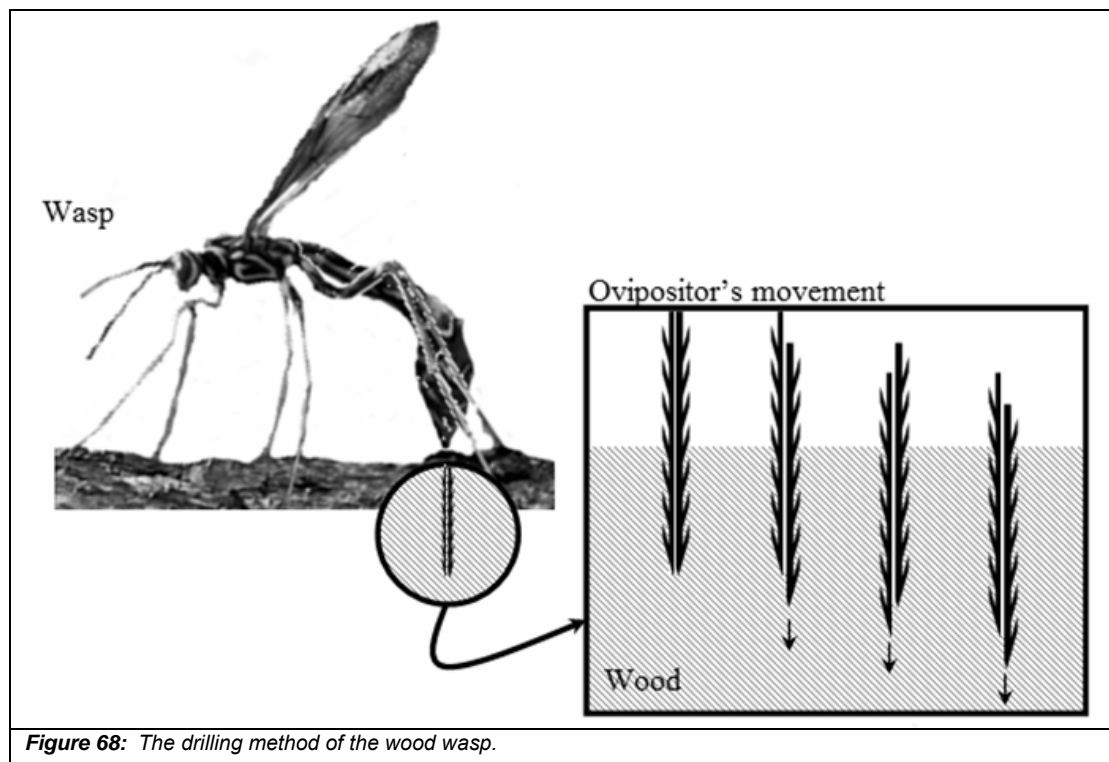
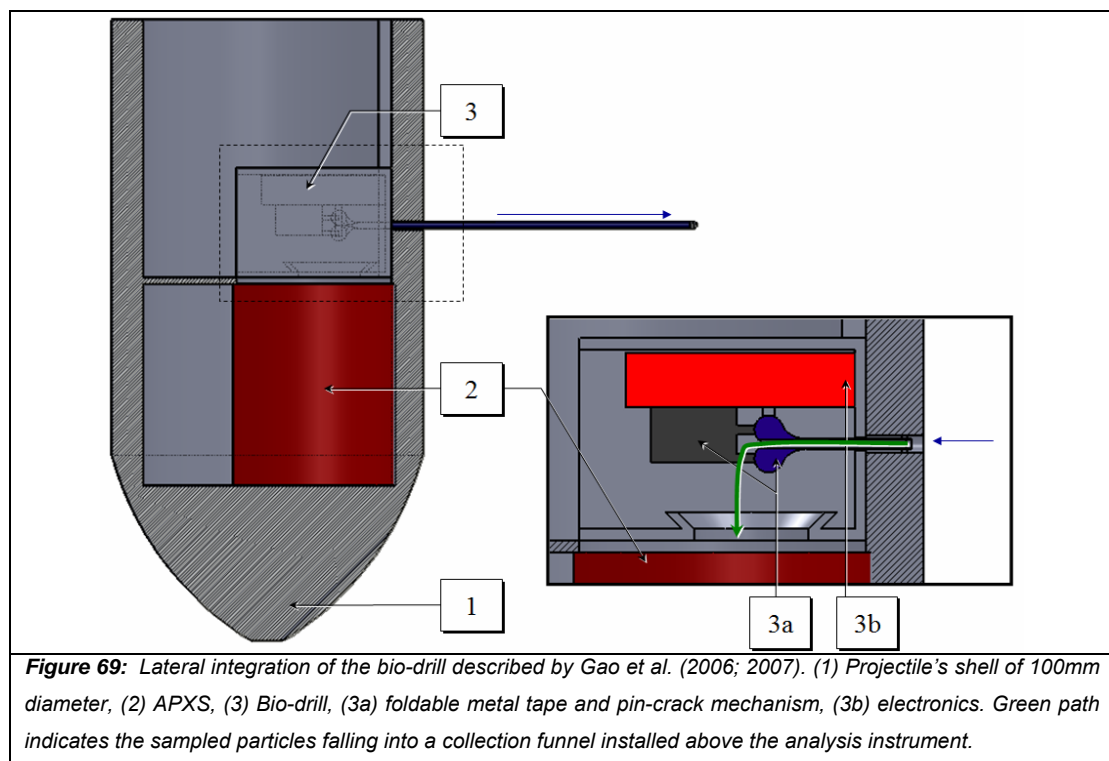


**Figure 68:** The drilling method of the wood wasp.

The current mechanism uses a piezoelectric motor. The drill penetrates in soft (chalk) to medium hardness substrate (clay) with a speed of 0.0056m/min to 0.0023m/min at an input power of 3W (Gao et al., 2007b). In conclusion, the bio-inspired drill is an attractive technique for impacting probes due to its low weight, low power consumption and capability to work on low-gravity targets with little pushing force necessary for sample penetration. It is adapted to sample medium to hard soil, potentially over large drilling distances. The mechanism does not need any particular probe orientation as long as it is assured that the drill bits penetrate the soil. Both papers of Gao et al. include technical drawings of the architecture of the driving

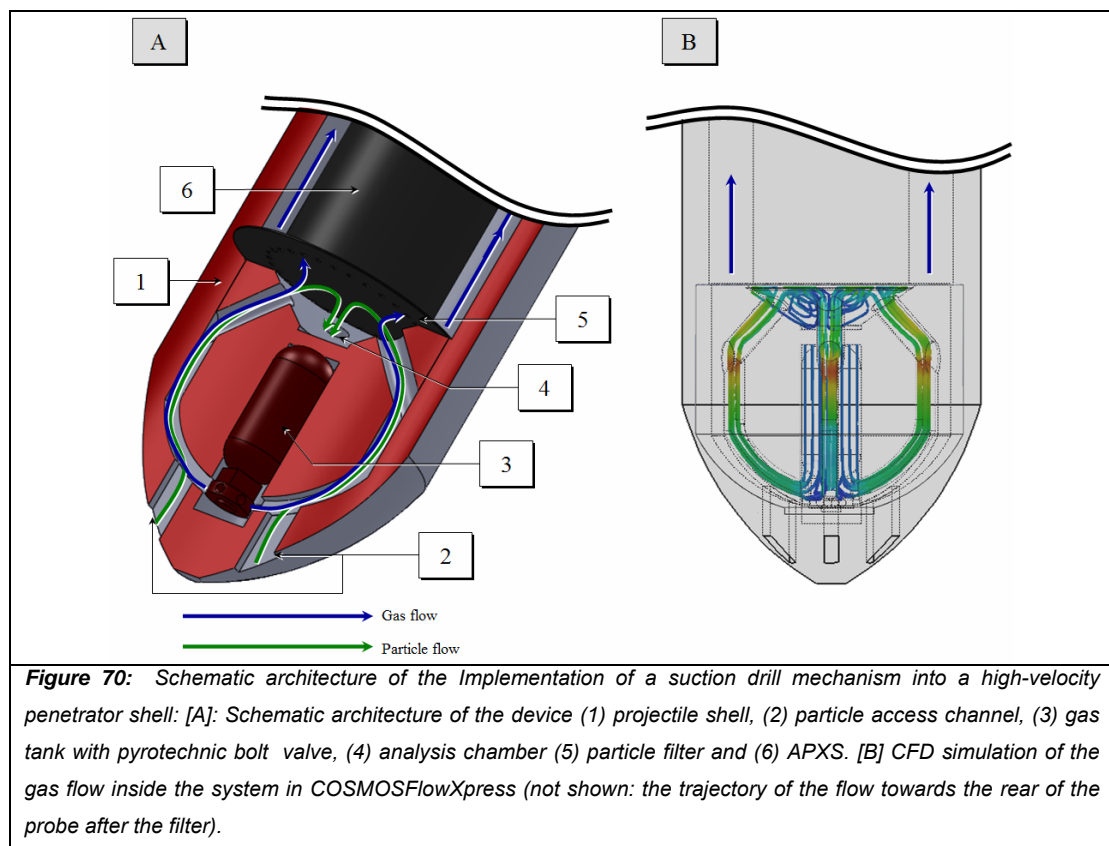
mechanism of the drill. The storage of a long drill bit comes with problems, especially for the design of a micro-probe. This is solved in an elegant way in the here presented concept: the drill consists of two metal tapes that can be unrolled to form a circular-shape. The concept of this foldable drill can be seen in more detail in the manuscript of Kömle et al., (2008b). The reciprocating movement of the bio-drill is done by a pin-crank mechanism which pays-out the half-shells of the drill in altering manner. The mechanism is small in dimensions (diameter 50mm x 75mm with casting) and can therefore be integrated in various sections of the impacting probe. The study of Gao et al., (2006; 2007b) suggests an integration of the probe in the nose. The following figure shows a possible configuration of such drill with a lateral payout. The driving mechanism itself is not detailed, but its elements are specified in the above mentioned publications.



### **6.2.5. Suction-drill**

A further concept that merits consideration for a penetrator-based sampling system is based on the use of a cold gas flow to transport surface material into an analysis apparatus. Such a system was studied as a conceptual design for regolith sampling by Kömle et al., (2008). This sampling device offers some specific advantages to

classical drilling systems. The transport of the soil sample is done by the hydrodynamic forces exerted on the soil particles by the gas flow. The use of gas as transporting medium greatly reduces the use of moving parts. No electrical power supply is necessary for the sampling device (eventually apart from the instruments that are necessary to control the gas flow). In the above mentioned study, due to its inert characteristics, Nitrogen gas is proposed as carrier. The contamination of the soil and its alternation are obviously critical in this extraction process. Nitrogen itself is not an element of interest from lunar geochemical investigations. Its strong triple bonds prevent reactions with other elements for exploration in lunar environment (Dinitrogen and Hydrogen are known to react only above 150atm and 450°C in the so-called Haber-Bosch Process). Figure 70 shows the integration of a suction sampling system into the shell of a high-velocity penetrator.



The sampling mechanism is integrated into the nose of the shell. This position has the advantage that it offers access to the deepest layers of the subsoil. However, it is the nose of the penetrator that will experience the largest deformations. A suction sampling mechanism does not require any moving parts apart from the control valve

of the gas tank, which can be actuated by a pyrotechnic bolt. Structure deformations in the system will, therefore, not lead to a failure of the system unless the nose is deformed to a point where the particle access channels are completely closed. The particles enter the probe through the channels that are integrated in the tip of the nose. The compression of the regolith during the impact of the probe will ultimately form a plug that helps avoid the gas from escaping through the surrounding soil. Kömle et al., ran mathematical simulations on the gas escape via the surrounding material and conclude that the lost amount is minimal compared to the gas flow towards the outlet. This loss might be more severe in the case where the probe is completely buried since this will influence the pressure of the gas outlet. However, it can be expected that the material in front of the penetrator is more compacted than the soil that falls back onto the penetrator's rear part. After impact of the probe, a pyrotechnic bolt can open the valve to release the gas (it is even imaginable that the impact force itself is used to open the valve, which would mean that the soil is sampled while the system penetrates the surface). A stream of gas will flow through the channel and flush the particles towards the rear of the probe. To lift the soil particles upwards, it must be assured that the drag force of the gas flow upon the particles is larger than the gravitational force. A filter separates the particles from the gas. The latter escapes from the probe at the rear of the penetrator (not shown), while the particles will fall into the analysis chamber.

#### **6.2.6. Shacking sampling system**

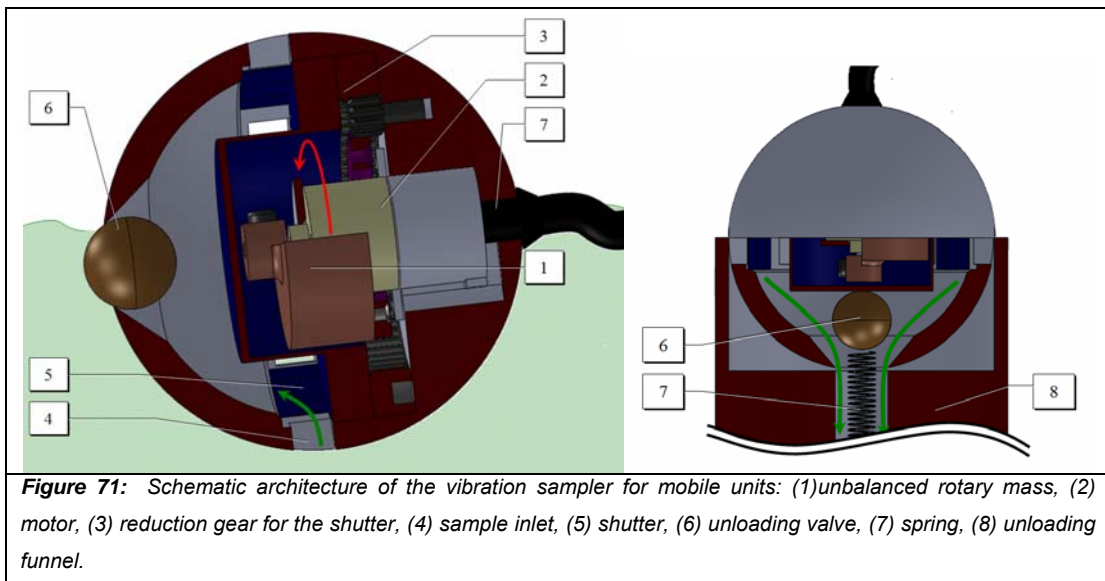
A novel sampling method for impacting probes was developed in the frame of this Ph.D: it is based on a concept to use vibration to transport a soil sample from the perimeter of the probe towards its inner instruments. A very simple baseline design is depicted in Fig. 71.

The system is based on a vibration mechanism like the ones known from mobile telephones: an unbalanced mass (1) is brought into rotation by a motor (2). The system will start to wobble like an unbalanced car wheel. The movement will shovel soil through the sample inlets (4) into the probe. The sample inlets are closed by a shutter mechanism (5) and the probe can be retrieved once the sampling is terminated. Such system is suited for sampling activities by robotic mobile units in rough terrain. The probe can be fired into inaccessible areas (i.e. the bottom of a shadowed crater



while the vehicle is positioned at its rim). A tether links the probe to the robot and serves as power line and recovery cable. Once the probe is retrieved to the robot, it is placed into an unloading funnel. The soil sample is evacuated from a trap in the probe as depicted in the lower schema of Fig. 71.

The amplitude of vibration depends on its overall mass. It is, therefore, not suited for orbital penetrators since their mass is too heavy and the probe is buried too firmly in the soil to induce a vibration. The system was originally designed to be deployed from a rover or by astronaut on the lunar surface (i.e. by rocket gun or even air gun) and is, therefore, light in mass. It has no measuring instrument onboard since the probe is retrieved back to the robot for the analysis. In order to use vibrations for the transport from the perimeter of an impactor to its instruments, a modified architecture has to be chosen.



### **6.2.7. Chladni-Sampler**

Another sampling concept is not derived from a biological model, but from the field of acoustics. Ernst Florens Friedrich Chladni (1756-1827) was a German physicist, and musician who performed, besides many other works, research on the vibration of plates. The law, which is named after him, relates the frequency of a surface under vibration to the number of (linear or radial) nodes. The phenomenon that brought

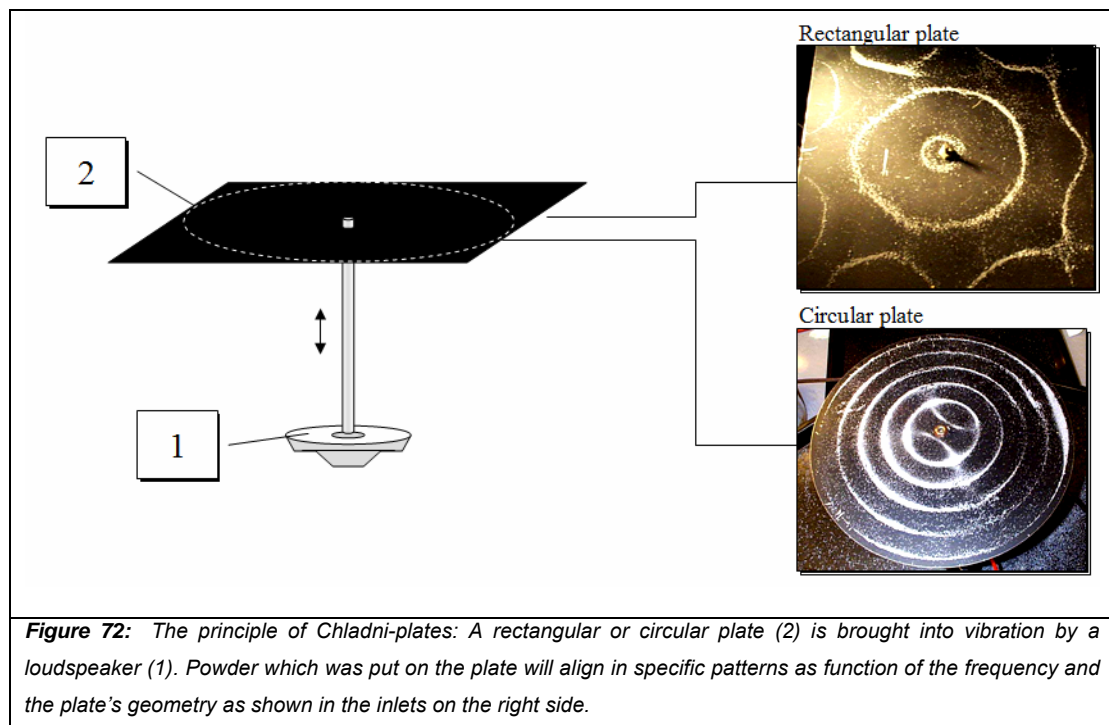
Chladni to formulate this law was his observation that powder on a plate in vibration aligns on specific patterns. A picture of the effect can be seen in Fig. 72.

The formula that defines the frequency as function of the number of modes (and verso) is shown in Eq. (6.1),

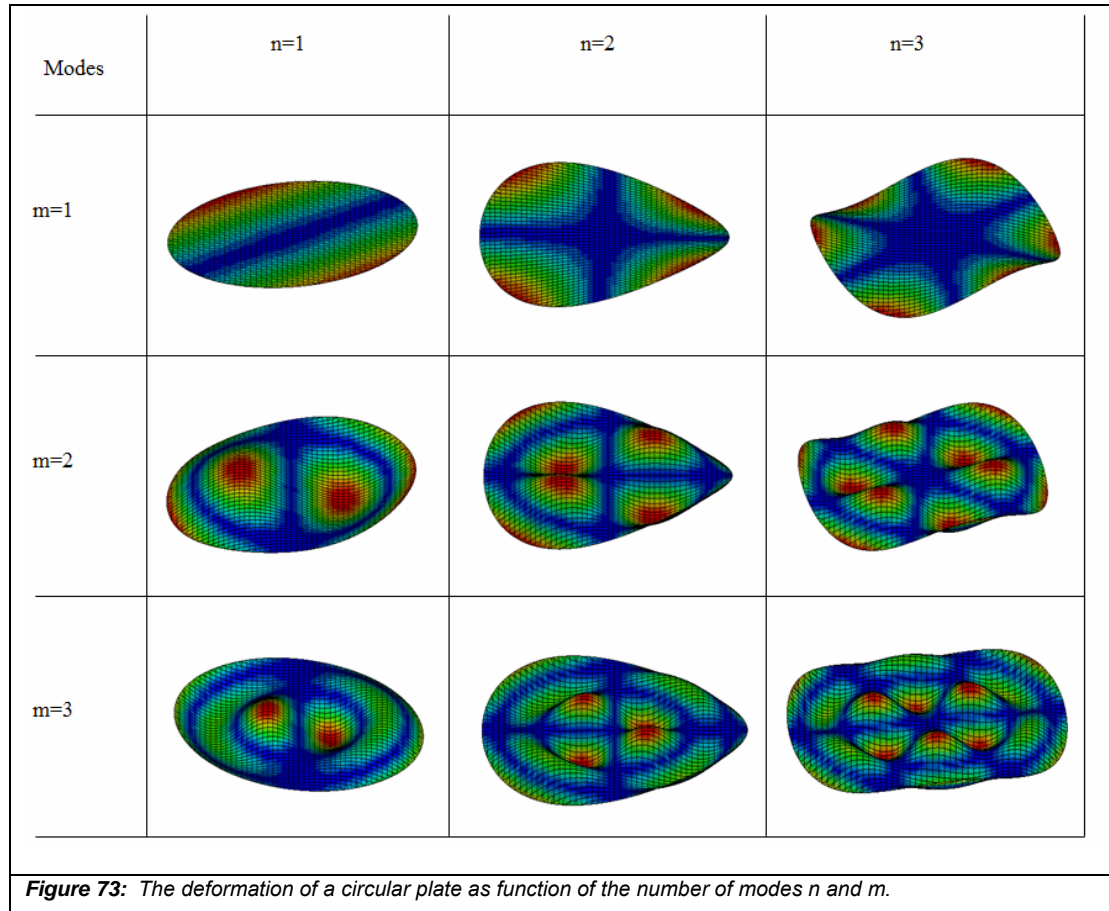
$$f = (m + 2n)^2 \quad (6.1)$$

where  $m$  is the number of circular modes and  $n$  is the number of radial modes.

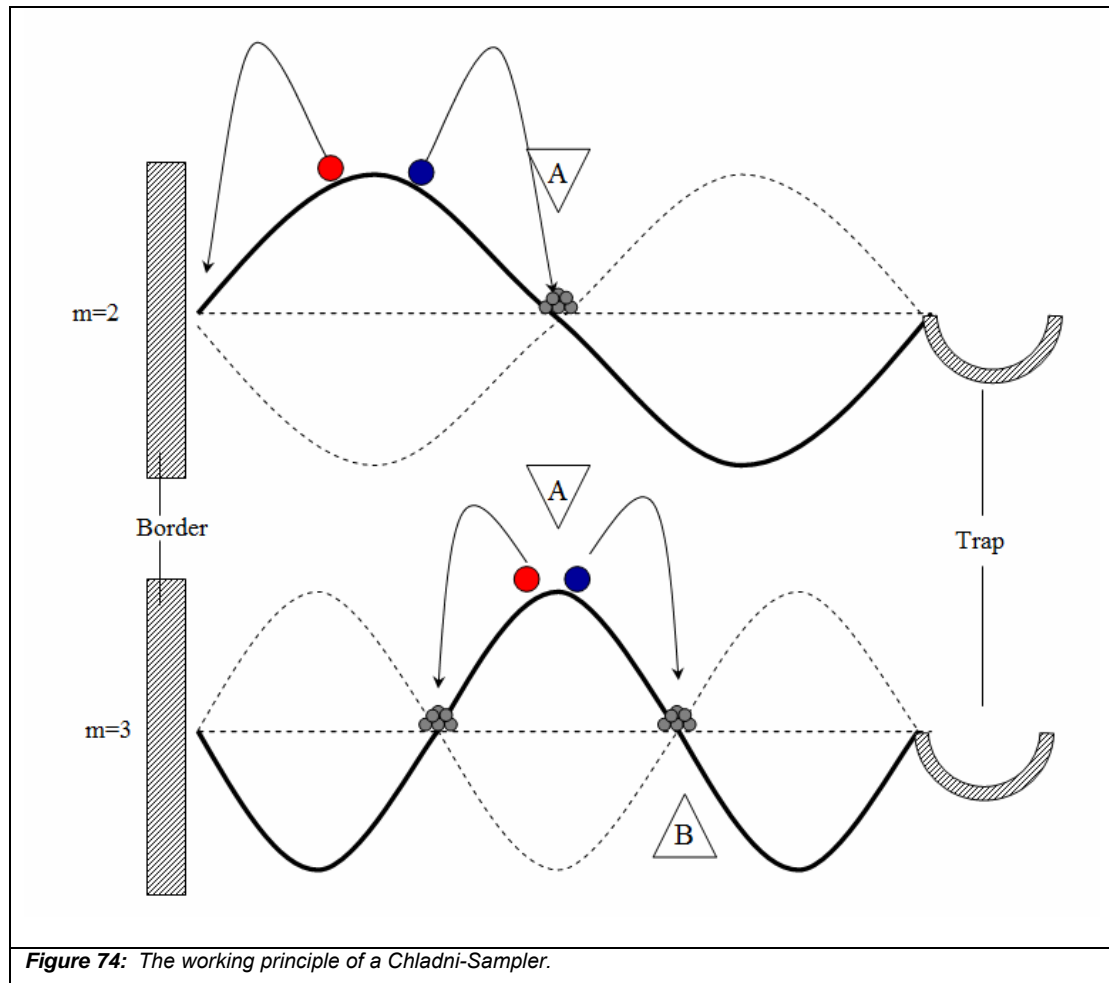
A LS-DYNA simulation of a circular plate is depicted in Fig. 73.



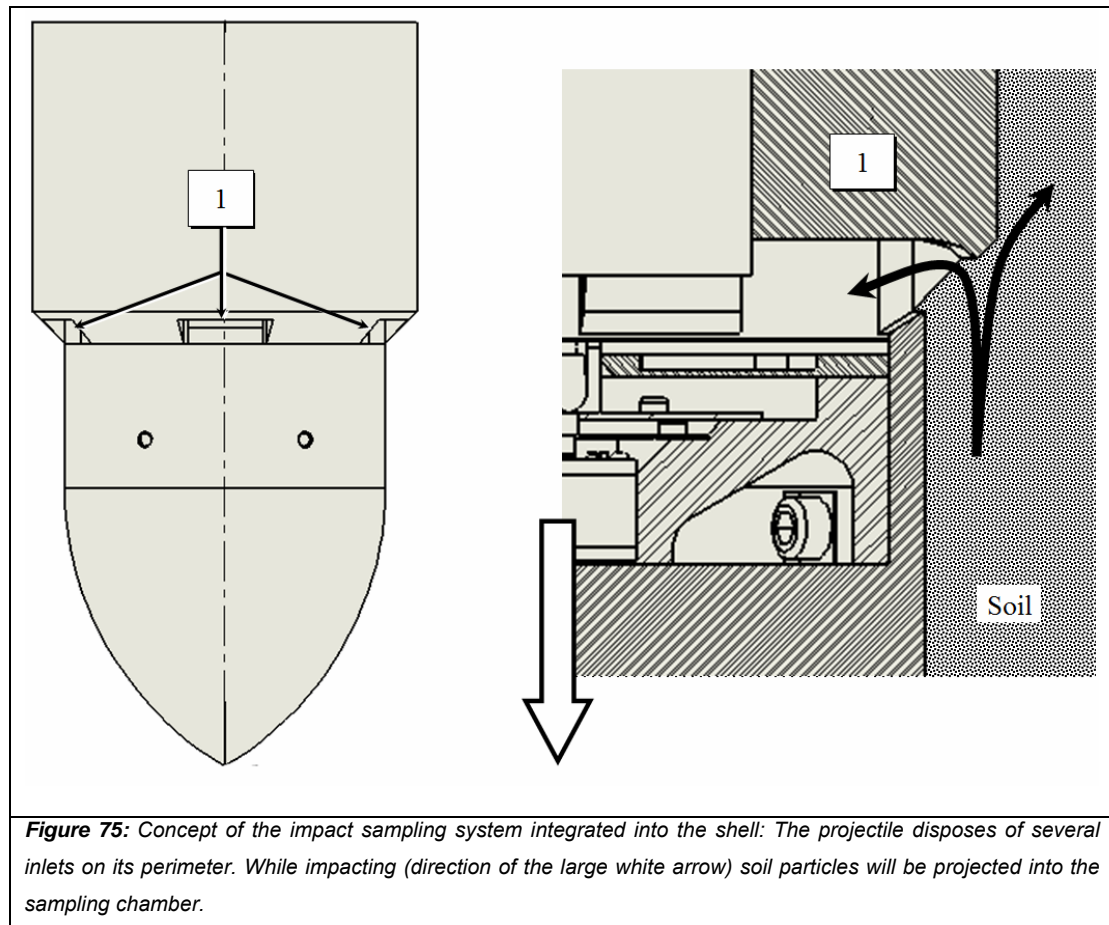
This effect can be used to transport (granular) soil samples from the perimeter of the system to a central analysis instrument: the particles can be made “walk” towards the centre of the plate by varying its frequency. Figure 74 shows the working principle of the concept. A particle will be projected by the amplitude of the plate. It will jump until it reaches a location on the plate where the amplitude is zero (indicated in Fig. 74 by the assembly of little grey dots). Statistically, half of the particles at an amplitude maximum will travel towards the centre, half towards the perimeter. In order to make the principle work, it is, therefore, necessary that the particles that reach the centre are blocked. This can be done by the trap indicated in the figure.



On the other side, it must be assured that the particles that reach the perimeter still remain in the system. This can be done by implementing a border that prevents the particles from falling out of the plate. A particle that reaches a rest position is brought thus back into movement once the frequency changes (in the Fig. 74 the upper blue particle will come to a rest at position A. Once the frequency changes [ $m=2$  becomes  $m=3$  in Fig. 74], the position A will become an amplitude maximum. This forces the particles that were at rest at this position to move further [forwards to the centre or backwards]). Since statistically half of the particles move towards the centre, and since the particles that reach the centre are blocked, a continuous flow of particles into the trap can be assured by changing the frequencies of the vibrator accordingly.



A precondition of its functionality is that the soil reaches the perimeter of the plate. The plate can obviously not be exposed to the outside, but needs to be protected during the impact by the shell of the penetrator. A solution to inject particles into the sampling chamber is accomplished by using the geometry of the shell to collect the sample: inlets are integrated over the perimeter of the shell that project particles during the impact into the plate-chamber. Figure 75 shows a possible architecture of such an impact sampling system. The shell of the probe penetrates in the direction of the large white arrow. During its trajectory through the soil, particles will be projected through the inlets into the chamber.



The particles enter the inlets during the impact of the probe. The mechanism is activated once the probe is at rest by an actuator that vibrates the plate at specific frequencies. The particles travel from the outer perimeter of the plate towards the centre where they fall into a trap. An APXS above the trap can either take continuous measurements of the particle flow, or point measurements after deactivation of the plate. Particles that have fallen into the trap are discarded by vibration into a second chamber below the plate. This allows taking measurements of a larger quantity of soil, which is unloaded into this space after analysis.

This method has several advantages compared to other sampling mechanisms: the soil is harvested during the impact of the system and further transported by vibration to the analysis instrument. Therefore, the actuator used for such application does not require large strains. Piezoelectric actuators are suited for this mechanism since they can operate at high frequencies (with low displacement). The use of monolithic actuators is more adapted to high-deceleration systems than multi-element actuators

such as motors. Although the Chladni Sampler disposes of a number of moving parts, those are relatively lightweight and robust.

A major drawback of the sampling system is the requirement that the probe is perpendicular to the surface: the particles simply slip over the plates if the latter is not aligned horizontally. As it was shown in simulations of the previous section, it is not guaranteed that a perpendicularly impacting probe will remain in its original orientation during the penetration of the soil. Several solutions to this problem exist. The geometry of the plate itself can inhibit slippage to a certain extent. The sampler could be integrated in a mechanism that works similar to an artificial horizon. However, this would penalize the simplicity of the system, requiring further mechanisms to assure its alignment.

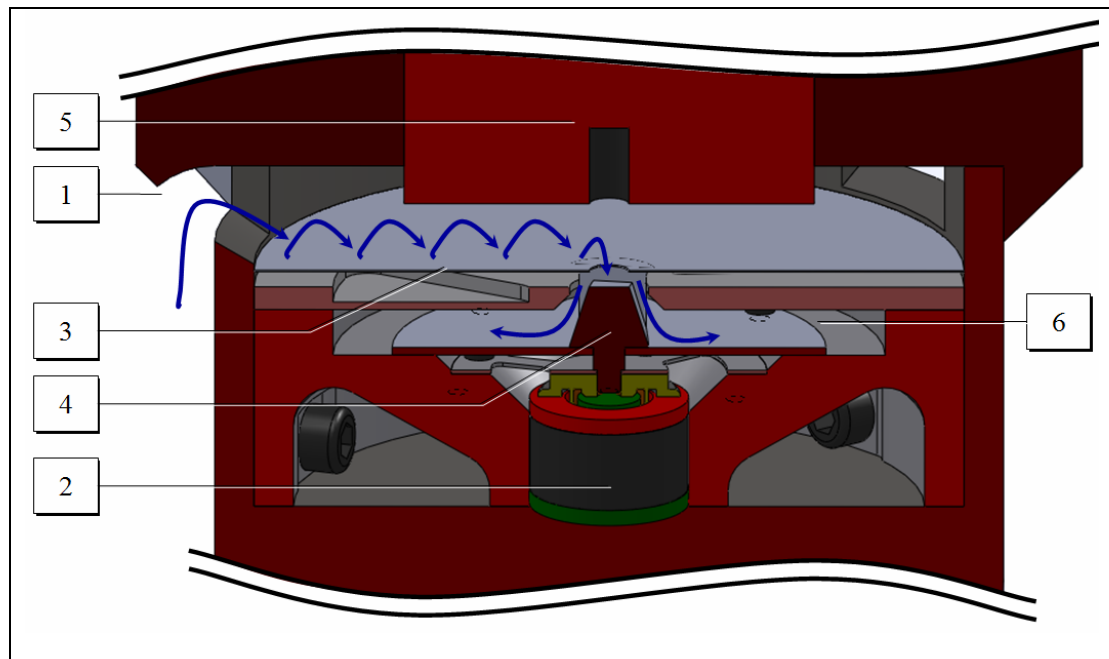
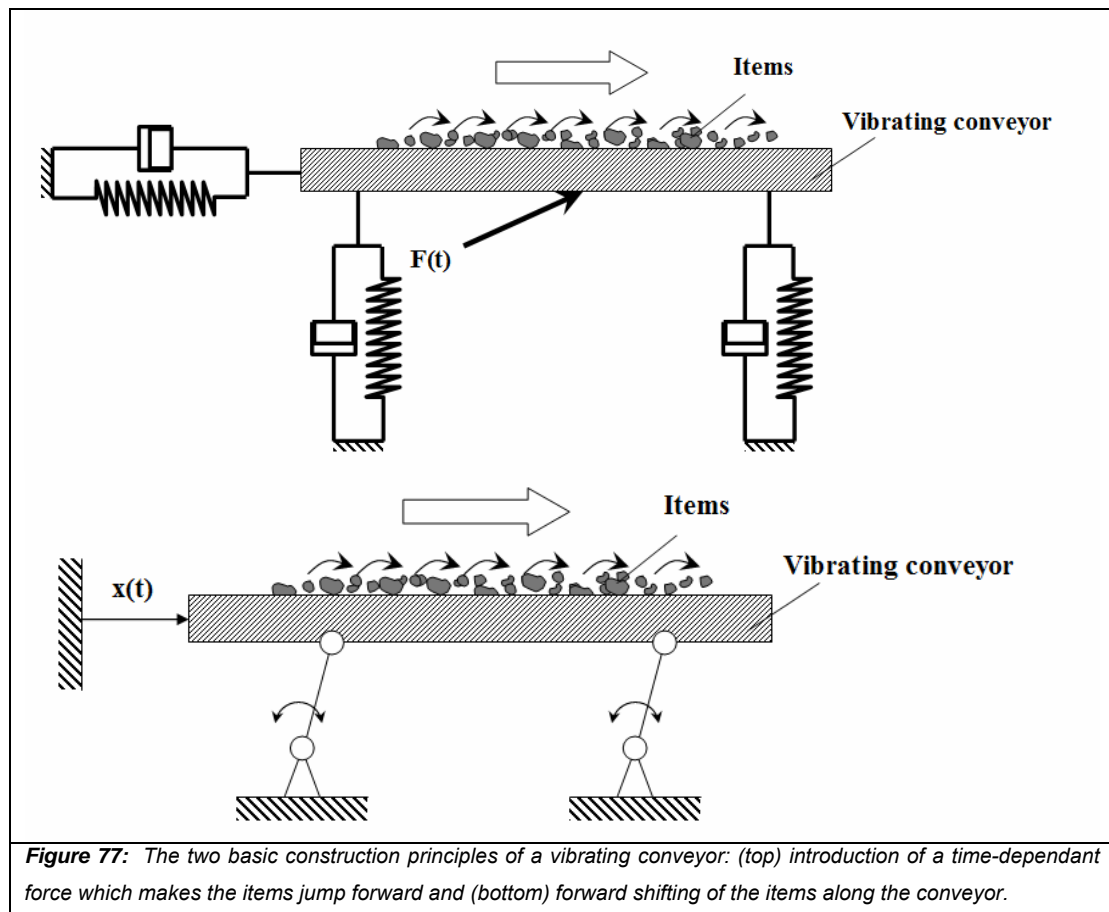


**Figure 76:** Inner structure of the Chladni sampling mechanism: The particles follow the blue path. They enter the probe during impact through the inlets in the penetrator's shell [1]. An actuator (here electromagnetic vibrator) [2] induces a vibration to the Chladni Plate [3]. The soil particles travel as a function of the frequencies used towards the centre of the plate where they fall into the trap [4]. An APXS [5] is aligned atop of the centre to take measurements of the particles composition in the trap. Measured particles are discarded into a second chamber [6] below the plate. The system allows continuous measurement of the particle flow from the perimeter into the discard chamber.



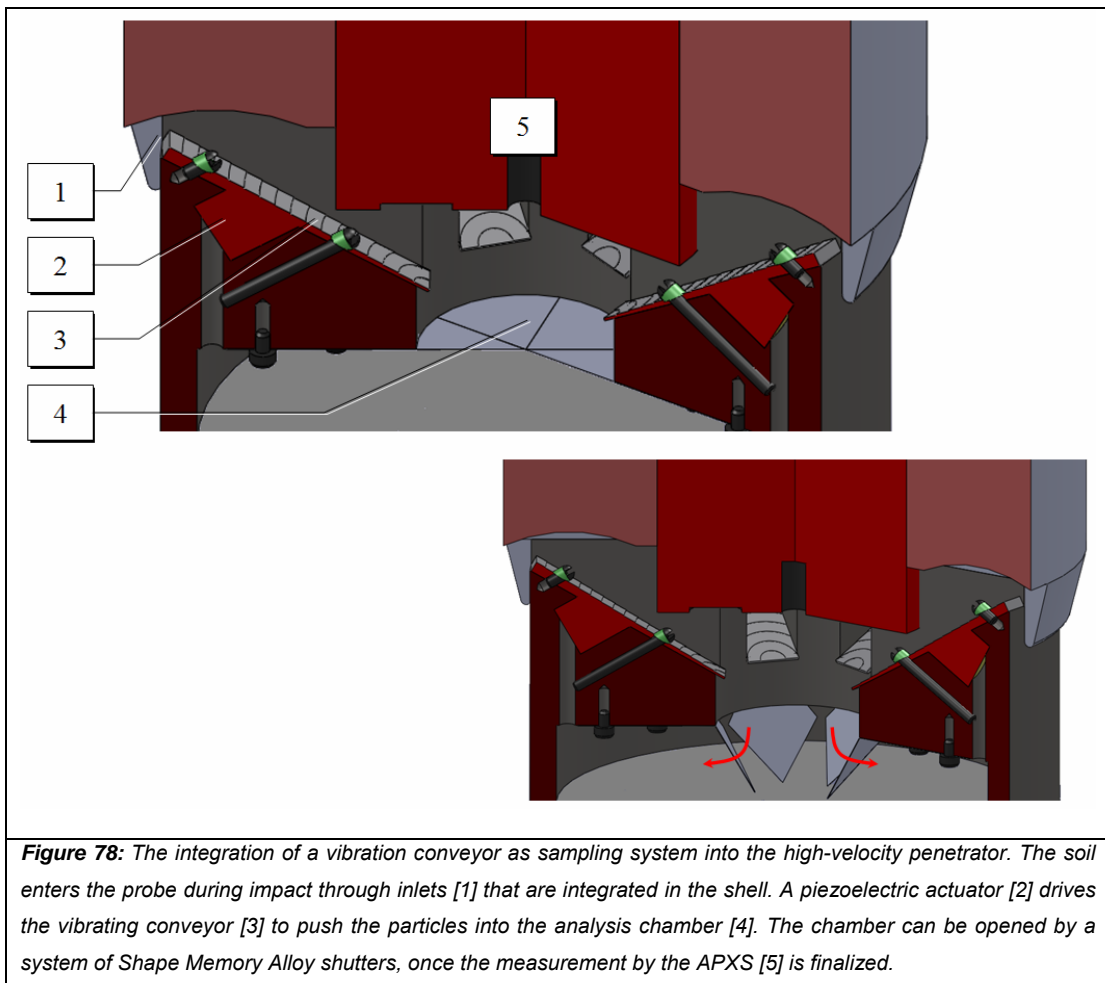
### 6.2.8. Vibrating conveyor

A third sampling system based on a vibration mechanism is inspired by the principle of a vibrating conveyor. The apparatus resembles very much the Chladni sampler in architecture and functionality; however, it is less sensible to a misalignment of the probe to the soil. Vibrating conveyors are used in many branches of industry to transport (small) items in the production process. The principle behind this method is to induce multiple micrometric forward-jumps to move the item from one location to another (see Fig. 77). The items (i.e. small bolts or granular material) are transported along the conveyor belt. Two principles are used to introduce the micro-jumps. Either a time dependent force  $F(t)$  is exerted or a forward-shift  $x(t)$  by moving the conveyor belt forward and backwards.



A similar system can be integrated in a high-velocity penetrator structure (see Fig. 78). The soil harvesting strategy is the same as described above. The soil enters the probe through several inlets which are integrated into the penetrator's shell.

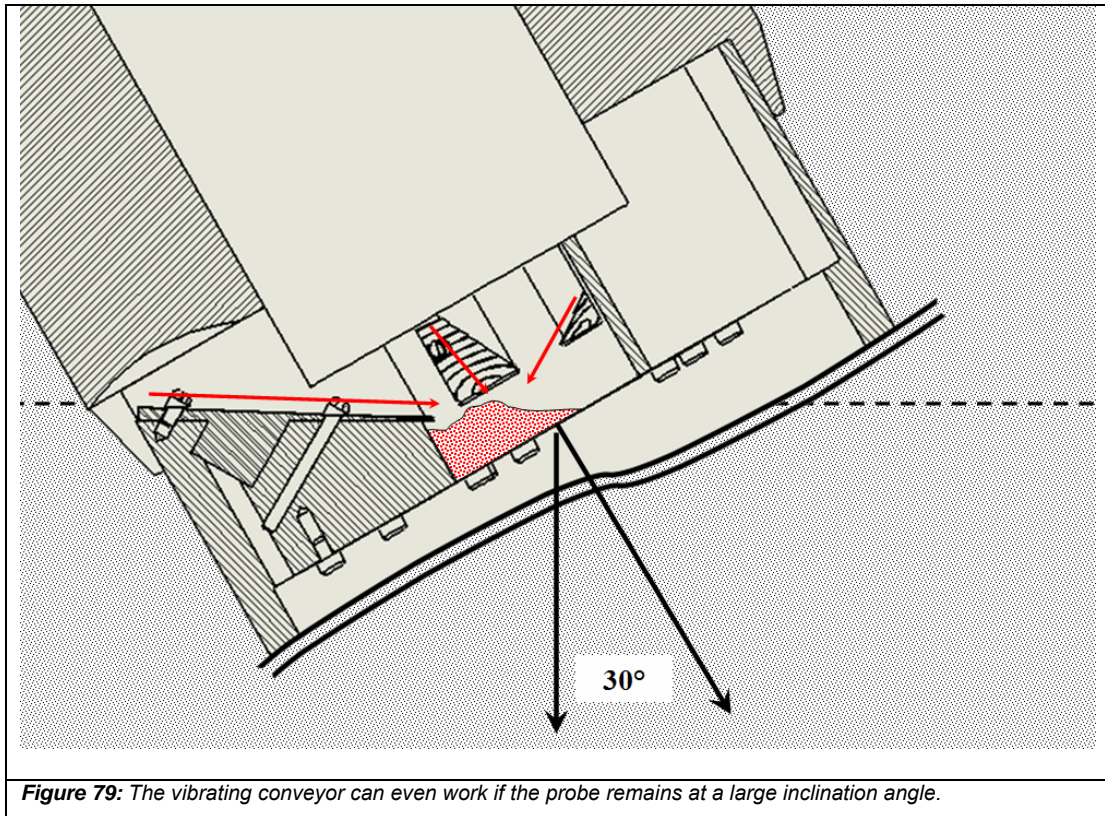
Vibrating conveyors lead the particles through a channel into the analysis chamber in the centre of the probe. The APXS is positioned above the chamber. Piezo-actuators vibrate the conveyor to achieve a forward movement (into the centre). A supplementary mechanism for this system, also based on smart materials, is a shutter door which could be activated by Shape Memory Alloys. The blades are opened by heating the alloys, through which the analyzed soil is discarded to a second space below the analysis chamber. This strategy would furthermore offer the possibility to examine sublimated gases (through the heating) after the measurements.



A vibrating conveyor has the advantages of vibrating systems as a sampling mechanism, while having a high tolerance to the final orientation of the probe. Even if the probe comes to a halt in an inclined position, the sampler is still able to transport soil into the chamber as shown in Fig. 79. Several conveyors are integrated into the perimeter of the shell, which increases the chances that at least one is in a position



where it can acquire soil samples. In the here presented architecture, the probe can be inclined  $30^\circ$  to enable the sampler to transport soil. However, the angle can even be larger, taking into account that several conveyors are used.



#### **6.2.9. Conclusions on the concept studies**

Several methods to sample soil for penetrator applications have been presented. Each of the concepts merits consideration in the application of future sampling systems. In the following, we will study the characteristics, advantages and drawbacks of these mechanisms in respect to the above-described mission for geochemical soil analysis.

The sampling strategies were evaluated to a list of criteria (see Tab. 19). We judged the usability of a system based on the number of moving parts (lowest possible), the possibility to use monolithic actuators (smart materials), and if any high-g tests have been done with such a similar system. A disqualifying criterion was the capability to work under different probe orientations, since it was shown that even if the system impacts perpendicular to the surface, it might reorient. A second eliminating criterion was its capability to take several soil samples. The latter's necessity is debatable, but

it is obvious that a geochemical soil analysis is more valid, if a larger quantity of soil can be analyzed. Unfortunately, most of the above-mentioned works do not specifically state if their system requires a specific orientation, or if it is capable of handling several soil samples. In these cases, we estimate the integration possibility of a multi-sample system and its sensibility to the probe's orientation. These cases are marked by asterisks in Tab. 19.

The objective of this exercise is to identify one sampling strategy which is most suited to this application, in order to study the concept in detail in the following sections.

Considering the multi-sample possibility, a necessity eliminates four of the sampling proposals: namely, the Mars-96 concept, the shacking sampler, the suction drill and the mole sampling concepts. The low tolerance of the probe's orientation disqualifies the Chaldni-Sampler concept, since it would need to be assured that the probe lands in almost perfect vertical direction. Both the Deep-Space 2 sample drill and the bio-inspired drill are highly valuable concepts for sampling systems onboard a penetration probe. Their only drawback would be the need of large displacement actuators, possibly the use of a motor. Furthermore, these systems have been extensively studied in the works mentioned above. Therefore, we retain the novel concept of a sampler that is based on a vibration conveyor for the following study.

Table 19: Comparison of different sampling strategies. Fields marked with \* are estimations.

System	Moving Parts	Monolithic Actuators	High-g proofed	Orientation Tolerance	Multi-sample possibility
<b>Mars-96 sampling strategy</b>	No	n.a.	Yes	any*	No*
<b>Deep-Space 2 micro sampler</b>	Yes	No	Yes	any*	Yes*
<b>Penetration mole sampling device</b>	Yes	No	No	any*	No*
<b>Bio-inspired micro-drill</b>	Yes	No	No	any*	Yes*
<b>Suction Drill</b>	No	n.a.	No	any	No
<b>Shacking sampling system</b>	Yes	No	No	any	No
<b>Chladni Sampler</b>	Yes	Yes	No	low <1°	Yes
<b>Vibrating conveyor</b>	Yes	Yes	No	high >30°	Yes

### 6.3 Modeling of the vibrating conveyor as sampling system

In the previous chapter, different sampling mechanisms were studied that can deliver a soil sample to the analysis instruments inside a penetrating probe. A novel concept based on a vibrating conveyor was identified as suitable for such applications.

Its principle offers several advantages compared to classical sampling techniques for planetary impact-penetrators:

- The mechanism is simple with a reduced number of moving parts (compared to a drill).
- Its drive can be built from smart-material devices like piezo-electric actuators. Such actuators are advantageous for applications in high velocity impact scenarios due to their monolithic structure, size and weight.

- The sampling principle offers a high potential for miniaturization. Therefore, it can be integrated in various positions and locations on impacting probes.

In this section, we study the architecture of such a system in more detail and develop a system design that suits the application of high-velocity penetrators. Several factors are of importance for the feasibility of a vibrating conveyor as a planetary sampling system:

- The effect of low-gravity environment on the conveyor's efficiency.
- The small motion range of monolithic actuators such as piezo ceramics for vibrating conveyors.
- The alignment sensibility of the transport process (determination of the maximal deployment angle  $\alpha_{\max}$ ).

### **6.3.1. General considerations in vibrating conveyor applications**

Vibrating conveyors can be based on two locomotion mechanisms: sliding and jumping.

#### **Sliding movement**

The first method to make a particle move along the conveyor's plane is a controlled forward sliding: the particles remain at their position in reference to the conveyor while the latter is moving forward. When the conveyor is retracted, the frictional forces between the particle and the conveyor are overcome, and the particle moves forward.

The mathematical framework for this process is given in Tmej (2001) with references therein. The following formulae are based on this work and have been adapted to our application. The conveyor's displacement  $S_R$  can be expressed by the following formula, using a sinus-formed output of the actuator:

$$s_R = A \sin(2 \pi f t) \quad (6.2)$$

The amplitude  $A$  is given through the travel range of the actuator while  $f$  is the frequency of the output signal. The velocity and acceleration can be calculated through the first and second derivate of formula (6.2):

$$\dot{s}_R = 2 \pi f A \cos(2 \pi f t) \quad (6.3)$$

$$\ddot{s}_R = -4 \pi^2 f^2 A \cos(2 \pi f t) \quad (6.4)$$

The z component of these vectors can be calculated by multiplying the vector s by the sine of the vibration angle  $\beta$ . The x component is obtained by a multiplication with  $\cos(\beta)$ .

Several factors determine if a particle slides on the surface of the conveyor:

- (i) The material dependant friction coefficient  $\mu$  and deployment angle  $\alpha$ ,
- (ii) The gravitation g,
- (iii) The waveform of the vibration (A, f) and geometry of the conveyor ( $\beta$ ).

The friction between the particle and the conveyor surface is determined by the normal force onto the surface; thus, by the gravity g and the conveyor's deployment angle  $\alpha$ .

$$F_R = \mu F_N \quad (6.5)$$

$$F_N = m g \cos(\alpha) \quad (6.6)$$

The particle sits on the conveyor if its parallel velocity is equal to the velocity of the conveyor,

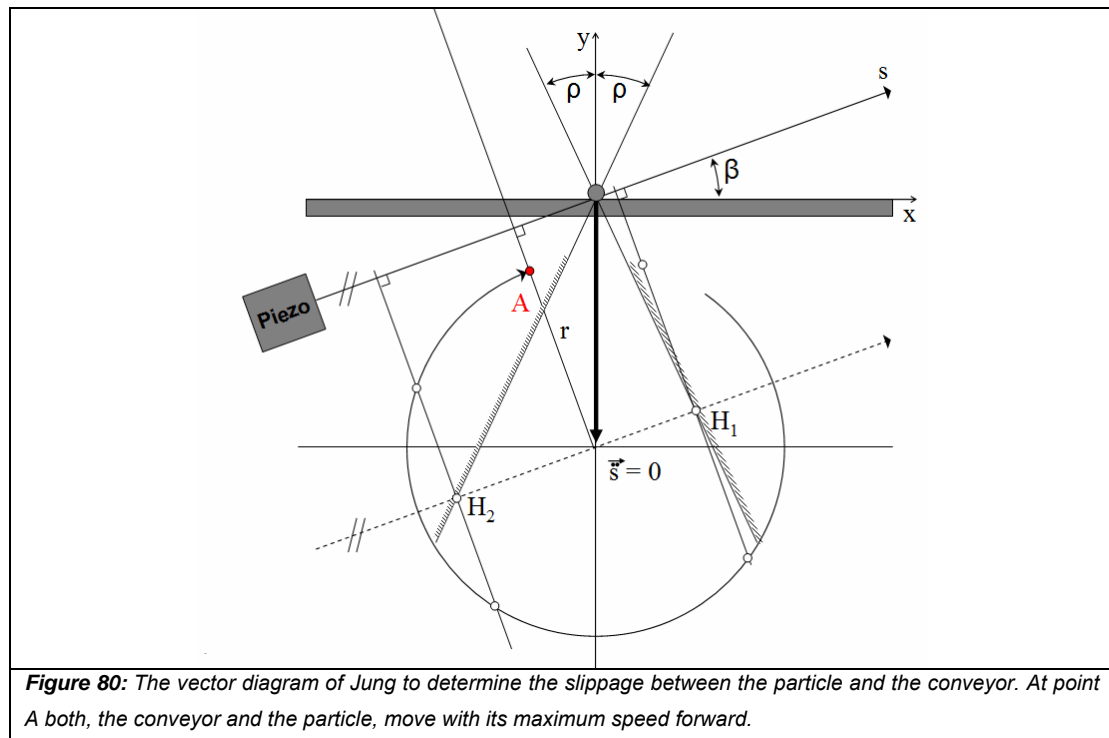
$$\dot{x}_P = \dot{x}_C \quad (6.7)$$

while it slides when both velocities draw from of each other:

$$\dot{x}_P \neq \dot{x}_C \quad (6.8)$$

Since the actuator will move periodically forward and backward, two slipping phases will occur where the inertia of the particle overcomes the friction force to the conveyor's surface. Tmej (2001) illustrates these relations by using Jung's vector diagram. Figure 80 illustrates the first phase of the periodical movement of the conveyor. The schema shows the conveyor with its principal parameters. The system is driven by a piezo-electric actuator (it could be any other device). The circle below represents the projection of a sin wave as rotating vector around the center. The circle

can be separated into four phases (delimited by the shadowed line left and right). At point A (Fig. 80) the speed of the conveyor has reached its maximum and the particle moves together with the conveyor in x direction (no relative movement between both). At the next moment, the conveyor will be slowed down; however, the particle will not start slipping forward immediately due to the friction between both.



At point B ( $\omega t = \delta_1'$ ), the conveyor is slowed down to a point where the particle's inertia overcomes the friction. The particle starts to slip forward relatively to the conveyor in x-direction.



At point D, the system enters the second slipping phase. The particle will now slip backwards due to its inertia, versus the acceleration of the conveyor.

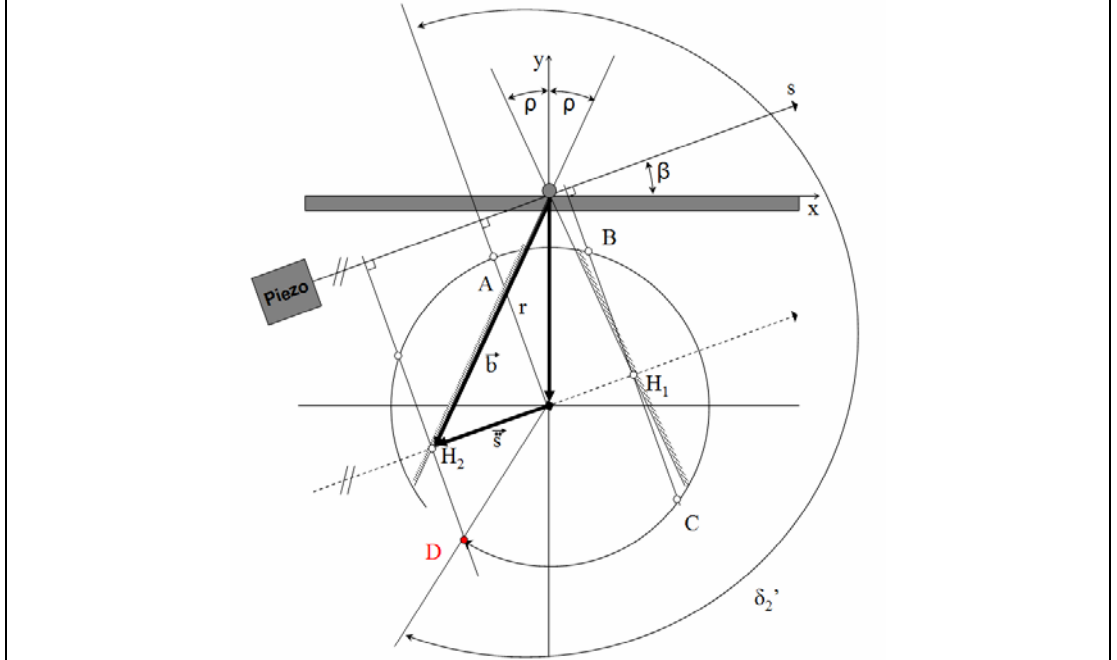


**Figure 83:** At point D the system enters a second slipping phase. This time the particle starts to slip backwards (negative x direction) due to the acceleration of the conveyor.

The angles that determine the slipping phases can be calculated through following formula by using the amplitude  $A$ , the gravitational constant  $g$ , the friction constant  $\mu$  and the angular speed  $\omega$  (Tmej, 2001):

$$\sin \delta_1' = \pm \frac{g}{A \omega^2} \frac{\mu}{\cos \beta \pm \mu \sin \beta} \quad (6.9)$$

$$\delta_1'' = \pi - \delta_1' \quad (6.10)$$

$$\delta_2'' = 3\pi - \delta_2' \quad (6.11)$$

To reach the highest transport efficiency, it is investigated to increase the first slipping phase while reducing the second one. For this, it is necessary that the actuating angle  $\beta$  is chosen so that the second angle  $\delta_2'$  is minimized. This is achieved when the plane defined by angle  $\beta$  is perpendicular to the line that crosses point  $H_1$  (first slippage phase).



It is now interesting to study how the lunar gravity will influence this process: the overall progression of the particle is determined by the difference between the forward slipping  $x_f$  and backward slipping  $x_b$  (relative to the conveyor). The relative particle velocity can, therefore, be calculated through the frequency of the actuator:

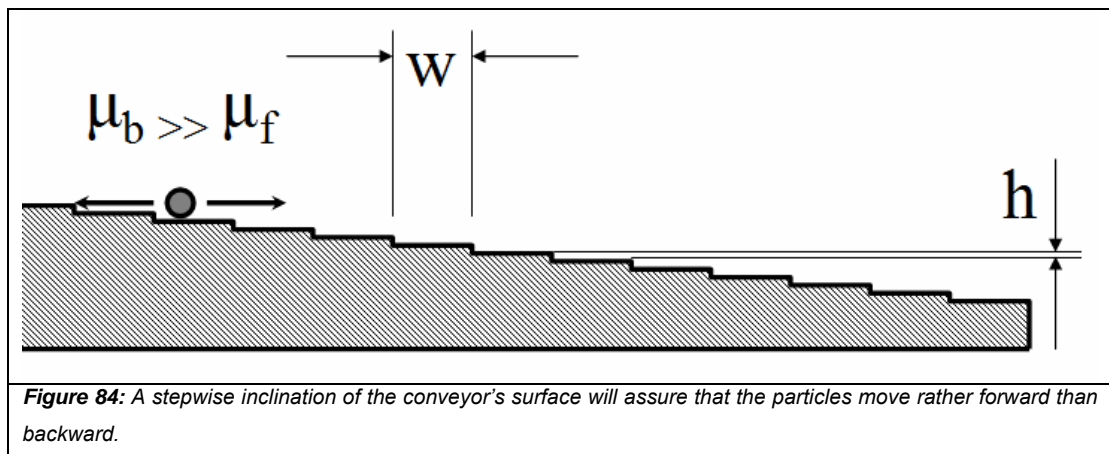
$$v = f(x_f - x_b) \quad (6.12)$$

The forward progression is given in Tmej (2001) by the following formula, where  $\varepsilon_1$  signifies the angle where the forward slippage stops and  $\varepsilon_2$  the angle where the backward slippage stops.

$$x_b = \pm \frac{\mu g}{2\omega^2} (\varepsilon_1 - \delta_1') - A(\cos\beta \pm \mu \sin\beta) [\sin\varepsilon_1 - \sin\delta_1' - \cos\delta_1' (\varepsilon_1 - \delta_1')] \quad (6.13)$$

The lower lunar gravitation will therefore increase the forward slipped trajectory, identically as it increases the backward slipped one.

The friction between the conveyor and the particle is the second variable that can be modified. Little data is reported on the mean frictional coefficient of lunar regolith. However, a design can be used that has a unidirectional friction, which means the friction is high in one direction, while low in the other direction. A simple stepwise inclination of the conveyor's surface will have the effect that particles will rather slip forward than backward (see Fig. 84).



A theoretical progression speed can be calculated using the following assumptions:

i) The angles  $\varepsilon_{1/2}$  where the particle stops slipping cannot be determined analytically. The transcendental equation for  $\varepsilon_{1/2}$  is given in Eq. (6.14):

$$\frac{\cos \varepsilon_{1/2} \cos \delta_{1/2}'}{\varepsilon_{1/2} \delta_{1/2}'} = \pm \frac{g}{A\omega^2} \frac{\mu}{\cos \beta \pm \mu \sin \beta} \quad (6.14)$$

$\varepsilon_{1/2}$  will be slightly larger than  $\delta_{1/2}'$ . As a first assumption, we therefore use the angle of  $\delta_{1/2}'$  as theoretical minimum of  $\varepsilon_{1/2}$  in Eq. (6.13).

ii) For the other parameters, we use the values of a piezo-electric actuator (Physical Instruments, 2009). We assume the amplitude  $A$  to be in the order of  $15\mu\text{m}$ .

iii) The frequency used is 240Hz, the vibration angle was chosen to be  $16^\circ$ .

iv) A friction coefficient of 0.6 was used. This is the mean friction coefficient between glass and metal (as previously indicated, no experimental data was found on the friction coefficient of lunar regolith) (Roymech, 2009).

Using the above data in Eq. (6.13), we obtain for  $x_f = 2.84\text{mm}$  and  $x_b = 2.27\text{mm}$ . The overall progress is thus its difference ( $x_{\text{total}} = 0.58\text{mm}$ ) per period. The theoretical progression speed of a particle can now be calculated over the frequency.

$$v_{\text{th}} = f (x_f - x_b) \quad (6.15)$$

The theoretical speed of the particle towards the centre of the probe would, therefore, be around  $139\text{mm/s}$ .

The length for the forward progression is of particular interest, because it can be used as design parameter for a mechanical restriction of the backward slippage. If the obstacle length is chosen to be  $x_f$ , then the particles will slip forward one step with each amplitude, while their backward movement is eliminated. The height of the step can influence the size of particles to be transported into the system: preferably smaller particles will be transported into the system if the step's height itself is small. Larger particles might jump over the step and will, therefore, have an  $x_b$  component in their movement.

The mass flow of soil into the system can be calculated based on formula (6.16) where  $A$  is the cross-sectional area of the aperture of the inlet and  $\rho_{\text{soil}}$  the density of the soil.

$$\dot{m} = A v \rho_{\text{soil}} \quad (6.16)$$

Using an effective coverage of the channel's aperture to 50% with soil, we estimate  $A$  to be  $25\text{mm}^2$ . As density of the soil, we use  $1.74\text{g/cm}^3$  as mean density of lunar regolith discussed in 5.1.2. The resulting mass flow would, therefore, be around  $6\text{g/s}$ .

### Jumping movement

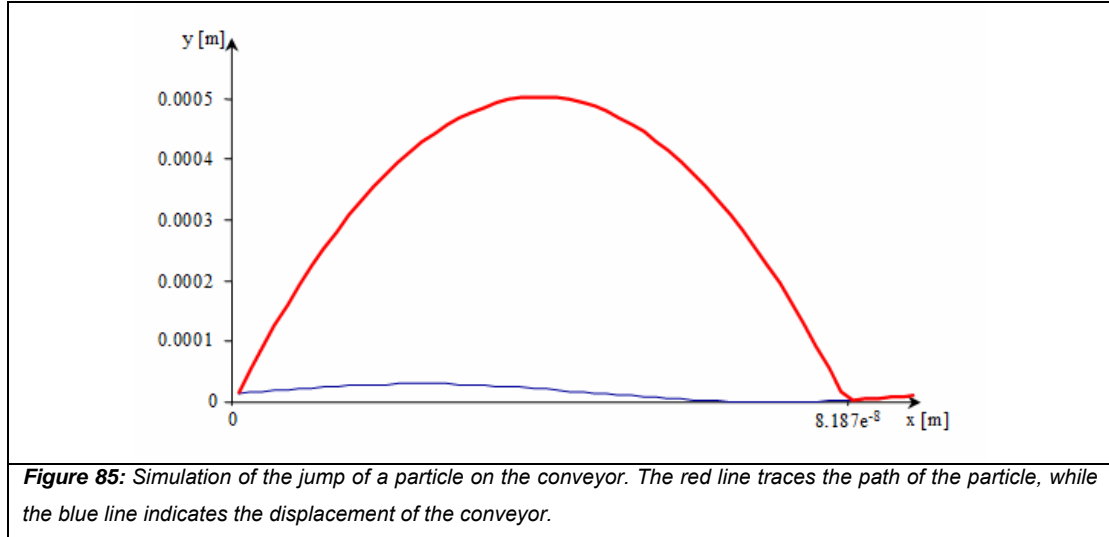
Vibration conveyors that are based on the forward and backward slipping movement are just one category of systems that are used nowadays. A second principle is to induce micro-jumps into the particles that make the soil move forward.

If the particle's acceleration in  $y$ -direction exceeds the gravitational force, then the particle will start jumping upwards. This relation is given by a jump coefficient which is the relation between the  $y$ -acceleration and the gravity (Tmej, 2001):

$$\Gamma = \frac{\ddot{y}}{g} = \frac{A \omega^2 \sin\beta}{g} \quad (6.17)$$

If  $\Gamma \leq 1$ , then the particle will not lift off, but will follow the movement of the conveyor. If  $\Gamma > 1$ , then the particle lifts off the conveyor and jumps to a second position. The jump's length can be estimated through a numerical simulation of the particle's path in reference of the swinging conveyor: Figure 85 shows the trajectory of a particle in lunar gravity with a conveyor at  $f=1000\text{Hz}$  with  $A=15\mu\text{m}$ . The formulae that govern the movement are indicated in Eq. (6.2) and (6.3) with a lift off at the highest velocity. After this point, the movement follows the trajectory of an object that is subject to gravity:

$$y(t) = v_0 t \sin\beta - \frac{g}{2} t^2 \quad (6.18)$$



The theoretical speed of a particle jumping along the conveyor can be calculated over the frequency, as indicated in Eq. (6.19):

$$v_{th} = f x_{th} \quad (6.19)$$

The result of this simulation is that the particles will advance with a speed of 0.082mm/s, which is significantly slower than in the slipping mode.

### **6.3.2. The problem of the probe's orientation**

The probe's orientation is a critical factor in the design of the sampling system based on the vibration conveyor. It is desirable to develop a system that disposes of sampling channels with a small angle  $\alpha$  (see Fig. 86). The smaller this angle is, the higher is the orientation tolerance for sampling. For the following study, we consider that the vibrating conveyor is only able to transport soil when the angle  $\delta$  between its transport plane and the normal force vector  $F_N$  is less or equal to  $90^\circ$ . If there are several sampling channels implemented in the projectile, it is possible to sample in various probe orientations.

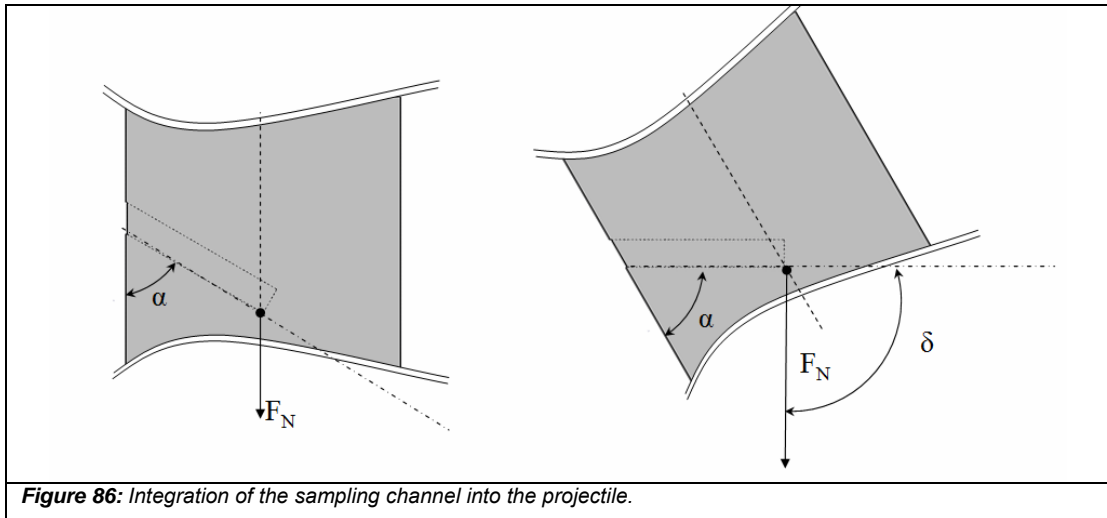
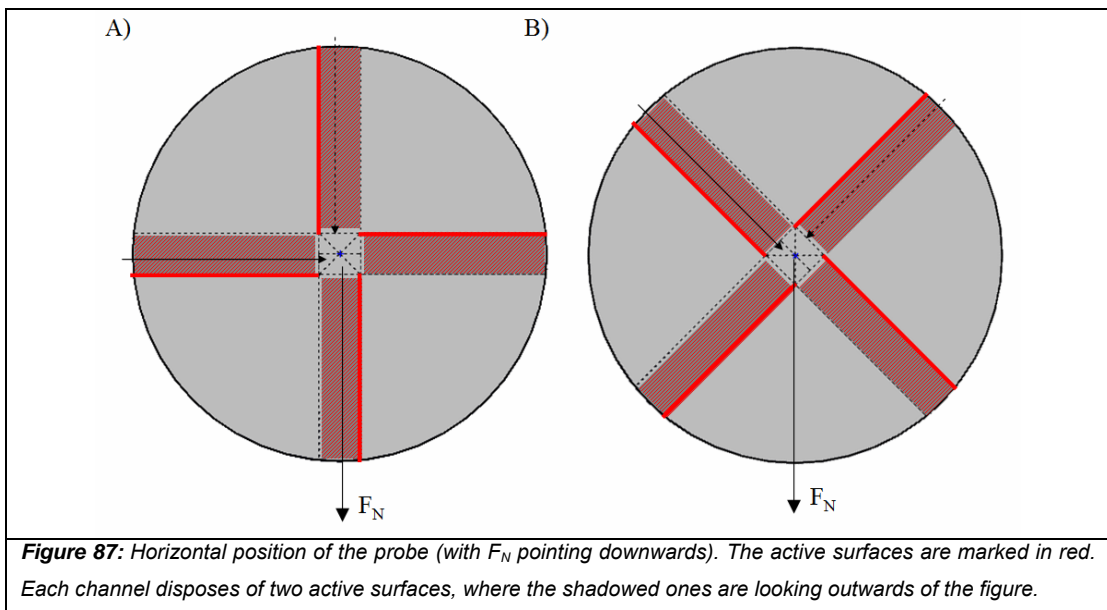


Figure 87 shows the extreme case when the probe comes to a halt at horizontal orientation. A system of four channels would still allow transporting soil into the analysis chamber if each channel disposes of two active surfaces (two sides of the chamber dispose of a conveyor). In situation A) of Fig. 87, it is the left-side channel that can work normally; it can also be expected that material will fall into the probe through the upper channel. However, this will mean that the lower channel is first to be filled up. In the situation B), we have a similar scenario: it is the upper left channel that can deliver material into the system since its active surface is looking upwards.



#### 6.4 The integration of the sampling mechanism in the projectile

The considerations on the vibrating conveyor system above lead to following conclusions:

- The more efficient transportation method is the mechanism that induces a sliding movement to the particles. Such system can deliver a mass flow of around 6g/s, using the above-given parameters. We will therefore now study the integration of such a mechanism into the penetrator's shell.
- Several sampling apertures need to be integrated into the shell in order to allow highest tolerances to different penetrator orientations. Four channels are, therefore, distributed over the perimeter of the penetrator. Each channel disposes of at least two active surfaces. From its four sides, at least two can be used to transport soil into the system.
- The conveyor cannot be directly in contact with the soil (i.e. overlap outside the penetrator's shell). Similar to the above-discussed Chladni-Sampler principle we will integrate a system to harvest the soil during impact.

For space reasons, no stacked piezo-actuator was chosen, but a piezoelectric bender actuator (Physical Instruments, 2009; page 24ff). This actuator has several advantages compared to other piezo-actuator designs.

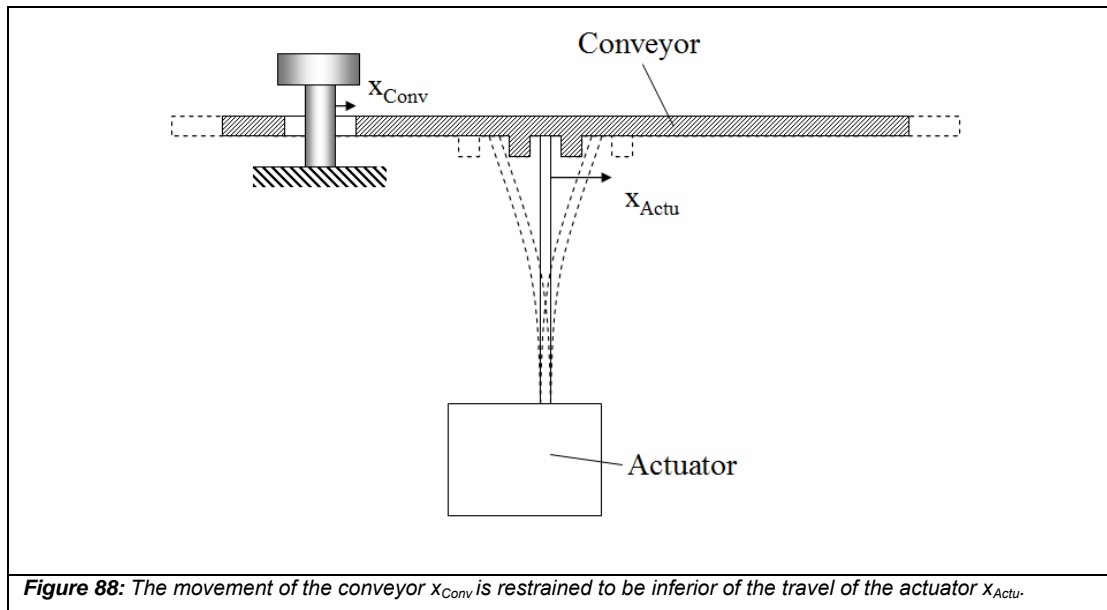
Firstly, its size is small enough to allow the integration even with large angles  $\alpha$  between the conveyor and the probe (the larger this angle is the further the actuator "sticks out" of the penetrator's shell). The length of model P 871.112 is 20mm which allows an integration angle  $\alpha$  of 30°.

The operation voltages are reduced, due to the thin layers of the piezo-ceramics in this actuator. The chosen actuator works at operation voltages of up to 60V only (other piezo-actuators work with voltages in up to the kV range).

The actuator does not dispose of polymer insulations and is therefore suited to UHV applications (no outgasing will occur in space environment).

Figure 88 shows the design constraints of the integration of the actuator. In order to protect it from damage from the impact shock, the bending surface needs to be separated from the conveyor itself. The stroke ( $x_{Actu}$ ) of model P 871.112 is  $\pm 80\mu m$ .

The conveyor needs to be fixed that its travel range ( $x_{Conv}$ ) is less than the admissible stroke of the actuator.



The system disposes of four sampling channels. Each channel has a three-sided conveyor which means that out of the four sides of the aperture, three can be used to transport soil into the system (see Figure 89).

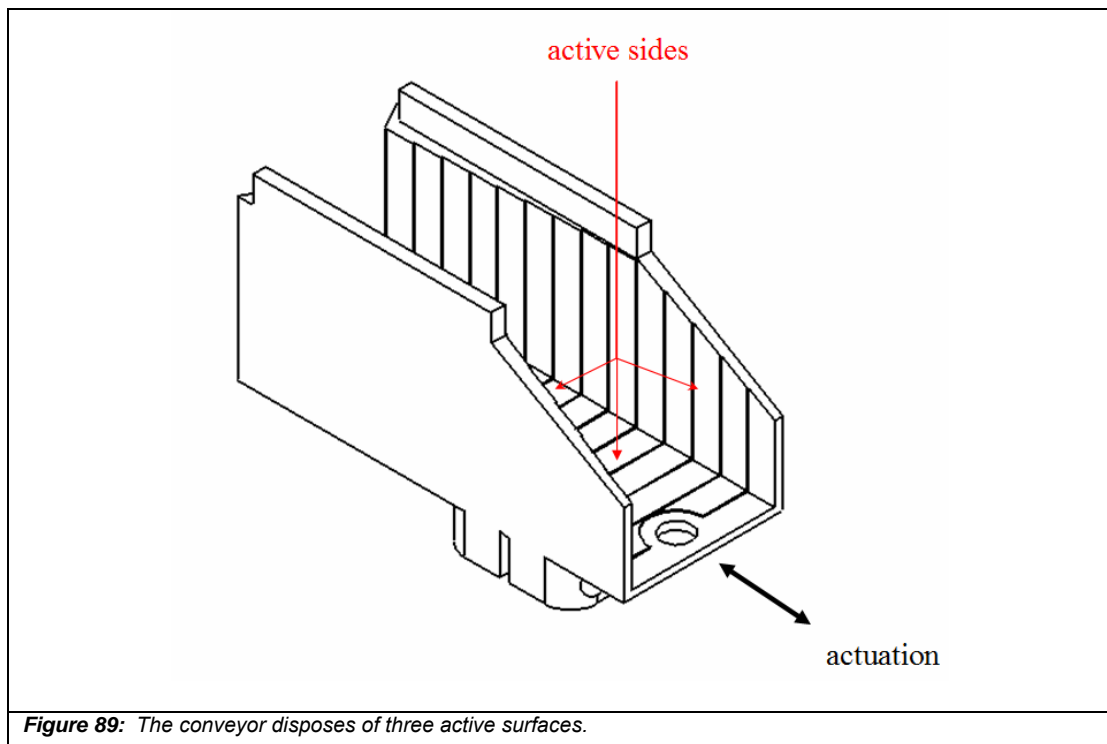
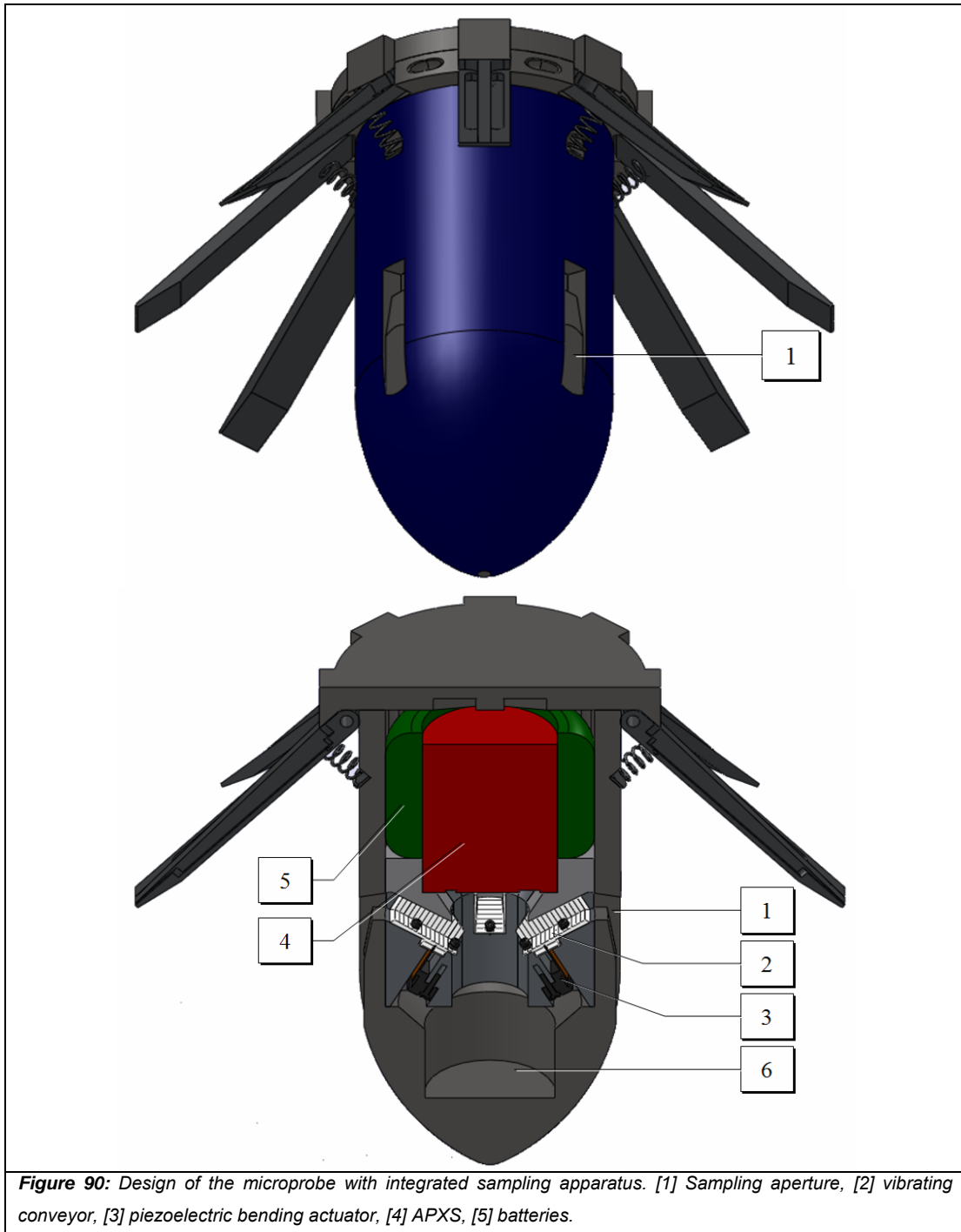


Figure 90 shows the overall design. The soil penetrates during impact through an aperture in the shell. The shape of the aperture facilitates the transport of the particles onto the vibrating conveyor. The APXS is integrated above the sampling mechanism. Analyzed soil samples are released into a disposal chamber below the mechanism (not shown).





The energy supply is one critical element in the design of the system. The batteries that are used will significantly influence the overall weight of the system. Different battery technologies can be used. Table 20 highlights the main technologies. Lithium-metal batteries are a promising technology for this penetrator application due to their advantageous energy density and low discharge rate. In the current design, a battery volume of 0.15l is assumed. Using a lithium-ion battery would, therefore, deliver a total energy of 45Wh. However, the use of this technology would lead to a battery weight of 0.32kg already. Table 21 estimates the power consumption of the system. With this choice of batteries, the penetrator could operate for 1.8h.

*Table 20: Battery technologies.*

<b>Technology</b>	<b>NiCd</b>	<b>NiMH</b>	<b>Li-Ion</b>	<b>Li-Metal</b>
Nominal Voltage [V]	1.2	1.25	3.6	3.0
Gravimetric Energy Density [Wh / kg]	45	55	100+	140+
Volumetric Energy Density [Wh / l]	150	180	225+	300+
Self-Discharge rate [% month]	25	20-25	8	1-2
Temperature Range [°C]	0 - 50	-10 - 50	-10 - 50	-30 - 55

*Table 21: Estimated power consumption*

APXS	0.33W
Communication	20W
Sampler	0.1W
Householding	0.1W
<b>Total</b>	<b>25W</b>
Operation time	1.8h
Total energy	45Wh

The overall system has a simulated weight of 4.7kg. Applying a weight penalty for the propulsion system for each probe of +60% leads to an overall weight of around 12kg per probe. The total weight of 31 probes would, therefore, be 312kg.

### **6.5 Conclusions on the sampling system**

The use of a sampling system based on a vibrating conveyor principle was studied. Such apparatus bears advantages compared to drilling systems since it can make use of monolithic actuators, like piezo-electric actuators. Vibrating conveyors used in industry already exist that use piezo-electrics as an actuator. However, in the here studied application, those can assure a large mass flow due to the lunar gravity.

The final orientation of the probe is a problem for such a sampling system. The particles cannot be transported into the analysis chamber if the conveyor's plane is oriented too steep. However, this problem can be solved by integrating four sampling channels in the perimeter of the probe, where each one disposes of three active (conveyor) surfaces. The device can still deliver a sample to the analysis instruments, even in the case where the probe comes to a halt in a horizontal position.

The study concluded with a design of the penetrator. Its weight estimation leads, however, to an overall weight of 12kg per probe (the probe itself is around 4.7kg; however, additional 60% is estimated for the propulsion part). The total payload weight for such a mission to the Moon would exceed 300kg. From this analysis it can be seen that the geochemical analysis of the lunar surface as presented in Chapter 4 would require a dedicated satellite to host the penetrator array of 31 probes.

# **CHAPTER 7**

## **Conclusions and suggestions for future research**

The system architecture and design of a micro-probe to analyze the geochemistry of extraterrestrial surfaces was studied. The work elaborated on several aspects which have not been tackled on previous mission proposals and system designs. The future objectives of missions to extraterrestrial surfaces were reviewed. Microprobes offer a significant advantage over larger landing stations in terms of global coverage of such surfaces. Nowadays, most solar system bodies are charted from orbit. Miniaturized penetrators, however, can reach numerous regions on a planet's or moon's surface to deliver the required in-situ data to complete the remote measurements. The study tries to analyze the multiple facets of a penetrator mission and its design. It clarified specific questions on such a mission strategy: how many probes are needed to develop a surface model on the geochemistry of an extraterrestrial surface? What kind of probe can be used to reach the surface, and how does it need to be built to survive the impact? How can soil samples be acquired for geochemical analysis through a sampling system?

The Moon was taken as case study. The future exploration of the lunar surface by manned space missions will rely on the identification and use of in-situ resources in the lunar soil. Elements such as Oxygen, Hydrogen, Helium and metals need to be charted precisely to choose the best spots for future landing missions. The work used the remote measurements done by the American Lunar Prospector mission to develop a Landing Site Decision Support System. This system calculates the uncertainties in remote measurement data of some elements. It was found that some element abundance exhibit specific correlations between each other. By using this correlation, we can establish theoretical models of the abundance of certain elements as function of the abundance of others. We compared the theoretical value and the measured one, and find that most of the surface can be correctly modeled by using this law.

However, some specific regions do not comply, and are consequently declared as uncertain. The deviation between the theoretical value and the measured one can be explained by two reasons: either there is a measurement error in the dataset, or there is indeed an exotic mixture of elements at the specific spot. The spatial distribution of these locations delivered further hints about the real situation. While isolated spots lead to the expectation that those are rather error measurements, clustered spots and areas that show the same behavior might lead to the conclusion that there is an exotic soil mixture present. We charted these areas and studied different exploration means to acquire surface samples. The Decision Support System assigned, by this methodology, a number of 31 locations on the lunar surface that might be interesting to be reached by impacting probes. This approach was novel from several aspects. It is to our knowledge the first attempt to study the number of in-situ measurements needed for the geochemical analysis of an extraterrestrial surface (the Moon in our case). Also, the method to analyze remote measurement datasets to derive landing spots by the use of a Geographic Information System and a Decision Support System is novel. The result of this study was that in order to reach all geochemically interesting sites on the lunar surface a large quantity of probes is needed.

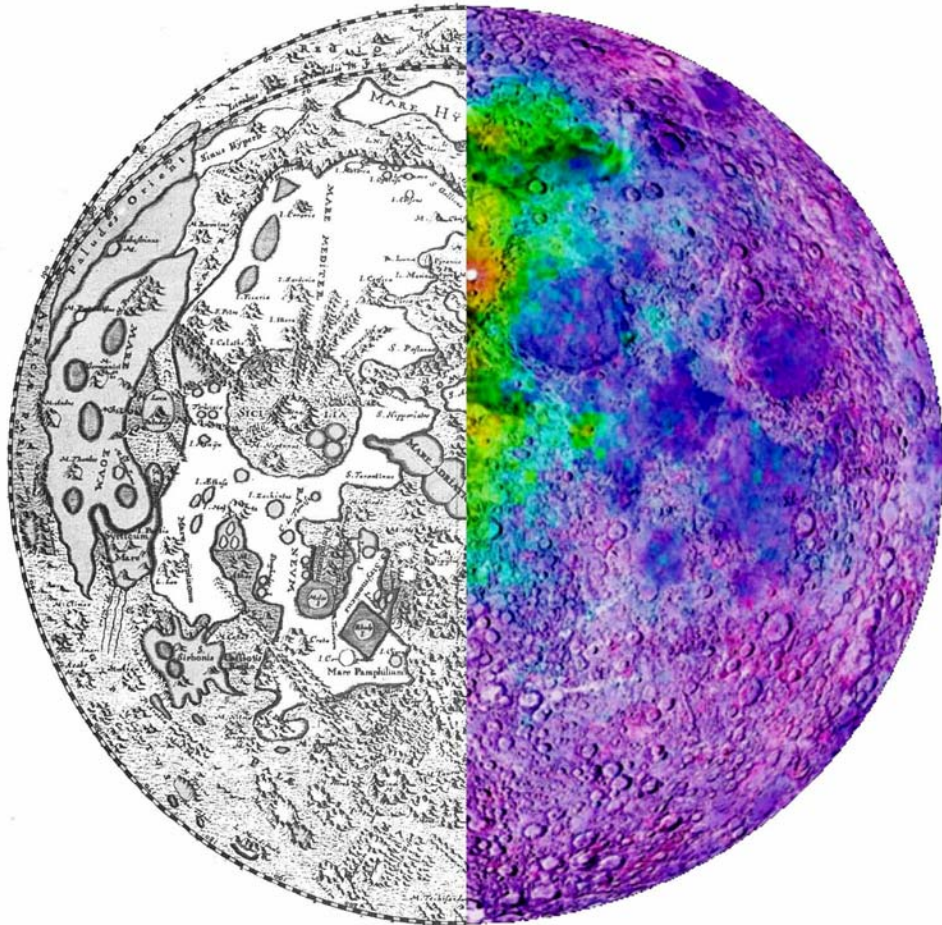
(The work had an unexpected “spin-off” finding; it showed that the element abundance of elements can be modeled as function of certain other elements. We show that these models are rather precise for the major regions of the moon. This has an interesting application for remote observations too: it would allow deriving a several element quantities only by measuring some elements in high spatial resolution.)

The microprobe was designed based on this first result. Different methods to deploy those systems onto the lunar surface were reviewed and studied. We came to the rather classic conclusion that the best way to deploy the penetrators is by a free-fall where the horizontal velocity has to be cancelled by a system of retrorockets. The propulsion system development was not part of this study; however, a weight penalty of +60% to the system’s weight was assigned to the overall weight budget. Two shell architectures were analyzed through formula and simulations in LS-DYNA: a slim shaped projectile and a larger diameter, disc-shaped shape. Each shape has specific advantages and drawbacks for a mission to analyze the chemistry of the surface. The

slimmer probe concentrates the deformations of the carrier to the frontal parts of the body. Its internal instruments are therefore better protected. Its impact behavior is more stable than the larger diameter probe; it can impact under steeper angles of attack. However, its penetration depths are very large. Although radio communication should not be a problem even from deeper depths in the lunar soil, deep penetration is not a requirement. Based on these results, a novel carrier architecture was derived and analyzed. This penetrator has a slim diameter with a system of pedals at the rear to reduce the penetration depth. The novel concept was studied in LS-DYNA, and we calculated the g-force that the system will experience at different impact velocities.

The geochemical analysis apparatus was studied in the last part of the work. Different instruments that can be used for geochemical soil analysis are reviewed. A technological readiness analysis was performed to study which system is best fitted to the application of miniaturized high-velocity impactors. With the current state-of-the-art, we found that an APXS is, under the current state-of-the-art, the best-suited instrument to perform such a mission. Subsequent to the choice of the measurement instrument, a sampling strategy was developed. A number of methods were reviewed and several new concepts presented. A novel sampling concept, which is based on the principle of a vibrating conveyor, was found to be a promising candidate for this application. The system was analyzed and designed. The work concludes with an overall architecture of a micro-probe and an evaluation of its performance. The detailed design allowed estimating the overall weight and size of the penetrator. We found that that a rather large mission will be required to carry such a number of penetrators since the overall weight of all 31 penetrators exceeds 300kg.

Future work on this concept will inevitably include real impact trials with a mock-up of such probe and its instruments. Such trials were not possible in the frame of this thesis. The related costs to use an existing airgun, or even the development of one, are much too high. (For the latter, this also comes with significant risk!). However, impact trials will be required to validate the concept and the parameters which were derived by numerical simulations.



*Measure what is measurable, and make measurable what is not so.*  
Galileo Galilei (1564 – 1642)

# References

- Allouis, E., Ellerya, A., Welchb, C.S. 2006. Entry descent and landing systems for small planetary missions: Parametric comparison of parachutes and inflatable systems for the proposed Vanguard Mars mission, *Acta Astronautica* 59, pp. 911 – 922.
- Araki, H., Tazawa, S., Noda, H., Ishihara, Y., Goosens, N., Sasaki, S., Kawano, S., Kamiya, I., Otake, H., Oberst, J., and Shum C., 2009. Lunar global shape and polar topography derived from Kaguya-LALT laser altimetry, *Science*, 323, pp. 897-900.
- Araki, H., Tazawa, S., Noda, H., Ishihara, Y., Goosens, S., Kawano, N., Sasaki, S., Kamiya, I., Otake, H., Oberst, J., and Shum, C. K., 2009b, The lunar global topography by the laser altimeter (LALT) onboard Kaguya (SELENE): Results from the one year observation, 40th, Lunar and Planetary Science Conference, Abstract # 1432.
- Atzei A. and Falkner P., 2003. Study overview of the Jovian Minisat Explorer (JME). An ESA Technology Reference Study, ESA Technology Reference Study 22/03/2005, [www.esa.int](http://www.esa.int).
- Atzei A.C., Falkner P., Van den Berg M.L. and Peacock A., 2006. The Jupiter Minisat Explorer a technology Reference Study, *Acta Astronautica* 59, 644-650, 2006.
- Bakich, M.E., 2000. The Cambridge planetary handbook, Cambridge, U.K.; New York: Cambridge University Press, 2000.
- Ball, A.J. and Lorenz, R.D., 1999. Penetrometry of extraterrestrial surfaces: A historical overview, in *Penetrometry of the solar system* (Kömle, Kargl, Ball and Lorenz editors), Verlag der Österreichischen Akademie der Wissenschaften.
- Ball, A.J., Garry, J.R.C, Lorenz, R.D. and Kerzhanovich, V.V. 2007. *Planetary Landers and Entry Probes*, Cambridge University Press 2007.
- Basilevsky, A.T., Keller, H.U., Nathues, A., Mall, U., Hiesinger, H., Rosiek, M., 2004. Scientific objectives and selection of targets for the SMART-1 Infrared Spectrometer (SIR), *Planetary and Space Sciences*, 52, pp.1261-1285.

- Basilevsky, A.T., Ivanov, M.A., Head, J.W., Aittola, M. and Raitala, J., 2007. Landing on Venus: Past and future, *Planetary and Space Sciences*, 55, pp. 2097-2112.
- Bienstock, B.J., 2003. Pioneer Venus and Galileo Entry Probe Heritage, International Workshop on Planetary Probe Atmospheric Entry and Decsne Trajectory Analysis and Science, Lisbon, Portugal 2003.
- Blue, R.C., 1999. Mars Microprobe project instrumentation package, *Acta Astronautica*, 45, pp.585-595.
- Boyle, W. S., Howard, B. T., James, D. B., 1962. Apollo and the unmanned program, NASA Report# NASA-CR-118875; TR-62-204-3.
- Braeunig R.A., 2008. Homepage Rocket and Space Technology, retrieved on June 26, 2009 from <http://www.braeunig.us/space/>
- Carrier, W.D., Olhoeft, G.R., and Mendell, W., 1991. Chapter 9 Physical properties of the lunar surface, In *Lunar sourcebook a user's guide to the Moon*, Editors G.H. Heiken, D.T. Vaniman, B.M. French, Cambridge University Press, Cambridge USA.
- Chaikin, A., 2004. The other Moon landings, in *Air&Space Smithsonian Online Magazine*, retrieved on June 03rd, 2009 at <http://www.airspacemag.com/space-exploration/other-moon.html>.
- Chassefière, E., Korablev, O., Imamura, T., Baines, K.H., Wilson, C.F., Titov, D.V., Aplin, K.L., Balint, T., Blamont, J.E., Cochrane, C.G., Ferencz, Cs., Ferri, F., Gerasimov, M., Leitner, J.J., Lopez-Moreno, J., Marty, B., Martynov, M., Pogrebenko, S.V., Rodin, A., Whiteway, J.A., Zasova, L.V., 2009. European Venus Explorer :an in-situ mission to Venus using a balloon platform, doi: 10.1016/j.asr. Advances in Space Research 2008.11.025.
- Chin, G., 2007. Lunar Reconnaissance Orbiter (LRO) Overview, The instrument suite and mission status, Proceedings of the ICEUM9 9th ILEWG International Conference on Exploration and Utilisation of the Moon,(B.H. Foing, S. Espinasse, G. Kusters, editors), ESA/ILEWG online publication, <http://sci.esa.int/iceum9>, Sorrento & ESTEC.



- Choate, R., Batterson, S.A., Christensen, E.M., Hutton, R.E., Jaffe, L.D., Jones, R.H., Ko, H.Y., Scott, R.F., Spencer, R.L., Sperling, F.B. and Sutton, G.H., 1969. Chapter 4. Lunar Surface Mechanical Properties, Surveyor Program Results, National Aeronautics and Space Administration, Compiled by Surveyor Program, Lunar and Planetary Programs Division, Office of Space Science and Applications, Washington D.C. 1969.
- Choi D., Banfield D., Gierasch P., Showman A.P., 2006. Velocity and vorticity measurements of Jupiter's Great Red Spot using automated cloud feature tracking, *Icarus*, 188, pp. 35-46.
- Committee on Planetary and Lunar Exploration, National Research Council, 1999. A Science Strategy for the Exploration of Europa, the National Academies, ISBN: 0-309-51657-9.
- Courrèges-Lacoste, G.B., Ahlers, B., Rull Pérez, F., 2007. Combined Raman spectrometer/laser-induced breakdown spectrometer for the next ESA mission to Mars, *Spectrochimica Acta Part A*, 68, pp. 1023-1028.
- Crawford, I.A., 2004. The scientific case for renewed human activities on the Moon, *Space Policy*, 20, pp. 91-97.
- Crawford, I., Fagens, S., and Joy, K., 2007. Full Moon exploration, *Astronomy and Geophysics*, 48, pp.3.18-3.21.
- Crawford I. and Smith A., 2007. Impact Site Options for a Lunar Penetrator Mission, Proceedings of the ICEUM9 9th ILEWG International Conference on Exploration and Utilisation of the Moon, (B.H. Foing, S. Espinasse, G. Kusters, editors), ESA/ILEWG online publication, <http://sci.esa.int/iceum9>, Sorrento & ESTEC 2007.
- Economou, T., 2001. Chemical analyses of martian soil and rocks obtained by the Pathfinder Alpha Proton X-Ray spectrometer, *Radiation Physics and Chemistry*, 61, pp. 191-197.
- Ellery, A., Richter, L., Parnell, J., Baker, A., 2006. A low-cost approach to the exploration of Mars through a robotic technology demonstrator mission, *Acta Astronautica*, 59, pp. 742 – 749.

- ESA, 2007. European Space Agency, Project homepage of the Young Engineer's Satellite 2, retrieved on June 26, 2009 at <http://www.esa.int/SPECIALS/YES/index.html>.
- Espinasse, S., and Di Pippo, S., 2007, Italy's Plans for Moon Exploration, Proceedings of the ICEUM9 9th ILEWG International Conference on Exploration and Utilisation of the Moon, (B.H. Foing, S. Espinasse, G. Kusters, editors), ESA/ILEWG online publication, <http://sci.esa.int/iceum9>, Sorrento & ESTEC 2007.
- Evans, L.G., Trombka, J.I, and Boynton W.V., 1986, (abstract) Elemental analysis of a comet nucleus by passive gamma ray spectrometry from a penetrator, *Journal of Geophysical Research*, 91, D525-D53.
- Fa W., Jin Y.Q., 2007. Quantitative estimation of helium-3 spatial distribution in the lunar regolith layer, *Icarus*, 190, pp. 15-23.
- Feldman, W.C., Barraclough, B.L., Fuller, K.R., Lawrence, D.L., Maurice, S., Miller, M.C., Prettyman, T.H. and Binder, A.B., 1999. The Lunar Prospector gamma-ray and neutron spectrometers, *Nuclear Instruments and methods in Physics Research A* 422, pp. 562-566.
- Flamini, E., Ori, G.G., 2007. The role of the terrestrial analogues studies in planetary exploration, Proceedings of the ICEUM9 9th ILEWG International Conference on Exploration and Utilisation of the Moon,(B.H. Foing, S. Espinasse, G. Kusters, editors), ESA/ILEWG online publication, <http://sci.esa.int/iceum9>, Sorrento & ESTEC.
- Foing B.H., and Ehrenfreund P., 2008. Journey to the Moon: Recent results, science, future robotic and human exploration, *Advances in Space Research* 42, pp. 235-237.
- Frank, H., Kindler, A., Deligiannis, F., Davies, E., Blakevoort, J., Ratnakumar, B.V., Surampudi, S., 1998. DS2 Mars microprobe battery, NASA Battery Workshop, Huntsville, retrieved on August, 11th, 2009 from <http://trs-new.jpl.nasa.gov/dspace/handle/2014/20612>.

- Gao, Y., Sweeting, M.N., Eckersley, S., Vicent, J.F.V., 2006. A "micro" concept for a planetary penetrator and drill package, in *Penetrometry of the solar system II* (Kömlé, Kargl, Ball and Lorenz editors), Verlag der Österreichischen Akademie der Wissenschaften.
- Gao Y., Phipps A., Taylor M., Clemmet J., Parker D., Crawford I.A., Ball A.J., Wilson L., Silva Curiel A. da, Davies P. Sweeting M., Baker A., 2007. UK Lunar Science Missions: MoonLITE and Moonraker, DGLR International Symposium "To Moon and beyond", Bremen, Germany 2007.
- Gao, Y., Ellery, A., Jaddou, M., Vincent, J., Eckersley, S., 2007b. Planetary micro-penetrator concept study with a biomimetric drill and sampler design, *IEEE Transactions on aerospace and electronic systems*, 43, pp. 875-885.
- Gao Y., Phipps A., Taylor M., Crawford, I.A., Ball A.J., Wilson L., Parker D., Sweeting M., Silva Curiel A. da, Davies P., Baker A., Pike, W.T., Smith, A., Gowen, R., 2008. Lunar Science with affordable small spacecraft technologies: MoonLITE and Moonraker, *Planetary and Space Sciences*, 56, pp. 368-377.
- Gavit et al. 1990. The new millennium program's Mars microprobe mission, *Acta Astronautica* Vol. 39, No 1-4 pages 273-280.
- Gavit S., Powell G., 1996. The new millennium program's mars microprobe mission. *Physica B: Condensed Matter*, Volumes 208-209, 1 March 1995, Pages 243-244.
- Genetay, I., Maurice, S., Feldman, W.C., Gasnault, O., Lawrence, D.J., Elphic, R.C., d'Uston, C. and Binder, A.B., 2003. Elemental content from 0 to 500 keV neutrons: Lunar Prospector results, *Planetary and Space Science*, 51, pp. 171-280.
- Gershman, R., Wallace, R.A., 1999. Technology need for future planetary missions. *Acta Astronautica*, 45, pp. 329-335.
- Gerzer, R., 2007. Working and living on the Moon: Challenges for medicine, *Proceedings of the ICEUM9 9th ILEWG International Conference on Exploration and Utilisation of the Moon*, (B.H. Foing, S. Espinasse, G. Kusters, editors), ESA/ILEWG online publication, <http://sci.esa.int/iceum9>, Sorrento & ESTEC.
- Gowen R.A., A. Smith, I. A., Crawford, A. J. Ball , S. J. Barber, P. Church, Y. Gao , A. Griffiths, A. Hagermann, W. T. Pike, A. Phipps, S. Sheridan, M. R. Sims, D. L.

- Talboys, and N. Wells, 2009. Micro-penetrator for in-situ sub-surface investigations of Europa, Proceedings of the International workshop “Europa lander: science goals and experiments” Space Research Institute (IKI), Moscow, Russia.
- Grant, J.A., Golombek, M.P., Parker, T.J., Crisp, J.A., Squyres, S.W., and Weitz C.M., 2004. Selecting landing sites for the 2003 Mars Exploration Rovers. *Planetary and Space Science*, v 52, n 1-3, January/March, 2004, p 11-21.
- Green, J.L. 2007. NASA Lunar Science Activities, Proceedings of the 9th ILEWG International Conference on Exploration and Utilization of the Moon, Editors: B.H. Foing, S. Espinasse and G. Kusters.
- Greeley, R., 1974. Apollo landing site exercise, NASA. Ames Res. Center A Primer in Lunar Geology, p 541-567., retrieved on June 11, 2009 from <http://hdl.handle.net/2060/19750005695>.
- Habib, A., Kim, E.M., Morgan, M. and Couloigner, I., 2004. ISPRS Congress 2004. Available online at: <http://www.isprs.org/HRS/> (accessed December 03rd, 2007).
- Haskin, L.A., 1985. Towards a spartan scenario for use of lunar materials, in Lunar bases and space activities of the 21st century (W.W. Mendel editor), Lunar and Planetary Institute, Houston, USA.
- Haskin, L. and Warren, P., 1991. Chapter 8 Lunar Chemistry. In Lunar sourcebook: A user’s guide to the Moon, G. H. Heiken, D.T. Vaniman and B.M. French (Ed.), pp. 357-474 (Cambridge University Press).
- Hayward, R., 2007. Impact modelling of a micro-penetrator dart for Martian soil sampling, Thesis at Cranfield University.
- Head, J.W., 1970. Scientific rationale summaries for Apollo candidate lunar exploration sites - Case 340, NASA Report #B70-03034; NASA-CR-109867.
- Heiken G.H., Vaniman D.T., French B.M., 1991. Lunar sourcebook a user’s guide to the Moon. Cambridge University Press, Cambridge USA (1991).
- Holmberg, N.A., Faust, R.P. and Holt, H.M., 1980. Viking '75 Spacecraft Design and Test Summary, Volume I, Lander Design, NASA Reference Publication 1027.

- Holsapple, K.A., 1993. The scaling of impact processes in planetary sciences, *Annu.Rev. Earth Planet. Sci.*, 21, pp. 333-373.
- Holsapple, K.A., 2009. Theory and equations for “Craters from Impacts and Explosions” retrieved online on 17<sup>th</sup>, July, 2009 from <http://www.lpi.usra.edu/lunar/tools/lunarcratercalc/theory.pdf>
- Hovland, S., and Foing, B., 2007. ESA Lunar Science and Exploration, Proceedings of the 9th ILEWG International Conference on Exploration and Utilization of the Moon, Editors: B.H. Foing, S. Espinasse and G. Kusters.
- Hubbard G., Feldman W., Cox S., Smith M., Chu-Thielbar L., 2002. Lunar Prospector: First results and lessons learned, *Acta Astronautica*, 50, pp 39-47, 2002.
- Hunter, D., 1978. Why send probes to Venus?, *Nature*, 274, pp. 306-307.
- ISRO, 2009, Indian Space Research Organisation Homepage, Moon Impact Probe, retrieved on June 23rd, 2009 from <http://www.isro.gov.in/Chandrayaan/htmls/mip.htm>.
- Jakeš, P., Microtel a TV microscope for planetary field geology and ressource evaluation, 1997. In *Situ Resource Utilization (ISRU II) Technical Interchange Meeting*, Lunar and Planetary Institute, Houston, Abstract #9010.
- JAXA, 2009, Kaguya: Japan's lunar explorer - Solving the mysteries of the Moon, retrieved on June 03rd, 2009 from [http://www.jaxa.jp/article/special/kaguya/seika01\\_e.html](http://www.jaxa.jp/article/special/kaguya/seika01_e.html).
- Johnson, J.R., Swindle, T.D., Lucey, P.G., 1999. Estimated solar wind-implanted Helium-3 distribution on the Moon, *Geophysical Research Letters*, 26, pp. 385-388.
- Jolliff B.L., 1997. Clementine UV-VIS multi-spectral data and the Apollo 17 landing site: What can we tell and how well? , 28th Lunar and Planet. Sci. Conf., Abstract #1770, Available online at [www.lpi.usra.edu/meetings/lpsc97/pdf/1770.PDF](http://www.lpi.usra.edu/meetings/lpsc97/pdf/1770.PDF) (accessed 90th July 2008).
- Jolliff, B.L., Lawrence, S.J., Stopar, J.D., Robinson, M.R., Gaddis, L.R., Hawke, B.R., and the LRCO Trageting Action Team, 2009. Targeting the Lunar

- Reconnaissance Orbiter Narrow Angle Cameras: Target sources and selection strategy, 40th Lunar and Planetary Science Conference, Abstract # 2343.
- JPL DS2 (2007), Jet Propulsion Laboratory, Deep-Space 2 Homepage. <http://nmp.jpl.nasa.gov/ds2/mission/mission.html>.
- Justice, C., Belward, A., Morisette, J., Lewis, P., Privette, J. and Baret, F., 2000. Developments in the 'validation' of satellite sensor products for the study of the land surface, *International Journal of Remote Sensing*, 21, pp. 3383-3390.
- Kellog L., 2007. Lunar Prospector Homepage, Retrieved from <http://lunar.arc.nasa.gov/> on November 24th, 2007.
- Khalid, A.A., ASCE, M., Hasan, A., 2009. Strength properties of JRC-1 A lunar regolith simulant, *Journal of Geotechnical and Geoenvironmental Engineering*, DOI: 10.1061/ ASCE GT.1943-5606.0000068.
- Kochan, H., Hamacher, H., Richter, L., Hirschmann, L., Assanelli, S., Nadalini, R., Pinna, S., Gromov, V.V., Matrossov, S., Yudkin, E.N., Coste, P., Pillinger, C.T., Sims, M.R., Ng, T.C., 1999. The mobile penetrometer (MOLE): A tool for planetary sub-surface investigations, in *Penetrometry of the solar system* (Kömle, Kargl, Ball and Lorenz editors), Verlag der Österreichischen Akademie der Wissenschaften.
- Kömle N.I., Weiss P., and Yung, K.L., 2008. Considerations on a suction drill for lunar surface drilling and sampling, *Acta Geotechnica*, 3, pp. 201-214.
- Kömle, N.I., Hütter, E.S., Kargl, G., Ju, H., Gao, Y., Grygorczuk, J., 2008b. Development of thermal sensors and drilling systems for applications on lunar lander missions, *Earth Moon Planets*, 103, pp. 119-141.
- Klosky, J.L., Sture, S., Ko, H.-Y., Members, ASCE and Barnes, F., 2000. Geotechnical behaviour of JRC-1 Lunar Simulant, *Journal of Aerospace Engineering*, 13, pp. 133-138.
- Kraft, S, 2005. Highly Integrated Payload architectures and instrumentation for future planetary missions, *Proceedings of the 5th ESQ Round Table on Micro/Nano Technologies for Space*, 3-5 October, 2005 ESTEC Noordwijk, NL.

- Kruijff M., and van der Heide, E.J., 2009. Qualification and in-flight demonstration of a European tether deployment system on YES2, *Acta Astronautica*, 64, pp. 882-905.
- Kulcinski, Gerald L.; Schmitt, Harrison H.; Cameron, Eugene N.; Sviatoslavsky, Igor N., 1990. Mining helium-3 from the moon. A solution to the earth's energy needs in the 21st century, *Adv Mater Appl Miner Metall Proces Princ*, 1990, p 217-228.
- Landis, G.A., 2001, Materials refining on the Moon, *Acta Astronautica*, 60, pp. 906-915.
- Lawrence, D. J., Feldman W.C., Blewett, D.T., Elphic, R.C., Lucey, P.G., Maurice, S., Prettyman, T.H. and Binder, A.B., 2001. Iron Abundances on the Lunar Surface as Measured by the Lunar Prospector Gamma-ray Spectrometer, 32nd Lunar and Planet. Sci. Conf., Abstract #1830, Available online at <http://www.lunar-research-institute.org/images/science/2001/1830.pdf> (accessed 29th April 2008).
- Lebreton, J.-P., Witasse, O., Sollazzo, C., Blancquaert, T., Couzin, P., Schipper, A.M., Jones, J.B., Matson, D.L., Gurbits, L.I., Atkinson, D.H., Kazeminejad, B., and Perez-Ayucar, M., 2005. An overview of the descent and landing of the Huygens probe on Titan, *Nature*, 438, pp. 758-764.
- Lofgren, G.E., 1993. The first lunar outpost: The design reference mission and a new era in lunar science, *Lunar and Planetary Inst., Twenty-Fourth Lunar and Planetary Science Conference. Part 2: G-M*, p 891-892.
- Lognonne, P., Shirashi, H., Giardini, D., Mimoun, D., Bulow, R., 2007. Returning to the Moon with Very Broad Band seismology onboard SELENE-2 and other landers of the international Moon exploration program, *Proceedings of the ICEUM9 9th ILEWG International Conference on Exploration and Utilisation of the Moon*, (B.H. Foing, S. Espinasse, G. Kosters, editors), ESA/ILEWG online publication, <http://sci.esa.int/iceum9>, Sorrento & ESTEC.
- Longley P.A., Goodchild M.F., Maguire D.J., Rhind D.W., 2005. *Geographical Information Systems and Science*, 2nd Edition, John Wiley and Sons, 2005.

- Lorenz, R.D., Moersch, J.E., Stone, J.A., Morgan Jr, A.R., Smrekar S.E., 2000. Penetration tests on the DS-2 Mars microprobes: penetration depth and impact accelerometry, *Planetary and Space Sciences*, 48, pp. 419-436.
- LSTC, (2007). LS-DYNA Keyword user's manual, Volume I, Livermore Software Technology Corporations (LSTC), Livermore, USA.
- Maguire D.J., Goodchild M.F and Rhind D.W., 1991. *Geographical Information Systems, Principles and Applications*, Vol 1: Principles, Longman Scientific and Technical, Essex, 1991.
- Mars Moessbauer Group, 2009. Homepage of the University of Mainz: Miniaturized Mössbauer spectrometer for the mineralogical analysis of the surface of Mars, retrieved on July 22<sup>nd</sup>, 2009 from <http://iacgu32.chemie.uni-mainz.de/mimos.php?ln=e>.
- Matsumoto, K., Hashimoto, T., Hosihino, T., Wakabayashi, S., Mizuno, T., Sawai, S., and Kawaguchi, J., 2007. Landing targets and technical subjects for SELENE-2, *Proceedings of the ICEUM9 9th ILEWG International Conference on Exploration and Utilisation of the Moon*, (B.H. Foing, S. Espinasse, G. Kusters, editors), ESA/ILEWG online publication, <http://sci.esa.int/iceum9>, Sorrento & ESTEC.
- McEntire, R., Managadze, G., Rosenbauer, H., Cheng, A., Murchie, A., Keath, E., 1996. Mass spectrometer instrumentation for landers on small bodies and planetary moons, *Acta Astronautica*, 38, pp.337-348.
- McEwen, A.S. and Robinson, M.S., 1997. Mapping of the Moon by Clementine, *Advances in Space Research.*, 19, pp. 1523-1533.
- McKay, D.S., Heiken, G., Basu, A., Blanford, G., Simon, S., Reedy, R., French B.M., and Papike, J., 1991, Chapter 7, The lunar regolith, In *Lunar sourcebook a user's guide to the Moon*, Editors G.H. Heiken, D.T. Vaniman, B.M. French, Cambridge University Press, Cambridge USA.
- Meek, T.T., Vaniman, D.T., Cocks, F.H., and Wright, R.A., 1985. Microwave processing of lunar materials: Potential applications, in *Lunar bases and space activities of the 21st century* (W.W. Mendel editor), Lunar and Planetary Institute, Houston, USA.



- Meyer, C., Treiman, A. H., and Kostiuk, T., eds., 1996. Planetary Surface Instruments Workshop. LPI Technical Report 95-05, Lunar and Planetary Institute, Houston.
- Mining, C.P., and Luers P., 1999. The new Millennium Program: Validating advanced technologies for future space missions, NASA Goddard Space Flight Centre, Jet Propulsion Laboratory, accessed online on August 11th, 2009 at <http://hdl.handle.net/2060/20000057365>.
- Munsell, K. and Smith, H., 2007. Nasa Solar System Exploration Homepage. Available online at: <http://solarsystem.nasa.gov/missions/> (accessed December 03rd, 2007).
- Namiki, N., Iwata, T., Matsumoto, K., Hanada, H., Noda, H., Goossens, S., Ogawa, M., Kawano, N., Asari, K., Tsuruta, S.-I., Ishihara, Y., Liu, Q., Kikuchi, F., Ishikawa, T., Sasaki, S., Aoshima, C., Kurosawa, K., Sugita, S., and Takano, T., 2009. Farside gravity field of the Moon from four-way doppler measurements of SELENE (Kaguya), *Science*, 323, pp. 900-905.
- National Research Council, 2006. The scientific context of exploration of the Moon: Final Report, Space Studies Board, Division on Engineering and Physical Sciences, National Research Council, National Academies Press, Washington, D.C., USA.
- Neal, C.R., 2009. The Moon 35 years after Apollo: What's left to learn? *Chemie der Erde - Geochemistry*, 69, pp. 3-43.
- Nozette S., 1995. The Clementine Mission: Past, Present and Future. *Acta Astronautica*, 35, pp 161-169, 1995.
- NSSDC, 2009. NASA NSSDC Master Catalog Lunar-A, retrieved on June 23rd, 2009 from <http://nssdc.gsfc.nasa.gov/nmc/masterCatalog.do?sc=LUNAR-A>.
- NSSDC, 2009b. NASA NSSDC Master Catalog Beagle 2, retrieved on June 23rd, 2009 from <http://nssdc.gsfc.nasa.gov/nmc/masterCatalog.do?sc=2003-022C>.
- NSSDC, 2009c. NASA NSSDC Master Catalog Huygens, retrieved on June 23rd, 2009 from <http://nssdc.gsfc.nasa.gov/nmc/masterCatalog.do?sc=1997-061C>.
- Okada, T., Sasaki, S., Sugihara, T., Saiki, K., Akiyama, H., Ohtake, M., Takeda, H., Hasebe, N., Kobayashi, M., Haruyama, J., Shirai, K., Kato, M., Kubota, T., Kunii,

- Y., Kuroda, Y., and the SELENE-B Rover Science Group 2006. Lander and rover exploration on the lunar surface: A study for SELENE-B mission, *Advances in Space Research*, Vol. 37, pp 88-92.
- Pardo, J.R., Serabyn, E., and Wiedner, M.C., 2005. Broadband submillimeter measurements of the full Moon center brightness temperature and application to a lunar eclipse, *Icarus*, 178, pp. 19-26.
- PDS, 2008. Lunar Prospector Reduced Spectrometer Data - Special Products, PDS Geosciences Node, University in St. Louis, USA, Available online at : [http://pds-geosciences.wustl.edu/missions/lunarp/reduced\\_special.html](http://pds-geosciences.wustl.edu/missions/lunarp/reduced_special.html) (accessed May 06th, 2008).
- Perminov V.G., 1999. The difficult road to Mars. A brief history of Mars exploration by the Soviet Union. NASA History Division Office of Policy and Plans and Office of Space Science. Retrieved on April 30th, 2007 from [http://klabs.org/richcontent/Reports/mars/difficult\\_road\\_to\\_mars.pdf](http://klabs.org/richcontent/Reports/mars/difficult_road_to_mars.pdf).
- Physical Instruments, 2009. Piezo Actuators & Components, Catalogue of Physical Instruments, retrieved on October 05, 2009 from [http://www.physikinstrumente.com/en/pdf\\_extra/2009\\_PI\\_Piezo\\_Actuators\\_Components\\_Nanopositioning\\_Catalog.pdf](http://www.physikinstrumente.com/en/pdf_extra/2009_PI_Piezo_Actuators_Components_Nanopositioning_Catalog.pdf)
- Pieters, C.M., and Englert, P.A.J., 1993. Remote geochemical analysis: Elemental and mineralogical composition, University of Cambridge Press, Cambridge, USA.
- Plescia, J., Bussey, B., Spudis, P., Lavoie, T., 2007. Rationale of NASA Lunar Precursor Robotic Program (LPRP), Proceedings of the ICEUM9 9th ILEWG International Conference on Exploration and Utilisation of the Moon,(B.H. Foing, S. Espinasse, G. Kusters, editors), ESA/ILEWG online publication, <http://sci.esa.int/iceum9>, Sorrento & ESTEC.
- Podnieks E.R., and Roepke, W.W. 1985. Mining for lunar base support, in *Lunar bases and space activities of the 21st century* (W.W. Mendel editor), Lunar and Planetary Institute, Houston, USA.
- Polishchuk, G., 2007. Program of the Moon exploration by automatic space complexes, Proceedings of the 9th ILEWG International Conference on

Exploration and Utilization of the Moon, Editors: B.H. Foing, S. Espinasse and G. Kusters.

Prettyman, T.H., Feldman, W.C., Lawrence, D.J., McKinney, G.W., Binder, A.B., Elphic, R.C., Gasnault, O.M., Maurice, S., Moore, K.R., 2002. Library least squares analysis of Lunar Prospector gamma ray spectra, 33rd Lunar and Planetary Science Conference, Abstract # 2012.

Reid, J.D., Coon, B.A., Lewis, B.A., Sutherlad, S.H., and Murray, Y.D., 2004. Evaluation of LS-DYNA soil model 147, US Department of Transportation, Federal Highway Administration, Report # FHWA-HRT-04-094.

Reniers, F., and Tewell, C., 2005. New improvements in energy and spatial (x,y,z) resolutions in AES and XPS applications, review, Journal of Electron Spectroscopy and Related Phenomena, 142, pp.1-25.

Rieder, R., and Wänke, H, 1996. An Alpha Proton X-Ray Spectrometer for Mars-96 and Mars Pathfinder, American Astronomical Society, Division for Planetary Sciences Meeting Abstracts, volume 28.0221R, page 1.

Rohner, U., Whitby, J.A., and Wurz, P., 2003. A miniature laser ablation time-of-flight mass spectrometer for in situ planetary exploration, Measurement Science and Technology, 14, pp. 2159-2164.

Roytech, 2009. Coefficients of Friction, Homepage, retrieved on October 05th, 2009 from [http://www.roytech.co.uk/Useful\\_Tables/Tribology/co\\_of\\_frict.htm](http://www.roytech.co.uk/Useful_Tables/Tribology/co_of_frict.htm).

Salisbury, J.W, Basu, A., and Fischer E.M., 1997. Thermal infrared spectra of lunar soils, Icarus, 130, pp. 125-139.

Satellite Imaging Corporation, 2007. Corporation Homepage: Orthorectification. Available online at: <http://www.satimagingcorp.com/svc/orthorectification.html> (accessed November 30th, 2007).

Scott, R.F., 1970. Mechanical properties of lunar surface material, Powder Technology, 3, pp. 41-50.

Schmitz, N., Biele, J., Grott, M., Knapmeyer, M., Oberst, J., Sohl, F., Spohn, T., Ulamec, S., 2007. Rationale for a geophysics and geodesy payload for lunar networks, Proceedings of the ICEUM9 9th ILEWG International Conference on

- Exploration and Utilisation of the Moon,(B.H. Foing, S. Espinasse, G. Kusters, editors), ESA/ILEWG online publication, <http://sci.esa.int/iceum9>, Sorrento & ESTEC.
- Scott, R.F., and Zuckerman, K.A., 1971. Examination of the Surveyor 3 surface sampler scoop returned by the Apollo 12 mission, NASA Report #NASA-CR-127521, retrieved on July 03rd, 2009 from <http://hdl.handle.net/2060/19730064630>.
- Seah, M.P., AES and XPS measurements: reducing the uncertainty and improving the accuracy, 1993. *Applied Surface Science*, 70/71, pp. 1-8.
- Sharpe, M.R., 1970. *Satellites and probes, the development of unmanned space flight*, Doubleday Science Series, Doubleday & Company, Inc. Garden City, New York, USA, 1970.
- Shi, J.W., 2007. *Lecture Notes: GIS Principles*, Hong Kong Polytechnic University, 2007.
- Shi, J.W., 2008, *Principles of modeling uncertainties in spatial data analysis*, *Spatial Data quality and uncertainty*, (London: Taylor & Francis) (in press).
- Shiraishi H., Tanaka S., Fujimura A. and Hayakawa H., 2007. Development of LUNAR-A penetrator: Current status and future prospect, *Proceedings of the ICEUM9 9th ILEWG International Conference on Exploration and Utilisation of the Moon*, Session 7.2, (B.H. Foing, S. Espinasse, G. Kusters, editors), ESA/ILEWG online publication, <http://sci.esa.int/iceum9>, Sorrento & ESTEC 2007.
- Silberberg, R., Tsao, C.H., Adams, J.H., 1985. Radiation transport of cosmic ray nuclei in lunar material and radiation doses, In *Lunar Bases and Space Activities of the 21st Century* (W. W. Mendell, ed.), pp. 663–669. Lunar and Planetary Institute, Houston.
- Silverman, S., and Christensen, P., 2006. Successful Mars remote sensor, MO THEMIS and MER Mini-TES, *Acta Astronautica*, 59, pp.1039-1047.
- Simpson, R., Tyler, L.G. 2001, Mars Global Surveyor Bistatic Radar Probing of the MPL/DS2 Target Area, *Icarus*, Volume 152, Issue 1, July 2001, Pages 70-74.

Smith, A., Crawford I.A., Gowen R.A., Ball, A.J., Barber S.J., Church, P., Coates A.J., Gao Y., Griffiths A.D, Hagermann A., Joy K.H., Phipps A., Pike W.T., Scott R., Sheridan S., Sweeting M., Talboys D., Tong V., Wells N., Biele J., Chela-Flores J., Dabrowski B., Flannagan J., Grande M., Grygorczuk J., Kargl G., Khavroshkin O.B., Klingelhoef G., Knapmeyer M., Marczewski W., McKenna-Lawlor S., Richter L., Rothery D.A., Seweryn K., Ulamec S., Wawrzaszek R., Wieczorek M., Wright I.P., and Sims M., 2007. LunarEx - A proposal to the ESA Cosmic Vision, Mullard Space Science Laboratory, Proposal to the ESA Cosmic Vision Call.

Smith A., Gowen R., Gao Y. and Church P. 2007b, Technical Trade Studies for a Lunar Penetrator Mission, Proceedings of the ICEUM9 9th ILEWG International Conference on Exploration and Utilisation of the Moon, Session 7.2, (B.H. Foing, S. Espinasse, G. Kusters, editors), ESA/ILEWG online publication, <http://sci.esa.int/iceum9>, Sorrento & ESTEC 2007.

Smith, A., Crawford I.A., Gowen R.A., Ball, A.J., Barber S.J., Church, P., Coates A.J., Gao Y., Griffiths A.D, Hagermann A., Joy K.H., Phipps A., Pike W.T., Scott R., Sheridan S., Sweeting M., Talboys D., Tong V., Wells N., Biele J., Chela-Flores J., Dabrowski B., Flannagan J., Grande M., Grygorczuk J., Kargl G., Khavroshkin O.B., Klingelhoef G., Knapmeyer M., Marczewski W., McKenna-Lawlor S., Richter L., Rothery D.A., Seweryn K., Ulamec S., Wawrzaszek R., Wieczorek M., Wright I.P., and Sims M., 2009. LunarEx - A proposal to the ESA Cosmic Vision, *Experimental Astronomy*, 23, pp. 711-740.

Spudis, P.D. and Hood, L.L., 1992. Geological and geophysical field investigations from a lunar base at Mare Smythii, NASA. Johnson Space Center, The Second Conference on Lunar Bases and Space Activities of the 21st Century, Volume 1, p 163-174.

Spudis, P.D., Stockstill, K.R., Ockels, W.J., Kruijff, M., 1985. Physical environment of the lunar south pole from Clementine data: Implications for future exploration of the Moon, *Lunar and Planetary Science Conference*, vol. 26: pp. 1339-1340.

- Spudis, P.D. and Taylor, G.J., 1992. The roles of humans and robots as field geologists on the Moon, Second Conference on Lunar Bases and Space Activities of the 21st Century, Volume 1, p 307-313.
- Spudis, P.D., Bussey, B., Lichtenberg, C., Marinelli, B. and Nozette, S., 2005. Mini-SAR: An imaging system for the Chandrayann 1 mission to the Moon. 36th, Lunar and Planet. Sci. Conf., Available online at: <http://www.lpi.usra.edu/meetings/lpsc2005/pdf/1153.pdf> (accessed December 01st, 2007).
- Surkov, Y.A., and Kremnev, R.S., 1998. Mars-96 mission: Mars exploration with the use of penetrators. Planetary and Space Sciences, Vol. 46, No. 11, pp. 1689-1696.
- Swindle T.D., 1992. Abundance of He-3 and other solar-wind-derived volatiles in lunar soil, NASA Space Engineering Research Center for Utilization of Local Planetary Resources.
- Tanaka, S., Okada, T., Shiraishi, H., Kato, M., Hashimoto, T., and Kubota, T., 2007. The Science objectives of the SELENE-II lunar landing mission, Proceedings of the ICEUM9 9th ILEWG International Conference on Exploration and Utilisation of the Moon,(B.H. Foing, S. Espinasse, G. Kusters, editors), ESA/ILEWG online publication, <http://sci.esa.int/iceum9>, Sorrento & ESTEC.
- Taylor, G.J., 1992. Future scientific exploration of Taurus-Littrow, Lunar Science Institute, Workshop on Geology of the Apollo 17 Landing Site, p 57-59.
- Thompson, W.B., 1964. Lunar landing site constraints: The arguments for and against one preselected site versus several sites, NASA Report# NASA-CR-116911; TR-64-211-4.
- Trueman, E.R., Black, S., Read, D., 2004. Technical Note: Characterization of depleted uranium (DU) from an unfired CHARM-3 penetrator, Science of the Total Environment, 327, pp. 337-340.
- Tmej, C., 2001. Betriebsverhalten eines Brennstofffödersystems für direkt-holzstaubgefeuerte Gasturbinen, Dissertation, Technische Universität Wien,Fakultät für Maschinenbau, Retrieved on October 2nd, 2009 from [http://publik.tuwien.ac.at/files/pub-mb\\_4122.pdf](http://publik.tuwien.ac.at/files/pub-mb_4122.pdf).

- Tompkins, S., Pieters, C.M., 1999. Mineralogy of the lunar crust: Results from Clementine, *Meteoritics and Planetary Sciences* 34, 24-41.
- Towner, M.C., Patel, M.R., Ringrose T.J., Zarnecki, J.C., Pullan, D., Sims, M.R., Haapanala, S., Harri, A.-M., Polkko, J., Wilson, C.F., Zent, A.C., Quinn, R.C., Grunthaler, F.J., Hecht, M.H., and Garry, J.R.C., 2004. The Beagle 2 environmental sensors: science goals and instrument description. *Planetary and Space Sciences*, 52, pp.1141-1156.
- Turkevich, A.L., Knolle, K., Franzgote, E., and Patterson J.H., 1966. The chemical analysis experiment for the Surveyor lunar mission, NASA Technical Report # NASA-CR-75748 , retrieved on July 25, 2009 from <http://hdl.handle.net/2060/19670003914>.
- Valero, F.P.J., Pieters, C.M., Paulikas, G.A., 2007. Report Overview: The scientific context for exploration of the Moon, Proceedings of the ICEUM9 9th ILEWG International Conference on Exploration and Utilisation of the Moon, (B.H. Foing, S. Espinasse, G. Kusters, editors), ESA/ILEWG online publication, <http://sci.esa.int/iceum9>, Sorrento & ESTEC.
- Vaniman, D., Dietrich, J., Taylor, G.J., and Heiken G., 1991. Exploration, samples, and recent concepts of the Moon, In *Lunar sourcebook a user's guide to the Moon*, Editors G.H. Heiken, D.T. Vaniman, B.M. French, Cambridge University Press, Cambridge USA.
- Vaniman, D., Reedy, R., Heiken, G., Olhoeft, G., and Mendell, W., 1991b. The lunar environment, In *Lunar sourcebook a user's guide to the Moon*, Editors G.H. Heiken, D.T. Vaniman, B.M. French, Cambridge University Press, Cambridge USA.
- Vargo J., 2004. Progress Letter. Pasteur Instrument Payload for the ExoMars Rover Mission. Number 3. (2004). Retrieved on May 09th, 2007 from [http://esamultimedia.esa.int/docs/Aurora/Pasteur\\_Report\\_3.pdf](http://esamultimedia.esa.int/docs/Aurora/Pasteur_Report_3.pdf)
- Vargo J., 2004b. Progress Letter. Pasteur Instrument Payload for the ExoMars Rover Mission. Number 4. (2004). Retrieved on May 09th, 2007 from [http://esamultimedia.esa.int/docs/Aurora/Pasteur\\_Newsletter\\_4.pdf](http://esamultimedia.esa.int/docs/Aurora/Pasteur_Newsletter_4.pdf).

- Waenke, H., 2009. Der Mars nach Pathfinder, Cosmochemistry-Online, Homepage of the Max-Planck-Institut für Chemie, Cosmochemistry Department, retrieved on August 10th, 2009 from [http://www.mpch-mainz.mpg.de/~kosmo/members/waenke/mars\\_np.htm](http://www.mpch-mainz.mpg.de/~kosmo/members/waenke/mars_np.htm).
- Wargo, M.J., Hill, L., 2007. Lunar precursor robotics program, Proceedings of the ICEUM9 9th ILEWG International Conference on Exploration and Utilisation of the Moon, (B.H. Foing, S. Espinasse, G. Kusters, editors), ESA/ILEWG online publication, <http://sci.esa.int/iceum9>, Sorrento & ESTEC.
- Weiss, P., Yung, K.L., Ng, T.C., Wai Leung, W.S., and Choi, S., 2007. Integrated Sampler Downhole Hammering Drill Head (ISDHH) for soft and hard soil sampling, presented at the European Geosciences Union, General Assembly 2007, Vienna.
- Weiss, P., Yung, K.L., Ng, T.C., Kömle, N., Kargl, G., and Kaufmann, E., 2007b. Study of a melting drill head for the exploration of subsurface planetary ice layers, presented at the European Geosciences Union, General Assembly 2007, Vienna.
- Weiss P. and Yung K.L. 2007. Closing the gap between remote observation and rover explorations: Lunar exploration by multiple micro-probes, Proceedings of the 9th ILEWG International Conference on Exploration and Utilization of the Moon, Editors: B.H. Foing, S. Espinasse and G. Kusters.
- Weiss, P., Shi, W.Z., Yung, K.L. 2009. Attribute uncertainty modeling in lunar spatial data, In press, International Journal of Remote Sensing.
- Wilhelms, D.E., 1985. Unmanned spaceflights needed as scientific preparation for a manned lunar base, Lunar and Planetary Institute, Retrieved on October 31st, 2008 from [http://www.lpi.usra.edu/publications/books/lunar\\_bases/1985lba.conf.245W.pdf](http://www.lpi.usra.edu/publications/books/lunar_bases/1985lba.conf.245W.pdf).
- Willhelms, D.E., 1987. The geologic history of the Moon, U.S. Geological Survey Professional Paper 1348.
- Williams, K.K., and Zuber, M.T., 1998. Measurement and Analysis of Lunar Basin Depths from Clementine Altimetry. Icarus 131, pp. 107-122.



- Williamson, M., 2006. *Spacecraft Technology: The early Years*, Institution of Electrical Engineers, London, 2006.
- Winchester, J., 2006. *Space Missions. From Sputnik to Space Ship One: The history of space flight*. Amber books Ltd (2006).
- Woods, D. 1989. *The illustrated encyclopedia of space technology: Probes to the moon*. Pages. 138 – 147, Second Edition, Salamander Books, London 1989.
- Wüest, M., Managadze, G.G., and Managadze, N.G., 2007. A combined Rama/laser ablation mass spectrometer instrument for exploration of small solar system objects, *Advances in Space Research*, 39, pp. 477-481.
- Yen, A.S., Smerkar, S.E., and Murray B., 1999. Future Mars micropenetrators based on New Millennium Deep Space 2 (DS2), 30th Lunar and Planetary Science Conference, Houston, Abstract # 1870.
- Yin, L.I., and Trombka, J.I., 1988. In-situ XRF and gamma ray spectrometer for Mars sample return mission, *Lunar and Planetary Inst., Workshop on Mars Sample Return Science*, p 182-183, retrieved on July 25th, 2009 from <http://hdl.handle.net/2060/19890008998>.
- Young, C.W., 1997. *Penetration Equations*, Sandia National Laboratories, Contractor Report SAND97-2426, retrieved on July 02nd, 2009 from <http://www.osti.gov/bridge/servlets/purl/562498-4aMCvY/webviewable/562498.pdf>.
- Yung K.L., Ng T.C., Yu C.H., Chan C, 2000. Design compromises of multi-function tools for both in-situ detection and particle return from asteroid, *Advances in Space Research*, 25, pp 323-328.
- Zacny, K., Glaser, D., Bartlett, P., Davis, K., Wilson, J., 2006. Drilling results in ice-bound simulated lunar regolith (FJS-1) as part of the construction and resource utilization explorer project (CRUX), 37th Lunar and Planetary Science conference, Available online at: <http://www.lpi.usra.edu/meetings/lpsc2006/pdf/2226.pdf> (accessed July 13th, 2009).

- Zakharov, A., 1996. Project Summary of the Mars-96 mission. Homepage of the Russian Space Research Institute IKI, Retrieved on January 22nd, 2007 from [http://www.iki.rssi.ru/mars96/00\\_mars\\_e.htm](http://www.iki.rssi.ru/mars96/00_mars_e.htm).
- Zhang J. and Goodchild M., 2002. Uncertainty in Geographical Information, Taylor and Francis, London, 2002.
- Zheng, Y., Ouyang, Z., Li, C., Liu, J. and Zou Y., 2008, China's lunar exploration program: Present and future, Planetary and Space Sciences, 56, pp. 881-886.
- Zhengming T., Jiang W., Xiaohui W. and Xin W., 1999. Hard Landing Impact Probe / 行星探测器的硬着陆撞击, 导弹与航天运载技术, 1999年第4期 总第240期.